Analyses of spinal muscular atrophy (SMA) modifiers and drug-dependent responses using motoneurons (MNs) derived from induced pluripotent stem cells (iPSCs)

The Doctoral Thesis "Analyses of spinal muscular atrophy (SMA) modifiers and drug-dependent responses using motoneurons (MNs) derived from induced pluripotent stem cells (iPSCs)" was performed at the Institute of Human Genetics and the Institute of Genetics of the University of Cologne and at the Institute of Reconstructive Neurobiology/Life&Brain Center of the University of Bonn from February 2009 to September 2014.

Berichterstatter: Prof. Dr. rer. nat. Brunhilde Wirth, Institut für Humangenetik

                       Prof. Dr. rer. nat. Jürgen Dohmen, Institut für Genetik

Tag der mündlichen Prüfung: 8.12.2014

Meinen Eltern

Table of Contents

Abbreviations

+	Positive
-	Negative
%	Percent
% (v/v)	Volume percent
% (w/v)	Weight percent
4F	Four reprogramming factors (Yamanaka factors)
A	Ampere (electric current)
A	Adenine
aa	Amino acid
AA	Ascorbic acid
AChR	Acetylcholine receptor
ANOVA	Analysis of variance (statistics)
Amp^r	Ampicillin resistance
AP	Alkaline phosphatase
approx.	Approximately
APS	Ammonium persulfate
ATP	Adenosine triphosphate
a.u.	Arbitrary unit(s)
AZ	Active zone
BDNF	Brain-derived neurotrophic factor
bFGF	Basic fibroblast growth factor
bp	Base pairs
BSA	Bovine serum albumin
BTX	Bungarotoxin
C	Cytosine
°C	Degree Celsius
C57Bl/6	C57 black 6 (dark brown mouse)
cAMP	Cyclic adenosine monophosphate
cDNA	Complementary DNA
cm	Centimetre
CNTF	Ciliary neurotrophic factor

CNV	Copy number variation
C-terminal	Carboxy-terminus
CTP	Cytidine triphosphate
Cy3	Cyanine 3
d	Deoxy-
Da	Dalton
DAPI	4',6-diamidino-2-phenylindole
DAPT	N-[N-(3,5-Difluorophenacetyl)-L-alanyl]-S-phenylglycine t-butyl ester
db-cAMP	Dibutyryladenosine cyclic monophosphate
DEPC	Diethylpyrocarbonate
$_{dd}H_2O$	Double-distilled water
DMEM	Dulbecco's Modified Eagle Medium
DNA	Deoxyribonucleic acid
DNase	Deoxyribonuclease
DRG	Dorsal root ganglia
DSHB	Developmental Studies Hybridoma Bank
DV	Dorso-ventral
EB	Embryoid body
EBV	Epstein-Barr virus
E. coli	*Escherichia coli*
EDTA	Ethylenediaminetetraacetic acid
e.g.	*exempli gratia* (for example)
EGF	Epidermal growth factor
ELISA	Enzyme-linked immunosorbent assay
ESC	Embryonic stem cell
ESE	Exonic splicing enhancer
ESS	Exonic splicing silencer
et al.	*et alii* (and others)
et seq.	*et sequens* (and following)
EtOH	Ethanol
FACS	Fluorescence-activated cell sorting
F-actin	Filamentous (polymeric) actin

FCS	Foetal calf serum
FGF2	Fibroblast growth factor 2
FL	Full length
Fn	Fibronectin
FVB	Friend Leukaemia Virus B-Type (white mouse)
g	Gravitation acceleration
g	Gram
G	Guanine
GABA	γ-Amino butyric acid
G-actin	Globular (monomeric) actin
GAD	Glutamate decarboxylase
GAPDH	Glycerinaldehyd-3-phosphate dehydrogenase
gDNA	Genomic DNA
GDNF	Glial cell line-derived neurotrophic factor
Gem	Gemini of coiled bodies
GFAP	Glial fibrillary acidic protein
GFP	Green fluorescent protein
GSK3	Glycogen synthase kinase 3
GTP	Guanosine triphosphate
h	Hour
HB	Homeobox
HBSS	Hank's balanced salt solution
HCl	Hydrochloric acid
HDAC	Histone deacetylase
HEK293	Human embryonic kidney cell line 293
HGK	Humangenetik Köln (iPCS line)
HN	Haemagglutinin/neuraminidase (SeV envelope proteins)
H_2O	Water
HRP	Horse radish peroxidase
i.e.	*id est* (that is)
IgG	Immunoglobulin isotype G
IgM	Immunoglobulin isotype M

iPSC	Induced pluripotent stem cell
k	Kilo-
kb	Kilo bases
kDa	Kilo Dalton (atomic mass unit)
l	Litre
LAAP	L-Ascorbic-Acid-2-Phosphate
LB	Luria-Bertani (medium)
LB	Lymphoblastoid (cells)
Ln	Laminin
lt-NES®SCs	long-term neuroepithelial-like self-renewing SCs
LS	Low salt
μ	Micro-
m	Milli-
M	Marker
M	Molar
mM	Millimolar
MAPT	Microtubule associated protein τ (Tau)
max.	Maximum
Mb	Mega bases
MCS	Multiple cloning site
MEFs	Murine embryonic fibroblasts
μg	Microgram
mg	Milligram
MG	Matrigel™
min	Minute
μl	Microlitre
ml	Millilitre
ML	Monolayer (fibroblast cell line)
μM	Micromolar
μm	Micrometre
mM	Millimolar
MMLV LTRs	Moloney murine leukaemia virus long terminal repeats

mRNA	Messenger RNA
n	Nano-
NaCl	Sodium chloride
NaOH	Sodium hydroxide (soda lye)
n.d.	Not determined
NEAA	Non-essential amino acids
NF	Neurofilament
ng	Nanogram
nm	Nanometre
NP	Nucleocapsid protein
NPC	Neural progenitor cell
ns	Not significant
NSC	Neural stem cell
nt	Nucleotide
NTP	Nucleoside triphosphate
N-terminal	Amine-terminus
Ω	Ohm (electrical resistance)
OMIM	Online Mendelian Inheritance in Men
ORF	Open reading frame
ON	Overnight
p	Passage
p	Pico-
p	Probability (statistical significance)
PAA	Polyacrylamide
PAGE	Polyacrylamide gel electrophoresis
PAX	Paired box protein
PBS	Phosphate buffered saline
PC12	Pheochromocytoma cell line 12 (rat adrenal medulla)
PCR	Polymerase chain reaction
Pen/Strep	Penicillin/Streptomycin
PFA	Paraformaldehyde
pH	*Pondus hydrogenii* (acidity value)

PLS3	Plastin 3
PLZF	Promyelocytic leukaemia zinc finger
pMN	Motoneuronal progenitor domain (in neural tube)
PO	Poly-L-ornithine
Pur	Purmorphamine
qRT-PCR	Quantitative real-time PCR
RA	Retinoic acid
RC	Rostro-caudal
RNA	Ribonucleic acid
RNase	Ribonuclease
ROCK	Rho-associated kinase
rpm	Revolutions per minute
RRP	Readily releasable pool
RT	Room temperature
RT-PCR	Reverse transcription PCR
SC	Stem cell
SD	Standard deviation (statistics)
SC-CM	Schwann cell-conditioned medium
SCID	Severe combined immunodeficiency
SDS	Sodium dodecyl sulfate
sec	Second
SEM	Standard error of the mean (statistics)
SHH	Sonic hedgehog
SMA	Spinal muscular atrophy
SMI-32	Non-phosphorylated neurofilament H (Sternberger Monoclonal)
SMN	Survival of motor neuron
smNPCs	small molecule neural precursor cells
SNP	Single nucleotide polymorphism
SOX	SRY (sex determining region Y)-box protein
SSEA	Stage-specific embryonic antigen
SV2	Synaptic vesicle protein 2
T	Thymine

TAE	Tris-acetate EDTA
TC	Tissue culture
TEMED	N,N,N,N-Tetramethylethylendiamin
TF	Transcription factor
TGFβ	Transforming growth factor β
TH	Tyrosine hydroxylase
T_m	Melting temperature
TRA	Tumour-related antigen
Tris	Tris(hydroxymethyl)aminomethane
tRNA	Transfer RNA
TTP	Thymidine triphosphate
TUJ1	β III-tubulin
U	Unit(s)
UV	Ultraviolet
V	Volt (voltage)
v-Glut 1	Vesicular glutamate transporter 1
Vol.	Volume
VPA	Valproic acid
W	Watt (power)
WNT	Wingless-type
WT	Wild type
ZO-1	Zona occludens 1 protein

1. Summary

Spinal muscular atrophy (SMA) is an autosomal-recessive neurological heredopathia caused by homozygous loss of the <u>s</u>urvival of <u>m</u>otor <u>n</u>euron 1 (*SMN1*) gene. Although SMN protein is ubiquitously expressed as core part of the nuclear spliceosomal machinery, SMN depletion exerts its deleterious effects mainly in lower α-motoneurons of the spinal cord. The subsequent motoneuronal death and disruption of neuromuscular connectivity evokes de-nervation and atrophy of skeletal muscles in proximal limbs and trunk causing a high morbidity in affected infants. In humans there is naturally a second *SMN* gene copy (*SMN2*) present almost identical to *SMN1*. Notably, a C>T transition in exon 7 interrupts an important exonic splicing enhancer site in *SMN2* nucleotide sequence. Consequently, diminished intron/exon border recognition frequently causes exon 7 skipping so that approximately 90% of total transcripts are shortened (Δ7-SMN isoform). Still, about 10% full-length *SMN* transcripts (FL-SMN) are produced per *SMN2* gene copy ensuring a basal expression of fully functional FL-SMN protein even in *SMN1*-deleted SMA patients, after all. Variable numbers of *SMN2* (2-6 copies) are present within the population and SMA patients due to high dynamics in this genomic region. Hence, the number of *SMN2* copies inversely correlates with SMA severity. *SMN2* was regarded as the sole genetic modifier in SMA until the discovery of actin bundling protein plastin 3 (PLS3) (Oprea *et al.* 2008). In rare "discordant" families, some individuals over-expressing PLS3 remain phenotypically asymptomatic despite sharing the same genotype as SMA affected siblings. Thus, PLS3 obviously acts as protective modifier in SMA. Findings in cell culture models as well as in zebrafish and mouse models proved PLS3-induced rescue of SMA-mediated deficits in respect of axonal outgrowth and NMJ maintenance. Yet, the ameliorating effects of PLS3 could not be directly investigated in motoneurons of discordant family members.

The same problem occurred in examining the effects of SMA drugs such as histone deacetylase (HDAC) inhibitor valproic acid (VPA) (Brichta *et al.* 2006; Swoboda *et al.* 2011). However, not all SMA patients exhibited the desired *SMN2* activation and elevation of blood FL-SMN levels pointing to a different responsiveness to VPA administration (Brichta *et al.* 2006; Piepers *et al.* 2011). The underlying molecular mechanisms remained elusive so far.

The general infeasibility to obtain living neuronal tissue inheres in any neurological illness in humans. Therefore, introduction of induced pluripotent stem cell (iPSC) technology (Takahashi *et al.* 2006) paved the way for the generation of individualised patient-derived *in vitro* cell culture models. Via ectopic over-expression of pluripotency-related transcription factors (OCT4, SOX2, KLF4, c-MYC) human somatic target cells are reprogrammed into a pluripotent state displaying typical characteristics of naturally pluripotent embryonic stem cells (ESCs) (Takahashi *et al.* 2007). Directed re-differentiation of these iPSCs towards spinal motoneurons enables the generation of a patient-derived *in vitro* SMA model (Ebert *et al.* 2009). The goal of this doctoral thesis was to establish such a personalised iPSC-based *in vitro* cell culture model of PSL3-discordant family members as well as individuals with different responsiveness towards VPA.

Fibroblasts of VPA responder/non-responder SMA patients as well as two PLS3 discordant SMA families (SMA III affected and their corresponding asymptomatic *SMN1*-deleted siblings) were successfully reprogrammed by classical retroviral 4F transduction or by application of state-of-the-art non-integrative Sendai virus. Subsequently, twelve iPSC lines were clonally expanded and subjected to standardised validation procedures affirming *bona fide* pluripotency in all iPSC lines, indeed. In addition, an optimised iPSC-derived embryoid body (EB)-based motoneuron differentiation protocol was set up with which patient-derived iPSCs

were differentiated into human motoneuron (MNs) cultures lacking sufficient MN numbers for meaningful studies, however. Instead, generation of stable small molecule neural precursor cell (smNPC) lines provided a valuable tool in SMA studies representing a homogeneous cell population with high MN yield upon differentiation. Stringent examination of four phenotypic groups (i.e. healthy controls, SMA I and PLS3 discordant SMA III and asymptomatic siblings) in several different cell populations representing the iPSC-derived *in vitro* MN development (i.e. fibroblasts, iPSCs, smNPCs and MN cultures) enabled monitoring of cell-specific features during developmental course.

Subsequent MN differentiation of correctly patterned smNPCs resulted in considerable yield of *bona fide* MN cultures stunningly displaying significant differences in MN survival rate with SMA I exhibiting a massive MN decline while SMA III and asymptomatic showed an intermediate MN number relative to control upon maturation. These findings perfectly matched patients' respective phenotypes.

Furthermore, SMN expression RNA and protein levels and concomitant gem numbers broadly mirrored familiar *SMN1/SMN2* copy number distribution amongst phenotype classes with regard to principally known decreasing SMN expression in adult vs. foetal cells or in proliferating cells vs. post-mitotic cells: SMA I cultures indicated lowest SMN expression rates as well as fewest gem numbers in comparison to controls. In contrast, only a moderate reduction in gem numbers and SMN expression levels was found in SMA III and asymptomatic siblings relative to controls. In addition, PLS3 expression on RNA and protein levels depicted strong over-expression in neural lineages of asymptomatic siblings highlighting the importance of tissue-specific PLS3 over-expression for exertion of the protective effect in mild SMA III.

Different neurite length was not observed among phenotype classes in early MN cultures. PLS3/actin co-localisation occured in neuronal growth cones of MN cultures. Co-culturing iPSC-derived motoneurons with human myotubes successfully established the initial prerequisites for studying deficits in neuromuscular synapse formation, a key feature of SMA pathology.

Application of iPSCs successfully presented VPA response in GABAergic neuronal cultures of VPA (non)responders. Altered GABA release ultimately corroborated data disclosing membrane fatty acid transporter C36 as causative element in VPA responsiveness (Garbes *et al.* 2013).

For the first time, this study profoundly and reliably recapitulated SMN deficiency-conditioned deficits in SMA diseased cell lines of different severity grades and healthy control at decisive steps of MN differentiation directly in the target tissue. Moreover, PLS3 expression course during MN development gave new insight into putative PLS3-mediated protection specifically in MN cultures of asymptomatic asymptomatic siblings. Additionally, similar VPA responsiveness as in fibroblasts and blood was verified in neuronal cultures

2. Zusammenfassung

Spinale Muskelatrophie (SMA) ist eine verheerende autosomal-rezessive, neurodegenerative Erkrankung. Das verantwortliche Gen *survival of motor neuron 1* (*SMN1*) ist bei den betroffenen Patienten homozygot deletiert. Obwohl das korrespondierende Protein SMN ubiquitär als Kernbestandteil der Spliceosom-Maschinerie exprimiert wird, entfaltet der SMN-Verlust seinen schädlichen Effekt selektiv in den unteren α-Motoneuronen der ventralen Hörner des Rückenmarks. Der Untergang dieser Nervenpopulation und die folgende Unterbrechung der neuromuskulären Signalübertragung verursachen eine fortschreitende Denervierung mit progressivem Muskelschwund in der proximalen Skelettmuskulatur. Allerdings besitzen Menschen eine mit *SMN1* fast identische Gen-Duplikation (*SMN2*). Bemerkenswerterweise zerstört eine C>T Transition im Exon 7 einen wichtigen exonischen Spleiß-Enhancer, woraufhin die verminderte Erkennung der Exon/Intron-Grenzen zu einem verstärkten Ausschluss von Exon 7 im Transkript (Δ7-SMN Isoform) führt. Daher fehlen in ungefähr 90% der *SMN2*-Transkripte Exon 7. Nichtsdestotrotz werden pro *SMN2*-Genkopie ca. 10-20% Volllänge-Transkript (FL-SMN) transkribiert, wodurch sogar in SMA-Patienten mit homozygoter *SMN1*-Deletion eine Grundexpression von funktionstüchtigem SMN-Protein gewährleistet wird. Die Lage von *SMN2* in einer variablen Genomregion resultiert in einer variierenden Anzahl von *SMN2*-Kopien (2-6) in der Bevölkerung und bei SMA-Patienten. Somit korreliert die Anzahl der *SMN2*-Kopien umgekehrt mit dem Schweregrad der SMA-Erkrankung. *SMN2* war lange Zeit deshalb der einzig bekannte genetische Modifier für SMA, bis in diesem Zusammenhang der protektive Effekt des actinbündelnden Proteins Plastin 3 (PLS3) entdeckt wurde (Oprea *et al.* 2008). In seltenen, sogenannten „diskordanten" Familien zeigten einige Personen, die PLS3 überexprimierten, phänotypisch keine SMA-Symptome trotz desselben Genotyps wie ihre von SMA III betroffenen Verwandten. Studien in Tiermodellen und Zellmodellen bestätigten den durch PLS3-Überexpression induzierten Schutzeffekt. Allerdings konnte der Schutzeffekt von PLS3 nicht direkt in den Motoneuronen der Betroffenen untersucht werden. Dieselbe Problematik trat bei Studien potentieller Medikamente auf wie dem Histon-Deacetylase (HDAC) Hemmstoff Valproinsäure (VPS) (Brichta *et al.* 2003; Swoboda *et al.* 2011). Allerdings wiesen nicht alle Probanden die erwünschte stärkere *SMN2* Transkription und einen höheren SMN Proteingehalt im Blut auf (Brichta *et al.* 2006; Piepers *et al.* 2011). Augenscheinlich sprachen SMA-Patienten unterschiedlich auf VPS-Behandlung an aufgrund unbekannter molekularen Ursachen.

Da es generell unmöglich bleibt, Menschen eine Biopsie lebender Neuronen zu entnehmen, ist jedwede Studie über neurologische Erkrankungen durch diese Unzugänglichkeit des eigentlichen Zielgewebes behindert. Die Einführung der iPSZ-Technologie (induziert pluripotente Stammzellen) eröffnete dagegen die Möglichkeit, individuell patientenspezifische Krankheitsmodelle *in vitro* zu erstellen (Takahashi *et al.* 2006). Mittels ektopischer Überexpression von vier Pluripotenz aufrechterhaltenden Transkriptionsfaktoren (OCT4, SOX2, KLF4, c-MYC) konnten humane somatische Zellen in einen pluripotenten Zustand reprogrammiert werden (Takahashi *et al.* 2007), der dem Zustand natürlich pluripotenter embryonaler Stammzellen (ESZs) glich. Eine gerichtete Re-Differenzierung dieser iPSZ zu spinalen Motoneuronen ermöglichte die Etablierung eines vom Patienten abgeleiteten *in vitro* SMA-Modells (Ebert *et al.* 2009). Das Ziel dieser Doktorarbeit lag in der Generierung eines ebenjenen personalisierten, iPSZ-basierten *in vitro* Zellkulturmodells von PLS3-diskordanten Familienmitgliedern sowie SMA-Patienten mit unterschiedlicher VPS-Reaktivität.

Fibroblasten von VPS-Responder/-Nichtresponder SMA-Patienten wie auch zwei PLS3-diskordanten Familien (SMA III-Patienten sowie ihre asymptomatischen

SMN1-deletierten Geschwister) wurden erfolgreich reprogrammiert mittels klassischer retroviraler 4F-Transduktion oder durch Anwendung des nicht-integrativen Sendai-Virus. Die erhaltenen zwölf iPSZ-Linien wurden klonal expandiert und einem standardisierten Validierungsprozess unterzogen zum Beweis echter Pluripotenz, den tatsächlich alle iPSZ-Linien erfüllten. Als weiteres Ergebnis dieser Arbeit wurde zusätzlich ein optimiertes, iPSZ-basiertes motoneuronales Differenzierungsprotokoll eingeführt, mit dem sich die Patienten-abgeleiteten iPSZ in Motoneuron (MN)-Kulturen differenzieren ließen, deren geringer MN-Gehalt weiterführende Untersuchungen jedoch beeinträchtigte. Statt dessen erbrachte die Generierung einer stabilen, homogenen neuralen Vorläuferzellpopulation (small molecule neural precursor cell, smNPCs) eine genügende MN-Ausbeute nach Differenzierung. Stringente Untersuchung von vier Phänotypklassen (d.h. gesunde Kontrollen, SMA I sowie PLS3-diskordante SMA III und asymptomatische Geschwister) in verschiedenen Zellpopulationen (Fibroblasten, iPSZ, smNPCs, MN-Kulturen) ermöglichten genauere Studien zell-spezifischer, SMA-bedingter Veränderungen während der *in vitro* MN-Differenzierung. Tatsächlich erbrachte die motoneuronale Differenzierung von smNPCs eine beträchtliche Menge echter MN, deren Anzahl signifikant und massiv bei SMA I abfiel nach fortgeführter Reifung, wohingegen die MN-Zahl der SMA III und asymptomatischen Geschwister einen mittleren Wert annahm relativ zur Kontrolle. Diese Resultate deckten sich perfekt mit den entsprechenden realen Phänotypen der Patienten.

Ferner spiegelten die SMN-Expression sowie die damit einhergehende Anzahl der Gems die Anzahl der respektiven *SMN1*/*SMN2*-Genkopien unter den Phänotypklassen wider. Zudem stimmten die vorliegenden Daten mit denen vorheriger Studien überein hinsichtlich variierender SMN-Expression in adultem oder fötalen Gewebe oder verschiedenen Zellpopulationen. SMA I-Kulturen wiesen die niedrigsten SMN-Expressionsraten und die geringste Gem-Zahl auf im Vergleich zur Kontrolle. Dahingegen zeigten relativ zur Kontrolle SMA III und asymptomatische Geschwister lediglich eine milde Reduktion in puncto SMN-Menge und Gem-Zahl. Des weiteren förderte die Untersuchung der PLS3-Expression auf RNA- und Proteinlevel eine beachtliche Überexpression in neuralen Entwicklungslinien der asymptomatischen Geschwister zutage, was zusätzlich die offensichtliche Bedeutung einer gewebsspezifischen PLS3-Überexpression für einen protektiven Effekt hervorhob. Unterschiedliche Neuritenlängen innerhalb der Phänotypklassen sind in jungen MN-Kulturen nicht gemessen worden. PLS3 und Actin ko-lokalisieren in Wachstumskegeln von Neuronen in MN-Kulturen. Indem man von iPSZ abgeleitete Motoneurone zusammen mit humanen Muskelzellen ko-kultivierte, wurden die Grundvoraussetzungen für eine erfolgreiche Untersuchung von Defiziten in der neuromuskulären Synapsenbildung geschaffen – einem Kernmerkmal der SMA-Pathologie.

Erfolgreich wurden iPSZ außerdem angewandt, um VPS-bedingte Veränderungen bei der GABA-Ausschüttung Neuronenkulturen von VPS-Respondern/Nichtrespondern zu verifizieren. Diese Daten untermauerten letztlich die verantwortliche Rolle des membranständigen Fettsäuretransporters CD36 hinsichtlich der abweichenden VPS-Wirkung bei SMA-Patienten (Garbes *et al.* 2013). Zum ersten Mal überhaupt rekapitulierte die vorliegende Studie in profunder und verlässlicher Weise die durch SMN-Defizienz bedingten Defizite bei SMA-Zelllinien mit verschiedenen Krankheitsschweregraden sowie bei gesunden Kontrollen an entscheidenden Punkten der motoneuronalen Entwicklung direkt im Zielgewebe. Ferner hob der PLS3-Expressionsverlauf während der MN-Differenzierung schlüssig die Rolle des mutmaßlichen, PLS3-vermittelten Schutzes speziell in MN-Kulturen asymptomatischer Geschwister hervor.

3. Introduction

3.1 Spinal Muscular Atrophy (SMA)

3.1.1 Classification and clinical symptoms

In the 1890s, Viennese neurologist Guido Werdnig and autonomously German neurologist Johann Hoffmann in Heidelberg firstly described the symptoms of an autosomal-recessively inherited neurodegenerative disease termed spinal muscular atrophy (SMA). After cystic fibrosis, SMA is the major monogenetic cause of infant mortality in the Western European population (Lefebvre *et al.* 1995; Montes *et al.* 2009). Its incidence ranges from 1:6,000 to 1:10,000 live births with a carrier frequency of 1:35 in the Caucasian population (Pearn 1978; Czeizel *et al.* 1989; Emery 1991; Lefebvre *et al.* 1995; Wirth *et al.* 1999). However, this carrier frequency differs among ethnic groups in which Caucasians exhibit the highest and Hispanics and African Americans the least carrier frequency (Hendrickson *et al.* 2009; Sugarman *et al.* 2012). The causative gene *SMN1* was mapped by linkage analysis to a complex region of chromosome 5q13 (Brzustowicz *et al.* 1990; Melki *et al.* 1990). The disorder is caused by the selective degeneration of lower α-motoneurons situated in the anterior (ventral) horns of the spinal cord. Loss of this specific motoneuronal subpopulation ultimately results in symmetrical progressive de-nervation and subsequent atrophy of proximal skeletal and intercostal chest musculature. In contrast, corticomotoneuronal function remains preserved (Farrar *et al.* 2012).

As common postnatal symptom, affected individuals suffer from gradual weakening of voluntary muscles in limbs and trunk. Legs are more affected than arms and proximal muscles more than distal ones (Markowitz *et al.* 2004). In a milder progression, distal muscles in hands and feet are also impaired later. Since leg muscles are damaged first, usually patients become wheelchair-bound or face strong difficulties concerning gait and locomotive system. Depending on severity and ongoing progression, further symptoms appear e.g. paralysis and joint contractures. Despite profound motor deficits in SMA patients, the sensory nervous system as well as cognitive abilities remain intact usually (Crawford 2002; D'Angelo *et al.* 2006) although hints exist that in severely affected mouse models brain development in hippocampal regions is disturbed (Wishart *et al.* 2010). Albeit diaphragmatic strength is maintained in SMA patients, atrophy in intercostal chest musculature eventually leads to respiratory failure, secondary infections and death. In severely affected SMA patients, first symptoms such as abnormally decreasing foetal movements (MacLeod *et al.* 1999) and concomitant motoneuronal degeneration occur already *in utero* (Markowitz *et al.* 2004).

According to genotype and disease severity, SMA is classified into four subgroups whose characteristics are outlined in the following (Munsat *et al.* 1992):

<u>Type I SMA (Werdnig-Hoffmann Disease, MIM #253300):</u>
The acute infantile form SMA I is the most severe type and renders the highest morbidity. It accounts for approx. 50% of all SMA cases (Werdnig 1891; Pearn 1978; Markowitz *et al.* 2004). SMA I neonates exhibit profound truncal and limb hypotonia ("floppy babies") often around birth, yet within the first six months at the latest. The generalised muscle debilitation makes these infants unable to sit or walk independently giving an overall poor prognosis. Death occurs within the first two years due to respiratory insufficiency with seven months as average

survival rate (Rudnik-Schöneborn *et al.* 2009). Just 6% of SMA I patients survive longer than two years (Cobben *et al.* 2008; Rudnik-Schöneborn *et al.* 2009).

Type II SMA (MIM #253550):
In the chronic intermediate form SMA II, the disease onset commences between six months and 18 years. Most patients are diagnosed between six to 18 months. Patients are able to sit, however, their ambulatory capabilities are massively impaired because they cannot stand or walk without aid. The long-term survival varies broadly depending on involvement of intercostal chest musculature and possible detrimental effects due to the development of kyphoscoliosis (Talbot 1999). Normally, SMA II patients survive beyond two years of age with 98.5% still living at five years and 68.5% at 25 years (Zerres *et al.* 1997).

Type III SMA (Kugelberg-Welander Disease, MIM #253400):
The chronic juvenile form SMA III manifests after the first 18 months (Kugelberg *et al.* 1956) and is mostly diagnosed before the age of adolescence (between two to twelve years) by Gowers' sign for instance. SMA III yields rather modest symptoms for patients are capable of sitting, walking and climbing stairs, but wasting musculature hampers mobility with rising age. SMA III patients do not show a reduced lifespan. SMA III is further subgrouped into type IIIa with onset before the age of three years and type IIIb with onset after the third year (Zerres *et al.* 1997).

Type IV SMA (MIM #271150):
The adult form SMA IV exhibits the mildest disease phenotype. The age of manifestation lies in the 30s (Pearn 1978; Zerres *et al.* 1995) and is marked by only minor restrictions concerning gait and general mobility. SMA IV patients possess a normal life expectancy.

3.1.2 SMA genetics – *SMN1* & *SMN2* as disease causing genes

In 1990, linkage analysis revealed the SMA determining gene *survival of motor neuron 1* (*SMN1*) in a complex region on human chromosome 5q11.2-q13.3 (Brzustowicz *et al.* 1990; Melki *et al.* 1990). This genomic region features a large inverted duplication with at least five genes present in telomeric and centromeric copies making humans the only species to possess two *SMN* genes (*SMN1* & *SMN2*) (Fig. 1). After intense investigation, a homozygous mutation of telomeric *SMN1* was identified as the cause of SMA (Lefebvre *et al.* 1995). The *SMN1* gene spans a 28 kb genomic region and consists of nine exons (1, 2a, 2b, 3, 4, 5, 6, 7 and 8) of which exons 1-7 are translated. The coding sequence of *SMN1* is 882 bp long and produces an approx. 1.7 kb transcript (containing 5' and 3' UTR) which is ubiquitously expressed, especially highly in spinal cord and brain. The mRNA encodes for a protein of 294 amino acids with a molecular weight of 38 kDa (FL-SMN). In addition, *SMN1* is highly conserved among all eukaryotic organisms underlining its essential function (Miguel-Aliaga *et al.* 1999; Paushkin *et al.* 2000).

500 kb centromeric							500 kb telomeric					
RAD17	OCLN	GTF2H2	NAIP	SMN2	SERF1		SERF1	SMN1	NAIP	GTF2H2	OCLN	BDP1

Fig. 1: Scheme of 500 kb genomic region in chromosome 5q containing *SMN1* and its centromeric duplication *SMN2*.

Yet, an almost identical *SMN1* copy termed *SMN2* is located in the centromeric region. This duplication differs from the original *SMN1* nucleotide sequence only at five sites. However, all base pair exchanges do not affect the amino acid (aa) sequence. In total, four point mutations are located in untranslated regions (UTR) in exon 8 (nt 27869 G>A), intron 6 (nt 27092 G>A) and two others in intron 7 (nt 27289 A>G and nt 27404 A>G). In the coding region, there is a C to T transition (c.840C>T, codon C280T) at position +6 in exon 7 (Lefebvre *et al.* 1995; Bürglen *et al.* 1996) (Fig. 2).

Nevertheless, this minor mutation in exon 7 tremendously interferes with the unique splicing pattern of *SMN* genes. *SMN1* produces exclusively full length transcript (FL-SMN) containing all exons and giving rise to proper SMN protein as seen in individuals who possess only two *SMN1* copies. On the other hand, control probands carrying both *SMN1* and additional *SMN2* copies generated a specific mRNA population lacking exon 7 (Δ7-SMN2) (Lefebvre *et al.* 1995). Exon 7 contains a weak splicing enhancer site at its 3' end. This exonic splicing enhancer (ESE) acts as a *cis*-regulatory element and facilitates binding of auxiliary *trans*-acting splicing proteins such as Tra2, hnRNPs and SF2/ASF which recruit further serine-rich (SR)-like splicing factors excising only intron 6 and intron 7 (Lorson *et al.* 1999; Cartegni *et al.* 2002). However, the nucleotide exchange c.C280T in exon 7 destroys the ESE thereby inflicting damage to the whole splicing process. Since the splicing boundaries of exon 7 are poorly recognised, the entire exon 7 is frequently skipped from pre-mRNA resulting in 90% Δ7-SMN2 and only 10% FL-SMN2 transcript (Lorson *et al.* 1999; Cartegni *et al.* 2002). Another hypothesis suggests that this C to T transition in exon 7 generates a novel exonic splicing silencer (ESS) which favours exon 7 exclusion by recruitment of splicing factor hnRNP A1 (Kashima *et al.* 2003). As exon 7 contains the original stop codon, an alternative stop codon in exon 8 terminates translation of Δ7-SMN2 transcript, thus solely producing a truncated protein. Δ7-SMN2 protein is unstable and possesses a reduced oligomerisation ability (Lorson *et al.* 1998) resulting in rapid degradation (Burnett *et al.* 2009).
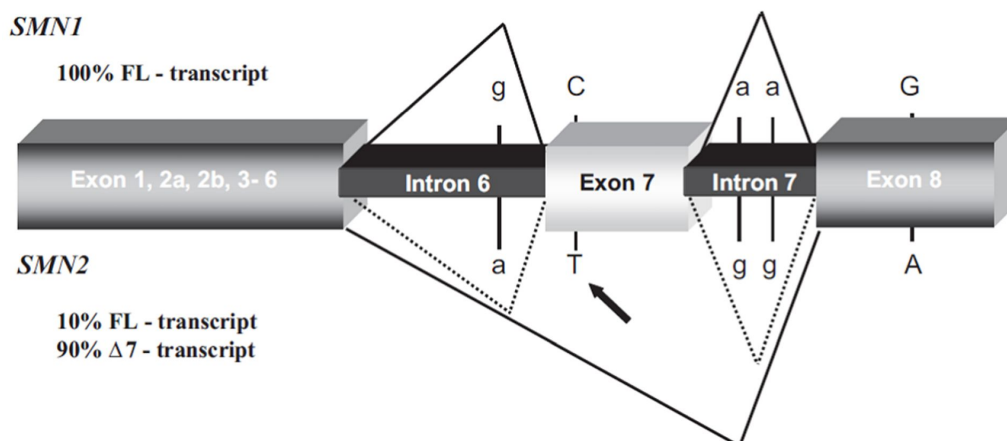
Fig. 2: Schematic illustration of nucleotide and splicing differences in *SMN1* and *SMN2* genes. Note the five differences in nucleotide sequence with C>T transition in exon 7 as the most influential one leading to frequent exon 7 skipping. Thus, *SMN2* generates almost exclusively Δ7-SMN2 transcript (90%) (from (Wirth *et al.* 2006a)).

Nearly all SMA patients show a homozygous deletion of *SMN1* gene or a conversion of *SMN1* into *SMN2* (Feldkötter *et al.* 2002; Mailman *et al.* 2002). However, some patients exhibit subtle intragenic missense mutations in *SMN1* (Alias *et al.* 2009; Vezain *et al.* 2011) or *de novo* rearrangements in the genomic region (Wirth *et al.* 1997). DNA based testing methods verify reliably and quickly clinical diagnosis of SMA in newborns beside overt motor impairments. The two most common techniques to detect loss in *SMN1* gene are (i) a PCR-based approach

with following test restriction enzyme digestion (Scheffer *et al.* 2001) or (ii) Multiplex Ligation-dependent Probe Amplification (MLPA) (Scarciolla *et al.* 2006; Zapletalova *et al.* 2007). Standard genetic sequencing procedure is alternatively usable in the rare case of subtle intragenic deleterious mutations within the *SMN1* gene (Alias *et al.* 2009; Vezain *et al.* 2011). In general, SMA I patients retain 1-2 *SMN2* copies (patients with solely one *SMN2* are sometimes denoted congenital SMA type 0), SMA II and SMA IIIa patients possess 3 *SMN2* copies, SMA IIIb patients carry 4 *SMN2* copies and SMA IV patients keep 4-6 *SMN2* copies (Feldkötter *et al.* 2002; Wirth *et al.* 2006b). Yet, there are exceptions with patients whose genotype does not match the phenotype diagnosed. For instance, Prior and colleagues reported that a SNP (c.859G>C substitution) in *SMN2* leads to a mild clinical progression in unrelated SMA patients even though they carry only 1-2 *SMN2* copies (Prior *et al.* 2009). So in conclusion, various factors may alter the outcome of SMA such as modifying genes, external factors, intragenic *SMN2* mutations and incomplete *SMN2* copies with partially deleted or duplicated *SMN2* copies (Feldkötter *et al.* 2002; Oprea *et al.* 2008; Chen *et al.* 2011; Wirth *et al.* 2013). Total loss of any *SMN* copy is embryonic lethal in humans and rodents (Burghes 1997; Schrank *et al.* 1997), yet 5-15% of the population possess no *SMN2* copies while they retain two *SMN1* copies (Feldkötter *et al.* 2002; Markowitz *et al.* 2012).

SMN2 copy number is variable within the human population because *SMN2* resides in a chromosomal region being susceptible for genomic rearrangements. In spite of a complete loss of *SMN1*-derived FL-SMN protein in SMA patients, every *SMN2* gene still delivers approx. 10% FL-SMN protein. Therefore, the SMA phenotype i.e. the disease severity inversely correlates with the *SMN2* copy number (Burghes 1997; Brahe 2000; Feldkötter *et al.* 2002; Wirth *et al.* 2006b).

3.1.3 SMN protein – Occurrence and function

SMN protein is an evolutionary highly conserved 294 aa housekeeping protein of 38 kDa in size encoded by 8 exons (Lefebvre *et al.* 1995). It is present at high levels in the central nervous system (CNS) and especially in spinal cord during embryogenesis and neonatal development emphasising the importance of a critical time window of developmental vulnerability in which SMN depletion causes its most detrimental effects (Burlet *et al.* 1998; Gabanella *et al.* 2007). SMN is ubiquitously expressed and found in both nucleus and cytoplasm of all cell types (Liu *et al.* 1996; Fallini *et al.* 2012), yet abundantly in spinal and brain stem motoneurons (Battaglia *et al.* 1997). An axonal SMN isoform has been delineated (Setola *et al.* 2007) but its disease-causing effect is regarded as unlikely (Burghes 2008). While SMN is diffusely distributed in the cytoplasm, in the nucleus SMN is present in distinct punctual nuclear sub-structures called "Gemini of Coiled bodies" (abbreviated "gems") which are located in close proximity to Cajal bodies (Liu *et al.* 1996). Vertebrate gems are stable multiprotein complexes comprising oligomerised SMN, UNRIP and diverse gemin proteins (GEMIN2-GEMIN8) (Meister *et al.* 2000; Meister *et al.* 2001; Gubitz *et al.* 2004; Carissimi *et al.* 2006). Cajal bodies are associated with the biogenesis of small nuclear ribonucleoprotein particles (snRNPs) (Carvalho *et al.* 1999; Jády *et al.* 2003). As part of the spliceosome, snRNPs conduct catalytic removal of introns from pre-mRNAs (Pellizzoni 2007). Most eukaryotic introns are excised by the major (U2-dependent) spliceosome whereas a small proportion of introns (~1%) are processed by the minor (U12-dependent) spliceosome (Patel *et al.* 2003; Lotti *et al.* 2012).

SMN protein contains different functional domains like a N-terminal RNA-binding domain in exons 2b/3, a Tudor-domain for interaction with Sm proteins in exon 3 and a poly-proline stretch in exons 4/5 mediating cytoskeletal interaction via profiling. As a characteristic of RNP

components, SMN protein possesses a C-terminal tyrosine-glycine (YG-)-box in exon 6 involved in self-oligomerisation (Lorson *et al.* 1998; Bertrandy *et al.* 1999; Selenko *et al.* 2001; Bowerman *et al.* 2007).

Turn-over of FL-SMN protein is regulated by proteasomal degradation ($T_{0.5}$ ~4.5 h). Δ7-SMN2 is a truncated protein of only 282 aa in size; however, degradation of Δ7-SMN2 is unlikely only due to lack of exon 7, reduced self-association ability and enhanced susceptibility to ubiquitinylation. Instead, low amounts of Δ7-SMN2 in patients are probably caused by its missing binding partner i.e. FL-SMN1 (Burnett *et al.* 2009). Despite poor oligomerisation ability *in vitro*, Δ7-SMN2 is able to inefficiently incorporate into heterotypic complexes with FL-SMN (Le *et al.* 2005). Without protection to proteasomal cleavage, however, Δ7-SMN2 amount drops rapidly (Burnett *et al.* 2009).

Recent studies demonstrated that SMN fulfils plenty of different functions in cellular processes. Its participation in the generation of small nuclear ribonucleoprotein particles (snRNPs) is well characterised. SMN oligomerises and forms a multiprotein complex with UNRIP and gemins (Lorson *et al.* 1998; Pellizzoni *et al.* 1999; Meister *et al.* 2001; Gubitz *et al.* 2004). This SMN complex mediates efficient and specific binding of a heptameric ring (Sm core) of Sm proteins (SmB/B', SmD1, SmD2, SmD3, SmE, SmF and SmG) onto a conserved sequence of newly exported uridine-rich snRNAs (U small nuclear RNAs, e.g. U1, U2, U4/U6, U5, U11 or U12) in an ATP-dependent manner in the cytoplasm (Liu *et al.* 1997; Pellizzoni *et al.* 1999; Raker *et al.* 1999; Meister *et al.* 2001; Pellizzoni 2007). As part of the spliceosomal machinery, this Sm core is required for snRNP stability and function (Fig. 3).
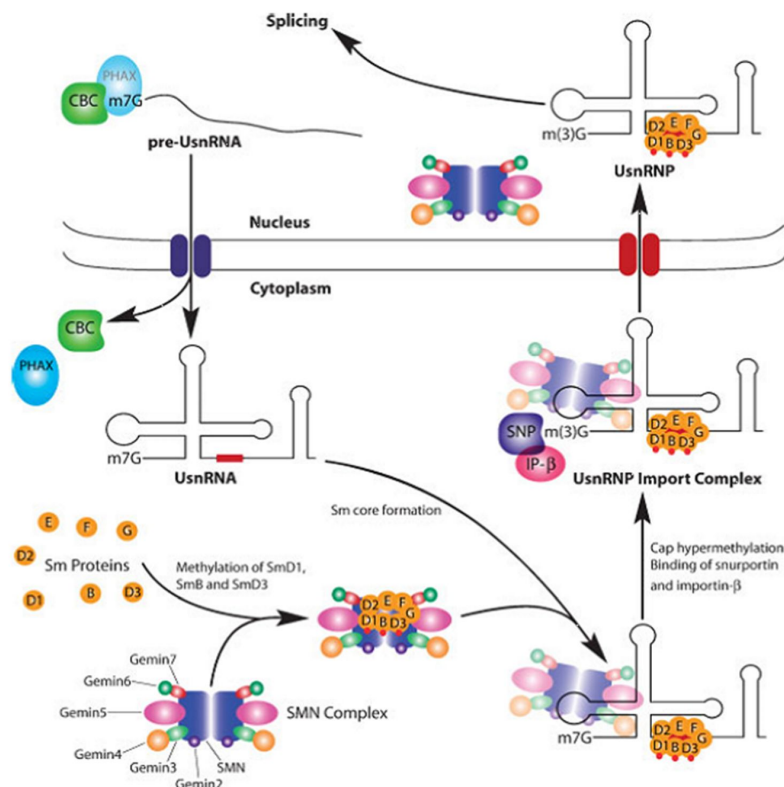
Fig. 3: SMN-mediated snRNP biogenesis. SMN complex consisting of SMN and gemin proteins conducts Sm ring formation and delivers the methylated Sm ring onto UsnRNA which is further modified. The resulting UsnRNP is imported into the nucleus and acts as part of the spliceosomal machinery (taken from (Briese *et al.* 2005)).

Moreover, the multimeric SMN complex interacts with various other proteins e.g. FUSE-binding protein; profilin II; WRAP53 and coilin for nuclear localisation nearby Cajal bodies; fragile-X mental retardation protein (FMRP); hnRNPs; Sm-like proteins; fibrillarin and GAR1 as components of small nucleolar RNPs (snoRNPs) (Pellizzoni *et al.* 1999; Williams *et al.* 2000; Pellizzoni *et al.* 2001; Rossoll *et al.* 2002; Sharma *et al.* 2005; Eggert *et al.* 2006; Piazzon *et al.* 2008; Mahmoudi *et al.* 2010).

In addition, SMN plays a more specific role in neurons since SMN protein can shuttle from nucleus and inner cytoplasm to the outer cellular periphery during CNS ontogenesis (Giavazzi *et al.* 2006). Furthermore, another study unveiled the bidirectional cytoskeleton-dependent transport of SMN granules along microtubules for long-range transportation and via actin filaments for short-range trafficking (Zhang *et al.* 2003). Thus, an additional function of SMN in neurons has been postulated possibly connecting SMN, motoneurons and the pathomechanism of SMA.

3.1.4 Pathomechanism in SMA

Disease onset often happens rather sudden with rapid decline in motor function followed by a long slow plateau period of deterioration (Sumner 2007). Considering strong SMN expression in embryonic and postnatal development with only residual expression during adulthood points at an important developmental time window in which SMN is absolutely essential (Burlet *et al.* 1998; Gabanella *et al.* 2007; Sleigh *et al.* 2011). Adenovirus-mediated SMN delivery (Foust *et al.* 2010) or compound-induced SMN elevation (Narver *et al.* 2008) in severe SMA mouse models rescue lethality at early but not later time points. These results are backed by the normal viability of SMA mice with doxycycline inducible SMN expression when SMN expression is triggered at both embryonic and early postnatal stages (Le *et al.* 2012). The importance of timely correct SMN expression during embryogenesis is thereby substantiated (Butchbach *et al.* 2007; Hammond *et al.* 2010).

The fact that SMN is an omnipresent protein provokes the puzzling question about elucidating the pathomechanism of SMA: Why does general impairment of snRNP biogenesis by SMN depletion cause fatal loss of just one specific neuronal subpopulation, i.e. lower α-motoneurons?

SMA and snRNP biogenesis

If failure of snRNP biogenesis is the major cause of motoneuronal death, dysfunctional splicing should cover a wide range of pre-mRNAs as well as alter the stoichiometry of snRNAs. Indeed, there are numerous aberrant transcripts which are not normally seen in tissues at physiological levels (Zhang *et al.* 2008). Cell lines from SMA patients do show reduced snRNP levels (Wan *et al.* 2005; Gabanella *et al.* 2007; Zhang *et al.* 2008) whose elevation rescues SMA phenotype in mice and zebrafish (Winkler *et al.* 2005; Workman *et al.* 2009). Even a negative feed-back loop is proposed in which SMN depletion and hampered snRNP synthesis attenuate exon 7 inclusion in *SMN2* mRNA especially in motoneurons (Ruggiu *et al.* 2012). Additonally, U1A protein, a component of the U1 snRNP assembled by the SMN complex, specifically inhibits 3' processing of the SMN pre-mRNA and might negatively influence SMN expression in SMA (Workman *et al.* 2013). Moreover, Lotti and colleagues recently demonstrated a tissue-specific decline in snRNP biogenesis, particularly affecting minor U12 splicing machinery (Lotti *et al.* 2012). Expression profiles showed that gene targets containing those U12 introns are frequently dysregulated in SMN deficient cells. Ostentatiously, some of these genes fulfil

essential functions in neurogenesis such as Stasimon. Similarly, pre-synaptic adhesion molecule Neurexin2a is down-regulated in smn-depleted zebrafish and SMA mice (See *et al.* 2013). mRNA of arginine methyltransferase CARM1 is also misdirected upon SMN depletion (Sanchez *et al.* 2012).

However, other data conjecture no direct congruence between splicing abnormalities/relevant RNA processing and SMA pathology because snRNP assembly activity in spinal cord extracts from severe SMA mice and milder Δ7-SMN2 mice is notably indistinguishable (Gabanella *et al.* 2007; Sleigh *et al.* 2011). Neither do motoneurons possess a specifically higher constitutive requirement for snRNP assembly (Sleeman 2013). In this context, alterations in RNA splicing appear rather as secondary effect in later stage of disease than as causative elicitor for SMA (Briese *et al.* 2005; Bäumer *et al.* 2009; Rossoll *et al.* 2009). Hence, difficulties remain to envision how a general cellular defect such as snRNP assembly could account for the motoneuron pathology underlying SMA (Shababi *et al.* 2013).

SMA and motoneuron maintenance

The aforementioned function of SMN in axonal RNA-trafficking sheds a more conclusive light on its potential role in SMA pathogenesis. SMN localises in RNA granules transporting *β-actin* mRNA along the axon (Glinka *et al.* 2010). Obviously, SMN facilitates recognition of mRNA-binding proteins (mRBPs) such as Hu antigen D (HuD) and insulin-like growth factor mRNA-binding protein 1 (IMP1) with their targets including the mRNAs of *β-actin*, the *microtubule associated protein tau* (*MAPT*) and *growth-associated protein 43* (*GAP-43*) (Hubers *et al.* 2010; Akten *et al.* 2011; Fallini *et al.* 2013; Yoo *et al.* 2013). Thereby, the assembly of mRNA-containing hnRNPs and their axonal transport is enhanced (Fallini *et al.* 2011). For example, SMN interaction partner hnRNP R binds 3' UTR of *β-actin* mRNA whereupon hnRNP R co-localises with murine Smn only in motor axons, but not in nuclear gems (Rossoll *et al.* 2002; Rossoll *et al.* 2003). Decrease and axonal mislocalisation of IMP1, a major protein regulating *β-actin* mRNA localisation and translation, exerts pathogenic effects in SMA (Fallini *et al.* 2013).

SMN associates with polyribosomal mRNPs and can repress translation in an *in vitro* luciferase assay (Sanchez *et al.* 2012). Growth cones do contain polyribosomal structures after several days in *in vitro* culture advocating vectored ribosome transport and protein synthesis ability (Twiss *et al.* 2009; Jablonka *et al.* 2013). Indeed, such local protein synthesis is crucial for axonal maintenance (Holt *et al.* 2009) supported by the observation that SMN deficient neurons exhibit defects in axonal outgrowth and path-finding (van Bergeijk *et al.* 2007; McWhorter *et al.* 2008; Oprea *et al.* 2008). Furthermore, related processes like axon elongation, growth cone size, β-actin dynamics and spontaneous excitability in primary motoneurons from lumbar spinal cord isolates of severe SMA mice are evidently impaired (Rossoll *et al.* 2003; Jablonka *et al.* 2007). In other words, these findings suggest that SMN might have a distinct motoneuron (MN)-specific role in maintaining motoneuronal functionality. The axonal pool of SMN and associated proteins like gemins hardly contributes to snRNP biogenesis (Cauchi 2010; Fallini *et al.* 2012) pointing to an additional function. Notably, those axonal RNA granules also differ from canonical SMN complex constitution for they lack Sm proteins (Zhang *et al.* 2006; Todd *et al.* 2010). Therefore, SMN seems to be involved in mRNP transport and maintenance of proper local translation in motor growth cones instead.

This essential function is even more highlighted when specific motoneuronal substructures like neuromuscular junctions (NMJs) are examined. SMN could be located at NMJs (Fan *et al.*

2002). Decrease in SMN elicits here cytoskeletal disorganisation, synaptic vesicle clustering and reduction of the readily releasable pool (RRP) retaining NMJs at an immature state and lagging overall neurotransmitter release (Torres-Benito *et al.* 2011; Ackermann *et al.* 2013). Moreover, two essential mRNAs for NMJ maintenance, i.e. *β-actin* and *candidate plasticity-related gene 15* (*cpg15*)/neuritin are significantly reduced in SMA motoneurons (Akten *et al.* 2011). In particular, the localisation and regional translation of *β-actin* mRNA in growth cones and axons are crucial for response to axonal guidance cues, maintenance and regeneration (Donnelly *et al.* 2013). Recent data suggest an enhanced demand for SMN during early post-natal days of murine NMJ maturastion while adult NMJs become refractory towards SMN depletion (Kariya *et al.* 2014). Most probably, SMA displays a foetal developmental maturation error at NMJs and a consecutive postnatal retrograde dying-back degeneration of α-motoneurons (Fidzianska *et al.* 2002; Ito *et al.* 2011). This circumstance is explained in 3.3.5 in detail.

The view is gaining momentum that effects of SMN demise do not exclusively derogate motoneurons (Hamilton *et al.* 2013). Instead, SMA encompasses lesions in further non-motoneuronal tissues and organs like heart (cardiac muscle), bones, lung, liver, intestine, pancreas, brain (telencephalon, hippocampus) and muscle (Finsterer *et al.* 1999; Felderhoff-Mueser *et al.* 2002; Ito *et al.* 2004; Rudnik-Schöneborn *et al.* 2008; Wishart *et al.* 2010; Mutsaers *et al.* 2011; Bowerman *et al.* 2012b; Schreml *et al.* 2013; Shababi *et al.* 2013). So, a threshold hypothesis delineates the pathogenesis in SMA the best: In SMA patients, there is a differential susceptibility of cell types and tissues to SMN reduction with motoneurons to be the most sensitive cell population at the very end of a vulnerability-resistance spectrum (Fig. 4) (Sleigh *et al.* 2011).
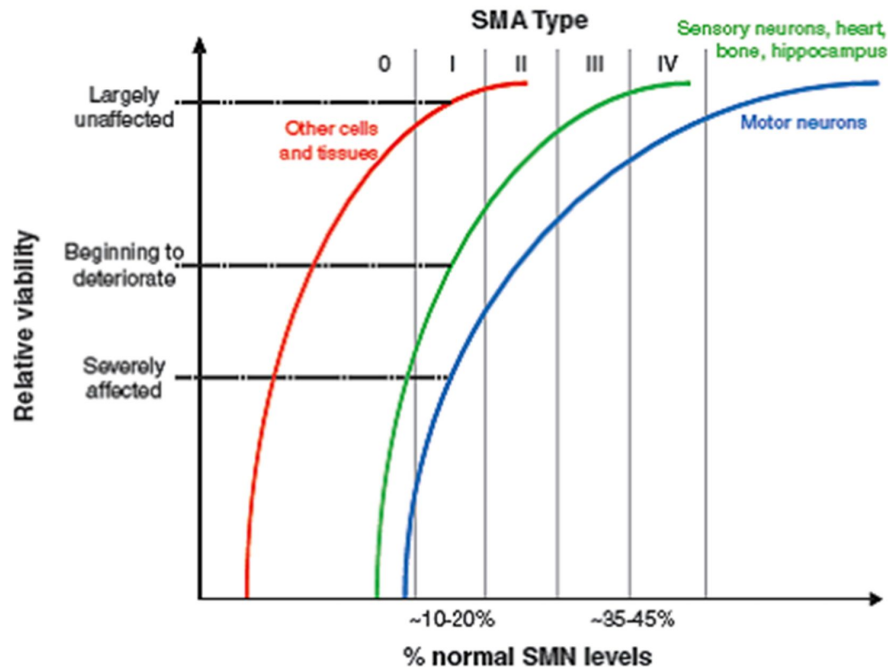
Fig. 4: Threshold hypothesis schematises the susceptibility of different tissues concerning SMN protein depletion with motoneurons as most vulnerable cells at the outermost end of the spectrum whereas other tissues tolerate lesser SMN levels (taken from (Sleigh *et al.* 2011).

3.1.5 Possible therapies in SMA

The outcome of many studies implies that mere increase of SMN exclusively in motoneurons does not rescue severe SMA mice. With a motoneuron-specific inducible *Hb9-Cre* allele, Gogliotti *et al.* managed to restore SMN in motoneurons autonomously. However, the overall effect in survival was just very moderate (Gogliotti *et al.* 2012). Similarly, when SMN was depleted specifically in motoneurons, only modest SMA symptoms occurred instead of the expected severe SMA phenotype (Park *et al.* 2010). Neuronal-specific SMN expression improved survival and weight gain in SMA mice whereas muscle-specific SMN expression had only little positive effect (Gavrilina *et al.* 2008). Significant extension of murine life span was achieved by an inducible *SMN* rescue allele which clarified the positive effect of temporal SMN expression, meaning early in all tissues (Lutz *et al.* 2011). This obvious requirement of SMN restoration in a spatiotemporal manner, i.e. at pre-symptomatic stage in all tissues, exacerbates any possible therapeutic treatment in SMA.

Nonetheless, several therapeutic approaches exist on genetic, transcriptional, translational and cellular levels. Different chemical compounds and other therapies have been examined in respect to these contact points of SMA phenotype; however, until now no absolute cure is available yet (Sumner 2006; Wirth *et al.* 2006a; Lorson *et al.* 2012).

Gene replacement strategies gave good results. Delivery of FL-SMN cDNA by self-complementary adeno-associated virus 9 (scAAV9) provided substantial improvement in severe SMA mice (Foust *et al.* 2010; Dominguez *et al.* 2011; Glascock *et al.* 2012; Shababi *et al.* 2013).

A direct transcriptional activation of FL-SMN expression is achieved by administration of hydroxyurea or histone deacetylase inhibitors (HDACi) such as short-chain fatty acids valproic acid (VPA) and sodium butyrate, the benazamide M344, suberoylanilide hydroxamic acid (SAHA), Trichostatin A (TSA) or JNJ-26481585 (Grzeschik *et al.* 2005; Riessland *et al.* 2006; Avila *et al.* 2007; Wirth *et al.* 2007; Riessland *et al.* 2010; Schreml *et al.* 2013). Restoration of correct splicing pattern of *SMN2* pre-mRNA is successfully established by quinazolines, the chemotherapeutic anthracycline antibiotic aclarubicin or the phosphatase inhibitor sodium vanadate (Andreassi *et al.* 2001; Zhang *et al.* 2001; Jarecki *et al.* 2005; Wirth *et al.* 2007).

Another utterly promising approach is the use of short antisense oligonucleotides (ASOs) which block the intronic splicing silencer ISS-N1 adjacent to exon 7, thereby facilitating the inclusion of exon 7 in *SMN2* transcripts and rescuing SMA phenotype in mice (Singh *et al.* 2009; Hua *et al.* 2011; MacKenzie 2012; Osman *et al.* 2012; Porensky *et al.* 2012). Recently, splicing modifiers were introduced which elevated SMN levels, MN numbers and survival rate and prevented motor dysfunction in SMA fibroblasts, iPSC-derived MNs and mice (Naryshkin *et al.* 2014).

On translational level, the antibiotic aminoglycosides are able to suppress the accurate identification of translation termination codons in eukaryotic cells. Oppressed recognition of the native stop codon in exon 8 of *SMN2* transcripts leads to a longer C-terminus and stabilised SMN2 protein. Thus, wild-type SMN localisation and quantity is restored (Wolstencroft *et al.* 2005) and lessens severity in SMA mouse models (Mattis *et al.* 2009; Mattis *et al.* 2012). Similar SMN protein stabilisation is exerted by the cyclooxygenase inhibitor indoprofen (Lunn *et al.* 2004). Protease inhibitors like MG132 block ubiquitin-mediated proteasomal SMN degradation (Chang *et al.* 2004). Inhibition of proteasome by bortezomib elevates SMN amounts in SMA mice and improves their motor function (Kwon *et al.* 2011).

Cellular replacement of diseased motoneurons is the ultimate goal in curing SMA. Yet, any stem cell therapy needs to overcome demanding hurdles including cell survival, generation of

functional motor units and sufficient axonal projection for long distances. Availability of primary motoneurons is restricted to isolation from fresh human or rodent foetal tissue touching ethical concerns as well as risking repulsion of xenograft transplants due to host immune response (Gowing *et al.* 2011). Generation of patient-derived motoneurons via direct reprogramming circumvents these problems indeed. However, transplantation of mature motoneurons and primed neural stem cells (NSCs) into SMA mice rather leads to engraftment of NSCs and development of supporting CNS cells than to insertion of exogenous motoneurons. Thus, the progressive loss of endogenous motoneurons is probably slowed down by secretion of neurotrophic factors from transplanted cells (Corti *et al.* 2008; Corti *et al.* 2010; Corti *et al.* 2012).

3.1.6 SMA models

Animal models are a suitable tool to elucidate the pathomechanism of diseases such as SMA. On account of high conservation of SMN genes between species throughout evolution, several transgenic animal models have been engineered to explore the consequences of SMN deficiency in different cell types, above all in neurons and muscle.

Thus, detrimental effects of SMN ablation have been modelled in nematode (*Caenorhabditis elegans*) (Briese *et al.* 2009), fruit-fly (*Drosophila melanogaster*) (Chan *et al.* 2003; Chang *et al.* 2008), zebrafish (*Danio rerio*) (McWhorter *et al.* 2008), cat (*Felis catus*) (He *et al.* 2005) and swine (*Sus scrofa*) (Lorson *et al.* 2011). The most important SMA animal models are house mice (*Mus musculus*) owing to an 82% homology in Smn aa sequence compared to human FL-SMN1. Murine gene orthologue *Smn* is only present as a single copy (DiDonato *et al.* 1997) so that homozygous *Smn* deletion inevitably leads to embryonic death by prevention of uterine nidation (Schrank *et al.* 1997). Introduction of human *SMN2* gene in different copy number into murine *null Smn*$^{-/-}$ background and subsequent cross-breeding resulted in mouse strains reflecting the whole bandwidth of human SMA phenotype with severe, intermediate or mild disease progression (Hsieh-Li *et al.* 2000; Monani *et al.* 2000; Le *et al.* 2005; Bowerman *et al.* 2009).

Nevertheless, every animal model is only capable of displaying a human disorder by approximation and hence incompletely. In particular, living human neurons cannot be obtained by biopsy obstructing the possibility to examine any neurodegenerative disease pathology in a patient-specific context. The emergence of direct reprogramming technology however circumvents the inaccessibility of neuronal target tissues in neurodegenerative diseases, thus enabling generation of a patient-derived *in vitro* model (see 3.2.4). Therefore, the set-up of such *in vitro* models is recently gaining more and more importance concerning drug screening studies and in-depth analyses of the actual pathomechanisms on molecular level.

3.2 Pluripotency and reprogramming

3.2.1 Pluripotency – An early starting point in development

Per definition in developmental biology, pluripotency describes the capability of unlimited differentiation into cell types of all three germ layers, i.e. into all >200 functional cell types of the human embryonic and adult organism (Thomson *et al.* 1998; Smith *et al.* 2009), however, excluding extraembryonic tissues (e.g. placentary trophectoderm). This ability of total organismal development – termed totipotency – is solely restricted to the fertilised ovum

(zygote) and the subsequent four blastomeres in mammals (Van de Velde *et al.* 2008; Smith *et al.* 2009).

Pluripotency is naturally found in embryonic stem cells (ESCs), embryonic germ cells (EGCs) and epiblast stem cells (EpiSCs) (Amabile *et al.* 2009). ESCs reside in the inner cell mass (ICM) of the blastocyst. The first explant of ESCs succeeded in 1981 in mice (Evans *et al.* 1981) and a decade later in humans in 1998 (Thomson *et al.* 1998). Moreover, there are reprogramming techniques artificially increasing potency and conferring "stemness" (the undifferentiated state): First, somatic cell nuclear transfer (SCNT) denotes the introduction of a donor nucleus of a fully differentiated somatic cell into an enucleated, mature, metaphase II-arrested oocyte (cytoplast). Oocyte-specific cytoplasmatic factors erase the donor epigenetic pattern, thus converting the somatic identity into a SC-like state. This "reproductive cloning" was firstly conducted in African clawed frog (*Xenopus laevis*) in the 1960s (Gurdon 1962), later also in mammals creating sheep "Dolly" in 1997 (Wilmut *et al.* 1997). In 2013, an optimised protocol for SCNT in humans was published (Tachibana *et al.* 2013). Second, cellular fusion of an ESC with a somatic recipient cell delivers tetraploid hybrids in which the developmental potential is reset to a pluripotent state (Tada *et al.* 2001; Cowan *et al.* 2005). These hybrids share many features with the ancestral ESC indicating a domination of the pluripotent state in these fusion products (Jaenisch *et al.* 2008). Third, a direct *in vitro* transdifferentiation back to pluripotency is manageable with spermatogonia. By prolonging culture conditions, pluripotent ES-like cells can be isolated from such cultures (Kanatsu-Shinohara *et al.* 2004; Golestaneh *et al.* 2009). Finally, in direct reprogramming, introduction and ectopic expression of defined pluripotency transcription factors (TFs) revert the somatic state to a pluripotent one (induced pluripotent SCs) (see 3.2.3).

3.2.2 Stem cells (SCs) – Occurrence and properties

Stem cells (SCs) are characterised by both the ability of undifferentiated proliferation (self-renewal) and the differential potency to develop into various functional cell types.

During normal ontogenesis, cells transit in a unidirectional way from totipotent zygotic SCs to pluripotent embryonic SCs until it narrows down to terminally differentiated somatic cells (Jaenisch *et al.* 2008). While their grade of potency gradually diminishes, cells become developmentally more restricted, thereby adopting distinct epigenetic modifications. Yet, this process is not irreversible as unambiguously proven by the aforementioned reprogramming methods to remodel the somatic epigenome and thus "rejuvenate" the entire cell. Additionally, adult SC populations are left in the organism: Multipotent SCs give rise to multiple cell types of one specific lineage (e.g. haematopoietic SCs for blood cells of myeloid and lymphoid lineage), whereas unipotent SCs are only capable of generating one specific cell type, e.g. spermatogonial SCs for sperm (Jaenisch *et al.* 2008).

In the adult human, NSCs solely populate two neurogenic brain regions: the subventricular zone (SVZ) of the lateral ventricle and the dentate gyrus of the hippocampus (Eriksson *et al.* 1998; Gage 2002; Hsu *et al.* 2007). In addition, adult NSCs in the neuroepithelium of the olfactory bulb exhibit crucial reparative potential of the sensory nervous system, yet these neuroblasts descend from the SVZ (Curtis *et al.* 2007; Leung *et al.* 2007).

3.2.3 Induced pluripotent stem cells (iPSCs) – Back to the roots

At Kyoto University in 2006, Yamanaka and Takahashi succeeded in the Nobel prize-awarded discovery of directly reprogramming somatic cells to an ES-like state (Takahashi *et al.* 2006).

This marked a revolutionary milestone in comprehension of cellular plasticity and developmental biology.

Out of 24 candidate genes related to ESC-pluripotency, the authors found that the combinatory over-expression of just four transcription factors (Oct4, Sox2, c-Myc & Klf4) sufficed to reprogram murine embryonic fibroblast (MEFs) and adult fibroblasts which thus acquired a pluripotent ESC-like identity. These cells are coined "induced pluripotent stem cells" (iPSCs) (Takahashi *et al.* 2006). Since then, immense endeavours have been undertaken to generate iPSCs from different sources and species and to fully characterise the process of reprogramming.

Human iPSCs were successfully generated from foetal and adult fibroblasts in 2007 (Takahashi *et al.* 2007; Yu *et al.* 2007). Moreover, generation of iPSCs was accomplished in further species such as cow (*Bos taurus*), dog (*Canis lupus familiaris*), horse (*Equus caballus*), rat (*Rattus norvegicus*), sheep (*Ovis aries*) and Tibetan miniature pig (*Sus scrofa*) (Esteban *et al.* 2009; Liao *et al.* 2009; Bao *et al.* 2011; Han *et al.* 2011; Luo *et al.* 2011; Nagy *et al.* 2011).

First successful attempts in direct reprogramming were carried out with dermal fibroblasts (Takahashi *et al.* 2006; Takahashi *et al.* 2007; Yu *et al.* 2007; Park *et al.* 2008b). Beyond fibroblast as frugal, easily accessible donor cell population, various other cell types were reprogrammed meanwhile, *inter alia* adipose SCs, B-lymphocytes, gastric cells, germ line SCs, hepatocytes, keratinocytes, melanocytes, NSCs, pancreatic β-cells and umbilical chord blood cells (Aasen *et al.* 2008; Aoi *et al.* 2008; Hanna *et al.* 2008; Kim *et al.* 2008; Stadtfeld *et al.* 2008; Ko *et al.* 2009; Sun *et al.* 2009; Utikal *et al.* 2009).

The initial reprogramming experiments were performed by retroviral-mediated transduction of the four transcription factors (4F) Oct4, Sox2, c-Myc and Klf4 (Takahashi *et al.* 2006), ever since named "Yamanaka factors" (Sommer *et al.* 2010). Oct4 is the crucial factor in that row with an expression exclusively restricted to pluripotent SCs, while the other factors are also present in other tissues. The human equivalents to the Yamanaka factors (OCT4, SOX2, KLF4 & c-MYC) unproblematically fulfilled their function in reprogramming human fibroblasts (Takahashi *et al.* 2007). In an additional study briefly published afterwards, Yu and colleagues announced LIN28 and NANOG as surrogates for c-MYC and KLF4, respectively, in 4F reprogramming (Yu *et al.* 2007).

iPSCs arguably depict a developmental stage equivalent to that of ESCs, however, nuanced comparison in early studies disclosed distinct disparities concerning global gene expression, epigenetics and miRNAome (Takahashi *et al.* 2006; Yu *et al.* 2007; Wilson *et al.* 2009). Thus, a broader consensus manifests concerning the equivalence of iPSCs and ESCs to date: Both populations are rather overlapping than identical or distinct. Their functional equality is more theoretical because in practice, both ESCs and iPSCs possess genetic and epigenetic differences mirroring their different history (Robinton *et al.* 2012). The most illustrative systematic comparison of transcriptional profile, epigenetic pattern and developmental potential in twelve human iPSC and 20 ESC lines solidified the common view that transcriptional and epigenetic variation is common within iPSC lines, among ESC lines and between iPSC and ESC populations (Bock *et al.* 2011).

3.2.4 Medical application of iPSCs – Going where no one has gone before

Introduction of iPSC technology marked a breakthrough in generating a unique platform for patient-specific disease models *in vitro*, drug-screening and putative cell-replacement strategies. Within the last years, several different human disorders have been displayed by iPSC technology such as Alzheimer's Disease, Down's Syndrome, Fanconi Anaemia,

Friedreich's Ataxia, Huntington's Disease, Hutchinson-Gilford Progeria Syndrome, Machado-Joseph Disease, Marfan Syndrome, Parkinson's Disease or β-Thalassaemia (Park *et al.* 2008a; Raya *et al.* 2009; Soldner *et al.* 2009; Ku *et al.* 2010; Quarto *et al.* 2010; Koch *et al.* 2011; Zhang *et al.* 2011; HD iPSC Consortium 2012; Israel *et al.* 2012; Ito *et al.* 2012; Wang *et al.* 2012). However, the patient's phenotype is not always successfully mimicked as it happened in Fragile X-Syndrome (Urbach *et al.* 2010).

Concerning generation of diseased motoneurons by iPSC technology, different groups pioneered in modelling SMA (Ebert *et al.* 2009) or familial and sporadic ALS (Dimos *et al.* 2008; Burkhardt *et al.* 2013).

Beside general understanding of human ontogenesis, the prospective goal of human SC research lies in elucidating the chances of application in medical context, i.e. replacement of diseased cell/organs (regenerative medicine). In comparison to other pluripotent SCs, iPSCs bear several advantages: First, no human embryo is destroyed in generating iPSCs, thus bypassing strong ethical and religious objections towards SC research in society. Second, iPSC technology enables to obtain "customised" ESC-like surrogate cells in respect of the relevant disorder. When genetic correction is possible *in vitro* like in the rescue of a humanised sickle cell anaemia mouse model (Hanna *et al.* 2007), healthy patient-specific cells could be applied, thereby circumnavigating potential host immune rejection response upon transplantation. Third, iPSC generation became in the meantime a robust method with reliable efficiency compared to alternative reprogramming strategies: SCNT is extremely ineffective on account of faulty reprogramming resulting in death of most animal clones soon after implantation or birth of clones with serious anomalies (Hochedlinger *et al.* 2003). Like ESCs, SCNT in humans fiercely touches ethical concerns since receiving enough unfertilised human oocytes is a tedious, straining procedure impeding applicability. Inherent disadvantages in cellular fusion are inefficiency and polyploidy in fusion products.

Nevertheless, any medical application is hampered by the incalculable risk of tumour formation which transplantation of pluripotent SCs bears. Even when iPSCs are generated in the absence of the oncogenic gene c-Myc or integrative approaches, the peril of tumorigenesis is immanent (Nakagawa *et al.* 2008; Okita *et al.* 2008; Kim *et al.* 2009a).

In conclusion, despite apparent current shortcomings in tissue repair direct reprogramming bears profound advantages in establishing disease-specific *in vitro* models, in particular when naturally inaccessible cell types are affected such as neurons or cardiomyocytes. In order to obtain the desired cell type, mimicking the natural developmental processes of embryogenesis is essential when differentiating iPSCs with reasonable efficiency and specificity.

3.3 Neuromuscular development and generation of motoneurons

3.3.1 Vertebrate neurogenesis

One cornerstone of vertebrate embryogenesis is the generation of the three germ layers endoderm, mesoderm and ectoderm (triploblasty). Vast knowledge has been gained by developmental studies with African clawed frog (*Xenopus laevis*) in which this process commences at the late blastula stage when most of the embryonic tissue is not determined yet. However, some pluripotent blastomeres specialise in a dorsal vegetal mesoderm region (Nieuwkoop Centre) and induce formation of a further inductive region in close vicinity to the dorsal lip of the blastopore. This primary "organiser" (Spemann's organizer) dorsalises the surrounding tissue during early gastrulation, thus defining the dorso-ventral (DV) axis and

simultaneously initialising gastrulation – a process in which the three germ layers are specified, the body axes are determined and wide cellular rearrangements herald organogenesis (Spemann *et al.* 1924; Nieuwkoop 1952; Harland *et al.* 1997; Carlson 1999; Weinstein *et al.* 1999; Smukler *et al.* 2006).

The primary organiser secretes BMP inhibitors such as chordin and noggin as well as TGFβ inhibitors like follistatin into the overlying ectodermal cells. Depleted from BMPs and TGFβ, de-repression of gene transcription enhances promoter accessibility of pro-neural genes. So, an intrinsic neural program is spurred enabling the ectodermal cells to adopt a neural fate (Weinstein *et al.* 1999; Muñoz-Sanjuán *et al.* 2001). In amniotes like chick, mice and humans, a similar inductive system (node) is active (Levine *et al.* 2007).

The rostro-caudal (RC) axis is marked by the specification of dorsal mesodermal cells forming a flexible rod-shaped structure (notochord) when the node regresses towards the posterior end of the primitive streak (Wilson *et al.* 2005). Concomitantly, the overlying dorsal ectodermal layer thickens (neural plate) designating the start of neurulation and the surrounding paraxial mesoderm segments into somites (somitogenesis) (Fig. 5) (Carlson 1999; Copp *et al.* 2003). By the end of the third gestational week, human neurulation begins with formation of a neural plate in the epiblast, a distinct ICM layer of a human blastocyst. Subsequently, the neural plate invaginates, thereby forming the neural groove and simultaneously elevating the surrounding tissue wall to neural folds. After all, the neural folds converge to the neural tube covered by non-neural epidermal ectoderm (Smith *et al.* 1997; Copp *et al.* 2003). Neurulation makes ectodermal cells competent to respond to morphogenic patterning from non-organiser mesoderm, hence specifying the RC axis between anterior and posterior pole of the embryo (Carlson 1999; Copp *et al.* 2003).
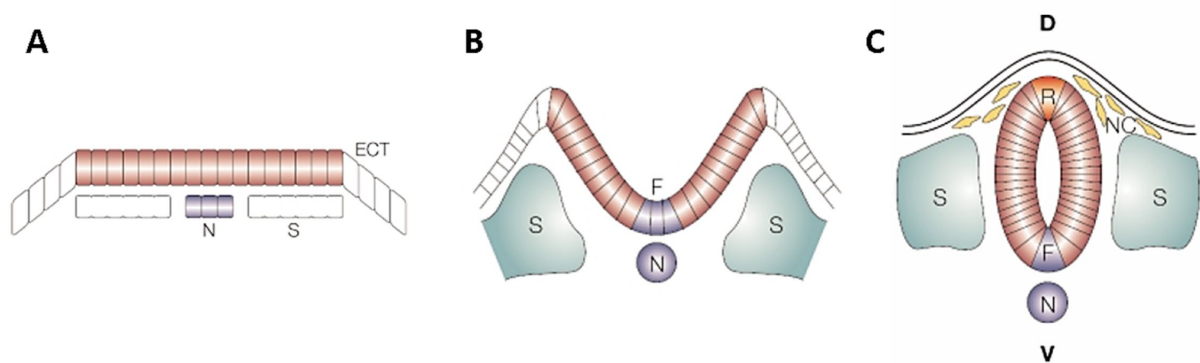
Fig. 5: Successive steps of neurulation and spinal cord development. Neurally primed cells form neural plate which are flanked by epidermal ectoderm (ECT) (**A**). Invagination of neural plate forms neural groove while the nethermost cells are primed to floor plate (F) by subjacent notochord (N) and somatic mesoderm begins to develop (S) (**B**). Once neural folds close to neural tube, roof plate cells (R) are determined. Neural cells are allocated along the dorso-ventral axis (D-V). Neural crest cells transiently delaminate from dorsal neural tube (**C**) (adapted from (Jessell 2000)).

3.3.2 Neural tube patterning and generation of motoneurons (MNs)

One of the most fundamental concepts of embryology is the establishment of morphogenetic fields in the developing embryo. A biochemical coordinate system of diffusible factors (termed "morphogens") defines different developmental zones in a spatiotemporal manner, thereby allocating every cell in developing tissues positional information (Jaeger *et al.* 2006). Wolpert's French Flag model schematises this concept in which a row of cells are exposed to an idealised

morphogen concentration gradient. Positional information is conveyed relative to field boundaries which coincide with the distance between source and sink of a morphogen in respect to temporal context (Wolpert 1969; Jaeger *et al.* 2006).

The node regressing head-to-tail along the primitive streak and pre-somitic mesoderm lying ahead secrete FGFs, in particular FGF8, thus establishing a proliferative caudal zone (Wilson *et al.* 2005). Behind it, the neural plate cambers and the resultant neural groove closes to the neural tube. There, the roof plate and dorsal ectoderm secrete BMPs and Wnt members defining dorsal progenitor (pd) domains pd1-pd6 plus pdIL (Fig. 6) (Helms *et al.* 2003). The ventral neural tube is specified by Sonic Hedgehog (SHH) protein secreted by the floor plate and notochord (Marti *et al.* 1995; Ericson *et al.* 1996). Retinoic acid (RA) is a soluble lipophilic molecule produced by the oxidation of its corresponding alcohol (retinol = vitamin A). RA exerts pleiotropic functions during embryogenesis including cellular proliferation, differentiation, apoptosis, tissue patterning and maintenance of bilateral symmetry via nuclear receptor binding (Duester 2008). The segmented paraxial mesoderm stretching on both sides of the neural tube (somites) secretes RA during neurulation, thus caudalising the neighbouring neuroepithelial tissue and allocating positional information along the RC axis (Sockanathan *et al.* 1998). Taken together, four major signalling systems (SHH, FGFs, BMPs and RA) determine position as well as time of progenitor domain generation in the neural tube in reference to both RC and DV body axes.

Within the nascent spinal cord, neuron subpopulations are topologically assigned according to their origin and function (Briscoe *et al.* 2001). Dorsal neurons mostly relay cutaneous sensory input whereas ventral neurons exert motor functions by the majority, thus reflecting ancient tetrapod locomotion. SHH signalling defines generic motoneuronal identity in motoneuronal progenitor domain (pMN). Later, mesodermal retinoid signals aid to specify identity and position (Jessell 2000). In neural tube, SHH either represses expression of transcription factors (TFs) (Class I, e.g. Pax6, Irx3) or induces synthesis of TFs (Class II, e.g. Nkx6.1, Nkx2.2) (Briscoe *et al.* 2001). Therefore, incremental concentration relative to the SHH source determines five different progenitor cell domains in the ventral neural tube (p0, p1, p2, pMN and p3) characterised by a unique TF combination (Fig. 6) (Wilson *et al.* 2005). On the other hand, RA promotes class I TF expression (Diez del Corral *et al.* 2003). As a common feature, an individual subset of basic helix-loop-helix (bHLH) and homeo-domain box (Hox) TFs is expressed conferring each domain a very specific TF profile. Typically, TFs in one progenitor domain cross-repress expression of complementary factors in abutting domains, hence avoiding hybrid identities (Briscoe *et al.* 2001; Lee *et al.* 2001). Nearly all domains give rise to interneurons, just pMN domain generates motoneurons early and later oligodendrocytes (Lee *et al.* 2001; Soula *et al.* 2001).

Within the emerging motor column of the developing neural tube, maturing MNs diversify further into motor pools, each innervating individual muscles. Organisation is evident in the alignment of motor neurons with common target projections into longitudinally oriented columns (Landmesser 1978; Jessell 2000). Post-mitotic MNs become divided into the medial and hypaxial motor columns (MMC and HMC) which innervate the back (epaxial) and trunk (hypaxial) musculature, respectively (Fig. 7). The third lateral motor column (LMC) is subdivided into a medial and lateral portion innervating the ventral part (LMCm) and the dorsal part (LMCl) of limbs, respectively (Sockanathan *et al.* 1998; Wilson *et al.* 2005). So along the RC axis, LMC is only found at brachial and lumbar levels of the spinal cord at putative limb buds (Lee *et al.* 2001). Motor column diversification is predominately regulated by RA expression in MNs at brachial and lumbar levels of the spinal cord (Sockanathan *et al.* 1998; Wilson *et al.* 2005; Ricard *et al.* 2013).

Lower motoneurons are among the largest cells in the human body. Their thin and extremely long axons connect the CNS with the periphery and function as relays for central signals by transducing electric stimuli to target skeletal muscles. Lower motoneurons themselves are wired to different afferent neurons including upper motor neurons, glutamatergic interneurons and sensory neurons. As each myelinated motor axon reaches its target, it divides into 20–100 unmyelinated terminal fibres, each of which innervates a single muscle fibre (Fallini *et al.* 2012).
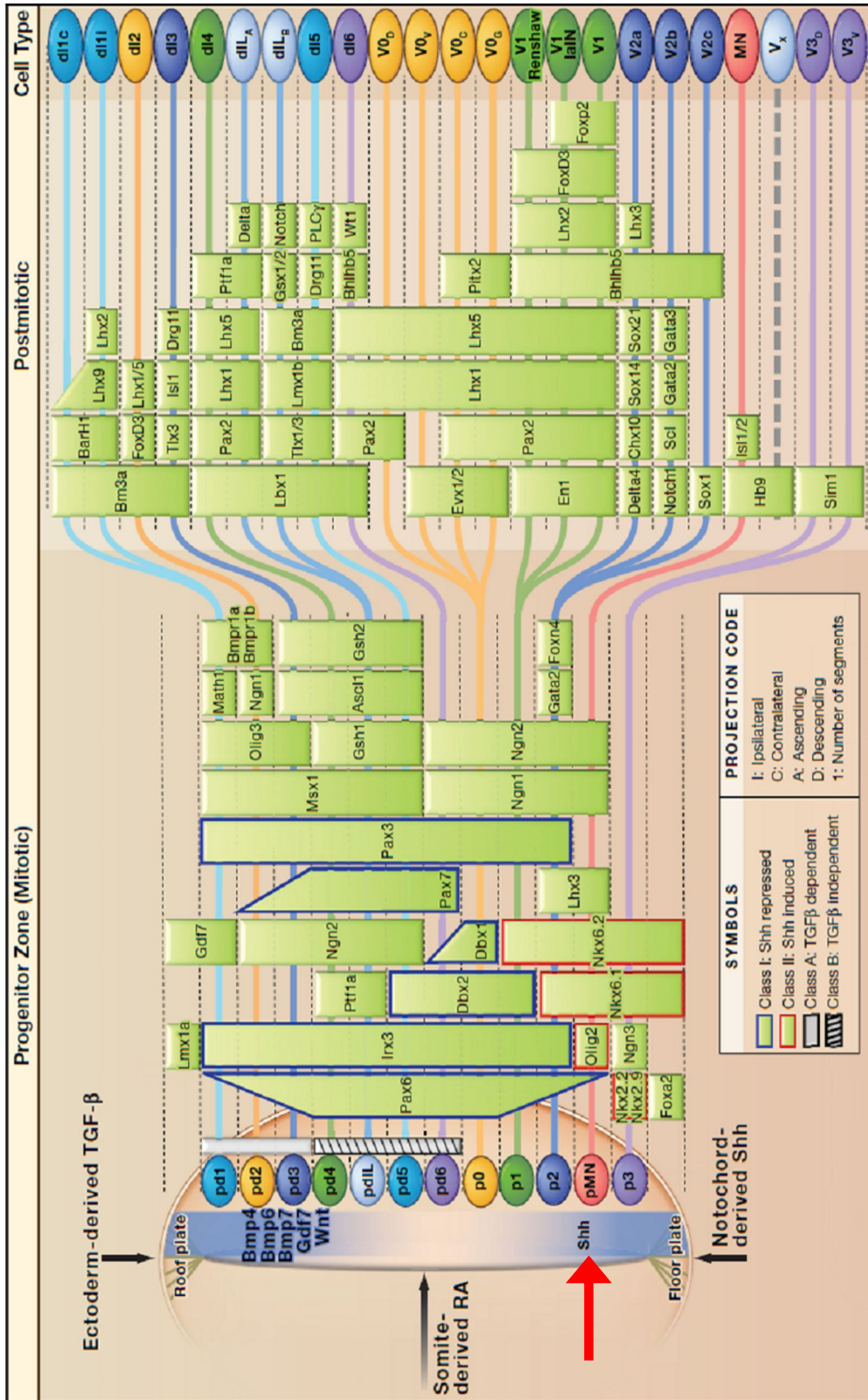
Fig. 6: Idealised segment of neural tube showing morphogen induced patterning into different domains. Secretion of Wnt proteins and TGFβ from roof plate/ectoderm determines dorsal progenitor (pd) domains (pd1-pd6). SHH secretion from floor plate/notochord defines ventral domains (p0-p3). Somite-derived RA caudalises neural tissue. The individual morphogen gradient conveys positional information to neural cells in each domain, thus leading to expression of characteristic domain-bound TFs and their down-stream targets. Note the ventral motoneuronal progenitor domain pMN (red arrow) and its TF composition (modified from (Alaynick *et al.* 2011)).
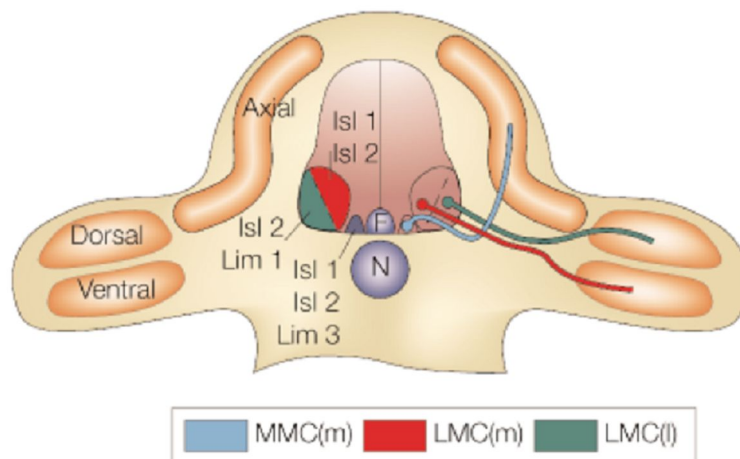
Fig. 7: Transverse section of a chick embryo at limb levels depicting the position of motor columns, their TF profile and the respective axonal projections into the target muscle fields (N, notochord; F, floor plate; MMC, medial motor column; LMC(m), medial portion of lateral motor column; LMC(l), lateral portion of lateral motor column) (taken from (Jessell 2000)).

3.3.3 Mammalian motor circuit – exerting force

The motor circuit of voluntary movements relies on a two-staged system (Fig. 8): First, axons of large pyramidal neurons (upper motoneurons) originating in layer V of the cerebral motor cortex extend through the medullary pyramids, where most fibres decussate in the caudal medulla before descending as lateral corticospinal tracts within the spinal cord (Carpenter 1991; Blackstone 2012). The second part consists of lower motoneurons whose axons connect to skeletal muscle fibres throughout the body via highly specialised terminal structures (NMJs). Even though some upper motoneurons directly contact their lower counterparts, in the vast majority interneurons are interconnecting both types of motoneurons (Carpenter 1991).

There are three sub-classifications of lower motoneurons (Manuel *et al.* 2011): (i) α-motoneurons (α-MNs) reside in the spinal cord with their axons projecting outside CNS via the ventral horns. They transmit nerve impulses via NMJs to ordinary extrafusal muscle fibres, thereby eliciting voluntary movements by contraction. In vertebrates, the release of neurotransmitter acetylcholine (ACh) mediates signal transduction. (ii) The smallest subgroup comprises β-MNs which innervate intrafusal & extrafusal muscle fibres. (iii) γ-MNs innervate intrafusal muscle fibres and refine their sensitivity. So, motoneurons are a

Fig. 8: Schematic illustration of human motor circuit. Upper MNs descend to the spinal cord where lower MNs extend axonal connections to skeletal muscles (from (Damjanov 2000)).

heterogeneous group of CNS neurons responsible for motricity (locomotive system) (Manuel *et al.* 2011).

3.3.4 Neuromuscular junctions (NMJs) – an extraordinary cell-cell contact

Motor axons end in a specially designed synaptic structure establishing connectivity between the pre-synaptic motor nerve site and the post-synaptic muscle site, denoted neuromuscular junction (NMJ) (Fig. 9). The NMJ is wholly capped by supportive terminal Schwann cells (TSCs) and kranocytes (Court *et al.* 2008) whose absence severely impedes NMJ functionality (Lin *et al.* 2000).
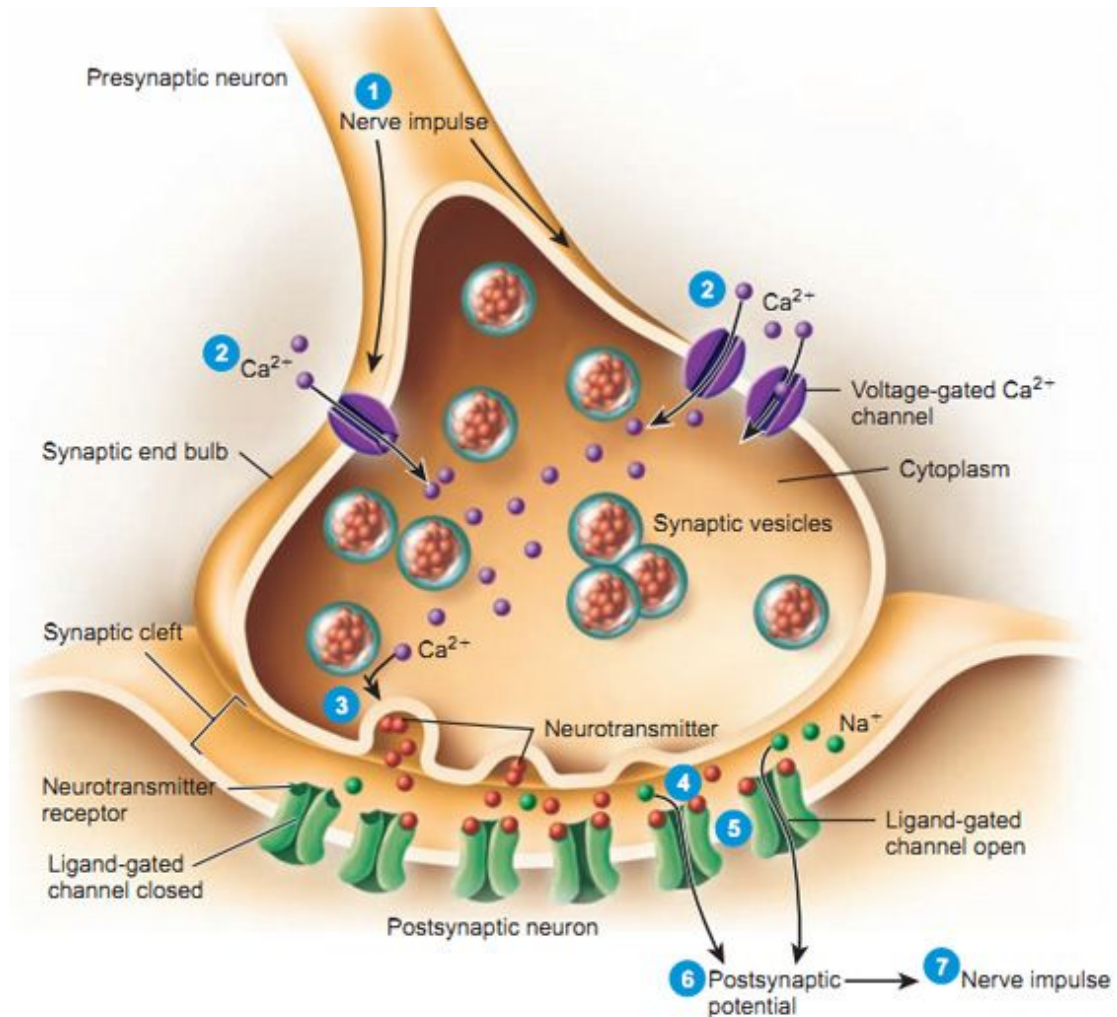
Fig. 9: Schematic depiction of a neuromuscular junction. Incoming action potential (**1**) causes opening of voltage-gated Ca^{2+} ion channels (**2**) and subsequent influx. Ca^{2+}-mediated synaptic vesicle fusion with the synaptic membrane leads to emptying of neurotransmitter molecules (i.e. ACh) into the synaptic cleft (**3**). Punctual high AChR occupation (**4**) on the post-synaptic site efficiently pursues signal transduction by induction of Na^+ influx (**5**) conducting local sarcolemma de-polarisation (end-plate potential) (**6**) which triggers large-scale muscular action potentials (**7**) and subsequently muscle contraction (taken from ©2013 neuroanatomyblog.tumblr.com).

Once a pre-natal motor axon approaches its target muscle, a number of events take place during synaptogenesis: (i) Prolonging motor axons secrete the proteoglycan agrin which binds to the transmembrane receptor muscle-specific kinase (MuSK) and its co-factor Lrp4. Thereupon, cytoskeletal re-distribution takes place by Rho GTPase induced signalling. At last,

rapsyn, a cytoplasmatic linker, mediates plaque-like clustering of acetylcholine receptors (AChR) anchored to the cytoskeleton on the myotube surface (Sanes *et al.* 2001; Wu *et al.* 2010). (ii) The post-synaptic sarcolemma folds to a lamella-like structure (motoric end-plate) massively equipped with AChRs (Sanes *et al.* 2001). (iii) Moreover, the de-myelinated motor axon tip bulges into a button-like swelling ("bouton") above the sarcolemmal invaginations, spacing the synaptic cleft (Sanes *et al.* 2001). (iv) Growing motor axons terminally branch and innervate several muscle fibres. Thus, one AChR cluster of a single muscle fibre might be transiently covered by numerous MN terminals of different MNs at birth (polyneuronal innervation) (Slater 2009).

Elimination of such redundant neuronal connections in the immature nervous system, termed axonal pruning, is a common feature of neurogenesis ensuring proper formation of neural functionality (Low *et al.* 2006). Therefore, in a postnatal selection process, motor axons compete for maintenance of their synapses leading to physiological weakening and retraction of most motor axons. Eventually, all exuberant but one pre-synaptic MN connections are removed so that only one single MN terminal innervates one endplate (Lichtman *et al.* 2000; Luo *et al.* 2005).

Further regular postnatal NMJ maturation comprises rearrangement of immature oval AChR plaque shape to a perforated, pretzel-like structure since AChRs agglomerate at the crests of junctional sarcolemmal folds (Wu *et al.* 2010). The area of AChR clusters moderately enlarges. Likewise, the composition of AChRs changes: AChR are heteropentamers composed of α-, β- and δ-subunits plus embryonic γ-isotype subunits which are substituted by adult ε-isoforms (Sakmann *et al.* 1978; Sine 2012). In adult muscle, the density of AChRs reaches >10,000 per μm^2 (Sanes *et al.* 2001). In summary, functional NMJ connections are established at birth, however, the mature adult configuration is adopted post-natally (Ruegg 2001). Stable neurotransmitter release and augmented receptor number and density yield an efficacious mature NMJ in the end (Sanes *et al.* 2001).

3.3.5 Effects of SMN depletion in the motoneuronal circuit

Summarising recent studies, hints accumulate that SMN protein function in motoneurons may go beyond snRNP biogenesis. Instead, necessary levels of SMN are essential for motor axon development and NMJ maintenance (Fallini *et al.* 2012).

In SMA patients, the greatest loss of muscular strength occurs at disease onset indicating an initial loss of lower motoneurons followed by a low deterioration (Sumner 2007). A SMA mouse model failed to exhibit any significant abnormalities in motor axon formation (McGovern *et al.* 2008), thus corroborating evidence that SMA is rather a disease of maintenance of MNs and NMJs. SMN loss in SMA patients and SMA mouse models is accompanied by pronounced synaptic defects and de-nervation: (i) Reduced stimulatory input onto motoneurons because of decrease in glutamatergic synapses of proprioceptive sensory neurons (Mentis *et al.* 2011); (ii) phosphorylated neurofilament aggregation in motoneuronal NMJs (Cifuentes-Diaz *et al.* 2002; Ling *et al.* 2010; Ling *et al.* 2011; Bowerman *et al.* 2012a); (iii) disturbed Ca^{2+} homeostasis (Ruiz *et al.* 2010); (iv) irregularities in synaptic architecture concerning pre-synaptic vesicle distribution and recycling as well as lower neurotransmitter release (Kariya *et al.* 2008; Kong *et al.* 2009); (v) atypical motor endplate appearance on pre-synaptic motoneuronal side indicated by poor arborisation, shortened axon length and reduced growth cone size (Murray *et al.* 2008; Ling *et al.* 2011; Torres-Benito *et al.* 2011; Bowerman *et al.* 2012a); (vi) delayed AChR clustering and NMJ maturation on post-synaptic muscle side (Arnold *et al.* 2004; Kariya *et al.* 2008; Martínez-Hernández *et al.* 2013). In SMA,

NMJs detain embryonic AChR subunits and keep the immature plaque form (Kariya *et al.* 2008; Kong *et al.* 2009; Bowerman *et al.* 2012a).

So, loss of motoneuron cells is caused by a dying-back axonopathy because MN-axon degeneration occurs before actual MN-cell death (Cifuentes-Diaz *et al.* 2002; Fallini *et al.* 2012). Considering a normal embryonic development, SMN seems more important for foetal NMJ maturation and NMJ maintenance in postnatal/adult stages (Fallini *et al.* 2012).

Disturbed ubiquitin homeostasis is additionally causal for MN death elicited by disrupted splicing of ubiquitin-like modifier activating enzyme 1 (*Uba1*) mRNA and lost interaction between UBA1 and SMN in several SMA model systems (Wishart *et al.* 2014). Axonal microRNA (miRNA) expression and distribution are dysregulated in SMN-deficient neurons (Kye *et al.* 2014). Moreover, autophagy dysregulation was recently connected to SMA pathology in mouse models (Custer *et al.* 2014; Garcera *et al.* 2013).

To which extent actin bundling protein PLS3 might positively influence the maintenance of SMA-diseased NMJs is still a matter of debate. Particularly with regard to the inability of a PLS3 over-expressing mouse model to appropriately phenocopying the SMA ameliorating effect of this SMA modifier (Ackermann *et al.* 2013), the significance of a human patient-derived PLS3 discordant cell model is highlighted.

3.4 Plastin 3 (PLS3) as disease modifier in SMA discordant families

3.4.1 The effects of modifiers in disease phenotype – no 1:1 translation from gene to malady

Genetic disorders oftentimes exhibit a broad spectrum of phenotypic characteristics owing to environmental as well as intrinsic genetic factors ("modifiers"). Monogenetic diseases like SMA provide the unique framework to examine the possible impact of those modifiers since they possess a uniform aetiology with a single causal gene, detailed clinical phenotype in affected individuals and familial cumulation (Cutting 2010). The type of genetic mutation often defines outcome and severity of a single-gene disorder. For instance, the kind of deletion in the dystrophin gene determines whether a nonsense/frame-shift mutation or an in-frame mutation occurs leading either to severe Duchenne Muscular Dystrophy or to milder Becker Muscular Dystrophy (Abmayr *et al.* 2006; Kanagawa *et al.* 2006). However, when patients with exactly the same genotype display a phenotypic variability, these observations point to the existence of modifiers.

For many years, *SMN2* was the sole known SMA-modifying gene displaying a strong inverse correlation between its copy number and SMA phenotype (Feldkötter *et al.* 2002). Beside *SMN2* copy number, SMA severity and progression is decisively influenced by different disease modifying factors: Barring an ameliorating SNP (c.859G>C substitution) in *SMN2* (Prior *et al.* 2009), over-expression of zinc finger protein 1 (ZPR1) in mice led to increase in SMN levels and gem formation as well as stimulation of neuritogenesis and rescue of axonal growth deficits (Ahmad *et al.* 2012). In contrast, stathmin, a ubiquitous microtubule-destabilising phosphoprotein enhancing the microtubule catastrophe rate, is aberrantly augmented in SMA mice. Stathmin reduction improved motor abilities and NMJ formation in SMA mice, but failed to prolong total viability. Ergo, microtubule depolymerisation apparently favours detrimental effects in SMA linking microtubule stability to disease severity (Wen *et al.* 2010; Wen *et al.* 2012).

3.4.2 PLS3 acts as protective modifier in SMA – but how?

In rare families, siblings showing the identical genotype, i.e. 3-4 *SMN2* copies and homozygous absence of *SMN1*, exhibit variable SMA phenotypes. Scrutinising this observation in so-called "discordant families" suggests the influence of unknown modifying factors in SMA penetrance (Helmken *et al.* 2000). In six such discordant families, some individuals with no *SMN1* copy and 3-4 *SMN2* copies suffer from SMA III whereas other relatives are totally asymptomatic despite sharing the same *SMN1/SMN2* genotype. Remarkably, the number of affected male SMA patients significantly outweighed the number of female patients alluding to a gender-specific effect. In this context, the actin filament bundling protein plastin 3 (PLS3) was eventually discovered by differential gene expression (micro-array) analysis as first SMA modifier beside *SMN2* copy number (Oprea *et al.* 2008).

Further qRT-PCR and protein analysis affirmed *PLS3*/PLS3 to be highly up-regulated in Epstein-Barr-virus (EBV)-transformed lymphoblastoid (LB) cell lines of asymptomatic individuals compared to their affected siblings. As expected, PLS3 protein is strongly expressed in solid tissues like foetal and adult human brain, muscle and spinal cord. Interestingly, a high PLS3 expression was also found in blood of asymptomatic individuals being unusual for this PLS3 isotype (see 3.4.3). In only 5% of healthy control probands PLS3 expression could be detected in native blood samples, at all. Yet, PLS3 over-expression in blood of asymptomatic individuals rules out that EBV-mediated cell immortalisation led to the finding in this study (Oprea *et al.* 2008).

Previous PLS3 over-expression studies in fibroblast-like cell lines *in vitro* demonstrated cell rounding, accumulation in the apical periphery and in microvilli of polarised epithelial cells, PLS3 withdrawal from adhesion foci and simultaneously a massive actin filament rearrangement to a polygonal meshwork (Arpin *et al.* 1994). To dissect the functional mechanism behind the protective effect of PLS3 as well as the connection between SMN and PLS3, different approaches have been undertaken in the original study by Oprea *et al.*:

On cellular level, healthy primary murine motoneurons exhibit a co-localisation of endogenous Smn, actin and Pls3 which accumulate in F-actin-rich growth cones. As soon as rat PC12 cells are differentiated into motoneurons, a similar distribution of Smn and Pls3 is visible with agglomeration at neurites/growth cones and diffuse cytoplasmatic disposition. PLS3 over-expression in HEK293 cells shifts G-/F-actin ratio in favour of filamentous actin whereas a PLS3 knock-down results in the opposite effect and elevation of G-actin. LB cells of asymptomatic siblings with high PLS3 expression reveal augmented F-actin levels. Knock-down of Pls3 in rat PC12 cell-derived motoneurons evoked a dramatic shortage in neurite length, whereas an over-expression of PLS3 caused markedly elongated neurite growth. Besides, PLS3 over-expression with concomitant Smn knock-down rescued neurite outgrowth in PC12 cell-derived motoneurons. No increase in SMN levels was detectable due to PLS3 over-expression. Co-immunoprecipitation experiments insinuate an indirect PLS3/SMN interaction. Summing up, these *in vitro* findings lead to the conclusion that PLS3 is likely to exert its positive effect by stabilising actin filaments at crucial hotspots of structural motoneuronal homeostasis e.g. axonal growth cones. Actin cytoskeleton dynamics, namely G-/F-actin ratio, is a key player in axogenesis and path-finding (Dent *et al.* 2003).

Additionally, this hypothesis is strikingly circumstantiated by *in vivo* findings: PLS3 over-expression is able to fully rescue axonal growth defects including precocious branching and truncations in smn depleted zebrafish embryos (Oprea *et al.* 2008; Hao le *et al.* 2012). Moreover, in *smn*$^{-/-}$ zebrafish mutants Pls3 protein levels are significantly mitigated, while *pls3* mRNA levels remain unchanged suggesting that SMN affects PLS3 protein synthesis (Hao

le *et al.* 2012). Ackermann *et al.* recently provided a conditional *PLS3* over-expressing mouse model SMA$_{PLS3}$ bred into the severe Taiwanese SMA background (*Smn$^{-/-}$; SMN2$^{+/-}$; PLS3$^{+/-}$* in pure C57Bl/6N background). In detail, the authors found an increased F-actin amount in pre-synapses, restoration of synaptic vesicle and active zone content, re-assembly of the readily releasable pool, increased endplate and muscle fibre size and improved neurotransmission, summarised a general amelioration in MN-synapse architecture, activity and neuromuscular connectivity (Ackermann *et al.* 2013). Furthermore, MN somata in SMA$_{PLS3}$ mice are bigger and receive more afferent proprioceptive inputs as compared to SMA mice. Yet, ubiquitous over-expression moderately improved survival and motor function only in mildly affected SMA mice with mixed background (50%C57Bl/6N/50%FVB/N), not in severe SMA$_{PLS3}$ mice reflecting the human state in which only putative SMA III patients (≥3 *SMN2* copies) benefit from PLS3 abundance. Over-expression of human PLS3 caused a significant delay in axon pruning until postnatal day 8 (P8) counteracting the poor synaptic connectivity seen in SMA mice. Axonal pruning is a major process of NMJ maturation in which exuberant axonal branches are removed and endplates finally become innervated by a single axon (Redfern 1970; Luo *et al.* 2005) (see 3.3.4). In addition, PLS3 orthologues fimbrin (Fim) and plst-1 in *D. melanogaster* and *C. elegans*, respectively, act as protective modifiers in SMA models of these invertebrates, verifying the human data from the previous study and implying the relevance of PLS3 as a cross-species modifier of SMA (Dimitriadi *et al.* 2010).

The nexus between PLS3, SMN and further microfilament components is illustratively investigated by Bowerman and colleagues (Bowerman *et al.* 2009). In MNs of their intermediate SMA mouse model (*Smn$^{2B/-}$*) they detected a cell-autonomous increase in profilin IIa levels, an actin monomer-binding protein and direct interaction partner of SMN, which was accompanied by a decrease of Pls3 levels.

Yet, only PLS3 expression rescued axonal growth deficits in *smn* morphant zebrafish whereas other proteins modifying actin filaments (e.g. cofilin, profilin or α-actinin) failed. Deletion of conserved PLS3 structural domains revealed that mutations in Ca^{2+}-binding residues in the EF hand motifs totally impaired the ameliorative impact of PLS3. Astonishingly, despite the loss of their actin-binding domains, PLS3 mutants still exerted a moderate protective effect in motor axons of *smn* morphants implying an actin-independent action of PLS3 (Lyon *et al.* 2013).

Further insight to the human state provided following study: Bernal *et al.* assessed *PLS3* expression in LB cell lines of non-consanguineous discordant families (Bernal *et al.* 2011). *PLS3* levels are 8-9 fold increased in asymptomatic siblings when compared to affected siblings. However, *PLS3* levels in fibroblasts of discordant siblings exceed those of blood and LB cells ~12-200-fold, questioning the validity of the observed subtle differences of *PLS3* expression in LB cells of asymptomatic individuals. If these results mirror the PLS3 expression state in the spinal cord remains to be elucidated in depth. Unlike the study from Oprea *et al.*, *PLS3* expression levels are different when comparing LB cell lines to native blood of the same patient. Thus, the authors do not exclude that other internal factors or the EBV-mediated transformation process causes these slight changes in *PLS3* expression (Bernal *et al.* 2011).

The gender-related aspect of PLS3 expression was examined in a cohort of SMA patients of both sexes with different severity and age. Pre-pubertal male and female patients possess the highest PLS3 expression. Yet, a stringent correlation between SMA type, *SMN2* copy number, gross motor function and PLS3 expression is only visible in mildly affected post-pubertal women making hormonal influences probable. Thus, PLS3 seems unsuitable as general biomarker for SMA in most clinical trials (Stratigopoulos *et al.* 2010).

3.4.3 PLS3 – Occurrence and function

The human *plastin 3* (*PLS3*) gene (also called *T-plastin*) is located on Xq23 spanning a chromosomal region of ~90 kb (Lin *et al.* 1988). It consists of 16 exons and generates three mRNA transcript variants (1, 2 and 3) which are expressed in epithelial and mesenchymal cells of solid tissue (Delanote *et al.* 2005). Apart from *PLS3*, there exist two gene paralogues in humans: *I-plastin* (*PLS1*) and *L-plastin* (*PLS2*) which are expressed in small intestine/kidney and haematopoietic cell lineages, respectively (Lin *et al.* 1993; Lin *et al.* 1994).

Human *plastins* (earlier called *fimbrins*) derive from one ancestral gene. In general, *plastin* genes are highly conserved in eukaryotic evolution (Lin *et al.* 1993; Delanote *et al.* 2005). The three plastin protein isoforms share 70% aa homology.

PLS3 is 630 aa long cytoskeleton-associated protein with a size of roughly 70 kDa. Its nuclear export signal (NES) ensures a strict cytoplasmatic localisation. Like its tissue-specific relatives, PLS3 cross-links F-actin filaments into rigid, tight bundles with the same polarity. Thus, PLS3 is involved in dynamics and re-organisation of any highly ordered microfilament structure, amongst others microvilli, lamellipodia, membrane ruffles, focal adhesions, sometimes stress fibres and invasion of intracellular prokaryotic pathogens like *Rickettsia parkeri* or *Shigella flexneri* (Delanote *et al.* 2005; Serio *et al.* 2010).

4. Aim of the study

One of the most frequent monogenetic cause of infant death worldwide is spinal muscular atrophy (SMA), a devastating autosomal-recessive neurodegenerative disorder. SMA is characterised by selective loss of lower α-motoneurons (MNs) in the spinal cord eliciting de-nervation and progressive wasting of proximal skeletal musculature in limbs and trunk. The responsible gene _survival of motor neuron 1_ (_SMN1_) is homozygously deleted. An almost identical copy of _SMN1_, i.e. _SMN2_, contains a C>T transition in exon 7 which destroys an exonic splicing enhancer site, thus negatively interfering with mRNA splicing because of undue skipping of exon 7. Consequently, ~90% of _SMN2_ transcripts are devoid of exon 7 (Δ7-SMN), leading to a truncated and instable SMN protein. Nevertheless, about 10% correct full-length _SMN_ transcripts (FL-SMN) are generated. Therefore, SMA severity is inversely correlated to the total number of _SMN2_ copies which is variable in human population (2-6 on average). Beside _SMN2_ copy numbers, up-regulation of actin bundling protein plastin 3 (PLS3) is linked to protective effects in _SMN1_-deleted asymptomatic individuals of SMA discordant families. Moreover, the SMA drug valproic acid (VPA) induced SMN elevation only in approx. ⅓ of SMA patients due to individual VPA responsiveness. Yet, studies on neurological disorders like SMA are hampered by the inaccessibility to patients' neurons. The emergence of direct reprogramming of patient-derived cells overcomes this obstacle by generating induced pluripotent stem cells (iPSCs) and subsequent motoneuronal differentiation.

The major aim of this study was to obtain such a SMA patient-derived iPSC-based _in vitro_ cell culture model. Firstly, fibroblasts of six members of PLS3-discordant families as well as one VPA responder/non-responder each were either reprogrammed by classical retroviral transduction or by a non-integrative approach with Sendai virus. Secondly, one to two clones per subsequent iPSC line were subjected to thorough standard validation procedure in order to verify _bona fide_ pluripotency. Thirdly, appropriate protocols for directed _in vitro_ re-differentiation of iPSCs into spinal motoneurons were set up. Thus, the _in vitro_ SMA disease model enabled further elucidation of the SMA pathomechanism directly in the target tissue, i.e. α-motoneurons.

In four phenotypic groups (i.e. healthy controls, SMA I and PLS3 discordant SMA III and asymptomatic siblings), SMA disease-related features (e.g. gem number, neurite length, MN survival, growth cone architecture and SMN expression on RNA and protein levels) were scrutinised during developmental course in order to recapitulate SMA pathology proven in mouse models and established _in vitro_ cell systems. Furthermore, previous findings in animal models and non-neuronal patients' cell lines like fibroblasts and immortalised lymphoblastoid cells substantiated the ameliorative impact of PLS3 in SMA phenotype. Thus, this study addressed the key question to which extent protective effects of PLS3 over-expression would display in this model representing a mild discordant SMA cell system for the first time.

Moreover, the importance of neuromuscular junctions (NMJ), specialised motor synapses at skeletal muscles, is gaining momentum concerning SMA pathology. Therefore, a co-culture model of iPSC-derived motoneurons with human myotubes was introduced enabling further studies of the mutual MN-muscle interaction in that putative hotspot of SMA pathology.

Finally, (moto)neuronal differentiation of VPA responders/non-responders was supposed to verify previous results from patients' fibroblasts and blood after VPA application and furthermore to elucidate molecular mechanisms underlying variable VPA responsiveness in SMA patients.

5. Materials

5.1 Technical equipment

Table 1: Technical equipment

Appliance	Name	Manufacturer	Registered Office
Autoclave	DX-150	Systec	Wettenberg, Germany
Balance	LA310S	Satorius	Göttingen, Germany
	BL610	Satorius	Göttingen, Germany
Block heater	Thermomixer compact	Eppendorf	Hamburg, Germany
Cell culture centrifuge	Megafuge 1.0R	Kendro	Hanau, Germany
Centrifuge tubes	Ultra Cone Polyallomer	Seton	Petaluma, USA
Counting chamber	Fuchs-Rosenthal	Laboroptik	Bad Homburg, Germany
Digital camera	Canon Power Shot G5	Canon	Krefeld, Germany
FACS	FACS® Canto II	BD Biosciences	San Jose, USA
Fluorescence camera	Axiocam MRm	Carl Zeiss	Jena, Germany
Fluorescence lamp	HXP 120c	Carl Zeiss	Jena, Germany
Fluorescence microscope	Axio Imager.M2	Carl Zeiss	Jena, Germany
Freezer -20 °C/-80 °C	HERAfreeze	Heraeus	Hanau, Germany
Freezing container	"Mr. Frosty" 5100 Cryo 1°C	Nalgene	Roskilde, Denmark
Gel documentation	Geldoc2000/ChemiDoc XRS	Bio-Rad	Munich, Germany
Gel electrophoresis chambers	Agagel	Biometra	Göttingen, Germany
	SGE-020-02	CBS-Scientific	San Diego, USA
Horizontal hood	HERAguard	Heraeus	Hanau, Germany
Incubator	HERAcell 150	Heraeus	Hanau, Germany
Inverse light microscope	Axiovert 40C	Carl Zeiss	Jena, Germany
Liquid nitrogen store	MVE 611	German cryo	Jüchen, Germany
Magnetic stirrer	SB162	Stuart Scientific	Staffordshire, UK
Micropipette	2.5 µl, 10 µl, 20 µl, 100 µl, 1,000 µl	Eppendorf	Hamburg, Germany
Microplate reader	TECAN Safire²	Tecan	Männedorf, Switzerland
pH-meter	Microprocessor pH meter	Hanna-instruments	Woonsocket, USA
Pipette-boy	Accu-Jet II	Brand	Wertheim, Germany
Power supply for agarose electrophoresis	Standard Power Pack P25	Biometra	Göttingen, Germany
Real time thermocycler	Light cycler® 1.5	Roche	Penzberg, Germany
	iCycler	Bio-Rad	Munich, Germany
Refrigerator 4 °C	KGEE36A	Bosch	Gerlingen, Germany
Spectrophotometer	Nanodrop® ND-1,000	Peqlab	Erlangen, Germany
	BioPhotometer	Eppendorf	Hamburg, Germany
Sterile laminar flow hood	HERAsafe	Kendro	Hanau, Germany
Table centrifuge	Centrifuge 5415D	Eppendorf	Hamburg, Germany
Thermocycler	T3000	Biometra	Göttingen, Germany
Ultracentrifuge	Sorvall® Discovery 90SE	Hitachi	Wiesbaden, Germany
Vacuum pump	Vacuubrand	Brand	Wertheim, Germany

| Vortexer | Vortex Genie 2 | Scientific Industries | Bohemia, USA |
| Water bath | W22 | Medingen-GKS | Dresden, Germany |

5.2 Chemicals and consumables

If available, chemicals used in this study are purchased as purity grade "pro analysis". For RNA isolation and analysis, only RNase-free chemicals are employed.

Table 2: Chemicals

Chemical	Manufacturer	Registered Office
Accutase	PAA	Cölbe, Germany
Advanced DMEM	Life Technologies	Darmstadt, Germany
Advanced DMEM/F-12	Life Technologies	Darmstadt, Germany
Alfazyme	PAA	Cölbe, Germany
Ascorbic acid	Sigma-Aldrich	Hamburg, Germany
B27® supplement	Life Technologies	Darmstadt, Germany
B27® supplement minus vitamin A (B27-RA)	Life Technologies	Darmstadt, Germany
β-mercaptoethanol	Life Technologies	Darmstadt, Germany
BDNF(rhBDNF)	R&D Systems	Wiesbaden, Germany
BSA Fraction V	Carl Roth	Karlsruhe, Germany
cAMP	Sigma-Aldrich	Hamburg, Germany
CHIR99021	Stemgent	Bergisch Gladbach, Germany
CNTF (rhCNTF)	R&D Systems	Wiesbaden, Germany
Collagenase type IV	Life Technologies	Darmstadt, Germany
DAPT	Sigma-Aldrich	Hamburg, Germany
DAPI	Sigma-Aldrich	Hamburg, Germany
db-cAMP	Enzo Life Sciences	Lörrach, Germany
D-Glucose	Carl-Roth	Karlsruhe, Germany
DMEM/F-12 (1:1)	Life Technologies	Darmstadt, Germany
Dispase	Life Technologies	Darmstadt, Germany
DMEM high Glucose	Life Technologies	Darmstadt, Germany
DMSO	Sigma-Aldrich	Hamburg, Germany
DNase I (for molecular biology)	Promega	Mannheim, Germany
Dorsomorphin	Sigma-Aldrich	Hamburg, Germany
EGF	R&D Systems	Wiesbaden, Germany
Ethanol (for molecular biology)	Merck	Darmstadt, Germany
FCS	Life Technologies	Darmstadt, Germany
FGF2 (= bFGF)	R&D Systems	Wiesbaden, Germany
FGF2 (= bFGF)	Life Technologies	Darmstadt, Germany
Fibronectin	Sigma-Aldrich	Hamburg, Germany
Fluorescein calibration dye	Bio-Rad Laboratories	Munich, Germany
Forskolin	Enzo	Lörrach, Germany
FuGENE® HD transfection reagent	Roche	Penzberg, Germany
GDNF (rhGDNF)	R&D Systems	Wiesbaden, Germany
Gelatine	Life Technologies	Darmstadt, Germany
Gentamicin	Life Technologies	Darmstadt, Germany
GlutaMAX™ Supplement	Life Technologies	Darmstadt, Germany

$_{dd}H_2O$ (Ampuwa® sterile water)	Fresenius Kabi	Bad Homburg, Germany
HBSS buffer	Life Technologies	Darmstadt, Germany
Heparin	Sigma-Aldrich	Hamburg, Germany
Horse serum	Life Technologies	Darmstadt, Germany
IGF-1 (rhIGF-1)	R&D Systems	Wiesbaden, Germany
iScript reverse transcriptase	Bio-Rad Laboratories	Munich, Germany
Knockout DMEM	Life Technologies	Darmstadt, Germany
Knockout Serum Replacement	Life Technologies	Darmstadt, Germany
L-Ascorbic-Acid-2-Phosphat (LAAP)	Sigma-Aldrich	Hamburg, Germany
Laminin	Sigma-Aldrich	Hamburg, Germany
LDN193189	Axon MedChem	Groningen, Netherlands
Magnesium chloride	Life Technologies	Darmstadt, Germany
Matrigel™	BD Biosciences	Heidelberg, Germany
Mowiol 4-88	Merck	Darmstadt, Germany
mTeSR™1	STEMCELL Technologies	Cologne, Germany
N2 Supplement	PAA	Cölbe, Germany
Neurobasal® medium	Life Technologies	Darmstadt, Germany
Non-essential amino acids (NEAA)	Life Technologies	Darmstadt, Germany
Opti-MEM®	Life Technologies	Darmstadt, Germany
PAGE Ruler Plus protein ladder	Fermentas	Pittsburgh, USA
Paraformaldehyde (PFA)	Sigma-Aldrich	Hamburg, Germany
PBS	Life Technologies	Darmstadt, Germany
PeqGOLD dNPT set	PEQLAB Biotechnologie	Erlangen, Germany
Penicillin/Streptomycin	Life Technologies	Darmstadt, Germany
Picric acid	Sigma-Aldrich	Hamburg, Germany
Poly-L-ornithine	Sigma-Aldrich	Hamburg, Germany
Purmorphamine	Merck	Darmstadt, Germany
Retinoic acid (RA)	Sigma-Aldrich	Hamburg, Germany
RIPA buffer	Sigma-Aldrich	Hamburg, Germany
SAG	Calbiochem	Läufelfingen, Germany
SB431542	Sigma-Aldrich	Hamburg, Germany
Sendai virus vector (SeV)	DNAVEC	Tsukuba, Japan
SkGM + supplement	PromoCell	Heidelberg, Germany
Sodium pyruvate	Life Technologies	Darmstadt, Germany
SYBR-green I nucleic acid gel stain (10,000 ×)	Sigma-Aldrich	Hamburg, Germany
Taq DNA polymerase recombinant	Life Technologies	Darmstadt, Germany
Triton-X100	Sigma-Aldrich	Hamburg, Germany
Trypan blue	Life Technologies	Darmstadt, Germany
Trypsin EDTA	Life Technologies	Darmstadt, Germany
Y-27632 (ROCK Inhibitor)	Merck	Darmstadt, Germany

Table 3: Consumables

Consumable	Manufacturer	Registered Office
Adhesive PCR films	Peqlab	Erlangen, Germany
Cellsive cell strainer (40 µm)	BD Biosciences	Heidelberg, Germany
Cell scraper	Corning	Kaiserslautern, Germany
Chamberslide (4-well glass)	Millipore	Schwalbach, Germany
Cotton swabs	Hartmann	Neuhausen, Schwitzerland

Coverglass (24×60 mm)	Paul Marienfeld	Lauda-Königshofen, Germany
(Ø 30 mm)	Glaswarenfabrik Karl Hecht	Sondenheim, Germany
Coverslips	Labomedic	Bonn, Germany
Cryovials (1 ml, 1.8 ml)	Nunc	Wiesbaden, Germany
Cuvettes	Brand	Wertheim, Germany
Glass pipettes	Hirschmann Laborgeräte	Eberstadt, Germany
Hyperfilm ECL	Amersham	Glattbrugg, Switzerland
KimWipes	Kimberly-Clark	Koblenz, Germany
OP-mask	Hartmann	Neuhausen, Switzerland
Parafilm	Bemis	Meckenheim, Germany
Pasteur pipettes	Brand	Wertheim, Germany
PCR plate (96 well)	PEQLAB Biotechnologie	Erlangen, Germany
PCR stripe tubes (0.2 ml)	PEQLAB Biotechnologie	Erlangen, Germany
Pipette tips	Axygen (FischerScientific)	Schwerte, Germany
	Greiner Bio One	Solingen, Germany
Reaction tubes (0.5 ml, 1.5 ml, 2 ml)	Sarstedt	Nümbrecht, Germany
Serological pipettes	Corning	Kaiserslautern, Germany
Single-use gloves	Ansell	Munich, Germany
Syringe filter (0.2 μm)	PALL Corporation	Dreieich, Germany
Syringes (1 ml, 5 ml, 10 ml)	BD Biosciences	Heidelberg, Germany
(50 ml)	Braun	Melsungen, Germany
Syringe needles	BD Biosciences	Heidelberg, Germany
Tissue culture dishes	BD Biosciences	Heidelberg, Germany
	Nunc	Wiesbaden, Germany
	Corning	Kaiserslautern, Germany
Tissue culture flasks (T75, T175)	Greiner Bio One	Solingen, Germany
Tubes (15 ml, 50 ml)	BD Biosciences	Heidelberg, Germany
48-well-plate (transparent, flat bottom	Corning	Kaiserslautern, Germany
96-well-plate (black, flat bottom)	Greiner Bio One	Solingen, Germany

5.3 Kits

Table 4: Kits

Kit	Manufacturer	Registered Office
Alkaline Phosphatase Substrate Kit III SK-5300	Vector Laboratories	Burlingame, USA
DNeasy Blood & Tissue Kit	Qiagen	Hilden, Germany
Fast Start DNA Master SYBR® Green I	Roche	Penzberg, Germany
GoTaq Flexi DNA polymerase Kit	Promega	Mannheim, Germany
iScript Reverse Transcription Kit	Bio-Rad	Munich, Germany
Plasmid Maxi Kit	Qiagen	Hilden, Germany
Quant-iT™ RiboGreen® RNA Assay Kit	Life Technologies	Darmstadt, Germany
QuantiTec Reverse Transkriptase Kit	Qiagen	Hilden, Germany
RNeasy Blood & Tissue Kit	Qiagen	Hilden, Germany
SuperSignal® West Pico Chemiluminescent Substrate	Pierce	Bonn, Germany

5.4 Software

Table 5: Software programs

Name	Application	Version	Producer
Axiovision	Fluorescence microscopy	4.8	Carl Zeiss, Germany
iCycler analysis software	qRT-PCR analysis	V.3.1	Bio-Rad, Germany
iControl software	Plate reader	1.6	Tecan, Switzerland
EndNote	Bibliography	9.0.1	Thomson, USA
GraphPad Prism®	Graph design	6	La Jolla, USA
LightCycler Software	qRT-PCR analysis	3.5	Roche, Switzerland
Microsoft® Office 2007	Figure and text processing	2007	Microsoft, USA
Openlab	Fluorescence microscopy	4.0.1	PerkinElmer, USA
Photoshop	Image processing	CS4	Adobe, Ireland
Quantity One	Electrophoresis gel documentation	4.6.3	Bio-Rad, Germany
XFluor4Safire² software	Plate reader	1.2	Tecan, Switzerland
ZEN	Fluorescence microscopy	2011	Carl Zeiss, Germany

5.5 Primers

All primers used in this thesis are designed by Johannes Jungverdorben or Dr. Bastian Ackermann. Primers are individually designed for specific DNA targets and purchased from Metabion or Life Technologies in lyophilised form. Upon arrival, lyophilised primers are diluted to 100 pmol/µl stock solutions using sterile $_{dd}H_2O$. Working solutions are produced by diluting stock solutions to a final concentration of 10 pmol/µl (FL-SMN, PLS3).

Table 6: Sequences of RT-PCR primers

Transcript	Forward sequence (5'-3') ff	Reverse sequence (5'-3') rev	T_{anneal}
18S rRNA	TTCCTTGGACCGGCGCAAG	GCCGCATCGCCGGTCGG	60 °C
c-MYC endo	TTCGGGTAGTGGAAAACCAC	CCTCCTCGTCGCAGTAGAAA	60 °C
c-MYC total	AAGACTCCAGCGCCTTCTCT	TCTTGTTCCTCCTCAGAGTCG	60 °C
FL-SMN	CCACCACCCCACTTACTATCA	GCTCTATGCCAGCATTCCTCCT	60 °C
GAPDH	TGACAACTTTGGTATCGTGGA	CCAGTAGAGGCAGGGATGAT	60 °C
NP	GAAAGAAATTTCACCGCTAGCGCGG CCGCATGCTAACACGGCGCAATG	CATTGCGCCGTGTTAGCATGCGGCC GCGCTAGCGGTGAAATTTCTTTC	60 °C
KLF4 endo	GACCAGGCACTACCGTAAACA	CTGGCAGTGTGGGTCATATC	60 °C
KLF4 total	CCCAATTACCCATCCTTCCT	ACGATCGTCTTCCCCTCTTT	60 °C
LEFTYA	AATGTGTCATTGTTTACTTGTCCTGTC	CAGGTCTTAGGTCCAGAGTGGTG	60 °C
LEFTYB	GTCCATCACCCATCCTAAGCAC	GCCAGCATTTCCTACTAGAGCTCA	60 °C
NANOG	CCTGTGATTTGTGGGCCTG	GACAGTCTCCGTGTGAGGCAT	60 °C
NODAL	GGCGAGTGTCCTAATCCTGTTG	GGTAACGTTTCAGCAGACTCTGG	60 °C
OCT4 endo	DACAGGGGGAGGGGAGGAGCTAG	GTTCCCTCCAACCAGTTGCCCCAAAC	60 °C
OCT4 total	GTGGAGGAAGCTGACAACAA	ATTCTCCAGGTTGCCTCTCA	60 °C
PLS3	GAACGTTGAGTGAAGCTGGA	TTGCCACTCTTCACAAGGTC	60 °C
REX1	GCACACTAGGCAAACCCACC	CATTTGTTTCAGCTCAGCGATG	60 °C
SOX2 endo	GTATCAGGAGTTGTCAAGGCAGAG	TCCTAGTCTTAAAGAGGCAGCAAAC	60 °C

| SOX2 total | GCCGAGTGGAAACTTTTCTCG | GCAGCGTGTACTTATCCTTCTT | 60 °C |
| TERT | GCGTTTGGTGGATCATTTCT | ACCACTGTCTTCCGCAAGTT | 60 °C |

Oligo-dT primers for qRT-PCR are purchased from Fermentas (Pittsburgh, USA).

5.6 Plasmids and bacterial strains

5.6.1 Plasmids

Table 7: Plasmids

Name	Description	Reference
pMXs-hOCT4	Expression vector; MCS, Ψ, MMLV LTRs, Amp^r	(Takahashi *et al.* 2007)
pMXs-hSOX2	Expression vector; MCS, Ψ, MMLV LTRs, Amp^r	(Takahashi *et al.* 2007)
pMXs-hKLF4	Expression vector; MCS, Ψ, MMLV LTRs, Amp^r	(Takahashi *et al.* 2007)
pMXs-hc-MYC	Expression vector; MCS, Ψ, MMLV LTRs, Amp^r	(Takahashi *et al.* 2007)

All plasmids (17217, 17218, 17219 and 17220) are purchased from Addgene (Cambridge, USA). Corresponding vector maps are listed in 10.3, Fig. 62.

5.6.2 Bacterial strains

Table 8: Bacterial strains

Strain	Description	Reference
E. coli DH5α	F$^-$, Φ80*lac*ZΔM15 Δ(*lac*ZYA-*arg*F) U169, *rec*A1, *end*A1, *hsd*R17 (rK$^-$-, mK$^+$) *supE*44, λ$^-$, *thi*-1, *gyr*A, *rel*A1	(Hanahan 1983)

5.7 Buffers and solutions

5.7.1 Media for bacterial work

All bacterial media are autoclaved before use (121 °C, 1 bar pressure, 20 min).

LB medium	
10 g	trypton
5 g	yeast extract
5 g	NaCl

Add up to 500 ml with $_{dd}$H$_2$O

pH 7.4-7.5 is adjusted by NaOH

SOC medium	
10 g	trypton
5 g	yeast extract
0.3 g	NaCl
0.09 g	KCl
1.02 g	MgCl$_2$ × 6 H$_2$O
1.23 g	MgSO$_4$ × 7 H$_2$O

Add up to 500 ml with $_{dd}$H$_2$O

After autoclaving 20 mM D-glucose is added

LB-agar is fabricated by adding 15 g agar per litre LB medium.

5.7.2 Antibiotics

Table 9: Antibiotics

Antibiotic	Stock concentration	Dissolved in
Ampicillin	100 mg/ml	$_{dd}H_2O$
Doxycycline	1 mg/ml	$_{dd}H_2O$
G418	50 mg/ml	$_{dd}H_2O$
Puromycin	10 mg/ml	$_{dd}H_2O$

5.7.3 Solutions for DNA and RNA work

TAE 50 ×	
242 g	Tris Base
57.1 ml	Acetic acid
100 ml	0.5 M EDTA (ph = 8.0)
Add up to 1 l with $_{dd}H_2O$ and store at RT	

PCR super mix	
1,520 µl	$_{dd}H_2O$
2,000 µl	5 × GoTaq Flexi Buffer
1,000 µl	MgCl$_2$ (25 mM)
80 µl	dNTPs (100 mM)
400 µl	DMSO

DNA loading buffer 10 ×	
2.5 ml	SDS (20%)
10 ml	EDTA (0.5 M, pH 7.2-8.5)
27.7 ml	Glycerol (87%)
0.05 g	Bromophenol blue
Add up to 50 ml with $_{dd}H_2O$	

qRT-PCR super mix	
1,511.5 µl	$_{dd}H_2O$
2,000 µl	5 × GoTaq Flexi Buffer (colourless)
1,000 µl	MgCl$_2$ (25 mM)
80 µl	dNTPs (100 mM)
400 µl	DMSO
7.5 µl	SYBR Green (1,000 ×)
1 µl	Fluorescine (100 µM)

TE^{-4}	
1 ml	Tris (1 M, pH 8.0)
20 µl	EDTA (0.5 M, pH 8.0)
Add up to 100 ml with $_{dd}H_2O$	

The super mixes are aliquoted and stored at -20 °C. 20 µl of each dNTP (dATP/dCTP/dGTP/dTTP) are taken which results in 0.4 mM final concentration. Primers are reconstituted in $_{dd}H_2O$ to 100 µM final concentration. Primer mix is generated by combining each forward primer with the corresponding reverse primer and diluting in $_{dd}H_2O$ to 3.3 µM final concentration.

5.7.4 Solutions for work with proteins

Laemmli buffer 2 ×	
0.757 g	Tris Base
20 ml	Glycerine
6 g	SDS
10 mg	Bromophenol blue
Add up to 90 ml with $_{dd}H_2O$ and store dark at RT	
1/10 β-mercaptoethanol is freshly added prior to use.	

Lower buffer (1.5 M, pH 8.8)	
91 g	Tris
Add up to 500 ml with $_{dd}H_2O$ and store at RT	

Upper buffer (1 M, pH 6.7)	
60.57 g	Tris
Add up to 500 ml with $_{dd}H_2O$ and store at RT	

Running buffer 10 ×	
30.29 g	Tris Base
144.13 g	Glycine
10 g	SDS

Add up to 1 l with $_{dd}H_2O$ and store at RT

10 × running buffer is diluted 1:10 with $_{dd}H_2O$.

Upper gel solution 3%	
330 µl	Acrylamid stock solution 30% (29:1)
250 µl	Upper buffer pH 6.7
1.4 ml	$_{dd}H_2O$
20 µl	SDS 10%
20 µl	APS 10% aqueous solution
2 µl	TEMED

TBS/Tween 10 ×	
8 g	NaCl
2.42 g	Tris
5 ml	Tween 20

Add up to 1 l with $_{dd}H_2O$ and store at RT

10 × TBS/Tween is diluted 1:10 with $_{dd}H_2O$.

Transfer buffer 1 ×	
4.84 g	Tris Base
22.52 g	Glycine
400 ml	Methanol

Add up to 2 l with $_{dd}H_2O$ and store at RT

Lower gel solution 10%	
2 ml	Acrylamid stock solution 30% (29:1)
1.3 ml	Lower buffer pH 8.8
1.7 ml	$_{dd}H_2O$
50 µl	SDS 10%
50 µl	APS 10% aqueous solution
2 µl	TEMED

Bradford solution	
100 mg	Coomassie Brilliant Blue G250
100 ml	H_3PO_4
50 ml	Ethanol

Add up to 1 l with $_{dd}H_2O$ and store at RT

5.8 Cell culture

5.8.1 Cell culture media

All media mixtures are stored at 4°C and used within two to four weeks. If necessary, Pen/Strep is added at a final concentration of 1%.
All sera utilised are heat-inactivated (30 min, 56 °C).

MEF medium	Final concentration
DMEM (high glucose)	88%
FCS	10%
Sodium pyruvate (100 ×)	1%
NEAA (100 ×)	1%

iPSC medium	Final concentration
Knockout-DMEM	78%
Knockout Serum-Replacement	20%
NEAA (100 ×)	1%
GlutaMAX™ (100 ×)	1%
β-mercaptoethanol (50 mM)	0.1 mM
bFGF (10 µg/ml)	6 ng/ml

N2 medium	Final concentration
DMEM/F12	98%
N2 Supplement	1%
D-Glucose stock (160 mg/ml)	1%

EB medium EB1	Final concentration
DMEM/F12	77%
Knockout Serum-Replacement	20%
NEAA (100 ×)	1%
Sodium pyruvate (100 ×)	1%
GlutaMAX™ (100 ×)	1%
β-mercaptoethanol (50 mM)	0.1 mM
freshly added:	
SB-431542 Inhibitor (50 mM)	5 µM
Dorsomorphin (5 mM)	1 µM

3 germ layer medium EB2	Final concentration
Knockout-DMEM	78%
Knockout Serum-Replacement	20%
NEAA (100 ×)	1%
GlutaMAX™ (100 ×)	1%

Neurosphere medium NSP1	Final concentration
N2 medium	97%
Pen/Strep (100 ×)	1%
freshly added:	
B27-RA (50 ×)	2%
Pur (10 mM)	1 µM
Heparin (1 mg/ml)	1 µg/ml
RA (1 mM)	0.75 µM

MN maturation medium MN1	Final concentration
N2 medium	98.5%
GlutaMAX™ (100 ×)	0.5%
NEAA (100 ×)	1%
freshly added:	
BDNF (10 µg/ml)	10 ng/ml
GDNF (10 µg/ml)	10 ng/ml
IGF1 (10 µg/ml)	10 ng/ml
CNTF (10 µg/ml)	10 ng/ml
Heparin (1 mg/ml)	1 µg/ml
RA (1 µM)	300 nM
Pur (10 mM)	0.5 µM
AA (200 mM)	200 µM
db-cAMP (200 mM)	5 µM

lt-NES®SC medium NSC1	Final concentration
N2 medium	100%
freshly added:	
B27-RA (50 ×)	0.1%
bFGF (10 µg/ml)	10 ng/ml
EGF (10 µg/ml)	10 ng/ml
CHIR99021 (10 mM)	1 µM

Original smNPC generation medium smEB1	Final concentration
Knockout-DMEM	77%
Knockout Serum-Replacement	20%
NEAA (100 ×)	1%
GlutaMAX™ (100 ×)	1%
Pen/Strep	1%
β-mercaptoethanol (50 mM)	1 mM
freshly added:	
Pur (10 mM)	0.5 µM
CHIR99021 (10 mM)	3 µM

Original smNPC medium smNPC1	Final concentration
DMEM/F12	49%
Neurobasal® medium	49%
B27-RA (50 ×)	1%
GlutaMAX™ (100 ×)	0.5%
N2 Supplement	0.5%
freshly added:	
LAAP (221 mM)	150 µM
Pur (10 mM)	0.5 µM
CHIR99021 (10 mM)	3 µM

smNPC medium NPC1	Final concentration
Advanced DMEM/F12	48%
Neurobasal® medium	48%
B27-RA (50 ×)	2%
GlutaMAX™ (100 ×)	1%
N2 Supplement	1%
BSA (5 mg/ml)	5 µg/ml
freshly added:	
LAAP (221 mM)	150 µM
Pur (10 mM)	1 µM
CHIR99021 (10 mM)	3 µM

smNPC medium NPC2	Final concentration
Advanced DMEM/F12	48%
Neurobasal® medium	48%
B27-RA (50 ×)	2%
GlutaMAX™ (100 ×)	1%
N2 Supplement	1%
BSA (5 mg/ml)	5 µg/ml
freshly added:	
LAAP (221 mM)	150 µM
SAG (1 mM)	1 µM
Pur (10 mM)	1 µM
RA (1 mM)	1 µM

smNPC medium NPC3	Final concentration
Neurobasal® medium	95%
B27-RA (50 ×)	2%
GlutaMAX™ (100 ×)	1%
N2 Supplement	1%
NEEA	1%
freshly added:	
BDNF (10 µg/ml)	10 ng/ml
GDNF (10 µg/ml)	10 ng/ml
IGF1 (10 µg/ml)	10 ng/ml
LAAP (221 mM)	0.2 mM
db-cAMP (100 mM)	500 µM

Schwann cell medium SC1	Final concentration
DMEM (high glucose)	96%
FCS	2%
Sodium pyruvate (100 ×)	1%
NEAA (100 ×)	1%
Forskolin (10 mM)	2 µM

Myocyte medium MYO1	Final concentration
SkMGM	88,5%
FCS	10%
GlutaMAX™ (100 ×)	1,5%
Gentamicin (50 mg/ml)	30 µg/ml

Skeletal muscle growth medium SkMGM = 100 ml SkMG basal medium + 5 ml SkMG supplement.

Myotube medium MYO2	Final concentration
DMEM (high glucose)	94%
Horse serum	5%
Sodium pyruvate (100 ×)	1%

Infection medium	Final concentration
Advanced DMEM	93%
FCS	5%
GlutaMAX™ (100 ×)	1%
Pen/Strep (100 ×)	1%

Table 10: Standard freezing media

Cell type	DMSO	Additive(s)
Fibroblasts	10%	90% FCS
Schwann cells	10%	90% FCS
Myocytes	10%	20% FCS + 70% DMEM
lt-NES®SCs	10%	25% N2 medium + 65% KO-SR
smNPCs	10%	25% N2 medium + 65% KO-SR
Human iPSCs	10%	90% KO-SR

5.8.2 Cell culture solutions

Table 11: Stock solutions in cell culture

Stock solution	Concentration	Dissolved in
Ascorbic acid	200 mM	$_{dd}H_2O$
B27® (-RA)	50 ×	/
BDNF	10 µg/ml	$_{dd}H_2O$ + 0.1% BSA
BSA Fraction V	7.5%	$_{dd}H_2O$, sterile filtered
cAMP	1 mg/ml (= 3 mM)	$_{dd}H_2O$
CHIR99021	10 mM	DMSO
Chloroquine	25 mM	$_{dd}H_2O$
CNTF	10 µg/ml	$_{dd}H_2O$ + 0.1% BSA
DAPT	10 mM	DMSO
db-cAMP	100 mM	$_{dd}H_2O$
D-Glucose	160 mg/ml	DMEM/F12, sterile filtered
Dorsomorphin	5 mM	DMSO
EGF	10 µg/ml	$_{dd}H_2O$ + 0.1% BSA + 10 mM glacial acetic acid
FGF2 (= bFGF)	10 µg/ml	$_{dd}H_2O$ + 0.1% BSA
Fibronectin	1 mg/ml	$_{dd}H_2O$
Forskolin	10 mM	DMSO
GDNF	10 µg/ml	$_{dd}H_2O$ + 0.1% BSA
Heparin	1 mg/ml	PBS
IGF-1	10 µg/ml	$_{dd}H_2O$ + 0.1% BSA
LAAP	64 mg/ml (= 221 mM)	$_{dd}H_2O$
Laminin	1 mg/ml	$_{dd}H_2O$
LDN193189	200 mM	DMSO
Picric acid	1.3% saturated supernatant	
Polybrene	4 mg/ml	$_{dd}H_2O$

Poly-L-ornithine	15 µg/ml	$_{dd}H_2O$
Purmorphamine	10 mM	DMSO/Ethanol 1:1
Retinoic acid	1 mM	DMSO/Ethanol 1:100
SAG	1 mM	$_{dd}H_2O$
SB431542	50 mM	DMSO
Y-27632	10 mM	$_{dd}H_2O$

Table 12: Working solutions in cell culture

Working solution	Concentration	Dissolved in
Collagenase Type IV	1 mg/ml	Knockout-DMEM, sterile filtered
Dispase	0.15 mg/ml	N2 medium, sterile filtered
DNase	1 mg/ml	$_{dd}H_2O$, sterile filtered
Gelatine	0.1%	$_{dd}H_2O$, autoclaved
Matrigel™	/	DMEM/F12
Poly-L-ornithine	15 µg/ml	$_{dd}H_2O$, sterile filtered
Trypsin/EDTA	1 ×	PBS

5.8.3 Cell lines

Table 13: Cell lines
Specific features of iPSC lines are given such as originating parental fibroblast, SMA phenotype, age, sex, *SMN1/SMN2* copy number, elevated (↑) PLS3 expression levels in blood and reprogramming technique. Note that numbers in HGK denote individual line and additional clone number of the same line.

iPS cell line	Fibroblast	Phenotype	Age (at biopsy)	Sex	*SMN1/SMN2* copies	PLS3 ↑ in blood	Reprogrammed
iLB-C31f-r1	AK1	healthy control	24 years		n.d.	n.d.	Retrovirus
iLB-C1-30m-r12	JS12	healthy control	34 years		n.d.	n.d.	Retrovirus
COII.2	F-CO-27	healthy control	61 years		n.d.	n.d.	SeV
HGK1	ML17	SMA I	6 months		0 / 2	n.d.	Retrovirus
HGK4	ML73	SMA II	10 years		0 / 3	n.d.	Retrovirus
HGK13	ML102	SMA III	18 years		0 / 3	–	Retrovirus
HGK16	ML101	asymptomatic	29 years		0 / 3	+	Retrovirus
HGK21.1 HGK21.8	ML11	asymptomatic	34 years		0 / 4	+	SeV
HGK22.17 HGK22.18	ML14	SMA IIIb	27 years		0 / 4	–	SeV
HGK27.10 HGK27.13	ML12	SMA IIIb	26 years		0 / 4	–	SeV
HGK28.9 HGK28.11	ML13	asymptomatic	37 years		0 / 4	+	SeV

5.9 Immunocytochemistry

5.9.1 Antibodies

Table 14: Primary antibodies
gt = goat, ms = mouse, rb = rabbit

Primary antibody	Species & isotype	Dilution	Manufacturer	Registered office
AFP	rb, IgG	1:100	Dako	Hamburg, Germany
AP2	ms, IgG	1:250	DSHB	Iowa City, USA
β-actin	ms, IgG	1:60,000	Sigma	Deisenhofen, Germany
ChAT	gt, IgG	1:100	Chemicon	Schwalbach, Germany
DACH1	rb, IgG	1:100	Proteintech	Herford, Germany
GAD65/67	rb, IgG	1:1,000	Chemicon	Schwalbach, Germany
GFAP	rb, IgG	1:1,000	Dako	Hamburg, Germany
HB9	ms, IgG	1:250	DSHB	Iowa City, USA
HN	ms, IgG	1:1,000	DNAVEC	Tsukuba, Japan
HOXB4	rat, IgG	1:250	DSHB	Iowa City, USA
ISL1	ms, IgG	1:250	DSHB	Iowa City, USA
MAPT	ms, IgG	1:500	Millipore	Schwalbach, Germany
Nestin	ms, IgG	1:100	Chemicon	Schwalbach, Germany
Nestin	rb, IgG	1:200	Millipore	Schwalbach, Germany
NF	ms, IgG	1:250	DSHB	Iowa City, USA
NF	rb, IgG	1:1,000	Millipore	Schwalbach, Germany
NKX2.2	ms, IgG	1:250	DSHB	Iowa City, USA
NKX6.1	ms, IgG	1:250	DSHB	Iowa City, USA
OLIG2	rb, IgG	1:500	Millipore	Schwalbach, Germany
PAX6	rb, IgG	1:300	Covance	Münster, Germany
PLS3	rb, IgG	1:50	Eurogentec	Cologne, Germany
PLZF	ms, IgG	1:25	Calbiochem	Läufelfingen, Germany
SMA	ms, IgG	1:100	Dako	Hamburg, Germany
SMI-32	ms, IgG	1:1,000	Covance	Münster, Germany
SMN	ms, IgG	1:100	immunoGlobe	Himmelstadt, Germany
SOX1	rb, IgG	1:100	Millipore	Schwalbach, Germany
SOX2	ms, IgG	1:500	R&D Systems	Wiesbaden, Germany
SSEA-3	rat, IgM	1:250	Millipore	Schwalbach, Germany
SSEA-4	ms, IgG	1:200	DSHB	Iowa City, USA
SV2	ms, IgG	1:100	DSHB	Iowa City, USA
TH	rb, IgG	1:500	Millipore	Schwalbach, Germany
TRA-1-60	ms, IgM	1:500	Millipore	Schwalbach, Germany
TRA-1-81	ms, IgM	1:500	Millipore	Schwalbach, Germany
TUJ1 (β III-tubulin)	ms/rb, IgG	1:1,000	Covance	Münster, Germany
v-Glut1	rb, IgG	1:1,000	Synaptic Systems	Göttingen, Germany
ZO-1	rb, IgG	1:100	Life Technologies	Darmstadt, Germany

Table 15: Secondary antibodies

Secondary antibody (conjugate)	Species & isotype	Dilution	Manufacturer	Registered office
Actin-Phalloidin (Alexa 555)	Death cap (*Amanita phalloides*)	1:40	Life Technologies	Darmstadt, Germany
anti-gt IgG (Alexa 488)	donkey, IgG	1:1,000	Life Technologies	Darmstadt, Germany
anti-gt IgG (Alexa 555)	donkey, IgG	1:1,000	Life Technologies	Darmstadt, Germany
anti-ms IgG (Alexa 488)	goat, IgG	1:1,000	Life Technologies	Darmstadt, Germany
anti-ms IgG (Alexa 555)	goat, IgG	1:1,000	Life Technologies	Darmstadt, Germany
anti-ms IgG (Alexa 647)	goat, IgG	1:1,000	Life Technologies	Darmstadt, Germany
anti-ms IgG (HRP)	goat, IgG	1:1,000	Dianova	Hamburg, Germany
anti-ms IgM (Alexa 555)	goat, IgG	1:1,000	Life Technologies	Darmstadt, Germany
anti-rat IgG/IgM (Cy3)	goat, IgG	1:250	Jackson/Dianova	Hamburg, Germany
anti-rb IgG (Alexa 350)	donkey, IgG	1:1,000	Life Technologies	Darmstadt, Germany
anti-rb IgG (Alexa 488)	goat, IgG	1:1,000	Life Technologies	Darmstadt, Germany
anti-rb IgG (Alexa 555)	goat, IgG	1:1,000	Life Technologies	Darmstadt, Germany
anti-rb IgG (HRP)	goat, IgG	1:1,000	Pierce	Bonn, Germany
BTX (Alexa 555)	Taiwanese banded krait (*Bungarus multicinctus*)	1:500	Life Technologies	Darmstadt, Germany

5.9.2 Solutions for immunocytochemistry

Solution	Concentration	Dissolved in
DAPI	0.1 µg/ml	PBS
Mowiol 4-88	0.415 g/ml	$_{dd}H_2O$ + 1 g/ml Glycerol + 2 volumes of Tris-HCl (pH=8.5)
PFA	4%	PBS
Triton-X-100	10%	PBS

Blocking solution: HBSS (+Ca^{2+}/Mg^{2+}) + 10% FCS + 0.1% Triton-X-100 (if necessary)
Antibody solution: HBSS (+Ca^{2+}/Mg^{2+}) + 5% FCS + 0.1% Triton-X-100 (if necessary)

6. Methods

6.1 Cell culture methods

6.1.1 Cell culture coatings

Coating TC dishes with different matrices provides cells with specific substrata for growth and adherence and is conducted by standard protocols as follows (Lindl 2002).

Gelatine coating

TC dishes/plates are incubated with an accordingly sufficient volume of gelatine working solution at 37 °C for at least 30 min. The gelatine solution is immediately aspirated before usage.

Matrigel™ (MG) coating

Overnight, 1 ml aliquots of Matrigel™ are thawed on ice. The other day, this Matrigel™ stock is dissolved in 29 ml ice-cold DMEM/F-12 medium according to manufacturer's data sheet. Always using pre-cooled equipment, this working solution is sufficiently spread onto TC dishes/plates. Those are sealed with Parafilm and stored for 24 h at 4 °C. The Matrigel™ solution is removed directly before plating any cells.

Poly-L-ornithine (PO) coating

TC dishes/plates are incubated with an accordingly sufficient volume of PO working solution at 37 °C for at least 1 h. The PO working solution is aspirated and dishes washed with PBS twice. Optionally, additional matrix protein coating may be performed.

Fibronectin (Fn) coating

The Fn working solution is freshly produced by diluting Fn stock in PBS (2-10 µg/ml final concentration). PO-coated TC dishes/plates are incubated with an accordingly sufficient volume of Fn working solution at 4 °C for 24 h to obtain PO/Fn coating. Plates are wrapped in Parafilm during storage.

Laminin (Ln) coating

The Ln working solution is freshly produced by mixing Ln stock with PBS (2-10 µg/ml final concentration). PO-coated TC dishes/plates are incubated with an accordingly sufficient volume of Ln working solution at 4 °C for 24 h to obtain PO/Ln coating. Plates are wrapped in Parafilm during storage.

6.2 General cell culture methods

6.2.1 Cultivation of human fibroblasts

Human fibroblast cell lines are grown in T75 cell culture flasks in MEF medium with medium change every two to three days. When fibroblasts are 70-75% confluent cells are split starting with a singular rinsing with PBS. Then, cells are incubated with trypsin/EDTA working solution for several minutes at 37 °C. As soon as cells start detaching, the trypsinisation reaction is stopped by adding fresh MEF medium at the ratio 1:1. Cells are collected and centrifuged (1,200 rpm, 3 min, 4 °C). The pellet is resuspended in fresh MEF medium. In a specific split ratio, cells are distributed on new culture dishes/flasks in respect to the desired time period until cells should have reached 70% confluence again (Lindl 2002).

6.2.2 Cultivation of human myocytes

Human myocyte line hMC is a kind gift of Prof. Hanns Lochmüller (University of Newcastle, UK). Myocytes are grown in T75 cell culture flasks in MYO1 medium which is changed every day according to collaborator's instructions. Myocytes must not become ever confluent to avoid loss of myogenic potential. Therefore, cells are split by standard trypsinisation when myocytes are 70-75% confluent at the latest.

6.2.3 Cultivation of murine Schwann cells (SCs)

Murine Schwann cell line iMS32 is a kind gift of Rebecca Conrad/Dr. Michael Karus (University of Bochum, Germany). iMS32 is a spontaneously immortalised Schwann cell line isolated from long-term cultures of adult murine DRG and peripheral neurons and is cultivated accordingly (Sango *et al.* 2006): Schwann cells are grown on 10 cm cell culture dishes (PO-coated) in MEF medium with medium change every other day. Splitting occurs by standard trypsinisation when SCs reach confluence of approx. 80% (see 6.2.1).
For the generation of Schwann-cell conditioned medium (SC-CM), Schwann cells are grown on 10 cm cell culture dishes until they reach total confluence. Subsequently, cells are fed with 10-15 ml SC1 medium (Kwiatkowski *et al.* 1998). For one week, medium is harvested each day, pooled and sterile filtered (0.2 μm).

6.2.4 Cultivation of human iPSCs

Human iPSC lines are grown in 6-well cell culture plates (MG-coated) in mTeSR™1 medium with daily medium change. iPSCs are split by the following standard singularisation protocol when cells are 70-75% confluent (StemcellTechnologies Version 3.0.0): Each well is rinsed once with PBS. Then, 0.5 ml of warm (RT) alfazyme is added and cells are incubated at 37 °C for 5-7 min. When cells begin to loosen, the alfazyme is diluted by addition of 2-3 ml pre-warmed (37 °C) DMEM/F-12 medium. Detached iPSCs are washed off with this medium at once. After centrifugation (800 rpm, 3 min, 4 °C) the cell pellet is resuspended only once with a 5 ml serological pipette in mTeSR™1 medium supplemented with 10 μM ROCK inhibitor Y-27632 to promote single cell survival and transferred to new 6-well-plates in the same medium. This way, human iPSCs are regularly split at a ratio of 1:6-1:14.

6.2.5 Freezing & thawing

For long-term cryopreservation, cells are detached according to the respective splitting protocol. However, after the centrifugation step the pellet is resuspended in ice-cold freezing medium (see 5.8.1, Tab. 10) instead of cultivation medium (Lindl 2002). Immediately, the cellular suspension is filled in pre-cooled cryovials and transferred into freezing boxes for one day at -80 °C. For long-term storage, cryovials are kept in liquid N_2.

For thawing cells, fast warming up is required in a 37 °C water bath. Before the icy cell mass is totally molten, cells are quickly transferred into a 15 ml tube filled with 5 ml pre-warmed (37 °C) medium. After centrifugation (800-1,200 rpm, 3 min, 4 °C), the pellet is resuspended in the correspondent maintenance medium and cells are seeded on new cell culture dishes/flasks at the desired ratio.
To spare sensitive single iPSCs, only low rotation values are used. Furthermore, any iPSC medium is supplemented with 10 µM ROCK inhibitor Y-27632 during the thawing process to enhance single cell survival (Watanabe *et al.* 2007).

6.2.6 Cell counting

From a single cell suspension, a 1:10 or 1:100 dilution is made according to the original cell density (Lindl 2002). 20 µl of this dilution is thoroughly mixed with 20 µl trypan blue solution. A counting chamber is prepared with half of the mixture. Cells in at least three smaller squares in one whole square are counted whereas dead cells marked by bluish colour are ignored. The sum is averaged and the result describes the mean cell numbers x $\times 10^4$/ml volume.

6.3 Induction of pluripotency

6.3.1 Preparation of feeder-plated TC dishes

Frozen cryovials with irradiated murine embryonic fibroblasts (MEFs) are thawed in a 37 °C water bath (Lindl 2002). Quickly, cells are transferred in a 15 ml tube filled with pre-warmed (37 °C) MEF medium. After centrifugation (1,200 rpm, 3 min, 4 °C), the pellet is resuspended in warm MEF medium and cells are sowed on gelatine-coated TC dishes at a density 3×10^4 to 4×10^4 cells per cm².

6.3.2 Generation of 4F retroviruses

In order to introduce the reprogramming factors into target cells, suitable retroviruses have to be generated. Here, the human HEK293-derived retroviral packaging cell line 293-GPG was employed yielding high virus titres (Ory *et al.* 1996). 293-GPG already contains the retroviral *gag-pol* cluster for capsid formation and reverse transcription. The G-protein of vesicular stomatitis virus (VSV) as envelope protein conveys a broad tropism for efficient host infection. Modified from Koch *et al.*, 2011, 293-GPG cells are sown on gelatine-coated 10 cm TC dishes at a density 9.5×10^6 per dish in MEF medium supplemented with antibiotics (2 µg/ml puromycin, 300 µg/ml G418, 1 µg/ml doxycycline). The next day, transfection is performed by mixing 500 µl Opti-MEM + 9.5 µl retro-DNA plasmid containing one single reprogramming factor (2 mg/ml) + 47.5 µl FuGENE® HD transfection reagent. During 15 min incubation,

transfection reagent and plasmids form complexes. In the meantime, medium is changed on 293-GPG cells with Opti-MEM supplemented with 25 µM chloroquine. This quinoline derivate prevents lysosomal acidification. Hence, retro-DNA plasmid containing endosomes escape lysosomal degradation and release a higher amount of plasmids increasing infecitivity (Fredericksen *et al.* 2002). The transfection mix is gently distributed dropwise in every TC dish. Seven to eight hours later, MEF medium is added to every TC dish. The next morning, the medium is wholly changed with plain MEF medium.

After three days, retrovirus containing medium is harvested separately for each reprogramming factor for the first time and cells are fed with fresh MEF medium. Further harvests are conducted on the following two mornings. The supernatant containing the retrovirus is sterile filtered (0.45 µm cellulose acetate filter) and stored at 4 °C. First and second harvests are pooled. Eventually, the retrovirus harvests of every factor fraction are concentrated by ultracentrifugation (4 °C, 50,000 g, 90 min). The supernatant is thoroughly removed and the retrovirus pellet is carefully resuspended in 50 µl reflux. The four factor fractions are coalesced in a specific ratio (OCT4:SOX2:KLF4:c-MYC=1.5:1:1:0.5).

To rid the ultraconcentrate from cytotoxic precipitations, this retroviral ultraconcentrate is spun again (4 °C, 15,000 g, 10 min) and the remaining supernatant is cautiously gathered.

6.3.3 Infection of target fibroblasts with 4F retroviruses

Following protocol is adapted from (Koch *et al.* 2011). At least two hours before infection, 5×10^4 fibroblasts are plated in a 12-well plate in MEF medium supplemented with 10 ng/ml bFGF to enhance proliferation and thus nuclear invasion of retroviral transgenes later.

The 4F ultraconcentrate is filled up with cold MEF medium to 350 µl final volume and supplemented with 4 µg/ml polybrene. This cationic polymer neutralises cellular surface charge and fosters uptake of retroviral particles by counteracting putative repellent effects of surface epitopes like sialic acid (Davis *et al.* 2002). At last, the target fibroblasts are infected (day 0) by aspirating the old medium and adding the retroviral ultraconcentrate mixture ON. The next morning, retroviral medium is removed and plain MEF medium allows fibroblast to recover. In the afternoon, infection is repeated with freshly prepared retroviral ultraconcentrate (day 1). From day 2 onwards, infected fibroblasts are maintained in MEF medium. On day 6, 4F fibroblasts are transferred onto MEF feeder coated TC dishes and cultivated in iPSC medium for the next weeks until first iPSC colonies appear.

6.3.4 Infection of target fibroblasts via SeV spinfection

Following protocol is modified from (Aasen *et al.* 2008). One day before infection, 10×10^4 target fibroblasts are seeded on uncoated 24-well-plates in MEF medium. The following day, ¼ of original commercially purchased Sendai virus (SeV) vector stock (see manufacturer's instructions) is diluted in infection medium while MEF medium is aspirated. Per well, 500 µl of diluted SeV vector solution are added. Fibroblasts are spun in a centrifuge for 45 min at 32 °C with 1,500 g (spinfection). Cells are incubated further with viral infection medium overnight. The next five days, daily medium change is performed with pure infection medium (without virus).

6.3.5 Induction of pluripotency

Protocol is adapted from (Koch *et al.* 2011). At day 5 post-infection, SeV infected fibroblasts are trypsinised and split onto two 10 cm feeder-plated TC dishes (10×10^4 and 15×10^4 cells, respectively) in 10 ml iPSC medium. Excessive cells can be frozen.
During the following weeks, medium is changed every other day until the first hints of reprogrammed cells emerge, normally between day 21 and day 28. If necessary, up to ¼ of the original amount of feeder cells are seeded onto the 10 cm dishes replenishing dying feeder cells.

6.3.6 Generation of clonal iPSC lines

As soon as new iPSC colonies emerging on primary 10 cm TC dishes reach a certain size, they can be manually picked to obtain single clonal iPSC lines. At the horizontal hood, one appropriate iPSC colony with proper stem cell morphology is quartered by a syringe cannula. Afterwards, the surrounding feeder layer is carefully scratched off. With a 100 µl pipette tip, iPSC colony fragments are collected and broken down further by pipetting up and down in a 96-well-plate several times. At last, these iPSC colony fragments are transferred into a 4-well-plate (MG-coated) filled with mTeSR™1 medium supplemented with 10 µM ROCK inhibitor Y-27632.
If a new clonal iPSC line grows properly in a stable manner without spontaneous differentiation, it will be split on 6-well-plates (MG-coated) and expanded according to standard maintenance protocol.
Particularly young iPSC lines tend to spontaneously differentiate partly at early passages sometimes. To purify these lines, differentiated parts of iPSC colonies are scratched off by a 10 µl pipette tip under a microscope at the horizontal hood during regular maintenance culture. Alternatively, incubation time with alfazyme is reduced to just 2-3 min. Detached iPSCs are washed off very gently only once with DMEM/F-12.

6.4 Directed motoneuronal differentiation *in vitro*

Subsequent protocol steps are adapted from (Hu *et al.* 2009).

6.4.1 Embryoid bodies (EB) formation

Three to five wells of a 6-well-plate (70-80% confluence) iPSCs are detached by collagenase (1 mg/ml) treatment for 60-70 min. Instead of densely packed colonies, iPSCs form delicate and fragile layers under feeder-free maintenance conditions. So, colonies are only very carefully washed off using a 10 ml serological pipette and pre-warmed (37 °C) DMEM/F-12. Cells are spun down (800 rpm, 30 sec, 4 °C) and the pellet is carefully resuspended in 2 ml EB1 medium supplemented with 10 µM ROCK inhibitor Y-27632. Cellular fragments are transferred to a 10 cm-Petri dish into total 10 ml EB1 medium + 10 µM Y-27632. Every other day, medium is totally changed by collecting the EBs in a 15 ml tube, letting them slump and congregate at the tube bottom for approx. 5 min. The supernatant is carefully aspirated and EBs are gently resuspended in fresh EB1 medium with subsequent re-transfer onto the Petri dish.

6.4.2 Neural rosette formation

On day 6, EBs are equally plated onto four to six 6 cm TC dishes (PO/Fn-coated) per cell line in 2.5 ml N2 medium + 10 ng/ml bFGF + 2 µg/ml Fn + 5 µM SB431542 + 1 µM dorsomorphin. The next day, only supplements are added (10 ng/ml bFGF + 0.75 µM RA) in 200 µl N2 medium per dish. Subsequently, daily medium change is carried out with 2-3 ml N2 medium + 10 ng/ml bFGF + 0.75 µM RA.

6.4.3 Neurosphere formation

On day 13, neural rosettes are enzymatically isolated from surrounding differentiating, non-rosette cells (e.g. neural crest cells). Neural rosettes are rinsed once with HBSS. Treatment with dispase working solution for 2-3 min selectively detaches neural rosettes. By tapping the dish and carefully washing with N2 medium, neural rosettes can be collected and centrifuged (800 rpm, 30 sec, 4 °C). After removing the supernatant, pelleted rosettes are gently resuspended and transferred in NSP1 medium to a 10 cm Petri dish to promote neurosphere formation. Even though the dish surface is non-adherent, the next day some neurospheres settled as well as differentiating cells in particular. To keep these spheres also into suspension, the Petri dish is moderately tapped without detaching differentiated aggregates. Any floating neurosphere is collected in a 15 ml tube and allowed to sediment for 5 min. In order to minimise stickiness of neurospheres due to cellular debris, 1:100 DNase might be added optionally. Then, the supernatant is aspirated slowly and pelleted neurospheres are transferred to a new Petri dish in 10 ml NSP1. Every other day, medium is fully changed according to the aforementioned suspension culture techniques.

On day 19, neurospheres are mechanically broken into smaller fragments. After having pelleted neurospheres in a 15 ml tube, spheres are vigorously pipetted two to three times with a 1,000 µl pipette tip in 1 ml NSP1 + DNase (1:100). Moreover, further titruation occurs by pipetting twice with a glass Pasteur pipette. The entire cell suspension is transferred to a new Petri dish in 10 ml NSP1. Often, neurospherical fragments attach owing to this previous splitting step. Therefore, Petri dishes are moderately tapped to loosen neurospheres on the following day. Floating spheres are transferred to a new Petri dish in 12 ml NSP1. After this cleaning step, ⅔ of the medium are replaced the other day. Since then, a full medium exchange is performed every second day.

6.4.4 Plating neurospheres and final MN maturation

On day 27, neurospheres are sown for the final maturation step. Mature, fully pMN-domain patterned neurospheres are collected and pelleted in a 15 ml tube. The supernatant is removed and spheres washed once with PBS. Afterwards, structural integrity of those spheres is loosened by incubation in 500 µl accutase + 30 µM ROCK inhibitor Y-27632 (5 min, 37 °C). To dilute accutase and to minimise its enzymatic activity thereby, 1.5 ml N2 medium + DNase (1:50) is added. Manual titruation is performed by moderately pipetting two to three times with a 1,000 µl pipette tip and once with glass Pasteur pipette. This cellular suspension is briefly centrifuged (800 rpm, 4 °C) and the supernatant containing any debris is removed. Hence, spherical fragments are gently resuspended in MN1 medium + 10 µM ROCK inhibitor Y-27632 and adequately distributed to MG-coated 3.5 cm TC dishes (for RNA/protein extraction) or chamberslides (MG- or PO/Fn/Ln-coated; for immunocytochemical stainings). Medium change is conducted at least every other day with an appropriate volume of MN1

medium (500 µl-1 ml with chamberslides; 2-4 ml with 3.5 cm dishes). In addition, it is recommendable to equilibrate MN1 medium beforehand by aseptically putting the medium in any TC dish in the cell culture incubator for 1 h (37 °C, 5% CO_2) as it is regularly done in this study.

6.5 Preparation of teratoma assay

Teratoma assay is adapted from (Takahashi *et al.* 2007). From one well of a 6-well-plate (80-90% confluence) iPSCs are detached by collagenase (1 mg/ml) treatment for 60-70 min. Cells are carefully washed off with pre-warmed (37 °C) DMEM/F-12 medium according to the EB formation procedure and centrifuged (800 rpm, 3 min, 4 °C). The supernatant is removed; the pellet is gently resuspended in 500 µl PBS to keep cells as bigger clumps and stored on ice. Cell clumps are injected in 10 µl liquor into the right testis capsule of six- to eight-weeks-old male SCID/Beige mice by Anke Leinhaas in the Haus für Experimentelle Therapie (HET), University of Bonn.
Between six to eight weeks after transplantation, the mice are sacrificed. Any tumour is surgically removed and fixed in a 4% PFA solution for at least one week. Afterwards, teratomas are dehydrated, embedded in paraffin and cut into sections of 7 µm thickness by Kristina Hupperich or Andrea Hoffmann. Standard eosin/haematoxylin staining is performed by 30 min incubation in xylol for de-paraffinisation. Then, sections are incubated in ethanol baths of decrementing concentrations (100%, 96%, 70%, 50% for 3 min each) and quickly rinsed in PBS. After 1 h incubation in H_2O, the sections are stained in haematoxylin for 6 min and washed in H_2O for 15 min afterwards. To remove redundant dye, the sections are briefly washed in H_2O and subsequently stained with eosin for 1 min. Thereafter, sections are purged in H_2O several times (6-7 ×), dehydrated in incrementing ethanol concentrations. Finally, tissue sections are air dried, embedded in Entellan® and histologically analysed.

6.6 Undirected differentiation of iPSCs into three germ layers

Protocol is adapted from (Itskovitz-Eldor *et al.* 2000). To induce spontaneous differentiation in human iPSCs, three to four wells of a 6-well-plate (70-80% confluence) iPSCs are detached by collagenase (1 mg/ml) treatment for 60-70 min. According to EB formation procedure, colonies are softly washed off and centrifuged. The pellet is carefully resuspended in 2 ml EB2 medium and cell clumps are transferred to a 10 cm-Petri dish into total 10 ml EB2 medium. Every two days medium is wholly changed. After six days, EBs are equally sown out in total 2 ml medium onto 3.5 cm cell culture dishes (gelatine-coated in MEF medium; PO/Fn-coated in EB2 medium) to promote either meso- and endodermal or neuroectodermal outgrowth, respectively. Cells are cultivated for further ten days with full medium change every other day and are then immunocytochemically analysed.

6.7 Generation and cultivation of smNPCs

Generating an appropriate neural precursor subpopulation massively shortens the time period of motoneuronal differentiation compared to the EB-based run-through protocol. Reinhardt *et al.* introduced human iPSC-derived, small molecule induced neural precursor cells (smNPCs) last year (Reinhardt *et al.* 2013).

Adapted from the published protocol, iPSC colonies are detached by collagenase treatment and transferred to a non-adherent Petri dish in smEB1 medium + 10 µM ROCK inhibitor Y-27632 + 0.5 µM LDN193189 + 10 µM SB431542. After two days, medium is changed omitting Y-27632. On day 4, dual SMAD-signalling inhibition is stopped by withdrawing LDN193189 and SB431542. Finally, EB-like spheres are collected and mildly chopped by titruation. Spheric fragments are plated on MG-coated dishes in smNPC1 medium + 10 µM ROCK inhibitor Y-27632. Soon, progenitor cells commence proliferating adherently.

Moreover, the original generation protocol was modified by Beatrice Weykopf and Dr. Michael Peitz to a fully adherent protocol for which iPSCs are grown in mTeSR™1 medium to approx. 70% confluence. Medium is switched to NPC1 plus 10 µM SB-431542 Inhibitor and 1 µM dorsomorphin, respectively for the following four days. Then, cells are detached by alfazyme treatment (5-7 min, 37 °C), washed off with NPC1 medium and spun down (1,000 rpm, 3 min, 4 °C). Finally, cells are split in a 1:8-1:10 ratio onto new MG-coated plates in NPC1 medium plus 10 µM ROCK inhibitor Y-27632. Both generation protocols are carried out with all cell lines in parallel.

After five passages, smNPCs are regularly growing stably. Then, medium is switched to NPC1 containing a higher portion of B27-RA and N2 Supplement thus allowing administration of a higher Pur concentration (1 µM). Expansion of smNPCs is conducted by further propagating cells up to 70% confluence. Regular splitting is carried out as described above in a ratio of 1:8-1:12 in NPC1 medium. NPC1 medium is changed every other day.

In order to pre-pattern smNPCs towards a ventral-caudal fate, 1 µM RA and 1 µM SAG are added to NPC1 medium with daily medium change.

6.8 Motoneuronal differentiation on smNPCs

Based on the original protocol by Reinhardt *et al.*, 2013, a modified MN differentiation protocol was developed with Dr. Michael Peitz and Johannes Jungverdorben. To differentiate smNPCs into MNs, smNPCs are seeded onto 6-well plates (PO/Ln-coated) in NPC1 medium. Once cells reach 70% confluence, medium is changed to NPC2 medium initiating motoneuronal patterning for the next seven days. On day 7, cells are singularised by alfazyme treatment (5-7 min, 37 °C). Bigger cell clumps are retained by a cell strainer (40 µm). 150,000 single cells per well of a chamberslide (PO/Ln/Fn-coated) are plated in NPC3 medium plus 10 µM ROCK inhibitor Y-27632 for final maturation during the following weeks. At least two million cells are sown on 3.5 cm-dishes (PO/Ln/Fn-coated) for harvesting RNA or protein. Medium is changed the next day. To thrust progenitor cells into motoneuronal differentiation, 10 µM notch-signalling inhibitor DAPT is added from d8-d12. Moreover, 0.5 mM Pur and 50 nM RA are subjoined to NPC3 medium from d8-d15 to ensure proper maturation of potentially present pMN-patterned progenitor cells. NPC3 medium is changed every other day. Motoneurons are matured until day 27 for three weeks in total.

6.8.1 Plating MN-primed smNPCs for growth cone assay

For precise measurement of axonal length or of growth cone architecture, special seeding technique is applied to avoid a tangled neuronal network in mature MN cultures which might impair further analyses adapted by Beatrice Weykopf from Tomishima *et al.* (Tomishima 2012). For this purpose, 75,000 MN-primed smNPCs are seeded to previously prepared chamberslides (PO/Fn/Ln-coated) of which the coating solution was aspirated beforehand.

The coating of those chamberslides is allowed to become touch dry under a sterile laminar flow hood for 10-15 min before usage.

In a single drop, the cells are set amidst in each chamberslide well, very cautiously put into the incubator and let sit for 10 min at least. Without any mechanic disturbance, the cells adhere to the coating matrix so that the wells can be flooded by 500 µl NPC3 medium + 10 µM ROCK inhibitor Y-27632 afterwards. Like regular MN cultures, medium is changed every other day. Punctiform plating enables coronal outgrowth of neurites and axons to the periphery.

6.9 Motoneuron-myotube co-culture *in vitro*

Based on previous protocols (Guo *et al.* 2011; Stockmann *et al.* 2011), the present co-culture technique was developed. Similar to the seeding procedure on day 27 (see 6.4.4), MN neurospheres are plated on 3.5 cm cell culture dishes (PO/Ln) and cultivated for the next nine days in MN maturation medium.

In parallel to this motoneuronal pre-maturation, human myocytes are seeded on 3.5 cm cell culture dishes (MG-coated) and grown until they reach nearly 90% confluence. Since that time, MYO1 medium is replaced by MYO2 medium to induce myocyte differentiation with subsequent syncytial myotube formation during the following four to six days under low-serum conditions.

On day 36, plated neurospheres are transferred *en bloc* atop differentiated myotubes. Therefore, medium is aspirated and neurospheres are incubated in 1.5 ml pre-warmed (37 °C) HBSS ($-Ca^{2+}/Mg^{2+}$) for 10 min. By gentle tapping, neurospheres detach and can be collected. 1 ml N2 medium + B27-RA (1:100) + DNase (1:100) is added. To separate the sticky neurospheres, cells are gently pipetted two to three times with a 5 ml serological pipette. Spheres are allowed to accumulate for several minutes before equally distributing those spheres on 3.5 cm cell culture dishes with myotubes whose medium was replaced in the meantime with Schwann-cell conditioned medium (see 6.2.3). Co-cultures are ideally cultivated for up to seven weeks or longer with medium change every two to three days.

6.10 Microbiological methods

6.10.1 Isolation of retro-DNA plasmids

Sufficient retro-DNA plasmids were kindly provided by Viola Poppe. To produce retro-DNA plasmids, 5 ng of each plasmid (pMXs-hOCT4, pMXs-hSOX2, pMXs-hKLF4, pMXs-hc-Myc) is added to 100 µl bacterial solution of heat-shock competent *E. coli* DH5α (in LB medium + 10% polyethylene glycol 400 + 5% DMSO + 50 mM $MgCl_2$ pH 6,5) and rested on ice for 20 min. Hereafter, the plasmids are incorporated via heat induction (42 °C, 40 sec). Immediately, bacteria are placed back on ice. After 2 min, they are dissolved in 900 µl SOC medium (RT) and shook for 1 h at 37 °C. Thereafter, transformed bacteria are centrifuged (RT, 10,000 rpm, 5 min). The supernatant is carefully removed and the pellet is resuspended in 100 µl reflux. Bacterial suspension is spread on LB-agar plates plus 100 µg/ml ampicillin and incubated ON at 37 °C.

The next morning, emerging bacterial colonies were positively selected for incorporated retro-DNA plasmids by Amp[r]. One distinct colony is picked and used for inoculation of 300 ml LB medium plus 100 µg/ml ampicillin. After one night shaking at 37 °C, bacterial suspension is

collected and spun down (4 °C, 4,500 g, 15 min). Retro-DNA plasmids are isolated by Plasmid Maxi Preparation Kit (Qiagen) according to manufacturer's instructions.

6.11 Molecular-biological methods

6.11.1 Polymerase chain reaction (PCR)

To amplify definite DNA fragments, PCR is a very productive and exact method due to its primer-mediated high specificity (Mullis *et al.* 1986). For this purpose, the DNA sequence has to be known in order to generate oligonucleotide primers flanking the DNA region of interest.

A typical PCR approach is prepared on ice and composes of the following:

Primer mix (3.3 µM)	1 µl
PCR super mix (2 x)	12.5 µl
$_{dd}H_2O$	10.375 µl
Template (cDNA/gDNA)	1 µl
GoTaq-Polymerase (5 U/µl)	0.125 µl
	25 µl

First, the DNA template turns into single stranded DNA owing to heating up the mixture to 95 °C (denaturation). Second, subsequently cooling the mixture to a definite temperature – usually 2-5 °C below T_m of the primers – enables the oligonucleotide primers to anneal specifically to the DNA template (annealing). Third, the temperature is risen again to the value of optimal working activity for the heat-stable Taq-polymerase which uses the final primer base as starting point for the synthesis of the complementary DNA strand (elongation). By cyclic repetition, the amount of target DNA is amplified exponentially.

For the house-keeping gene *GAPDH*, PCR program is as follows:

Initial denaturation	95 °C	5 min	
Denaturation	95 °C	30 sec	
Annealing	60 °C	30 sec	30 cycles
Elongation (1 min/kb)	72 °C	1 min	
Final elongation)	72 °C	5 min	

For all other trancripts, cycle number is elevated to 35.

6.11.2 Agarose gel electrophoresis

The functional principle of agarose gel electrophoresis is the size-dependent separation of DNA fragments by migration through a polymeric agarose matrix in an electric field. Since the deoxyribose-phosphate backbone of DNA is negatively charged, DNA always migrates towards the positive pole (cathode) in an electric field.
To check for the amplification success of PCRs or the expression rate of specific mRNA transcripts in a semi-quantitative Reverse Transription (RT)-PCR, samples are analysed via agarose gel electrophoresis. 1.2% agarose gels supplemented with 0.1 µl ethidiumbromide per ml gel are run in TAE buffer.

Loading dye is already included in PCR samples. 15 µl of each PCR sample is applied to every gel slot. Gel electrophoresis runs for 30-40 min at 100 V. Documentation and analysis are done at the BioRad ChemiDoc XRS with program Quantity One.

6.11.3 Isolation of DNA

Genomic DNA (gDNA) of iPSCs is isolated from one well of a 6-well-plate (65-75% confluence) by DNeasy Blood & Tissue Kit (Qiagen) according to manufacturer's instructions. Elution is done with first 50 µl TE^{-4} and second 80 µl TE^{-4} and 5 min incubation time each. Samples are stored at -20 °C.

The concentration of nucleic acids is determined by spectrophotometric measurement. 1 µl of each sample is measured at "Nanodrop" spectrophotometer with solvent as blank sample. Particular attention has to be paid whether the wave length ratios for protein contamination (260/280: ≥ 1.8) and organic reagents contamination (260/230: ≥ 2.0) fulfil purity criteria.

6.11.4 SNP-array

The maintenance of genomic integrity during the reprogramming process is verified by SNP-array analysis. From every iPSC clone gDNA is isolated and 50 µl (60 ng/ml) are processed for whole genome amplification. The amplified DNA is fragmented and hybridised to sequence-specific oligomers bound to beads on an Affymetrix® Genome-Wide Human SNP Array 6.0 for HGK13 and HGK16 by Prof. Peter Nürnberg at Cologne Centre of Genomics (CCG). All other iPSC lines are processed by an Illumina® Human610-Quad chip or a HumanCytoSNP-12 chip in the Institute of Human Genetics, University of Bonn. Data analysis is conducted with Illumina® BeadStudio.

6.11.5 Isolation of RNA

Whole RNA is isolated by RNeasy Blood & Tissue Kit (Qiagen) according to manufacturer's instructions. Cells are washed once with HBSS and any liquor is removed thoroughly. Lysis buffer is supplemented with β-mercaptoethanol (1:100 = 120 mM) to reduce sample-intrinsic RNase activity.

Digestion of contaminating gDNA is performed directly on extraction columns by DNase I treatment. Total RNA is eluted first by 50 µl $_{dd}H_2O$ and 5 min incubation time. Second elution occurs with first eluate plus 20 µl $_{dd}H_2O$ extra. Samples are stored at -80 °C and always thawed on ice due to higher degradation sensitivity of RNA. Sufficient concentration is verified by spectrophotometric determination (see 6.11.3) and for higher precision by using the Quant-iT™ RiboGreen® RNA Assay Kit according to the manufacturer's instructions. The fluorescent dye solely emits light if bound to RNA. Therefore, the fluorescence intensity directly correlates to the sample's RNA concentration. The assay is always conducted as triplicates in black 96-well-plates and analysed with the TECAN Safire2 microplate reader.

6.11.6 Synthesis of cDNA

RNA has to undergo reverse transcription into a single cDNA strand, because RNA is not capable of serving directly as template for a quantitative real-time (qRT)-PCR. 2 µg of total

RNA are subjected to reverse transcription with Bio-Rad iScript™ kit according to manufacturer's manual. The cDNA is diluted (1:5) with $_{dd}H_2O$ and used for RT-PCR applications. Alternatively, whole RNA is re-transcribed to cDNA by QuantiTec Reverse Transkriptase Kit according to manufacturer's instructions. In addition, to ensure exclusive mRNA transcription, oligo-dT primers binding to the mRNA-specific poly-A tail are utilised. For the individual samples 300 ng of total RNA are transcribed in a volume of 20 µl. From the defined standard 600 ng of total RNA are transcribed in a volume of 20 µl. cDNAs are diluted in a ratio of 1:5 in TE^{-4}, after all.

6.11.7 Quantitative real-time PCR (qRT-PCR)

Real-time RT-PCR is carried out in order to quantitatively determine the amount of mRNA transcripts. A typical qRT-PCR approach is prepared on ice and is composed of the reagents as mentioned for a PCR with cDNA as template (see 6.11.1).
The qRT-PCR is performed and analysed in the iCycler with the following parameters:

Initial denaturation	95 °C	5 min
Denaturation	95 °C	1 min
Annealing	60 °C	1 min
Elongation (1 min/kb)	72 °C	40 sec
Final elongation	72 °C	5 min
Melting curve	from 65 °C to 99 °C in 0.1 °C/sec increment	

40 cycles (Denaturation, Annealing, Elongation)

All experiments are done as triplicates. Expression levels are normalised to *GAPDH* expression level.

Alternatively, qRT-PCR and its subsequent analysis are performed at the LightCycler with FastStart DNA Master SYBR® Green. First, a standard has to be defined by mixing 16 µl with 24 µl of TE^{-4} properly. Then, the standard solution is diluted eight times in a ratio of 1:2 to obtain nine dilutions, at last. 3 µl of the diluted sample as well as the standard samples are needed in a standard qRT-PCR on a LightCycler 1.5 instrument using Fast Start DNA Master SYBR® Green I with the following reaction approach:

Primer ff (10 pmol/µl)	1 µl
Primer rev (10 pmol/µl)	1 µl
Fast start DNA Master mix	0.83 µl
$_{dd}H_2O$	2.7 µl
MgCl$_2$	1.2 µl
Template (cDNA)	1 µl
Polymerase	0.27 µl
	8 µl

All annealing temperatures used in qRT-PCRs are in accordance with the values of 5.5, Tab. 6. Experiments are conducted in triplicates all the time. Second derivative maximum method of the LightCycler software is operated for analyses. Expression levels are normalised to total RNA expression level.

6.12 Protein-biochemical methods

6.12.1 Isolation of protein

To isolate total protein, cells are washed once with HBSS and any liquor is removed thoroughly. On ice, 120 µl RIPA buffer are applied and incubated for 15 min. Then, cells are scratched off using a cell scraper, transferred to a 1.5 ml reaction tube and several times mechanically titruated by vigorous pipetting and vortexing. After further 15 min incubation on ice, cells are centrifuged (12,000 rpm, 15 min, 4 °C) to pellet insoluble cellular debris. Supernatant is carefully collected and frozen (-80 °C).

Sufficient concentration is verified by colorimetric determination according to Bradford (Bradford 1976). Bradford dye is able to bind to proteins whereupon their absorption maximum is shifted from 470 to 595 nm. 498 µl Bradford solution is mixed with 2 µl protein lysate and incubated for 10-15 min at RT. 50 µl of each sample are transferred to cuvettes and protein concentration is determined at the BioPhotometer with pure Bradford solution as blank. The final protein concentration is calculated by means of comparison to a BSA standard curve and divided by 2.

6.12.2 SDS polyacrylamide gel electrophoresis (SDS-PAGE)

The protein content of cells can be investigated by SDS-PAGE. Proteins migrate with varying speed in an electric field through a meshwork of polymeric acrylamide threads. The SDS excessively sets a negative charge to proteins which cloaks the intrinsic charge and enables a separation depending on size and weight (Laemmli 1970).

Protein-biochemical experiments were supportively conducted by Kristina Hupperich and Irmgard Hölker. In general, 7.5-10 µg protein are prepared for a SDS-PAGE sample. The corresponding volume of protein sample is added to 5 µl 2 × Laemmli buffer. The mixture is denaturated (5 min, 95 °C) to unfold proteins, briefly chilled on ice and shortly centrifuged. The total sample volume is filled into the gel slots.

After having assembled the glass panels (0.5 mm thickness) to the chamber scaffold, the acrylamide gel is ready to be cast. Firstly, the so called lower "separation gel" solution (10%) is prepared. When the solution is filled into the casting chamber, some water is added on top to generate an even rim line. As soon as this lower gel has hardened, the water layer is removed and the upper "stacking gel" solution (3%) is prepared and cast on top of the lower gel. Directly, the slot comb is put into the still liquid upper gel solution. Upper and lower gels differ in pore size and pH. The upper gel contains only little PAA leading to bigger pores and enabling the proteins to move easily between a dipolar front of glycine and Cl⁻-ions until all SDS-protein molecules accumulate at the borderline of the two gels. As soon as the molecule front enters the lower gel, glycine disperses owing to the increased pH. Thereupon, the SDS-protein molecules are free to migrate through a denser PAA network in the lower gel according to their size difference.

When the upper gel has polymerised, the gel is put into the running chamber which is filled with 1 × running buffer. The comb is drawn so that the slots fill with running buffer.

Every protein sample is loaded into one slot cautiously. PAGE Ruler Plus protein ladder is loaded to one lane to estimate protein size. The gel is run for 30 min at 50 V until the colour front reaches the separation gel and later for approx. 3 h at 70 V.

6.12.3 Western blotting

Western blotting describes the transfer of electrophoretically separated proteins from a polyacrylamide gel to a nitrocellulose membrane. The proteins migrate in an electric field to the wet membrane thereby copying the original separation pattern.

After the SDS-PAGE, the blotting device is equipped with pieces of Whatman paper and sponge pads which were soaked in $1 \times$ transfer buffer beforehand. The gel is stapled between sponge pad, wet Whatman paper pieces and the nitrocellulose membrane also pre-wetted in $1 \times$ transfer buffer. To remove possible air bubbles, a pipette is rolled over the sandwich. Finally, the sandwich is inserted into the blotting device. A cooling pack is added, everything closed and put into the running chamber filled with $1 \times$ transfer buffer. The blotting takes place ON (30 V, 4 °C).

6.12.4 Immunoblotting

The next morning, the nitrocellulose membrane is washed 5 min in $1 \times$ TBS/Tween. To saturate any unspecific binding site, the membrane is incubated for at least 3-4 h in blocking solution ($1 \times$ TBS/Tween + 6% skimmed milk powder). Afterwards, the primary antibody is applied ON in $1 \times$ TBS/Tween + 1.5% skimmed milk powder. The other day, the membrane is washed five times in $1 \times$ TBS/Tween. Next, the membrane is incubated in the secondary antibody solution ($1 \times$ TBS/Tween + 1.5% skimmed milk powder) for 1 h. Again, the membrane is washed five times in $1 \times$ TBS/Tween. Subsequently, the immunoblot is developed for 5 min in a chemiluminescent reaction with SuperSignal® West Pico Chemiluminescent Substrate kit. The membrane is carefully wrapped in plastic foil, placed in a developing cassette and exposed to Hyperfilm ECL. Densitometric analysis of the films is performed with ChemiDOC XRS analysis software.

When β-actin is applied as loading control, the primary antibody is incubated only for 10 min.

6.13 Immunocytochemistry

For immunocytochemical analyses, cells are rinsed once with HBSS (always +Ca^{2+}/Mg^{2+}), fixed in a 4% PFA solution for 10 min at RT and again washed with HBSS twice. Alternatively, cells are fixed by adding an appropriate volume of 8% PFA solution directly to the medium to obtain a final concentration of 4% PFA. For ChAT-staining, addition of 0.2% picric acid to the PFA fixation solution is recommended to decrease unspecific background noise (Hu *et al.* 2009). For co-localisation studies in growth cones, samples are fixed with 4% PFA/4% sucrose (37 °C) vibration-free for 10 min at RT (Dr. Min Jeong Kye, personal communication).

In order to block any unspecific binding sites, samples are next incubated in blocking solution for at least 1 h at RT. Samples are usually processed in a serial manner, i.e. the primary antibody (5.9, Tab. 14) is added separately in an appropriate dilution in antibody solution overnight at 4 °C. The next morning, specimens are washed three times with HBSS. The corresponding secondary antibody (5.9, Tab. 15) is then administered in antibody solution for 1 h at RT (dark). Again, samples are washed three times with HBSS and nuclear staining is performed by addition of DAPI solution for 2-3 min at RT (dark). At last, samples are washed twice with HBSS, mounted in Mowiol 4-88 solution and covered with glass covers. Stained samples are stored at 4 °C in the dark.

6.14 Microscopy

Immunocytochemical stained samples are further analysed using Zeiss microscopes (objectives 10 ×, 20 ×, 63 ×) in bright field or suitable fluorescence channels (excitation wavelengths: 335-383 nm, DAPI; 450-490 nm, GFP; 538-562 nm, Ds Red). Pictures are taken with Openlab, Axiovision or ZEN program and further processed by Photoshop if necessary.

For quantitative analysis, 7-10 pictures are randomly chosen. In each image section, the total number of vital cells is ascertained by counting DAPI$^+$ nuclei whereas the number of neurons is determined by β III-tubulin$^+$ cells. Then, the structures of interest (e.g. HB9$^+$ motoneurons or gems) are quantified and their number is computed as ratio of positive cells relative to total cells or total neurons (day 8: HB9: 1,200-2,000 cells; ISL1: 1,400-2,400 cells in total; day 27: HB9: 800-1,700 cells; ISL1: 300-900 neurons in total).

For gem quantification, gems are counted and their ratios calculated relative to total number of nuclei. Fibroblasts: 150-300 cells in total; iPSCs: 950-1,300 cells in total; smNPCs: 1,200-1,700 cells in total; MN cultures: 300-450 cells (day 8) and 200-550 cells (day 27) in total.

For neurite length measurement, outgrowth of SMI-32$^+$ cells or β III-tubulin$^+$ protrusions of HB9$^+$ or ISL1$^+$ motoneurons are manually surveyed starting from the soma until the neurite tip by "spline curve" analysis tool. Normally, 90-160 neurites are counted for β III-tubulin$^+$ neurons and on average 30-60 neurites for SMI-32$^+$ neurons, respectively.

Properly shaped growth cones are sought out in three weeks old MN cultures on day 27 (see 6.8.1). In total, ten growth cones are visualised by confocal laser scanning microscopy so far using Zeiss Meta 510 microscope in the Imaging Facility of the Cluster of Excellence in Cellular Stress Responses in Aging-associated Diseases (CECAD, Cologne, Germany) with assistance of Dr. Astrid Schauss and Ira Hensen. Pictures are taken with ZEN program and further analysed by Fiji program.

6.15 Statistical methods

Statistical significance of measurements are determined by GraphPad Prism software. Countings from immunocytochemical staining and expression rates from molecular-biological experiments are expressed as mean values ± SEM. D'Agostino-Pearson omnibus normality test determines non-Gaussian distribution of values. Thus, all data are analysed by Kruskal-Wallis non-parametric ANOVA test with Dunn's *post hoc* correction for multiple comparisons. Data is compared to single healthy control r1, single healthy control r12 or pheno-grouped healthy controls r12 and COII.2, respectively. Differences are considered significant when $p < 0.05$. Levels of statistical significance were pictured as asterisk and distinguished as follows: $p < 0.05$ = *, $p < 0.01$ = ** and $p < 0.001$ = ***.

7. Results

7.1 Induction of pluripotency

The original strategy to induce somatic conversion into pluripotent stem cells involves a retrovirally mediated transfer of the classical four Yamanaka-factors (OCT4, SOX2, KLF4, c-MYC) by pMXs-based vectors in human adult cells (see 10.3) (Takahashi *et al.* 2006; Takahashi *et al.* 2007).

Human fibroblast cell lines ML17 (SMA I, VPA responder), ML73 (SMA II, VPA non-responder) and family 1 discordant siblings ML101 (asymptomatic) and ML102 (SMA III) were reprogrammed that way at iPierian Inc. (San Francisco, USA) by Dr. John Dimos. Only one non-validated clone per cell lines was delivered (see 5.8.3, Tab. 13). Furthermore, healthy control cell line r1 was generated this way by retroviral transduction and validated by Matthias Brandt at the Institute of Reconstructive Biology (RNB, University of Bonn). There, control line r12 was generated by Dr. Michael Peitz and fully characterised by Johannes Jungverdorben (Koch *et al.* 2011). In addition, control cell line COII.2 was generated and validated by Swetlana Ritzenhofen at RNB (unpublished data).

Not only is generation of sufficient retrovirus a time-consuming elaborate process, but also does this method not always yield an appropriate number of iPSC colonies. Numerous attempts to reprogram human fibroblast cell lines of SMA discordant family 2 asymptomatic members (ML11, ML13) and SMA III patients (ML12, ML14) (Fig. 10) via retroviruses did not result in stable iPSC lines (data not shown). Moreover, random insertion of retroviruses into the human host genome does not necessarily lead to a complete silencing of those proviral transgenes (Takahashi *et al.* 2006). Thus, incomplete silencing in iPSCs may cause further problems during subsequent differentiation processes.

To avoid the aforementioned difficulties, non-integrative reprogramming techniques promised better results. In 2009, Fusaki and colleagues reported Sendai virus (SeV) based vectors which are merchandised by DNAVEC Corp. (Tsukuba, Japan) (Fusaki *et al.* 2009). This SeV system derives from an unsegmented (-) ssRNA virus from the *Paramyxoviridae* family performing a cytoplasmatic replication cycle. So, neither a DNA-intermediate nor integration into the host genome occurs. The SeV vectors are simply diluted over time due to cellular division. SeV vectors are non-transmissible in cellular systems and devoid of fusion-inducing factors (F-protein deficient) thereby possessing only little cytotoxicity (Inoue *et al.* 2003).

After all, SeV vectors turned out to be the most reliable reprogramming system in our hands transforming even cell lines which proved to be reluctant to retroviral reprogramming before. Human fibroblast cell lines from discordant family 2 (ML11, ML12, ML13 and ML14) were reprogrammed by SeV vector system (Fig. 11; 10.4, Fig. 64). When target fibroblasts underwent spinfection with SeV vectors containing the four Yamanaka factors (4F), some dead cells were visible afterwards on account of mechanic or infection-conditional stress. However, the overall viability was not massively impaired since vital fibroblasts with typical longish spindle-like shape and undisturbed adherence behaviour were visible in two representative cell lines (Fig. 12). In addition, the surviving fibroblasts still proliferated.

Infected fibroblasts were transferred to feeder-prepared primary plates after six days. Within the next three to four weeks, dozens of early iPSC colonies appeared on primary 10 cm TC dishes. Nevertheless, SeV-mediated reprogramming did not always induce transformation of fibroblasts into pluripotent SCs successfully. Colonies disintegrated or began to transform into immensely proliferative cell types marked by differentiated cellular morphology particularly

in the colony's rim area. Furthermore, a three-dimensional growth with brown or yellow cells was apparent (Fig. 13 **A**). On the contrary, proper iPSC colonies were denoted by round colony form and distinct clearly defined rims (Fig. 13 **B**).

Pedigree of discordant family 1
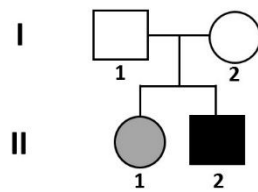
	II.1	II.2
Fibroblasts	ML101	ML102
iPSCs	HGK16	HGK13
SMN1/SMN2 copies	0 / 3	0 / 3
PLS3 ↑ (in blood)	+	–

Pedigree of discordant family 2
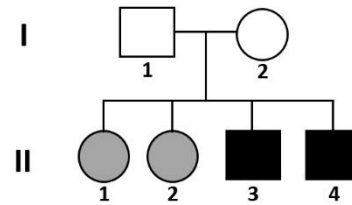
	II.1	II.2	II.3	II.4
Fibroblasts	ML13	ML11	ML12	ML14
iPSCs	HGK28	HGK21	HGK27	HGK22
SMN1/SMN2 copies	0 / 4	0 / 4	0 / 4	0 / 4
PLS3 ↑ (in blood)	+	+	–	–

Fig. 10: Pedigrees of PLS3 discordant family 1 and family 2 presenting SMA III affected brothers (black quadrats) and asymptomatic sisters (grey circles). Roman numbers defined parental and filial generations, respectively. Age of onset in HGK27 was 13 years and in HGK22 18 years. Table below denoted corresponding fibroblast and iPSC lines, respectively. Additionally, *SMN1* and *SMN2* copy number was given as well as lifted (↑) PLS3 expression levels in blood.
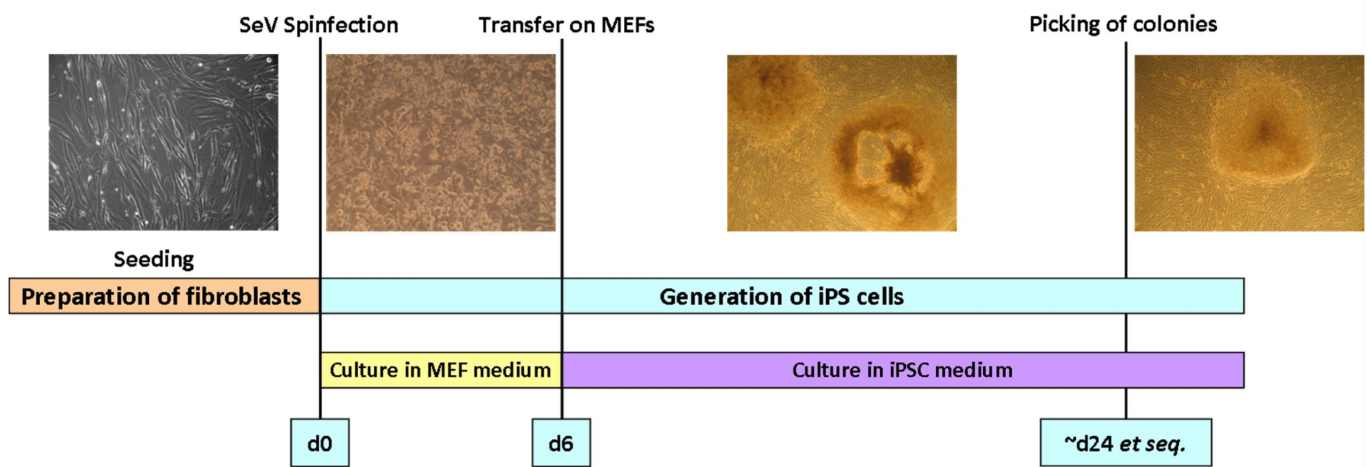
Fig. 11: Schematic picture of generation of iPSCs via reprogramming human fibroblasts by SeV spinfection. Target fibroblasts were seeded several days before infection. On day 0, fibroblasts were infected once by spinning SeV containing medium onto target fibroblasts (spinfection). After one week further culturing in MEF medium, 4F-fibroblasts were transferred onto feeder-plated TC dishes in iPSC medium on day 6. Since then, cells were fed with iPSC medium. Within the next weeks, 4F-fibroblasts reprogrammed to iPSC colonies which were picked, after all.
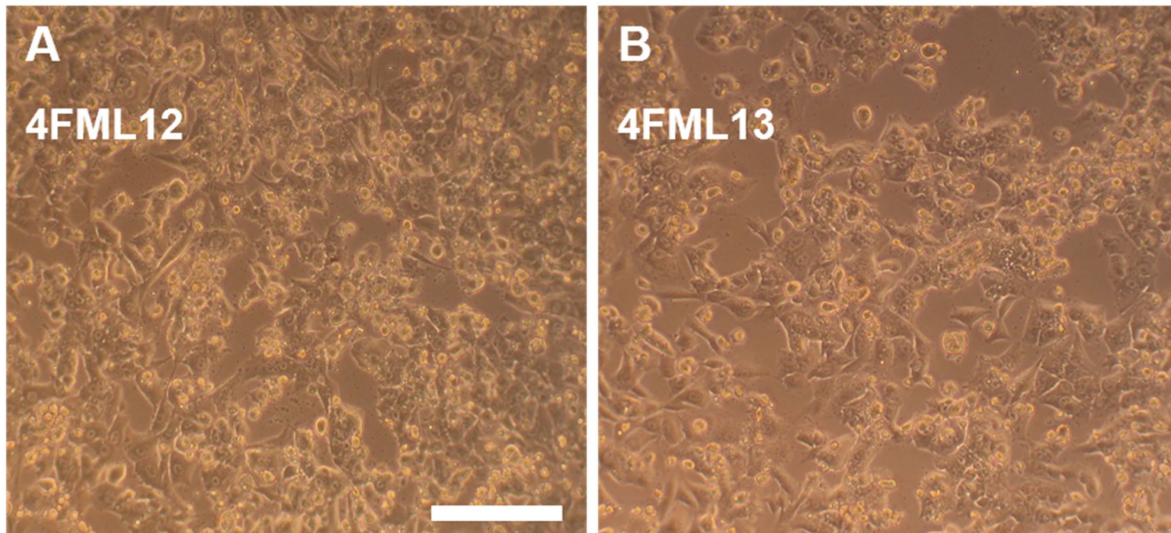
Fig. 12: Representative phase image of fibroblast cell lines three days after viral infection with four Yamanaka factors (4F) SeV representing a male SMA III patient (**A**) and his asymptomatic sister (**B**) from PLS3 discordant family 2. Cells sustained spinfection and exhibited viability and proliferation activity (scale bar 200 µm, valid for all images).
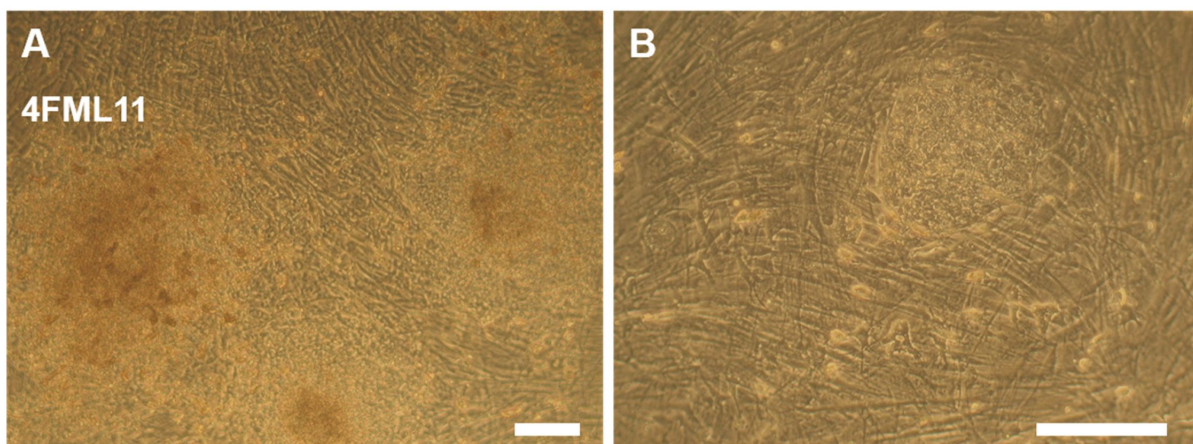
Fig. 13: Representative phase images of transferred 4F fibroblasts. (**A**) Improper iPSC colonies from infected fibroblast cell line 4FML11 on primary TC plates displayed irregular shape with differentiated cells at the rim and coloured overgrowth. (**B**) Proper iPSCs were marked by typical ESC-like appearance including defined round colony formation, small cell size and dense cellular package (scale bar 200 µm).

In total, 16-18 new iPSC clones per individual cell line were picked, stabilised and expanded (see 10.1, Tab. 19). From these, two to three clones per cell line were selected to undergo further characterisation.

HGK1, HGK4, HGK13 and HGK16 as well as healthy control lines r1 and r12 had initially been cultivated on MEF feeder layer in iPSC medium. Later, they and all following newly generated human iPSC lines were grown in mTeSR™1 medium by standard.

7.2 Validation of iPSC lines

For validation of HGK1 and HGK4 see Garbes *et al.*, 2013.

7.2.1 Morphology and expression of pluripotency surface markers

In feeder-free cultivation of human iPSCs with mTeSR™1 medium and MG-coated plates, iPSCs formed rather irregularly shaped colonies consisting of a thin layer than a densely packed colony as seen when propagated on MEF-feeder layers (Ludwig *et al.* 2006; StemcellTechnologies Version 3.0.0).

All new iPSC lines exhibited the aforementioned hESC-like appearance including a small cell body with high nucleus/cytoplasm ratio, flat growth and characteristic colony shape (Fig. 14). Activity of alkaline phosphatase (AP) is a key marker of pluripotent SCs (Takahashi *et al.* 2007; Smith *et al.* 2009). By converting a specific substrate into a chromogenic product, AP$^+$ cells were coloured in blue. Overt enzymatic AP activity was visualised by strong blue colour in all human iPSC lines here (Fig. 14).

Furthermore, undifferentiated SCs expressed specific surface antigens (e.g. SSEA-3, SSEA-4, TRA-1-60, TRA-1-81) as pluripotency markers (Smith *et al.* 2009). Immunocytochemical staining of these ESC markers revealed an overall strong expression in all human iPSC lines (Fig. 14).

7.2.2 Expression of typical pluripotency markers in human iPSC lines

Not only do pluripotent SCs express outer surface markers, but also characteristic transcription factors and enzymes essential for the maintenance of stemness.

In reference to human ESC line I3 (Amit *et al.* 2002) as control, expression of those pluripotency-related marker genes (e.g. *NANOG*, *TERT*) was determined on mRNA level by semi-quantitative RT-PCR with human iPSC lines HGK13 and HGK16 (Fig. 15).

In the agarose gel, comparable intensity of bands regarding *GAPDH* expression proved equal cDNA amounts. Despite individual differences between the three cell lines in respect of signal intensity, human iPSC lines HGK13 and HGK16 expressed every marker gene like control ECS line I3. As minor validation criterion, this semi-quantitative RT-PCR was not conducted for HGK21, HGK22, HGK27 and HGK28.
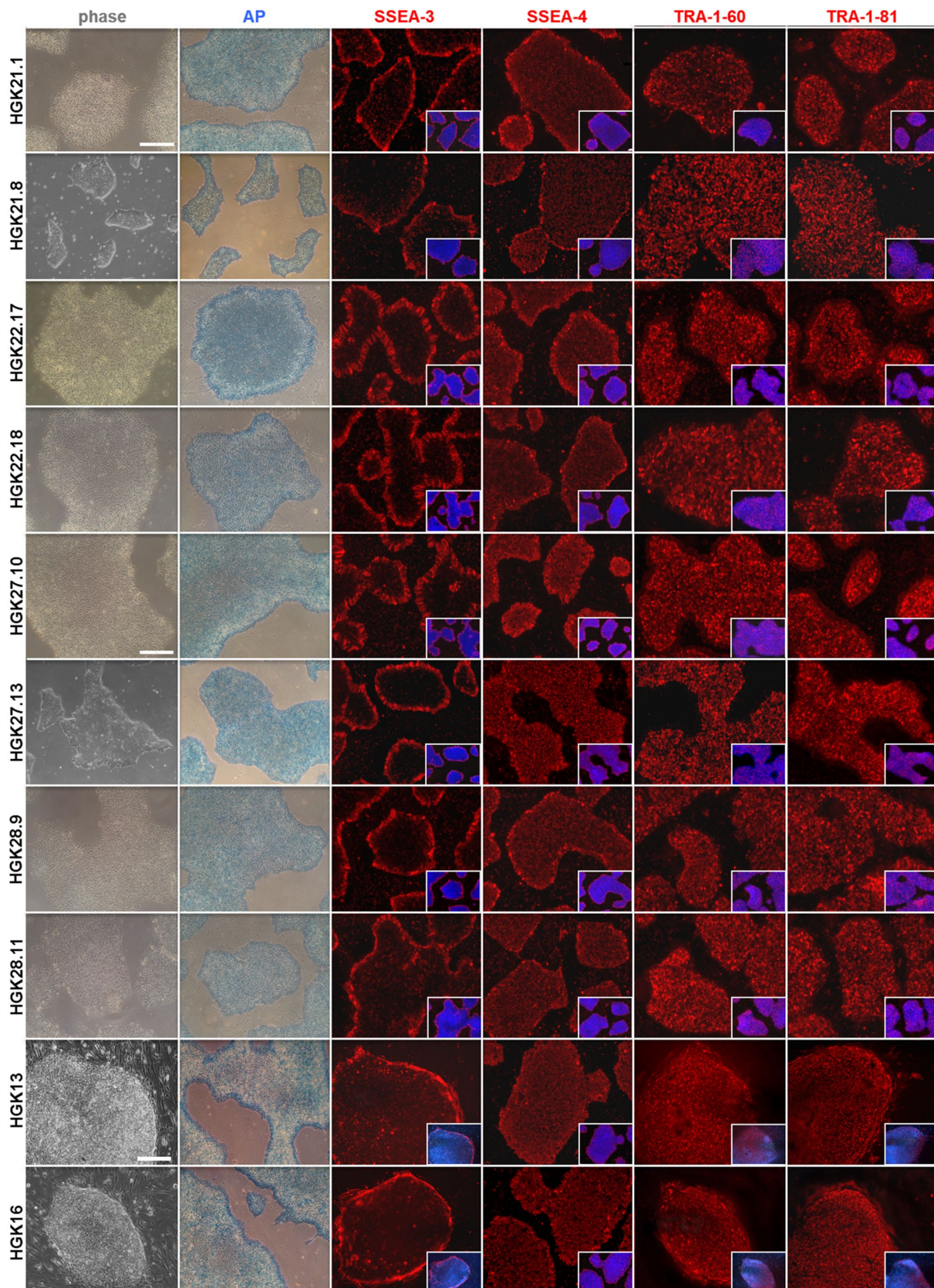
Fig. 14: Human iPSCs maintained in mTeSR™1 according to standard protocol showed a typical flat colony appearance with dense centre in phase contrast. Note the difference between HGK13 and HGK16 (on MEF feeder layer) and other HGK iPSCs (in feeder-free conditions) in regard to colony appearance. Blue staining of iPSC colonies palpably evidenced stemness due to AP activity. Immunocytochemical staining visualised classical pluripotency surface markers SSEA-3, SSEA-4, TRA-1-60 and TRA-1-81 were detectable on all human iPSC lines (all red). In insets, nuclei were counterstained with DAPI (blue) (scale bar 200 µm, valid for all images).
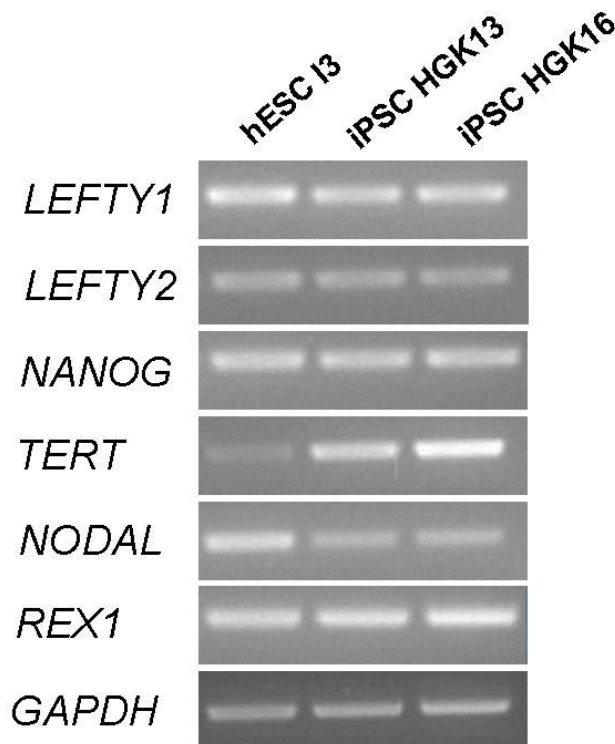
Fig. 15: Semi-quantitative RT-PCR with RNA extracted from iPCSs demonstrated the expression of stemness-related genes. Human embryonic stem cell line I3 served as reference, while GADPH was used as loading control.

7.2.3 Human iPSCs were genomically intact

By SNP-array analysis, all new iPSC lines were scrutinised for any potential genomic aberration which might have occurred during the gross overall cellular conversion processes of reprogramming. Whole gDNA was isolated and amplified for subsequent SNP-array analysis. Standard karyotyping did not suffice as validation criterion because it did not cover more subtle genomic aberrations. High-resolution SNP-arrays revealed genomic aberrations in established human iPSC lines initially catalogued as "genomically intact" after traditional karyotyping (Hussein *et al.* 2011).

Illumina® chips were employed to verify genomic integrity of HGK21, HGK22, HGK27 and HGK28. Fig. 16 depicted the iconographic scheme of every chromosome together with the corresponding Log R ratio as well as B allele frequency to discover copy number variations, aneuploidy or structural imbalances such as duplications, insertions or deletions for iPSC line HGK21.1 as example. For data of other lines, please refer to 10.2, Fig. 61.

Chromosomes were thoroughly screened and any aberration visible in this overview picture was marked in red circles (Fig. 16). If the mutation occurred in all clones plus the originating fibroblast cell line, the defect was regarded as inherited intrinsic feature of this individual cell line (Tab. 16).

Any additional obvious alteration ultimately led to the exclusion of the clone (e.g. HGK21.12, data not shown) for a potential detrimental effect could not be ruled out later during propagation or differentiation.

HGK13 and HGK16 were analysed by Affymetrix® Genome-Wide Human SNP Array 6.0. Comparison of cluster signals in human iPSC lines HGK13 and HGK16 with corresponding fibroblast donor cell lines ML102 and ML101 did not indicate any major detrimental alterations (10.2, Fig. 62).
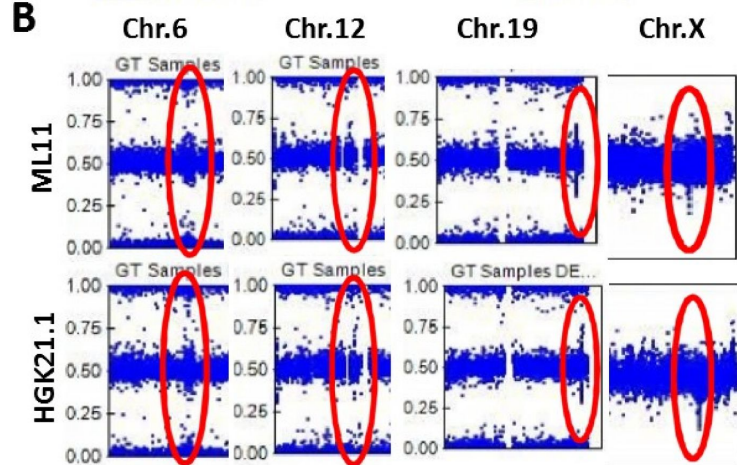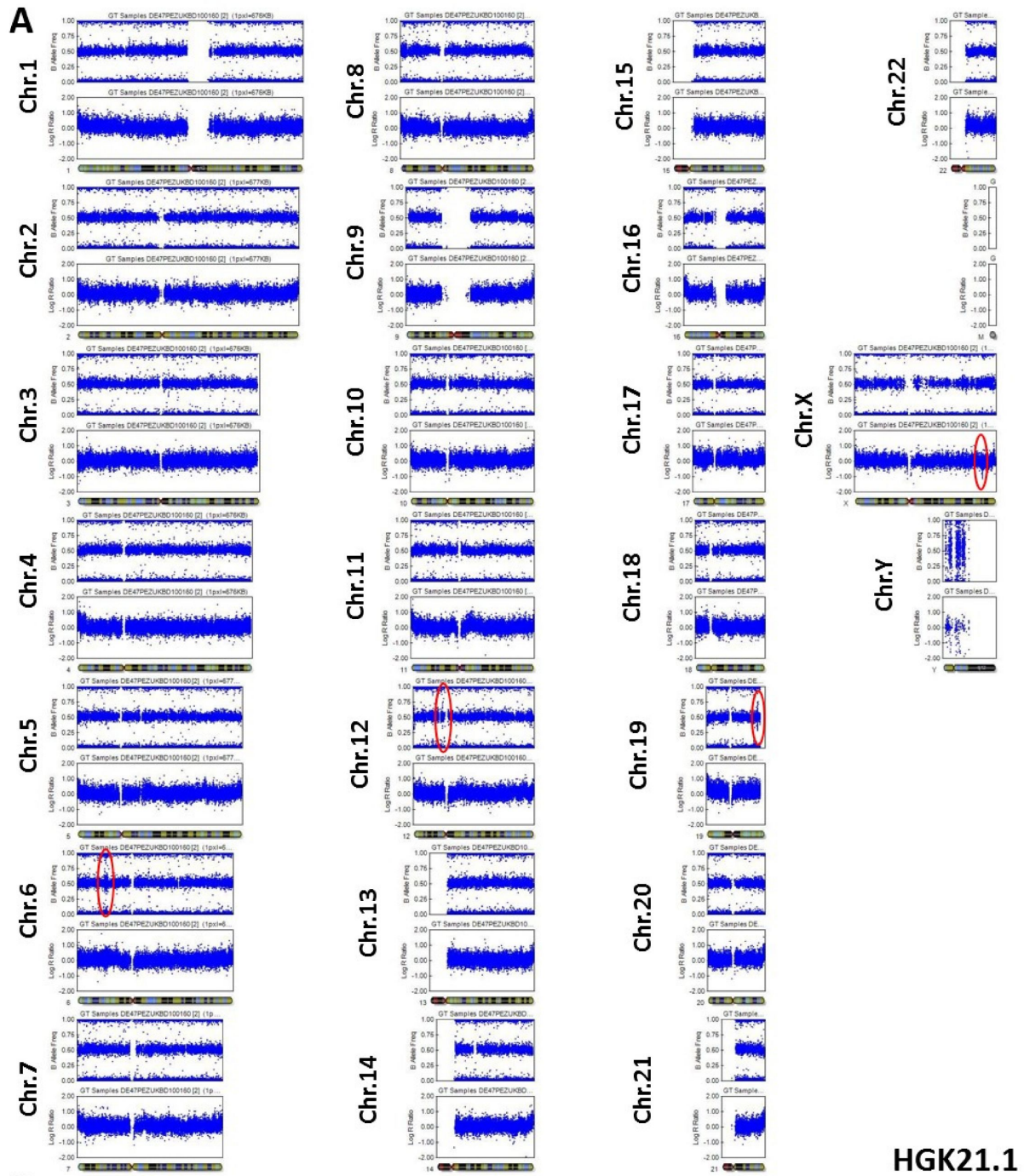
HGK21.1

Fig. 16: (**A**) Exemplary karyogram of human iPSC line HGK21.1 displayed every chromosome schematically together with its corresponding B allele frequency (upper panel) and Log R ration (lower panel). Note that regular SNPs show a Log R ratio of 0 and a B allele frequency of 0, 0.5 or 1 when homozygous. A heterozygous deletion will result in a Log R ratio of <0 and a B allele frequency of only 0 or 1, whereas a duplication will cause a Log R ratio of >0 and a B allele frequency of 0, ⅓, ⅔, or 1. (**B**) Visible genomic aberrations in this overview were encircled in red, magnified and compared to present mutations in original fibroblast cell line ML11 (see Tab.16).

Table 16: Overview about genomic mutations prevailing in iPSC lines HGK21, HGK22, HGK27, HGK28 and corresponding parental fibroblast cell lines. Original fibroblast lines were given with respective iPSC progeny. For other cell lines, see 10.2, Fig. 61

Cell line	Chromosomal position	Type of mutation
ML11 = → **HGK21.1** → **HGK21.8**	Chr.6 p21.32 Chr.12 p11.1 Chr.19 q13.33 Chr.X q27.2	Minor duplication Duplication Duplication Minor deletion
ML12 = → **HGK27.10** → **HGK27.13**	Chr.4 q28.3 Chr.6 p21.32 Chr.17 q12 Chr.19 q13.33	Duplication Minor duplication Minor duplication Duplication
ML13 = → **HGK28.9** → **HGK28.11**	Chr.4 q28.3 Chr.6 p21.32 Chr.12 p11.1 Chr.19 q13.33 Chr.X q27.2	Duplication Minor duplication Very minor duplication Duplication Minor deletion
ML14 = → **HGK22.17** → **HGK22.18**	Chr.6 p21.32	Minor duplication

7.2.4 Human iPSC lines HGK13 and HGK16 largely showed inactivation of retroviral transgenes

After having reached a pluripotent state, proviral transgenes *OCT4*, *SOX2*, *KLF4* and *c-MYC* are silenced in iPSCs favoured by the specific pMXs-architecture (Takahashi *et al.* 2006). In human iPSC lines HGK13 and HGK16, inactivation of retroviral transgenes was examined by qRT-PCR in which two different primer sets were used: One to detect expression of endogenous transcripts only whereas the other recognised endogenous as well as transgene mRNA (total). Each expression rate was normalised to *GAPDH* expression. A complete genetic silencing was achieved when the overall expression rate was generated by the endogenous gene only. All expression rates were referenced to those of respective genes in human ESC line H9 (Thomson *et al.* 1998) as control.

In general, both iPSC lines showed similar expression rates of endogenous *OCT4*, *KLF4* and *c-MYC*. Just endogenous *SOX2* was relatively low expressed in HGK16. HGK13 showed a rather high total *KLF4* expression indicating residual transgene activity. On the contrary, the amount of transgenic *SOX2* transcripts was elevated in HGK16 hinting at an insufficient silencing here. Yet, there was no generalised silencing defect noticeable (Fig. 17).
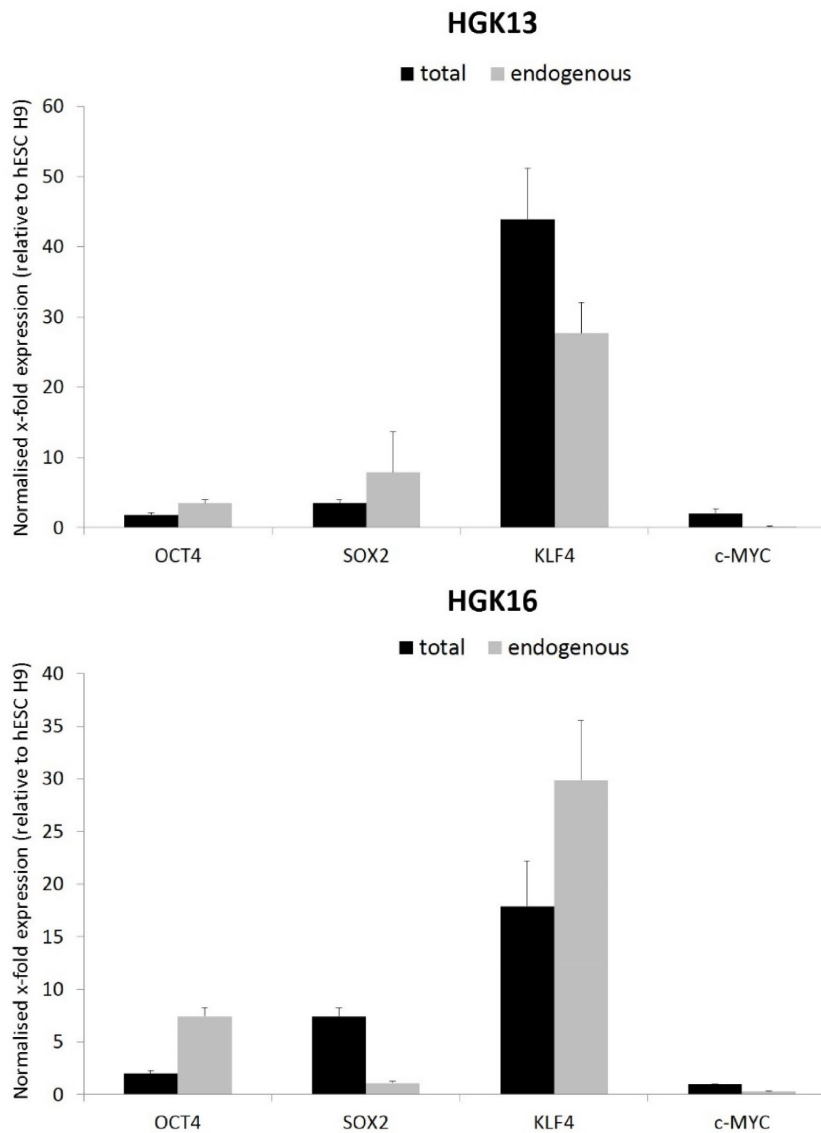
Fig. 17: Quantitative assessment of the residual expression of the four retroviral transgenes *OCT4*, *SOX2*, *KLF4* and *c-MYC* via qRT-PCR in both iPSC lines HGK13 and HGK16 compared to the respective endogenous expression of pluripotency-associated genes *OCT4*, *SOX2*, *KLF4* and *c-MYC*. Complete proviral silencing was indicated when total expression rate equated the endogenous expression rate. Thus, residual transgene expression was detectable in HGK13 concerning *KLF4* and in HGK16 concerning *SOX2*, respectively. Black bars represented total expression levels, grey bars represented endogenous levels. Expression was normalised to *GAPDH* level and shown as x-fold expression relative to human ESC line H9. Error bars represented ± SEM of triplicates (n=3).

7.2.5 Clones of human iPSC lines HGK21, HGK22, HGK27 and HGK28 did not contain SeV vectors at later passages

In SeV vector transduction, no insertion of viral genes occurs into the host cell genome. Therefore, viral transcripts are diluted over time by cell division. Between passages 5-10, new iPSC lines lose their viral expression profile which may be enhanced by lifting the cultivation temperature to 39 °C for a couple of days due to the thermal sensitivity of SeV vectors (Fusaki *et al.* 2009).

Every clone of human iPSC lines HGK21, HGK22, HGK27 and HGK28 was checked for expression of viral envelope protein haemagglutinin/neuraminidase (HN) by immunocytochemistry. At early passages (<7), some parts of iPSC colonies were still HN[+] pointing to a residuary expression of SeV genes. This HN expression was also visible in differentiated cells outside iPSC colonies (Fig. 18 **A**). However, at later time points no HN staining could be detected in iPSC lines anymore (Fig. 18 **B**).

However, a more precise method to examine whether iPSCs were SeV-free was to assess the expression of viral nucleocapsid protein *NP* via semi-qRT-PCR (Nishimura *et al.* 2011). Whole RNA was isolated at different passages and examined by semi-qRT-PCR with cDNA Alpers#2 (courtesy of Swetlana Ritzenhofen) as positive control. 18S rRNA acted as loading control.

Clearly, a strong expression of SeV *NP* transcript was only visible in the positive control, whereas the expression of these viral transcripts had completely disappeared in all iPSC lines verifying the total loss of any viral vector expression activity in those iPSCs (Fig. 19).
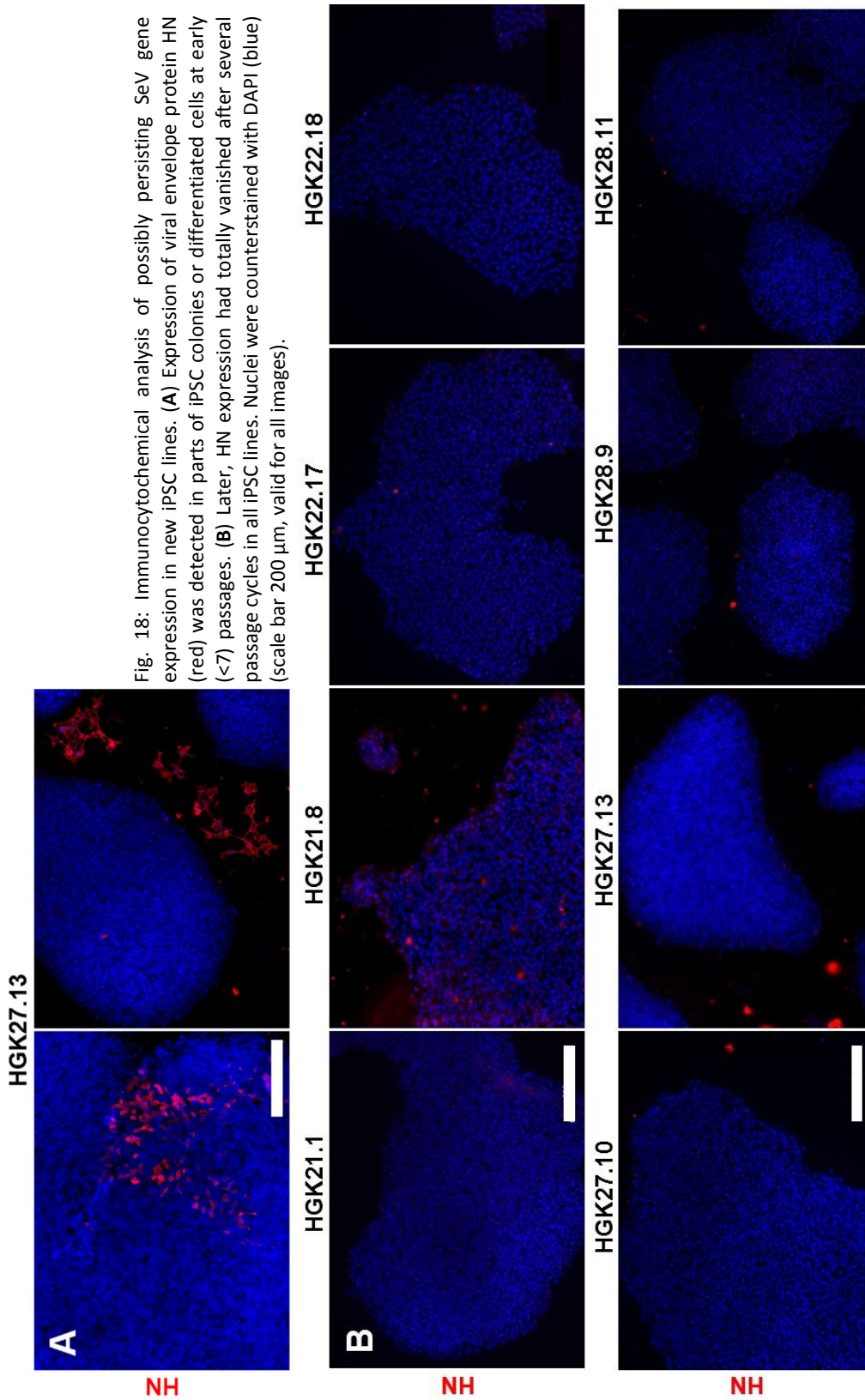
Fig. 18: Immunocytochemical analysis of possibly persisting SeV gene expression in new iPSC lines. (**A**) Expression of viral envelope protein HN (red) was detected in parts of iPSC colonies or differentiated cells at early (<7) passages. (**B**) Later, HN expression had totally vanished after several passage cycles in all iPSC lines. Nuclei were counterstained with DAPI (blue) (scale bar 200 µm, valid for all images).
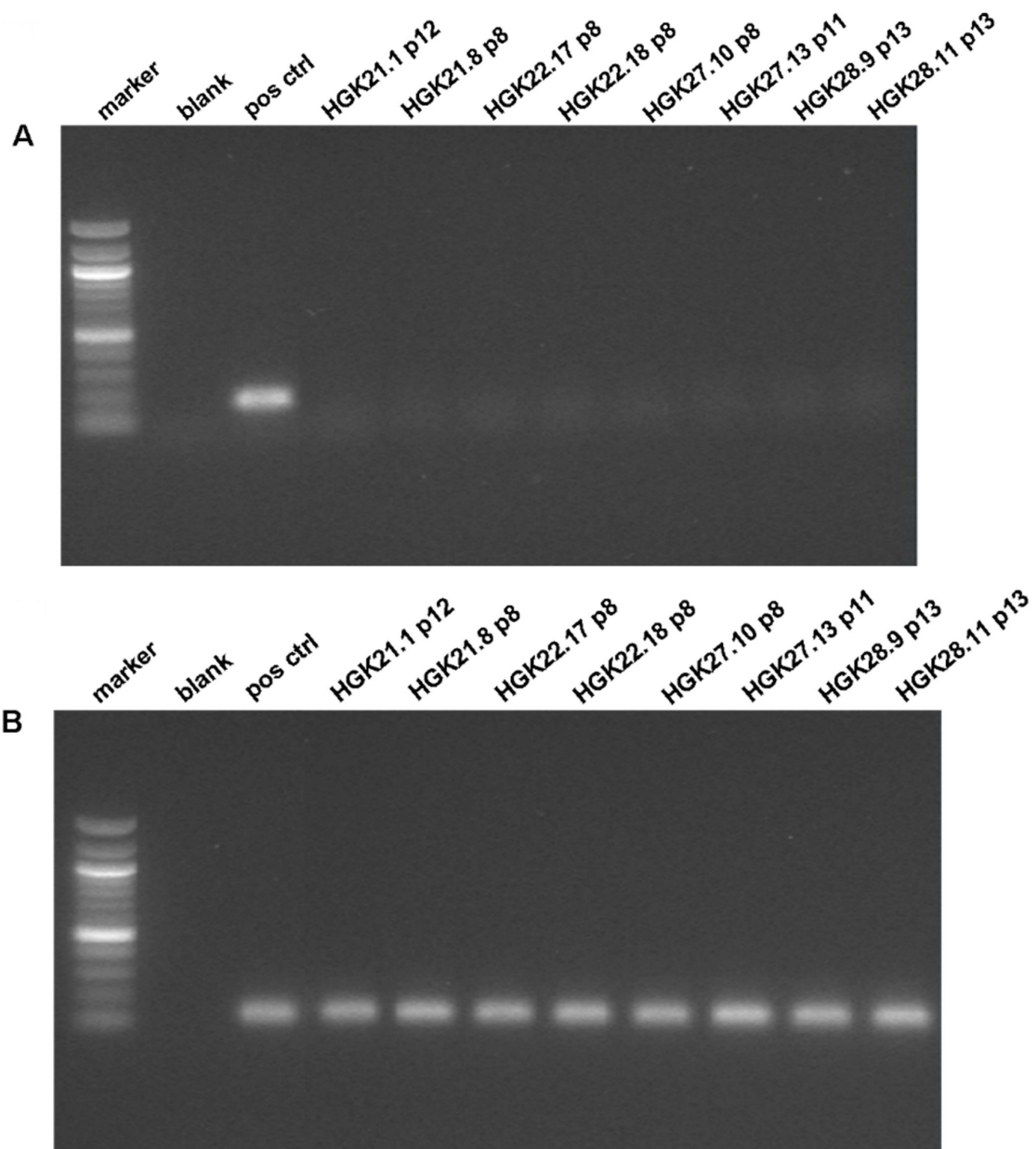
Fig. 19: Semi-quantitative analysis of SeV *NP* mRNA expression (**A**) in iPSCs in comparison to 18S rRNA as loading control (**B**). cDNA Alpers#2 (by Swetlana Ritzenhofen) served as positive control (pos ctrl). (**A**) At later passages (>p7), SeV vector activity was lost which rendered every iPSC clone virus-free. Only in the positive control a strong *NP* expression was detectable proving the functionality of the PCR. (**B**) All samples contained functional cDNA as seen in homogenous 18S rRNA expression.

7.2.6 Human iPSC lines developed into all three germ layers *in vitro*

Pluripotency is defined as the capability of unlimited differentiation into cells of all three germ layers (i.e. endoderm, mesoderm, neuroectoderm) without extra-embryonic tissue however (i.e. trophectoderm) whose generation is exclusively restricted to totipotent zygote and early blastomeres (Thomson *et al.* 1998; Smith *et al.* 2009).

To test the developmental potential of pluripotent SCs *in vitro*, iPSC colonies were gently lifted as whole colonies by enzymatic treatment and grown in suspension as embryoid bodies (EBs) (see 6.6). Upon withdrawal of pluripotency-maintaining growth factors such as bFGF, pluripotent SCs spontaneously started to differentiate into cells of all three germ layers within those EBs (Itskovitz-Eldor *et al.* 2000).

When plated and immunocytochemically analysed after further growth, all iPSC lines exhibited evident presence of tissue of endodermal (α-fetoprotein, AFP), mesodermal (smooth muscle actin, SMA) as well as neuroectodermal origin (β III-tubulin) (Fig. 20).

7.2.7 Human iPSC lines developed into all three germ layers *in vivo*

Unlike in murine iPSCs, chimera formation and germ line transmission as most powerful pluripotency quality criteria are ethically not accomplishable in this case even though human/mouse chimeras have been generated with human ESCs (James *et al.* 2006). Thus, the most stringent method for human iPSCs is teratoma formation assay (Smith *et al.* 2009).

All human iPSCs were injected into the testicular capsule of immuno-deficient male SCID/Beige mice. There, the iPSCs were exposed to a varying cellular environment inducing uncontrolled differentiation into tissues of all three germ layers (i.e. endoderm, mesoderm, neuroectoderm). After several weeks, tumour-like transplants were excised and immunohistochemically analysed for the presence of tissues of all three tissue lineages.

Endodermal tissue was displayed as adenoid goblet cell-like cells in an epithelial columnar arrangement with strong purple staining (Fig. 21). As mesodermal tissue, cartilage was visible in most cells as accumulation of huge bright cells which was clearly separated from neighbouring tissues by a distinct seam. In HGK28.11 typical densely packed reddish muscle cells were found as mesodermal derivative comparable to other studies (Huangfu *et al.* 2008; Hayashi *et al.* 2010). Neural rosettes derived from ectodermal cells and appeared in nests as dark-coloured, densely packed cells orientated in a petal-like arrangement. Instead, HGK27.13 displayed clusters of darkly stained retinal pigment epithelium as neuroectodermal tissue similar to previous studies (Park *et al.* 2008; Kallos 2011; Garbes *et al.* 2013).

Taken together, all iPSC clones fulfilling the aforementioned validation criteria could be regarded as fully pluripotent SCs.
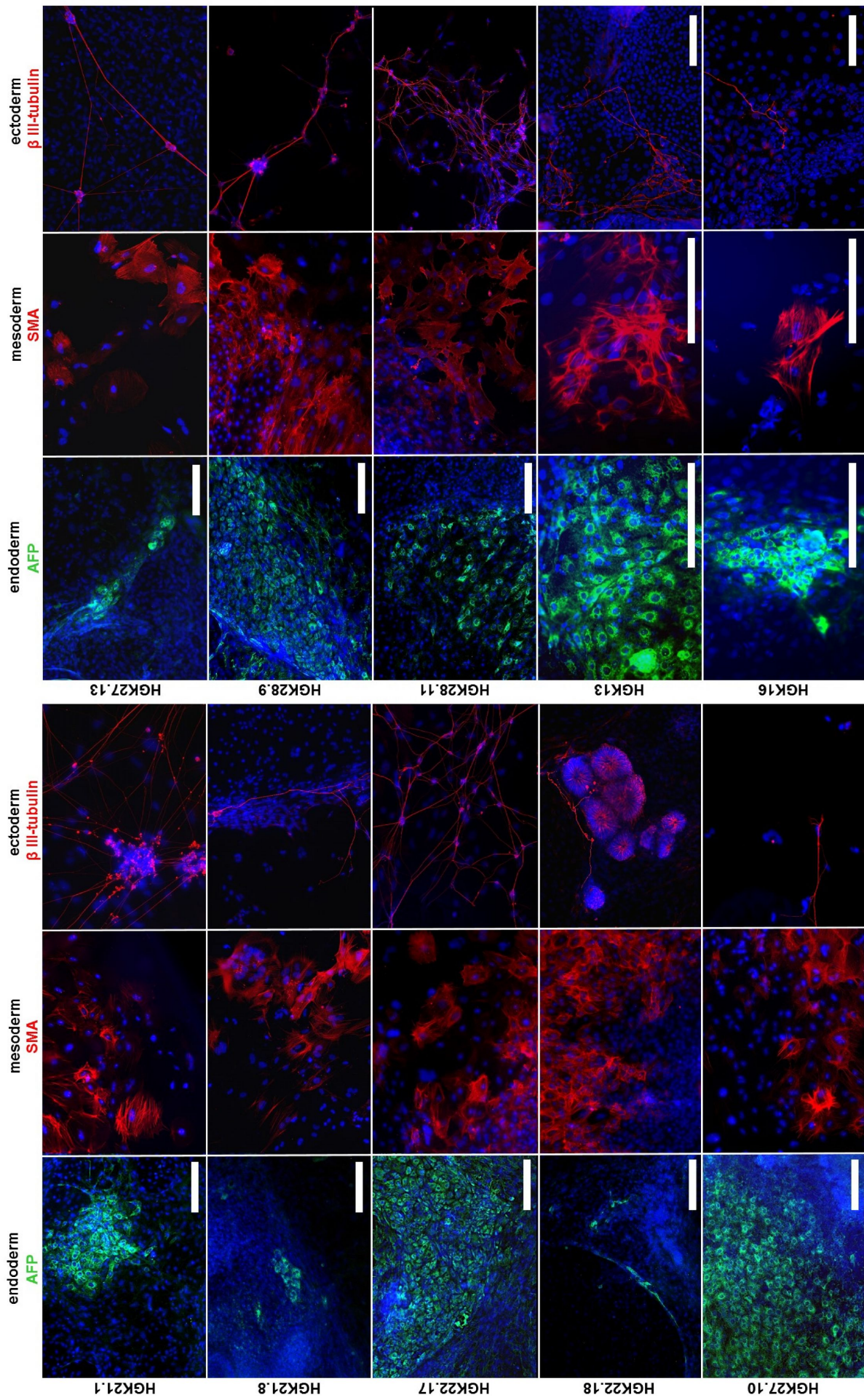
Fig. 20: Undirected differentiation of human iPSCs gave rise to cell types of all three germ layers as visualised by immunocytochemical staining. Endodermal cells showed punctual cytoplasmatic dispersion of AFP (green). Mesodermal cells contained cytoskeletal assembly of SMA (red). Ectodermal cells extended β III-tubulin⁺ axonal protrusions (red). Nuclei were counterstained with DAPI (blue) (given scale bar 200 μm, valid for images in respective row).
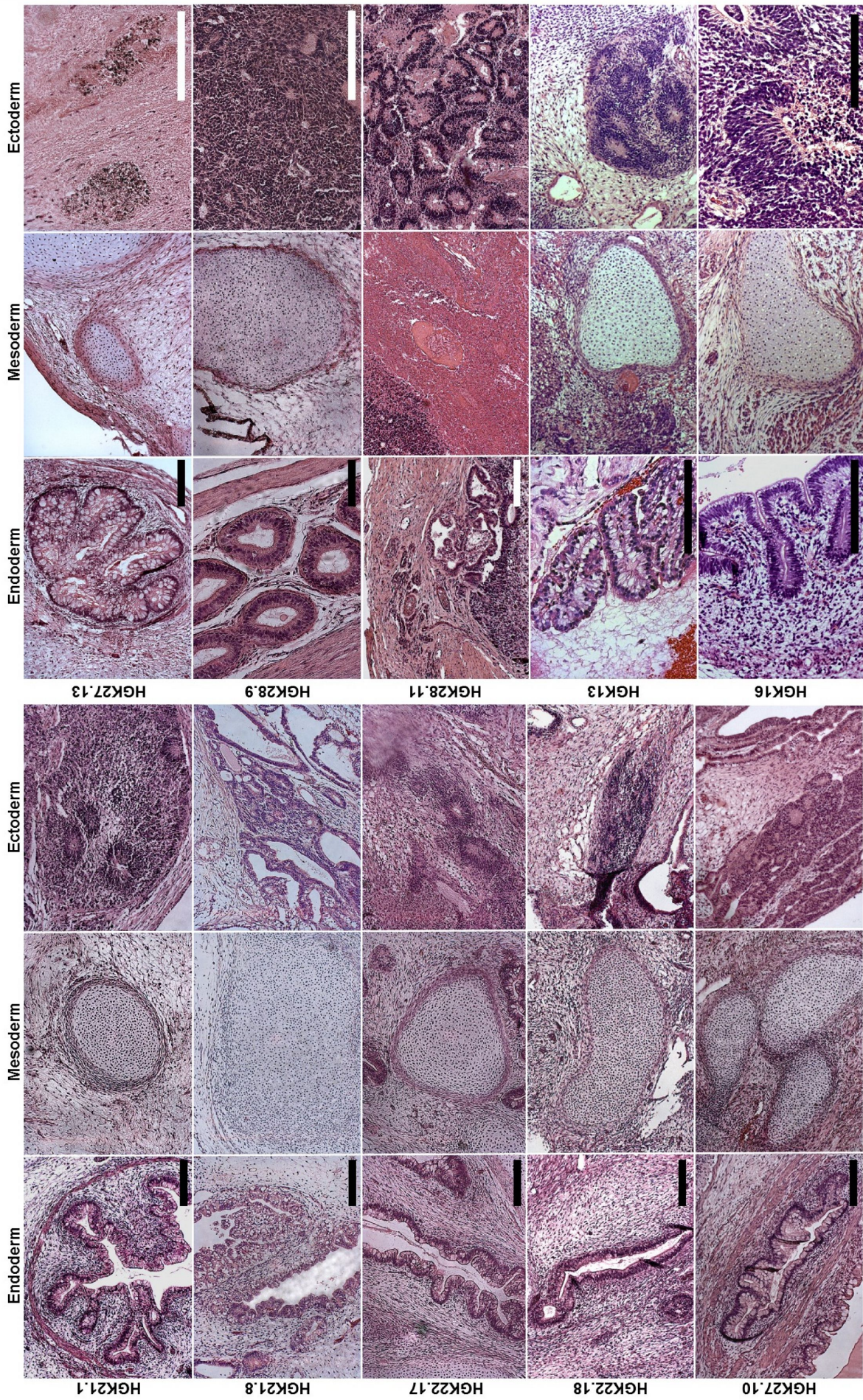
Fig. 21: Testing developmental potential of iPSCs in an *in vivo* teratoma formation assay successfully proved sufficient pluripotency by generating tissue of all three germ layers. Representative samples were subjected to immunohistologic HE staining Endoderm appeared as gland-like epithelium with lamella-like cavitations; as mesoderm, cartilage was present as marked-off agglomeration of bigger, pale cells. Note that HGK28.11 showed reddish muscle as mesoderm; ectoderm was illustrated by deep-purple cells arranged around a lighter centre in a rosette-like manner as neural rosettes. Note that HGK27.13 exhibited clusters of dark retinal pigment tissue as ectoderm (given scale bar 200 µm, valid for images in respective row).

7.3 Directed differentiation of human iPSCs into mixed motoneuronal cultures by an EB-based run-through protocol

Lacking accessibility of the actual SMA target tissue, i.e. lower α-motoneurons, has ever impaired research in the SMA research field. Previous studies examining the role of PLS3 in SMA or VPA responsiveness relied on patient-derived LB cell lines or fibroblasts providing valuable data (Brichta *et al.* 2006; Oprea *et al.* 2008). Still, the actual situation in patients' MNs remained elusive. With iPSCs as unlimited source of cells, the major aim of this study was the generation of such patient-derived MNs whose examination ideally ought to equip previous studies with strong further validity.

Many different protocols exist to differentiate functional motoneurons from human pluripotent stem cells (Wichterle *et al.* 2002; Ebert *et al.* 2009; Patani *et al.* 2011; Amoroso *et al.* 2013). However, pioneering studies were performed by Zhang and colleagues in 2005 *et seq.* (Li *et al.* 2005; Li *et al.* 2008; Hu *et al.* 2009). Testing up to five various protocols (data not shown), the EB-based run-through protocol of Hu and Zhang turned out as the most robust and applicable one.

Since the original study had been carried out with human ESCs, minor modifications were introduced to improve MN differentiation efficiency using human iPSCs (see Fig. 22): Firstly, a shift towards neuroectodermal germ layer development in pluripotent SCs was ensured by synergistic application of TGFβ-inhibitor SB431542 and BMP-inhibitor dorsomorphin during EB stage. Thus, a dual SMAD-signalling inhibition was exerted which efficiently directed neural conversion in human pluripotent SCs (Chambers *et al.* 2009; Kim *et al.* 2010). Secondly, the RA concentration was increased from 0.1 µM to 0.75 µM to ensure full caudalisation. Thirdly, RA administration began earlier on day 7 instead of day 10 as in the original publication. Those changes optimised the overall MN yield for the iPSC lines used in this study when compared to using the original run-through protocol of Hu and Zhang (see 6.4).
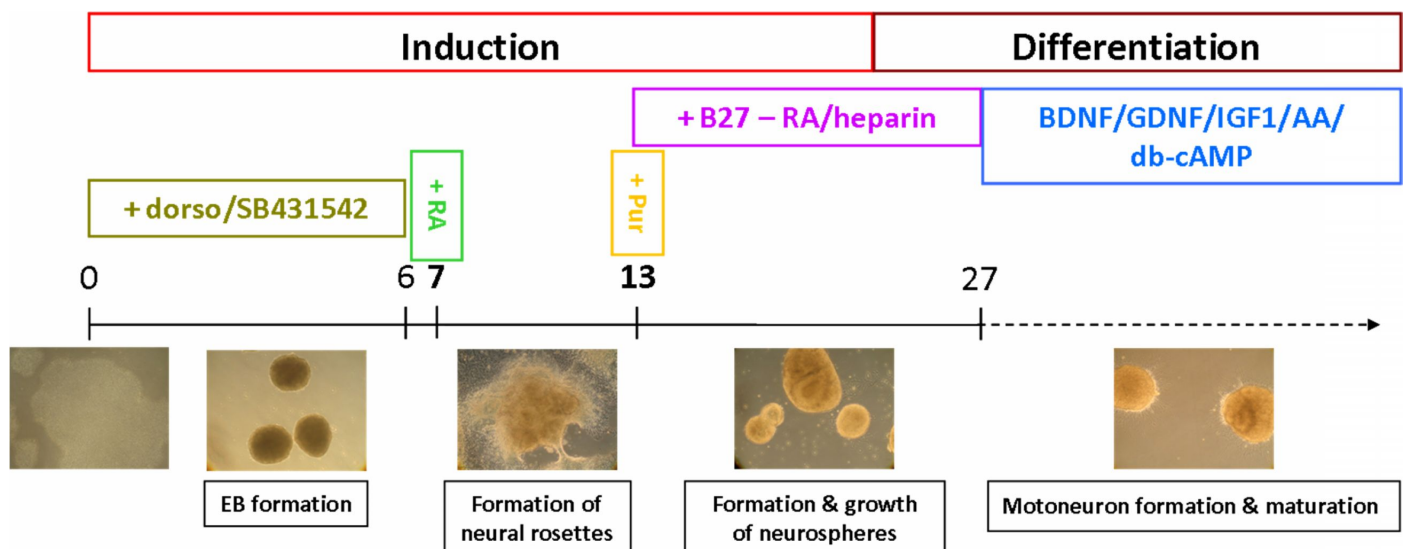
Fig. 22: Schematic picture of modified differentiation regimen to generate human motoneurons from iPSCs. Proper iPSC colonies were lifted and grown in suspension as embryoid bodies (EBs). To enhance neural development, inhibitors of BMP and TGFβ pathways – dorsomorphin and SB431542 – were administered. EB plating resulted in formation of neural rosettes which were primed to caudal development by RA treatment. On day 13, neural rosettes were isolated and cultivated in suspension as neurospheres. Administration of SHH agonist purmorphamine finally ventralised neural progenitors in neurospheres leading to proper motoneuronal precursor development. At last, neurospheres were seeded for final motoneuronal maturation in presence of neurotrophic factors.

7.3.1 Differentiating iPSCs according to a standard protocol resulted in low numbers of mature MNs

The first times, human iPSC lines were differentiated into MNs according to the original publication by Hu *et al.*, 2009. This meant that caudalisation started on day 10 with 0.1 μM RA. Nonetheless, dual SMAD-signalling inhibition was already carried out by administering SB431542 and dorsomorphin from day 0 to day 6 during EB generation. However, neuroectodermal development into pMN-regionalised cells yielded only a moderate number of OLIG2$^+$ progenitor cells (Fig. 23 **A**). After further maturation, only few neuronal cells express typical MN-markers like ISL1, HB9 or ChAT indicating a rather poor overall efficiency (Fig. 23 **B**).
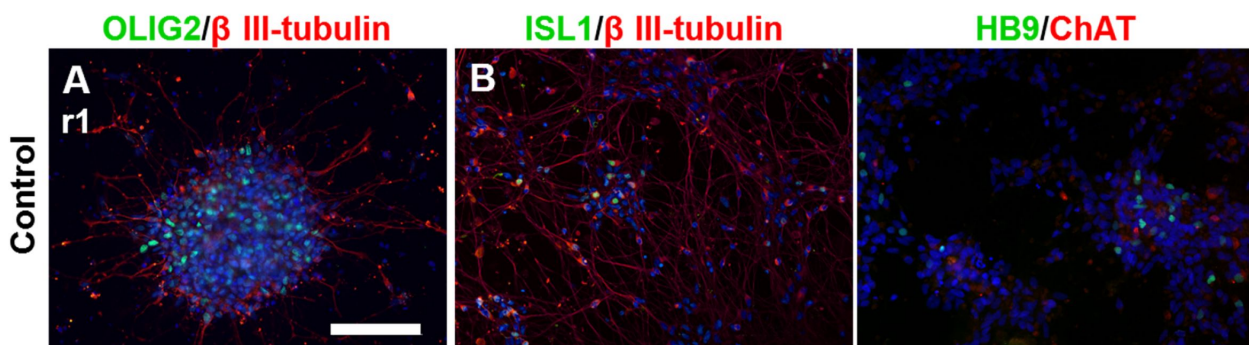
Fig. 23: Human control iPSC line r1 was differentiated according to the original EB-based run-through protocol published by Hu and Zhang (Hu *et al.* 2009) plus administration of small compounds SB431542 and dorsomorphin during the first seven days to favour neuroectodermal development (dual SMAD-signalling inhibition) (Chambers *et al.* 2009; Kim *et al.* 2010). Thus, regionalisation began on day 10 with application of 0.1 μM RA. (**A**) Before final maturation, just few OLIG2$^+$ progenitor cells (green) of the correct pMN domain were present on day 28 after immunocytochemical staining. (**B**) Moreover, the overall yield of proper MNs was low as well marked by the sporadic presence of ISL1$^+$ neurons (green) or HB9$^+$ (green) cholinergic ChAT$^+$ (red) motoneurons on day 46. Nuclei were counterstained with DAPI (blue) (scale bar 100 μm, valid for all images).

Characteristic MN markers include the following: As cholinergic neurons, mature spinal MNs express ChAT and vesicular acetylcholine transporter (VAChT) (Li *et al.* 2005). Homeobox TFs HB9, ISL1 and LIM3 (LHX3) suffice to induce and consolidate post-mitotic MN differentiation (Tanabe *et al.* 1998; Briscoe *et al.* 2001) and are regarded as *bona fide* MN-specific markers while co-expression of ISL1, PHOX2a/2b and TBX20 bestows MNs a fate of cranial visceromotor neurons (Arber *et al.* 1999; Jessell 2000). In addition, SMI-32 antibody detects a neuronal intermediate filament in spinal MNs (Carriedo *et al.* 1996).

7.3.2 Motoneuronal differentiation of iPSCs according to a modified protocol performed demonstratively better

To improve the global efficiency of MN-generation, the aforementioned modifications were introduced to the protocol, i.e. an earlier RA administration at higher concentration (0.75 μM RA from day 7 onwards) combined with dual SMAD-signalling inhibition.
Immunocytochemical staining showed a successful differentiation into MN-progenitor cells (Fig. 24) indicated by strong expression of characteristic markers of the pMN domain such as OLIG2 and NKX6.1 for ventral neural tube and upper spinal cord marker HOXB4 for caudalisation (Li *et al.* 2008). Hitting the correct domain was furthermore denoted by only rudimentary expression of markers of domains neighbouring pMN: PAX6 was expressed in upper ventral domains (p0-pMN) (Davis-Dusenbery *et al.* 2014), but only sporadically in these

MN-differentiated cells. NKX2.2 is a marker of the very ventral domain p3 (Alaynick *et al.* 2011), yet it was scarcely found in these MN-differentiated cells. General neural identity was proved by overt expression of SOX2 and nestin in all cell lines. Human NSCs endogenously express SOX2 (Kim *et al.* 2009b) while intermediary filament nestin is found in proliferating NSCs of the CNS (Michalczyk *et al.* 2005). Taken together, a higher RA-application at an earlier time-point demonstratively enhanced the generation of correctly regionalised pMN-like progenitor cells in comparison to the original protocol.

Further maturation of such progenitor cells eventually led to plenty of neurons exhibiting typical motoneuronal markers like ISL1, HB9 and ChAT (Fig. 25). The yield of double HB9^{+}/ChAT[+] *bona fide* MNs in this modified protocol appeared convincingly higher than in the standard protocol. Particularly, the control line r1 as well as the representative PLS3 discordant sibling pair HGK13 (SMA III patient) and HGK16 (asymptomatic) featured more *bona fide* MNs as when control line r1 is differentiated according to the standard protocol (compare Fig. 23). Thus, in this study an optimised motoneuronal differentiation protocol has been set up for further experiments in the actual human target tissue now. Several trials (~20) were conducted, however, loss of usable samples and parallel attempts to increase MN yield by additional modifications (e.g. additional administration of SHH protein for ventralisation) prevented collection of enough data for scientifically valid comparison. Especially the examination of quantitative differences concerning growth and long-term survival of MNs between PLS3 discordant siblings in comparison to healthy controls and HGK1 as severely affected SMA I patients was derogated.

Nonetheless, this new *in vitro* iPSC-based human MN model facilitated the detection of additional SMA-specific disease features like the number of SMN-containing gems since motoneuronal cultures of the representative PLS3 discordant sibling pair HGK13 (SMA III patient) and HGK16 (asymptomatic) exhibited the typical nuclear dot-like gem localisation (Fig. 26).

Furthermore, these iPSC-derived MNs did contain PLS3 as proven in Fig. 26 where HB9^{+} MNs clearly expressed PLS3 in MNs of the PLS3 discordant sibling pair HGK13 and HGK16. This fact will open an avenue to further elucidate how the molecular mode of action of PLS3 may exert its protective effect in discordant siblings' MNs.

Fig. 24: Human iPSC lines representing a healthy control (r12), a SMA I patient (HGK1) and PLS3 discordant siblings (SMA III patient HGK22.18 and his asymptomatic sister HGK28.11) were differentiated into MN progenitors according to a modified run-through protocol based on Hu *et al.*, 2009. On day 28, immunocytochemical staining revealed correct regionalisation into the pMN domain by strong presence of ventral markers OLIG2 (green) and NKX6.1 (red) and caudal marker HOXB4 (red) in all cell lines. Markers of adjacent neural tube domains like PAX6 (green; upper ventral domains e.g. p2) or NKX2.2 (green; lowest ventral domain p3) were hardly present. General neural priming was betokened by expression of neural markers SOX2 (green) and nestin (red). Nuclei were counterstained with DAPI (blue), also in insets (scale bar 100 µm, valid for all images).

Fig. 25: Final maturation of iPSC-derived mixed motoneuronal cultures from a healthy control (r1), a SMA I patient (HGK1) and PLS3 discordant siblings (SMA III patient HGK13 and his asymptomatic sister HGK16). Immunocytochemical staining on day 42 visualised the presence of ISL1+ (green) MNs as well as HB9+ (green) and ChAT+ (red) *bona fide* MNs in every cell line. Nuclei were counterstained with DAPI (blue) (scale bar 100 µm, valid for all images).

Fig. 26: HB9+ MNs (green) in mixed motoneuronal cultures of PLS3 discordant sibling pair HGK13 (SMA III patient) and HGK16 (asymptomatic) evidently expressed PLS3 (red). β III-tubulin+ neurons (red) in mixed motoneuronal cultures of HGK13 (SMA III patient) and HGK16 (asymptomatic) palpably expressed SMN (green) and showed characteristic dotted gem localisation in the nucleus (arrows) on day 41. Nuclei were counterstained with DAPI (blue) (scale bar 20 μm, valid for all images).

7.3.3 Expression of PLS3 and SMN on RNA and protein levels in mixed motoneuronal cultures

To determine the quantity of SMN and PLS3 on transcriptional and translational level, respectively, total RNA and proteins were extracted from mature mixed motoneuronal cultures.

Expression levels of *SMN* and *PLS3* were calculated relative to expression rate of total RNA. Analysis of mRNA expression rates in representative MN differentiation runs via qRT-PCR revealed a low *PLS3* expression rate for SMA III patient HGK13 whereas his asymptomatic sister HGK16 showed a slightly reduced *PLS3* expression rate when compared to *PLS3* expression of control line r1 (Fig. 27). In contrast, the *SMN* expression level in both discordant siblings was nearly equal (~30%) matching their genotype with three *SMN2* copies and significantly reduced to healthy control lines.

The amount of translated protein was valued by Western blotting and subsequent immunoblotting (Fig. 28). Protein expression was normalised relative to β-actin expression for quantification. The bands on the blot clearly represented the correct weight of the respective proteins (PLS3: 72 kDa; β-actin: 50 kDa; SMN: 36 kDa) with equalised β-actin bands allowing proper normalisation. Knock-down of PLS3 identified upper band as correct PLS3 signal (10.5, Fig. 65). Notably, SMA III patient HGK13 exhibited evident decrease in PLS3 expression when compared to controls. His asymptomatic sister HGK16 indicated a strong PLS3 expression in

the immunoblot which was also reflected in the quantification but without exceeding control values. Asymptomatic HGK16 showed rather equal PLS3 expression as healthy control r1. SMN expression was visibly diminished in both siblings' samples and reached just half of the amount of control line r1 (~50%).
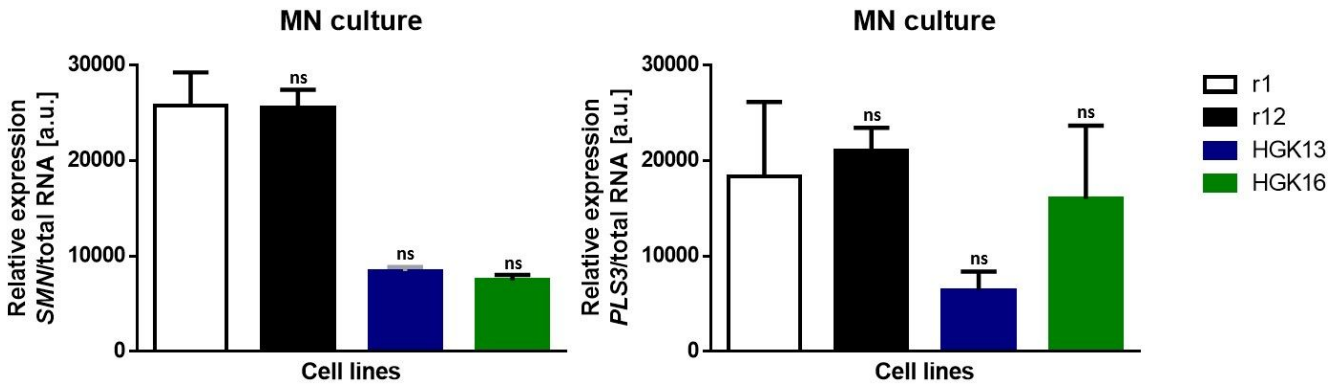
Fig. 27: Quantitative analysis of RNA expression levels in representative MN differentiation runs via qRT-PCR from a mixed motoneuronal culture of healthy controls (r1 & r12) and PLS3 discordant siblings (SMA III patient HGK13 and his asymptomatic sister HGK16). *PLS3* expression exhibited no significant differences between siblings yet HGK13 showed a lower expression whereas HGK16 did not display any higher *PLS3* expression in comparison to control lines. Contrarily, the *SMN* expression of both siblings was similarly high at approx. 30% congruent with their genotype of three *SMN2* copies. Expression was standardised to total RNA levels (Kruskal-Wallis test). Graphs were plotted from data of qRT-PCRs of three independent MN differentiation runs (n=3) apart from control line r12 (n=2). Error bars represented ± SEM of biological duplicates (n=2).
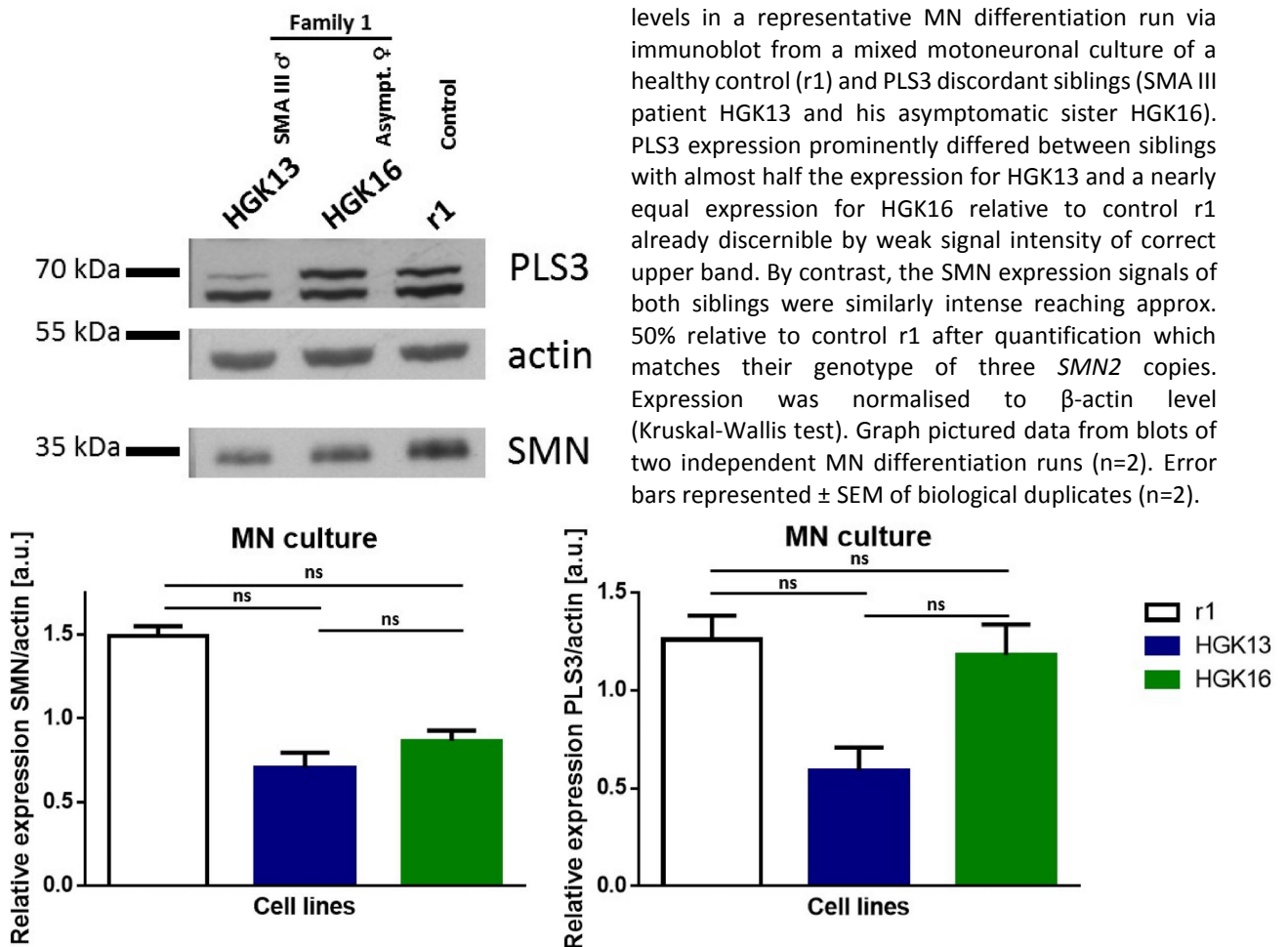
Fig. 28: Quantitative analysis of protein expression levels in a representative MN differentiation run via immunoblot from a mixed motoneuronal culture of a healthy control (r1) and PLS3 discordant siblings (SMA III patient HGK13 and his asymptomatic sister HGK16). PLS3 expression prominently differed between siblings with almost half the expression for HGK13 and a nearly equal expression for HGK16 relative to control r1 already discernible by weak signal intensity of correct upper band. By contrast, the SMN expression signals of both siblings were similarly intense reaching approx. 50% relative to control r1 after quantification which matches their genotype of three *SMN2* copies. Expression was normalised to β-actin level (Kruskal-Wallis test). Graph pictured data from blots of two independent MN differentiation runs (n=2). Error bars represented ± SEM of biological duplicates (n=2).

7.3.4 Analysis of the composition of mixed motoneuronal cultures

Although the modified MN differentiation protocol performed better than the standard differentiation procedure, the overall efficiency remained conspicuously below expectations. The number of ISL1^{+} and HB9^{+} *bona fide* MNs ranged on average from 5%-8% of total cells, seldom exceeding 12%. In Fig. 29 the quantification of a representative single MN differentiation run was pictured. Both controls exhibited comparable numbers of ISL1^{+} cells on low level (~6.5%). With control line r12, there was even the fewest number of HB9^{+} MNs whereas MN culture of control line r1 included almost 10% HB9^{+} MNs. In asymptomatic sibling HGK16, the amount of HB9^{+} and ISL1^{+} cells added up to approx. 6% whereas SMA III patient HGK13 tended to lower numbers in HB9^{+} MNs (~4.5%) whereas the numbers of ISL1^{+} MNs even exceeded the MN numbers in the controls (~12%).
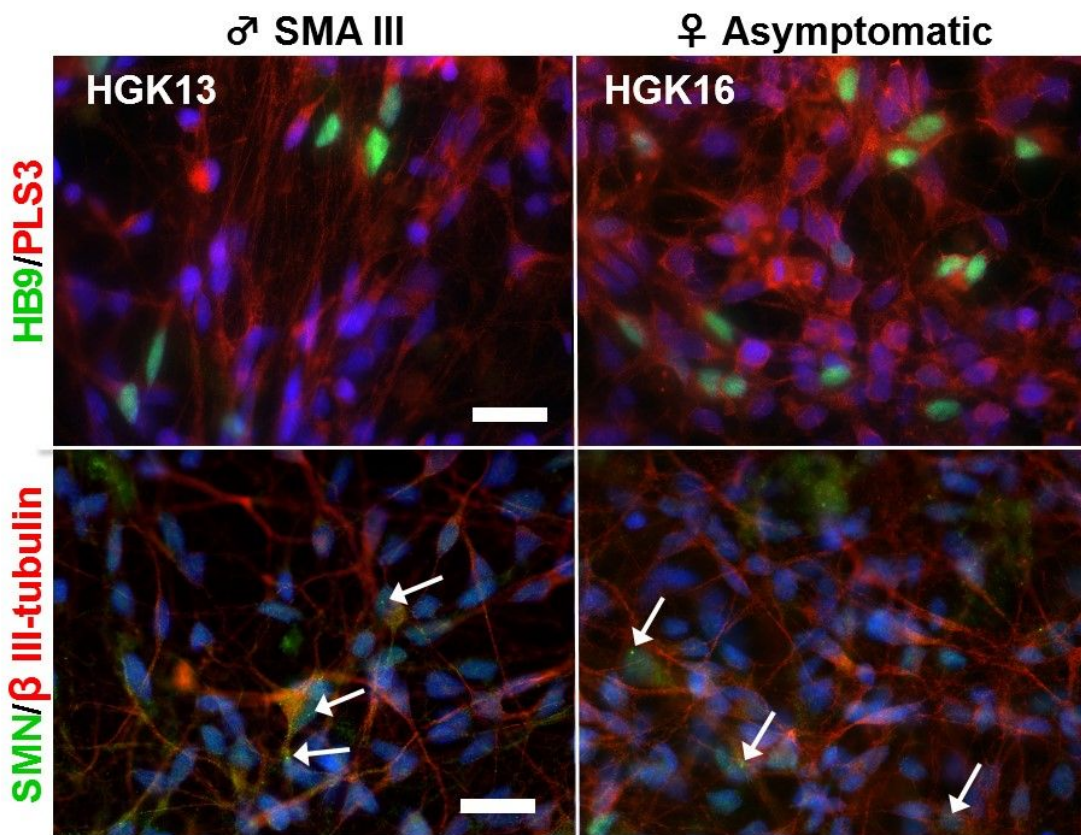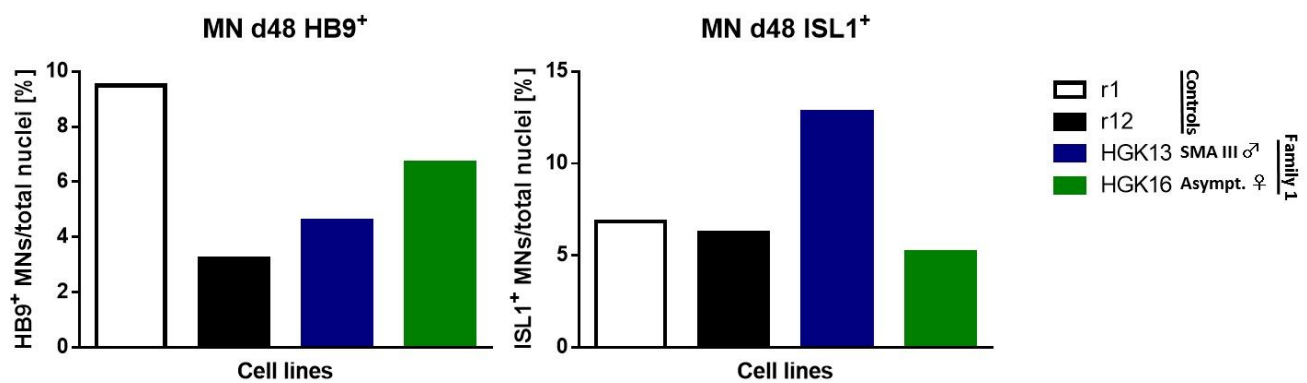

Fig. 29: Representative single quantification of HB9^{+} and ISL1^{+} MNs in a mixed motoneuronal culture of PLS3 discordant sibling pair HGK13 (SMA III patient) and HGK16 (asymptomatic) as well as healthy control lines r1 and r12. On day 48, the total number of HB9^{+} and ISL1^{+} cells was determined by immunocytochemical staining. Cultures of control lines r1 and r12 comparably contained ISL1^{+} MNs whereas there were gross differences between the lines concerning HB9^{+} cells. With HGK16 the MN number ranged around 6% whereas her affected brother HGK13 showed lower HB9^{+} MN numbers but even more ISL1^{+} MNs than the controls. Graph pictured data from quantification of one MN differentiation run (n=1).

In order to identify further neural populations within the mixed motoneuronal cultures, samples of healthy control line r12, positive control HGK1 (SMA I patient) and the representative PLS3 discordant sibling pair HGK22.18 (SMA III patient) and HGK28.11 (asymptomatic) were stained for different neuronal and glial markers. Cultures of cells which had been directly differentiated towards the respective neuronal populations or glia served as correspondent positive controls to verify antibody's functionality.

Clearly, cultures of all cell lines predominantly consisted of non-MN cells (Fig. 30). Whereas only very few TH^{+} dopaminergic neurons existed in those cultures, GABAergic neurons (GAD65/67[+]) and in particular glutamatergic neurons (v-Glut 1[+]) strikingly prevailed. In addition, GFAP^{+} glial cells were present. Yet, the longish morphology with neurite-like extensions rather hinted at radial glia cells than at astrocytes as it was also detectable in the corresponding positive control. Besides, iPSC-derived human astrocytes need longer maturation periods (>90 days) (Krencik *et al.* 2011) and GFAP is known to label radial glia cells as well (Campbell *et al.* 2002). Since the samples were stained on day 35, the presence of astrocytes was unlikely.

After all, the high degree of non-MN cells in mixed cultures as well as the low efficiency of MN generation raised the question if an iPSC-based differentiation protocol biased the overall results with too high variance during such a long differentiation period. Instead, a strategy

basing on neural stem cells (NSCs) may serve better and more reliably on account of a standardised starting situation with a homogenous cell population.
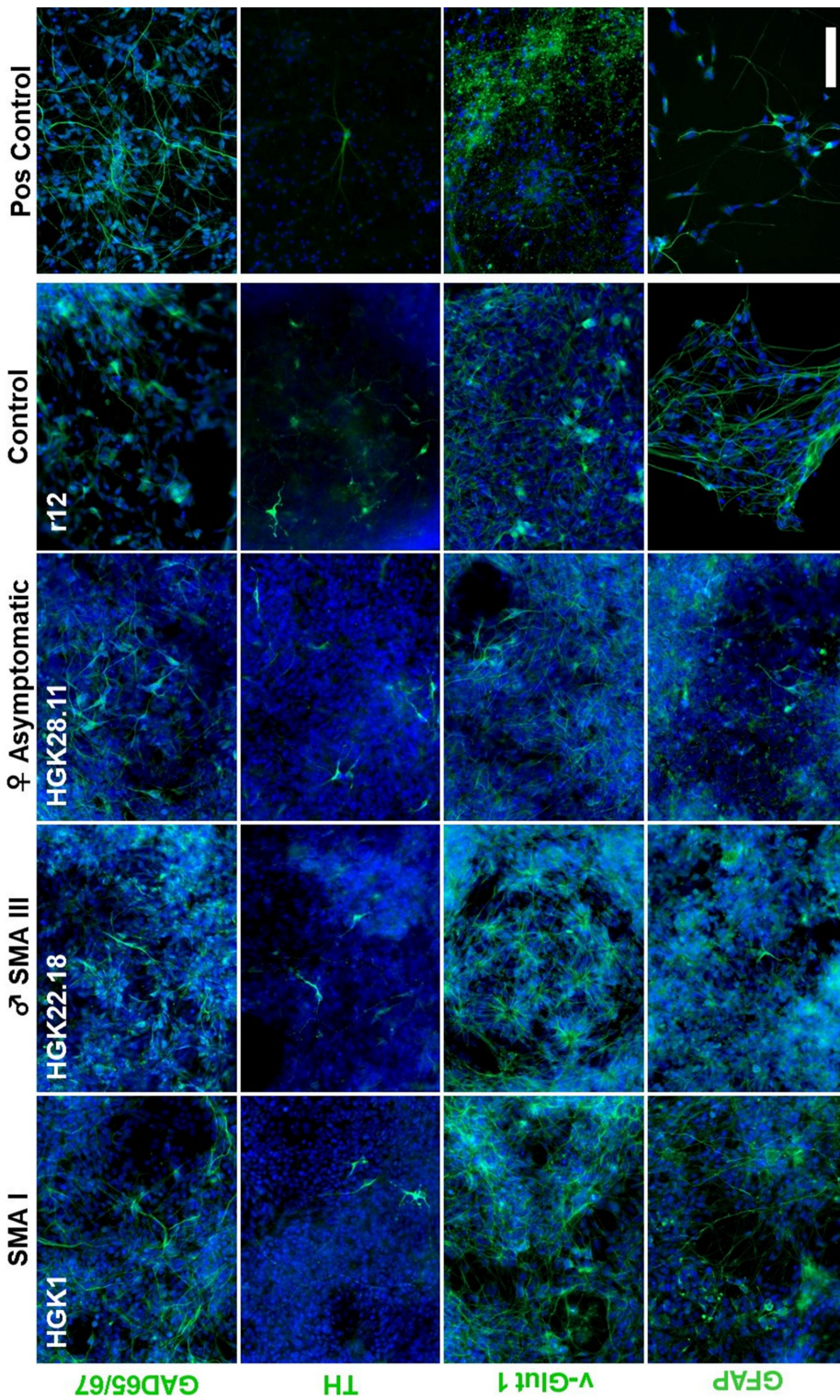
Fig. 30: Immunocytochemical staining of various neuronal and glial markers identified v-Glut 1⁺ glutamatergic and GAD65/67⁺ GABAergic neurons (both green) as prevailing neuronal populations in mixed motoneuronal cultures from a healthy control (r12), a SMA I patient (HGK1) and PLS3 discordant sibling pair HGK22.18 (SMA III patient) and HGK28.11 (asymptomatic). Dopaminergic TH⁺ neurons appeared solely sporadically. Frequently, GFAP⁺ glial cells arose. The supremacy of non-MN cells punctuated the need of more robust motoneuronal differentiation strategies. Directly differentiated cultures served as positive controls (pos ctrl). Nuclei were counterstained with DAPI (blue) (scale bar 100 μm, valid for all images).

7.4 Motoneuronal differentiation of iPSC-derived small molecule NPCs (smNPCs)

7.4.1 Generation of iPSC-derived small molecule NPCs (smNPCs)

Taking into account a very long differentiation period of up to seven weeks as well as a rather low efficiency in the modified EB-based run-through protocol, the establishment of a stably expandable fully patternable NSC population comprises several advantages. First, the already advanced developmental state of those neuroectodermally primed precursor cells curtails the duration of MN differentiation. Second, neural precursor cells (NPCs) form an initially more homogenous cellular population than during the EB-based protocol, subsequently leading to presumptively higher efficiencies. Third, by early administration of pattering morphogens during routine cultivation NSCs can be driven more easily into the neuronal subpopulation desired. Finally, a stable NSC population allows to monitor the entire developmental process of *in vitro* MN generation: From original fibroblasts via iPSCs to NSCs and ultimately to MN cultures, thus enabling to examine possible PLS3 mediated changes in different cell populations of an *in vitro* SMA cell culture model.

A couple of human NSC lines have been previously established e.g. long-term self-renewing neuroepithelial SCs (lt-NES®SCs) (Koch *et al.* 2009), primitive NSCs (Li *et al.* 2011) or rosette neural cells (Elkabetz *et al.* 2008). Yet, every line suffers from drawbacks such as a bound neural identity, costly growth factors for expansion or limited number of cultivable passages (Reinhardt *et al.* 2013).

Recently, Reinhardt and colleagues introduced a novel type of NSCs which combines the advantageous feature of robust cost-effective propagation and solid differentiation capability (Reinhardt *et al.* 2013). These small molecule NPCs (smNPCs) are easily derived from iPSCs by use of small compounds.

Therefore, all 13 iPSC lines were converted into corresponding smNPC lines according to a modified fully adherent protocol as well as a modified original published protocol which included an EB-like suspension step and dual SMAD-signalling inhibition (see Fig. 31 and 6.7). Since the adherent protocol failed to generate proper smNPCs (data not shown), only the smNPC lines obtained by the sphere-based original protocol were maintained and propagated. To prove the presence of a homogenous NSC population, every smNPC line (p8-p10) was checked for the same marker set as in the original publication by Reinhardt *et al.* (Fig. 32; 10.6, Fig 65). Evidently, all smNPC lines expressed standard CNS NSC markers like SOX1, SOX2, nestin and PAX6 in a comparable pattern compared to the original protocol. Moreover, forebrain marker FORSE-1 which had been associated with early NSC populations (Allendoerfer *et al.* 1995; Li *et al.* 2011) was clearly present in diffuse distribution in given smNPC colonies. By default, smNPCs comprise an early pre-rosette NSC population. As it was also shown in the original paper (Reinhardt *et al.* 2013), expression of classical rosette-markers PLZF and ZO-1 did not reveal the typical petal-shape arrangements with centred ZO-1 accumulation (compare Fig. 38). Only when grown very densely, some smNPC (e.g. HGK21.8 or HGK27.10) lines exhibited ring-like ZO-1$^+$ foci (Fig. 65). Thus, smNPCs fulfilled given validation criteria additionally demonstrating neural plasticity.
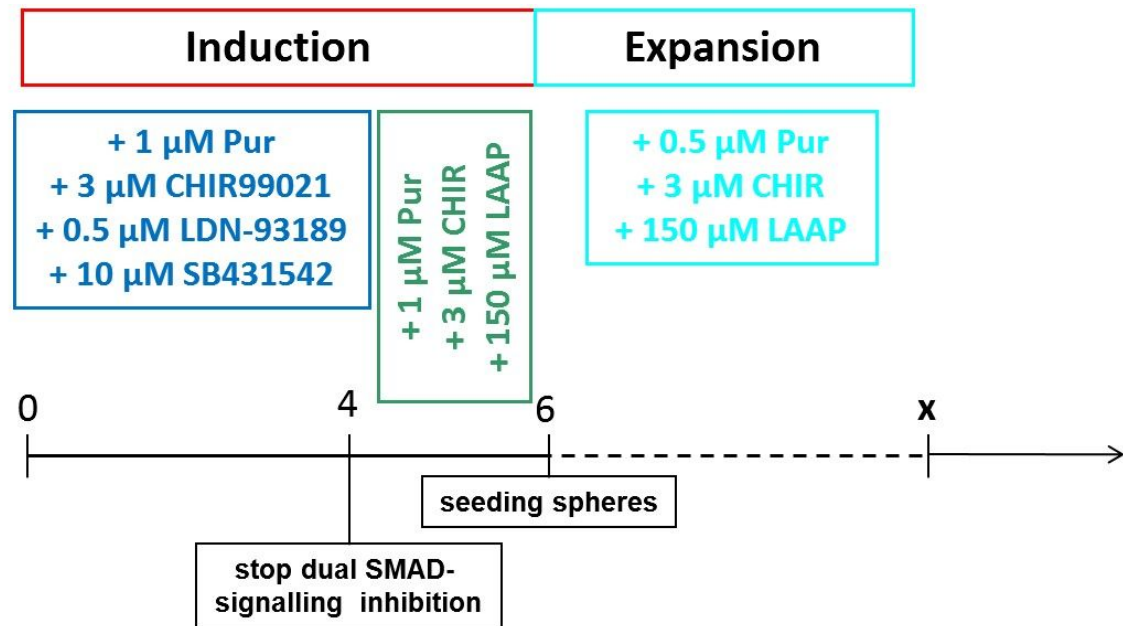
Fig. 31: Schematic picture of smNPC generation according to original protocol by Reinhardt *et al.*, 2013. iPSC colonies were enzymatically lifted and grown as EB-like spheres in suspension with smEB1 medium + 10 µM ROCK inhibitor Y-7632. For four days, dual SMAD-signalling was inhibited by administration of SB431542 and LDN-93189. After all, spheres were sown out on MG-coated dishes for further stabilisation and expansion of smNPCs.
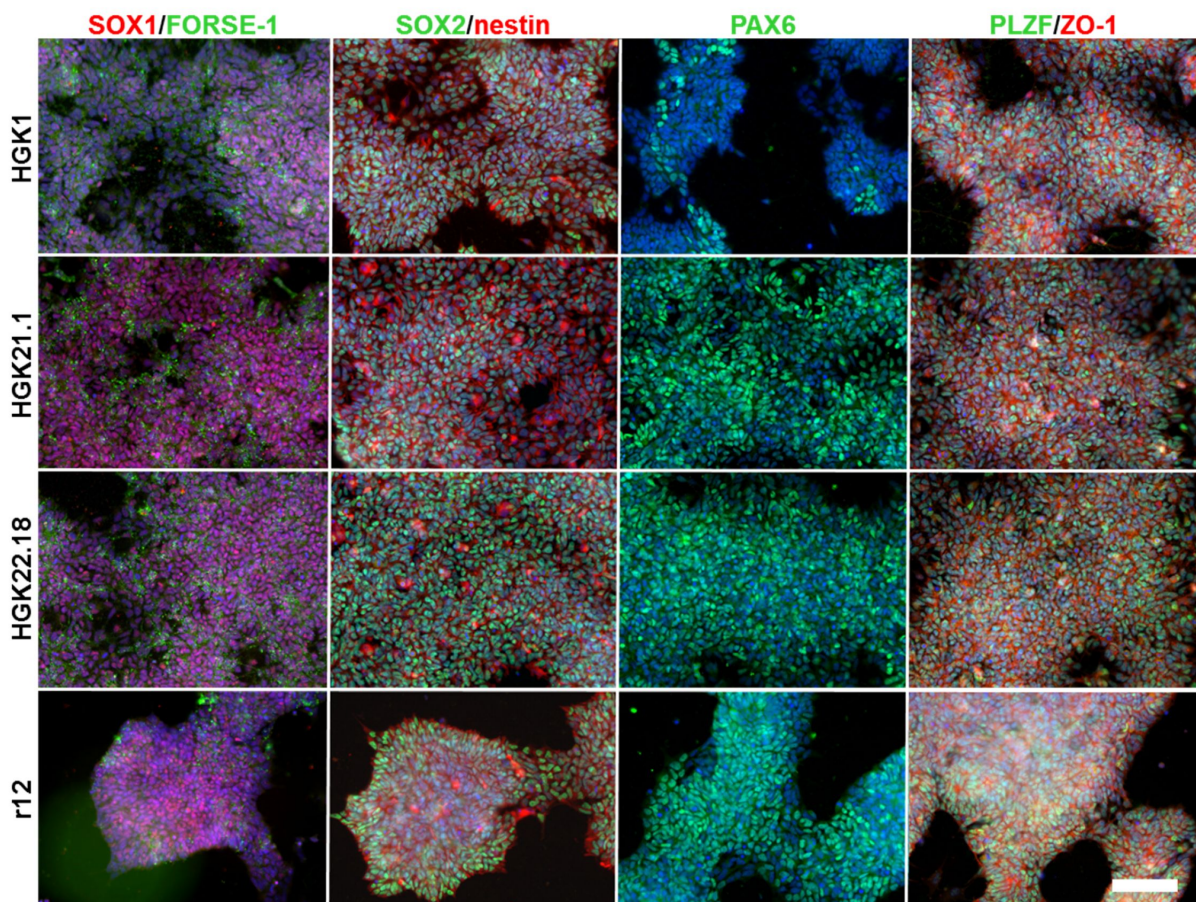
Fig. 32: iPSC-derived smNPC lines evidently exhibited typical NSC markers PAX6 (green), SOX1 (red), SOX2 (green) and nestin (red) in four representative cell lines upon immunolabelling. Expression of anterior marker FORSE-1 (green) was visualised as well. Since smNPCs possess an early pre-rosette NSC fate expression of characteristic rosette-markers PLZF (green) and ZO-1 (red) did not reveal the typical petal-like arrangement of lt-NES®SCs. Taken together, all smNPC lines were comparable to those of the original publication according to their marker profile. Nuclei were counterstained with DAPI (blue) (scale bar 100 µm, valid for all cell lines). For other cell lines, see 10.6, Fig. 66.

7.4.2 smNPCs differentiate into motoneurons with high efficiency

In an initial proof-of-principle experiment, an OLIG2-GFP smNPC reporter cell line (courtesy of Lisa Neumann) was differentiated into MNs. OLIG2-GFP iPSC reporter line was a kind gift of Ying Liu (University of California San Diego, USA).

This reporter cell line contains a knock-in of a GFP cassette into the human *OLIG2* gene locus enabling to monitor motoneuronal *in vitro*-differentiation (Liu *et al.* 2011). Upon patterning into the pMN domain, distinct *OLIG2*-expression is marked by GFP fluorescence in OLIG2-GFP reporter line.

OLIG2-GFP reporter smNPCs presented the same morphologic appearance during standard cultivation as the smNPCs in the original publication by Reinhardt *et al.*, 2013. One day after splitting, OLIG2-GFP reporter smNPCs assembled in smaller colonies with a cobblestone-like composition and flat growth (Fig. 33 **A**). Subsequently, those smNPCs aggregated to more condensed colonies with distinct round edges and 3D growth similar to murine iPSCs (Fig. 33 **B**).
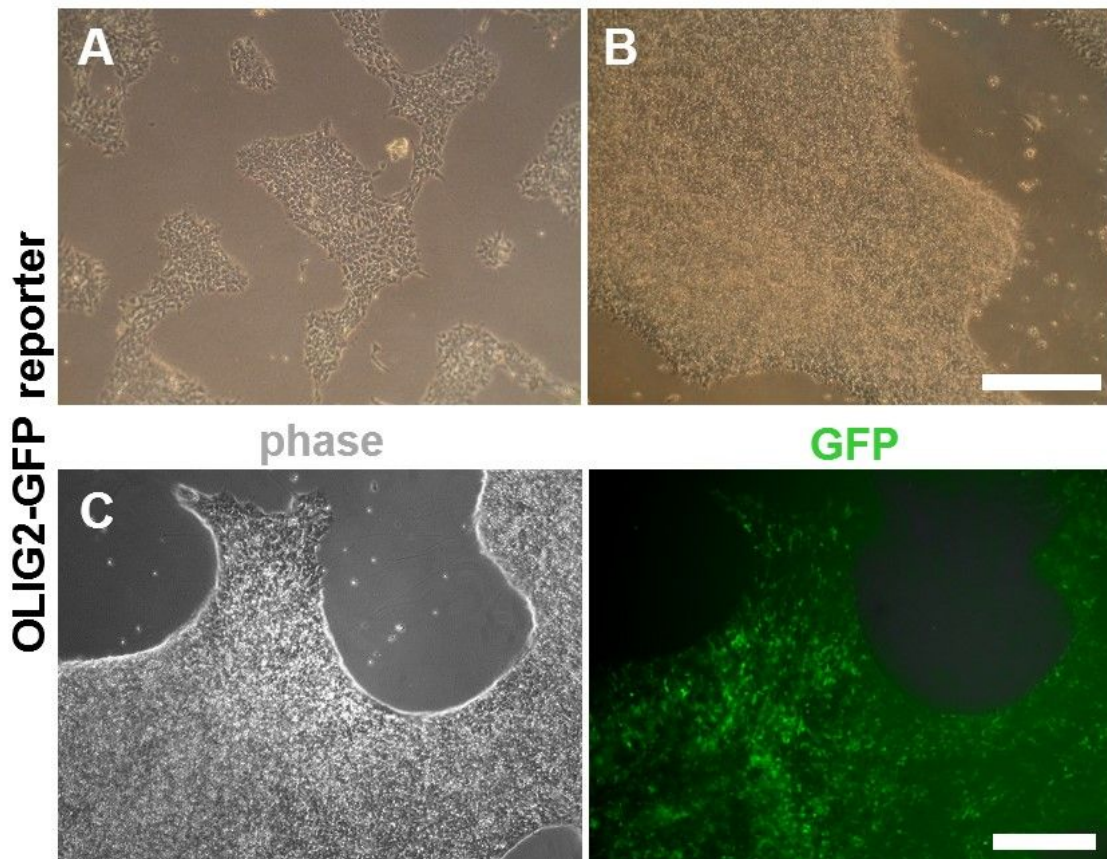
Fig. 33: (**A**) OLIG2-GFP reporter smNPCs aligned to smaller flat colonies with frayed rims one day after splitting in phase images. Single cells could still be recognised in the cobblestone-like assembly. (**B**) On day 4 after splitting, smNPCs agglomerated more densely and formed tightly packed 3D colonies with sharp edges comparable to murine iPSCs. (**C**) On d5 after motoneuronal induction, OLIG2-GFP reporter smNPCs considerably showed GFP fluorescence indicating a strong *OLIG2* expression. Thus, a correct regionalisation of smNPCs into the pMN domain took widely place (scale bar 200 µm, valid for all images).

Treatment with caudalising morphogen RA (1 µM) and ventralising agents Pur (1 µM) and SAG (1 µM) for one week evidently induced motoneuronal patterning. After five days, OLIG2-GFP reporter gene was widely expressed in smNPCs (Fig. 33 **C**) notifying intense endogenous *OLIG2* gene expression which hallmarked patterning of neural progenitor cells into the pMN domain.

Indeed, immunocytochemical staining of OLIG2-GFP reporter smNPCs on day 7 revealed strong expression of characteristic pMN-markers OLIG2, NKX6.1 and upper spinal cord marker HOXB4. NKX2.2^{+} cells were also detectable denoting a strong ventralisation because NKX2.2 is a marker of the outermost ventral domain p3. Already at this early time point which is comparable to day 28 in the iPSC-based run-through protocol, there were proper MNs identifiable by staining HB9, ISL1 or SMI-32 (Fig. 34). Final motoneuronal maturation for further 2-3 weeks gave rise to a considerable amount of *bona fide* MNs betokened by expression of ChAT, HB9 and ISL1 (Fig. 35).
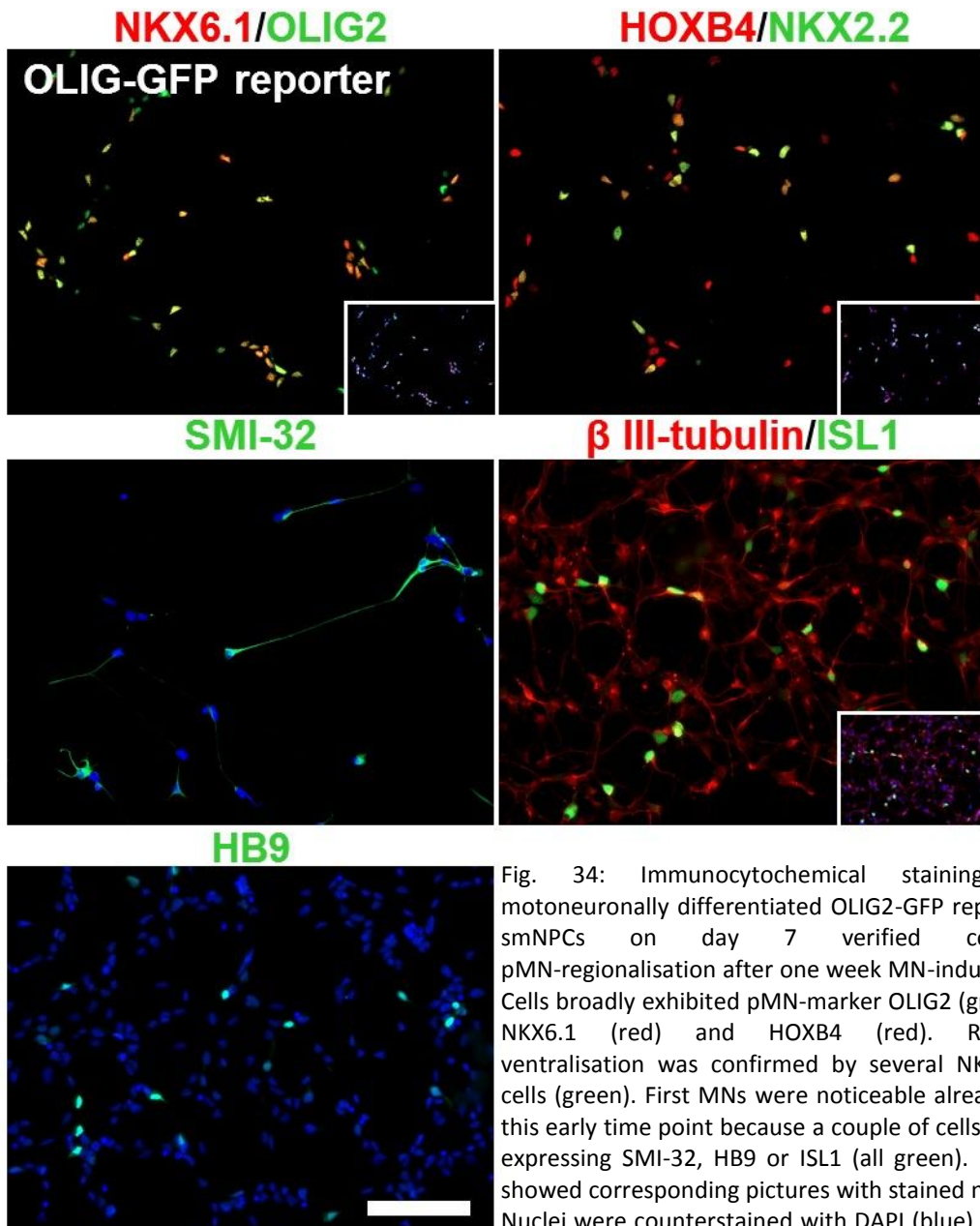
Fig. 34: Immunocytochemical staining of motoneuronally differentiated OLIG2-GFP reporter smNPCs on day 7 verified correct pMN-regionalisation after one week MN-induction. Cells broadly exhibited pMN-marker OLIG2 (green), NKX6.1 (red) and HOXB4 (red). Robust ventralisation was confirmed by several NKX2.2^{+} cells (green). First MNs were noticeable already at this early time point because a couple of cells were expressing SMI-32, HB9 or ISL1 (all green). Insets showed corresponding pictures with stained nuclei. Nuclei were counterstained with DAPI (blue) (scale bar 100 μm, valid for all images).
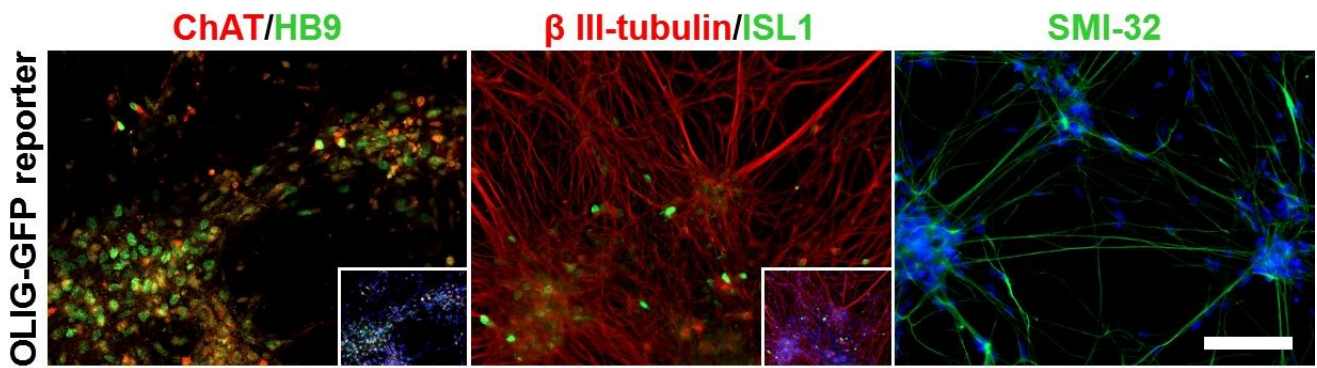
Fig. 35: Two weeks final MN maturation yielded a substantial number of ChAT⁺ (red)/HB9⁺ (green) or SMI-32⁺ (green) MNs in immunocytochemical staining. Strong neuronal differentiation was marked by excessive amount of β III-tubulin⁺ neurons of which a sufficient portion comprised ISL1⁺ MNs. Insets showed corresponding pictures with stained nuclei. Nuclei were counterstained with DAPI (blue) (scale bar 100 µm, valid for all images).

7.4.3 smNPCs were convertible into another NSC subpopulation

Among the first stably expandable human NSC lines, lt-NES®SCs were described by Koch *et al.* (Koch *et al.* 2009). Demonstrating cellular plasticity of smNPCs and concomitantly generating another possibly MN-differentiable NSC line, OLIG2-GFP smNPC reporter cells could be easily converted into these lt-NES®SCs by simple medium change (Fig. 36).

With 50% confluent smNPCs medium was switched to NSC1 medium containing 20 ng/ml bFGF for two days in total. Immediately, cells underwent obvious morphological changes indicated by re-arrangement to the typical rosette-type shape (Fig. 37 **A**). Upon standard trypsinisation regimen (Koch *et al.* 2009), smNPC-derived lt-NES®SCs were stably expandable in NSC1 medium (Fig. 37 **B**) even when 150 nM RA and 1 µM SAG were added during expansion to induce motoneuronal patterning (Fig. 37 **C**). Indeed, constant RA- and SAG-administration shifted OLIG2-GFP lt-NES®SCs reporter cells towards a ventral-caudal pMN-like cellular fate. OLIG2 expression in these lt-NES®SCs reporter cells was marked by GFP-fluorescence already after one week (Fig. 37 **D**)

OLIG2-GFP lt-NES®SCs reporter cells showed characteristic expression of typical NSC markers such as neural intermediate filament nestin or embryonic developmental transcription factors SOX2, PAX6 and DACH1. Moreover, rosette markers PLZF and ZO-1 clearly visualised characteristic blossom-like arrangement of lt-NES®SCs with a concentration of tight-junction protein ZO-1 in the centre. Neural crest marker AP2 was only found sporadically within lt-NES®SCs culture (Fig. 38).

For final motoneuronal differentiation, OLIG2-GFP lt-NES®SCs reporter cells were seeded in MN1 medium. Pre-treatment with RA and SAG occurred during regular expansion culture for either eleven days (11d+RA/SAG) or 21 days (21d+RA/SAG), respectively. As negative control (neg ctrl) served lt-NES®SCs which were never pre-treated with RA or SAG.
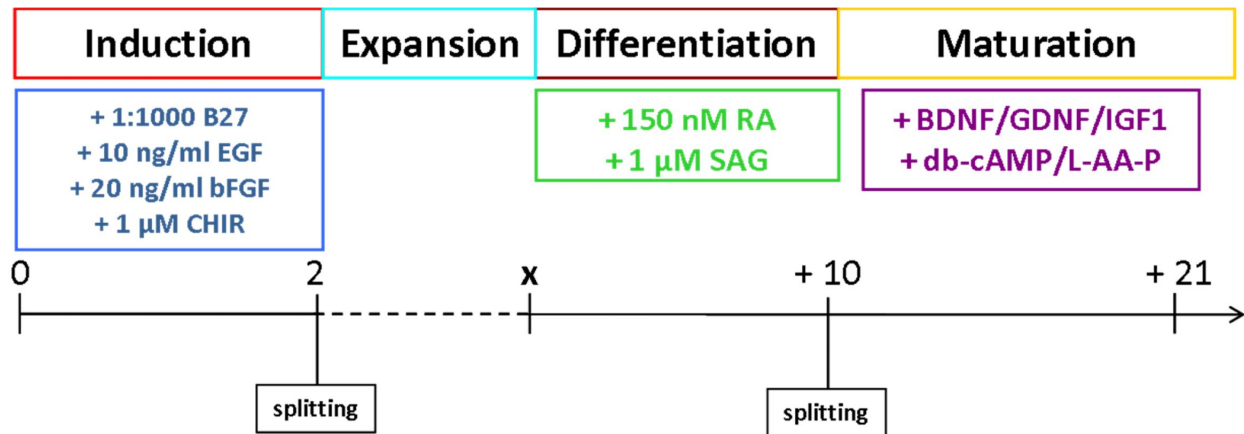
Fig. 36: Schematic picture of conversion of smNPCs into lt-NES®SCs and prospective motoneuronal differentiation modified from (Koch *et al.* 2009). Adherent smNPCs were converted into lt-NES®SCs by simple medium change for two days applying EGF, bFGF, B27 and GSK3 inhibitor CHIR99021. Obtained lt-NES®SCs were stably expandable and capable of motoneuronal differentiation by RA and SAG administration and consecutive maturation.

OLIG-GFP reporter
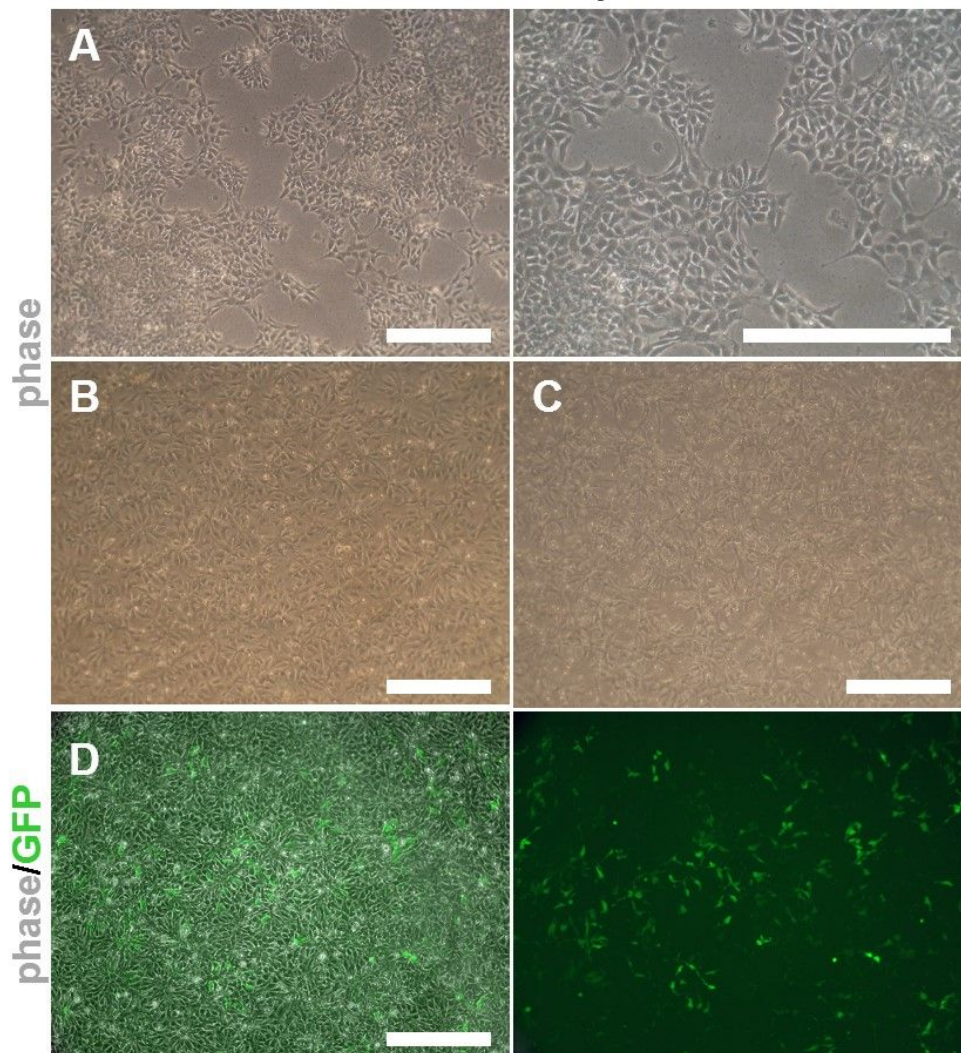
Fig. 37: (**A**) Changing medium converted OLIG2-GFP smNPC reporter cells immediately into lt-NES®SCs marked by overt appearance of neural rosettes. (**B**) lt-NES®SCs kept this typical morphology throughout expansion (**C**) even when MN patterning morphogens RA (150 nM) and SAG (1 µM) were added to regular cultivation medium NSC1. (**D**) OLIG2-GFP lt-NES®SCs reporter cell line proved functional since evident GFP fluorescence was visible in regular culture indicating *OLIG2* expression upon RA- and SAG-treatment after one week (scale bar 200 µm, valid for all images).

Immunocytochemical staining on day 1 after plating for MN maturation pictured the presence of diverse pMN regional markers. In untreated OLIG2-GFP lt-NES®SCs reporter cells, there was no expression of HB9, ISL1, OLIG2, NKX6.1 or HOXB4 visible. Yet, growth factor withdrawal by medium change from NSC1 to MN1 obviously induced rapid neuronal development of lt-NES®SCs towards β III-tubulin+ neurons even in untreated lt-NES®SCs. SMI-32 antibody detected non-phosphorylated neurofilament-H in ventral horn motoneurons in spinal cord slices and stained furthermore a subset of neurons in dissociated spinal cultures which morphologically resembled motoneurons identified *in vitro*: large (>20 µm) cell body, prominent neuritic arborisation and generally a single long axon (Carriedo *et al.* 1996). Thus, SMI-32 was regarded as a typical motoneuronal marker (Ebert *et al.* 2009). However, SMI-32 antibody also recognised neurons in the PNS and CNS such as human GABAergic cortical neurons (Campbell *et al.* 1989). Therefore, sporadic SMI-32+ cells apparent in negative control rather depicted those non-motor neurons (Fig. 39 **A**).
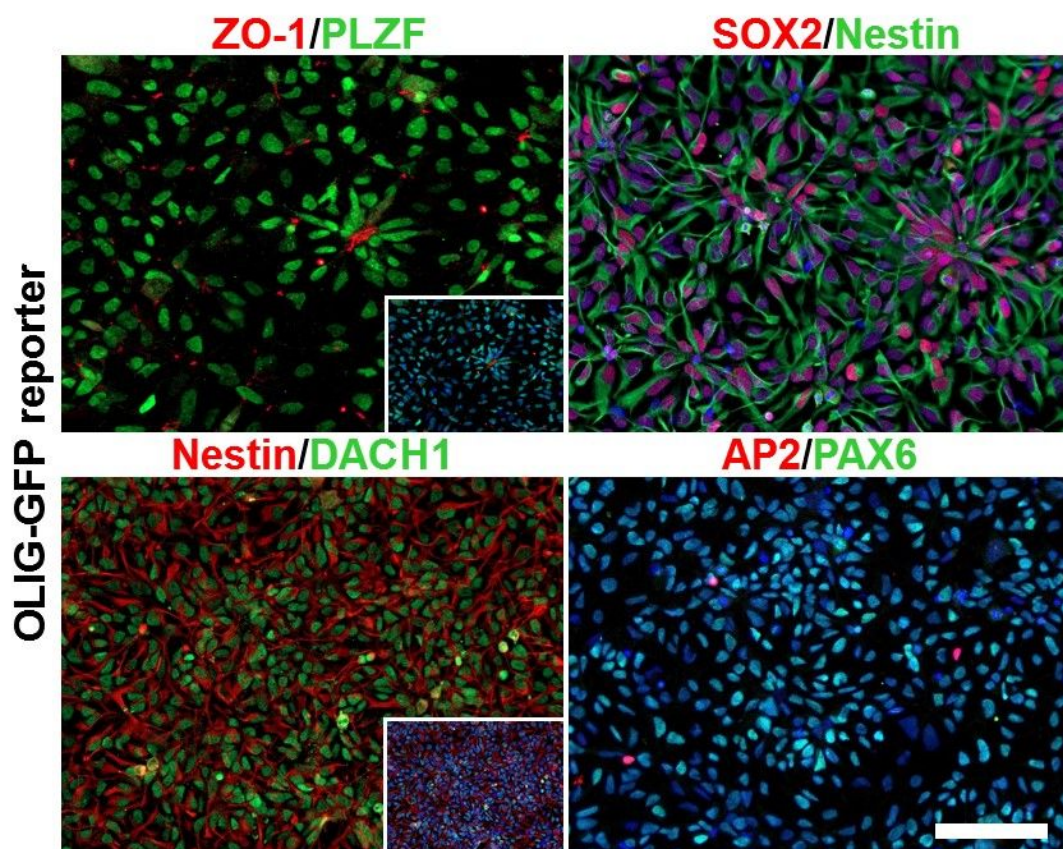
Fig. 38: Immunolabelling of smNPC-derived lt-NES®SCs verified the rosette-like character by expressing typical NSC markers PAX6 (green), SOX2 (red), nestin (red/green) and DACH1 (green). Characteristic rosette-shape was visualised by staining PLZF (green) and ZO-1 (red) displaying a strong central ZO-1 signal with petal-like arrangement of PLZF+ NSCs. Contamination of neural crest cells was hardly detectable by only few AP2+ cells (red). Insets showed corresponding pictures with stained nuclei. Nuclei are counterstained with DAPI (blue) (scale bar 100 µm, valid for all images).

In contrast, lt-NES®SCs treated with RA and SAG beforehand for eleven days (11d+RA/SAG) or 21 days (21d+RA/SAG), respectively, clearly showed expression of characteristic pMN markers like OLIG2, NKX6.1 and HOXB4. So, correct patterning did take place. However, OLIG2/NKX6.1 double-positive progenitor cells were noticeably rather found in lt-NES®SCs treated for 21 days indicating that a longer patterning period led to higher number of correct MN progenitor cells. Moreover, already one day after plating patterned lt-NES®SCs developed into MNs expressing HB9, ISL1 and SMI-32 (Fig. 39 **A**).

After 16 days maturation in MN1 medium, pre-treated lt-NES®SCs exhibited distinct expression of MN markers HB9, ISL1, ChAT and SMI-32. To evidence reliability of GFP fluorescence as reporter signal of *OLIG2* expression, cells were stained for both epitopes simultaneously revealing a decent number of GFP/OLIG2 double-positive cells. So, there were still MN progenitor cells present in this culture (Fig. 39 **B**).

However, untreated lt-NES®SCs lacked expression of HB9 and ChAT. Only very few ISL1$^+$ and SMI-32$^+$ neurons were present. Since MN1 medium still contained low concentrations of RA (50 nM) and Pur (0.5 µM), spontaneous MN differentiation might have occurred even in untreated lt-NES®SCs.

Taken together, initial proof-of-principle experiments denoted feasibility of using stable NSC lines for MN differentiation and advantages of RA/SAG pre-treatment.
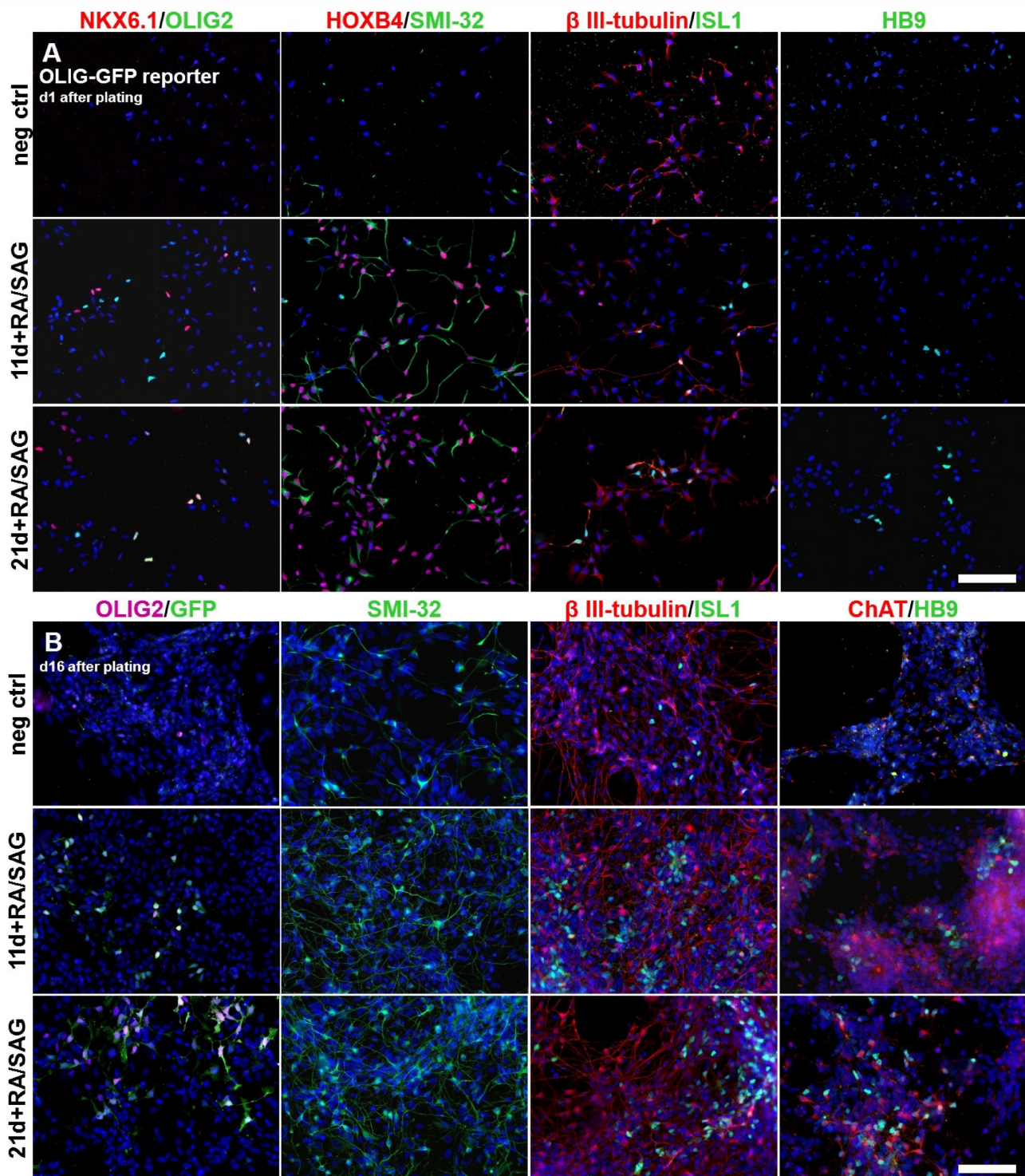
Fig. 39: (**A**) OLIG2-GFP reporter lt-NES®SCs pre-treated with RA and SAG for eleven days (11d+RA/SAG) and 21 days (21d+RA/SAG), respectively as well as untreated cells as negative control were seeded for final MN maturation and subjected to immunocytochemistry. One day (d1) after plating, negative control did not exhibit pMN marker gene expression but only differentiation into β III-tubulin⁺ neurons (red) and very few SMI-32⁺ neurons (green). Treated lt-NES®SCs contrarily expressed typical pMN markers OLIG2 (green), NKX6.1 (red) and HOXB4 (red). In addition, first ISL1⁺ and HB9⁺ motoneurons (green) appeared. (**B**) Longer maturation period for 16 days (d16) increased obvious numbers of mature motoneurons in treated lt-NES®SCs illustrated by positive staining for ChAT (red), HB9, ISL1 and SMI-32 (all green). MN cultures still contained MN progenitors marked by double-positive OLIG2⁺ (purple)/GFP⁺ (green) cells which were missing in negative control. Just very few ISL1⁺ and SMI-32⁺ cells were apparent in untreated lt-NES®SCs hinting at only rare spontaneous MN differentiation for they were also devoid of mature ChAT⁺/HB9⁺ mature motoneurons. Nuclei were counterstained with DAPI (blue) (scale bar 100 μm, valid for all images).

7.4.4 Differentiation of smNPCs from SMA patients and asymptomatic PLS3 discordant siblings into motoneuronal cultures

The preceding experiments with OLIG2-GFP smNPC reporter cell line strikingly pointed out the advantages of this NSC line concerning feasibility, duration and differentiation efficiency.

In addition, successful application of pMN-domain inducing morphogens RA and SAG during regular maintenance of smNPC-derived lt-NES®SCs demonstrated a visible enhancement of efficiency in MN generation. Thus, the same approach was undertaken with the other smNPC lines.

The regular cultivation medium NPC1 was additionally supplemented with 1 µM RA and 1 µM SAG for at least two weeks with every cell line before the standard MN differentiation procedure (i.e. withdrawal of GSK3 inhibitor CHIR99021 and administration of 1 µM RA/SAG/Pur respectively for one week) was applied (Fig. 40).
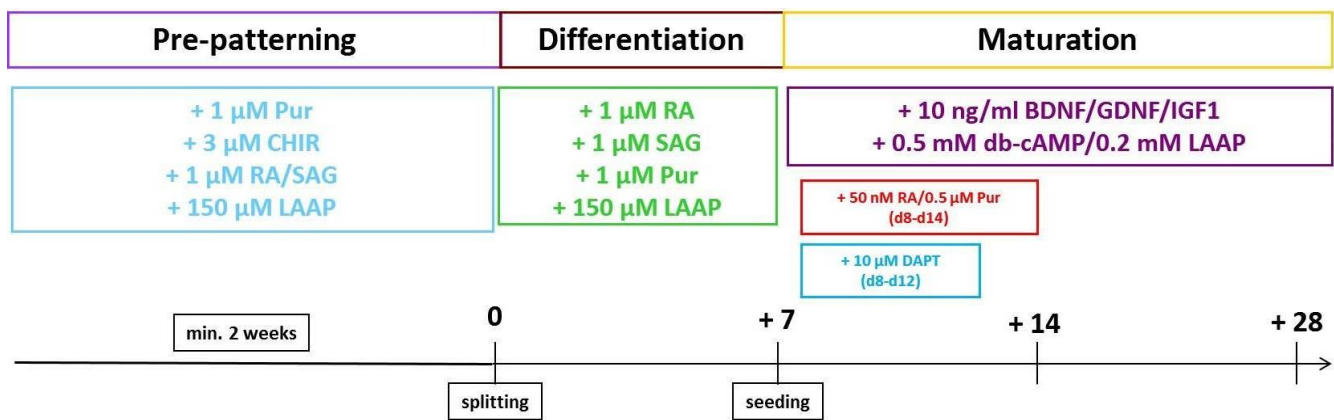
Fig. 40: Schematic presentation of smNPC differentiation according to a protocol modified from Reinhardt *et al.*, 2013. For at least two weeks, smNPCs were primed into pMN-domain by additional application of 1 µM RA and 1 µM SAG in standard cultivation medium NPC1 during regular maintenance. Once cells were 70% confluent, CHIR99021 was withdrawn and cells grown for one week. On day 7, patterned smNPCs were seeded for final maturation in NPC3 medium containing growth factors. Furthermore, 0.5 mM Pur and 50 nM RA were added from d8-d15 to warrant full motoneuronal differentiation of remaining progenitor cells. Additionally, notch-signalling was inhibited from d8-d12 by administration of γ-secretase inhibitor DAPT to push neuronal differentiation. At last, MN cultures were analysed after three weeks maturation.

In order to illustrate a correct shift into the pMN domain, representative cell lines of every phenotype (i.e. SMA I, SMA III, asymptomatic discordant and healthy control) were exemplarily examined for expression of standard CNS markers as well as classical motoneuronal progenitor markers on day 8 (Fig. 41). The overt expression of pan-CNS markers SOX2 and nestin depicted the NSC-like character of RA-treated smNPCs. Obviously, all four cell lines exhibited a strong expression of ventral pMN markers OLIG2 and NKX6.1 and caudal marker HOXB4 irrespective of their phenotypic background. The moderate presence of PAX6^{+} cells as well as the little amount of NKX2.2^{+} cells highlighted the exact shift of originally anterior smNPCs into the ventral-posterior pMN domain.

Exemplary immunocytochemical staining of motoneuronally differentiated smNPC lines representing the different phenotype classes revealed a broad expression of typical MN markers HB9, ISL1 and SMI-32 on day 8 (Fig. 42 **A**). Furthermore, HB9^{+} MNs also expressed PLS3 making this *in vitro*-disease model suitable for further studies on PLS3-specific influence in discordant families. Remarkably, at this early time point of MN differentiation there were

not fewer MNs in severely affected SMA I line HGK1. Quantification of MN number in all cell lines highlighted this fact (Fig. 43 **A**, **B**). From three independent MN differentiation runs (n=3), cells with these two markers were manually counted (HB9: 1,200-2,000 cells; ISL1: 1,400-2,400 cells in total) and their ratios computed in relation to total number of cells.

With most of the cell lines, the percentage of HB9$^+$ MNs ranged between 20-30% of all cells (Fig. 43 **A**). Only HGK13, HGK16, HGK21.8 and HGK28.11 generated fewer HB9$^+$ MNs (6-12%) pointing out variable differentiation efficiency among individual cell lines *in vitro*. Astonishingly, female control line COII.2 underperformed delivering just 2% HB9$^+$ MNs. Irrespective of the genetic background, there was no detectable trend in HB9 efficiency measurable since members of all three disease-related phenotype classes (i.e. SMA I, SMA III, asymptomatic discordant) generated a high amount of HB9$^+$ MNs. Thus, in comparison to control line r12 efficiency differences with statistical significance were only found for low HB9-expressing cell line COII.2 probably reflecting more intrinsic cell line-specific features than disease-related reasons. Therefore, no significant difference in HB9 generation was detected when results were summarised according to the phenotype (Fig. 43 **E**). Note that for comparability reasons, control line COII.2 was always excluded from phenotypic summaries since it did not represent a proper MN culture and additionally did not give rise to sufficient MNs until day 27 either.

Similarly, ISL1 expression on day 8 did not significantly differ amongst the cell lines (Fig. 43 **B**). On average, MN cultures comprised 10-30% ISL1$^+$ MNs independent of their corresponding phenotypic background. Of course, grouping all values according to the phenotype did not result in statistically significant differences (Fig. 43 **F**). Moreover, there was no strict congruency between the two MN markers HB9 and ISL1 within the cell lines observable. For example, HGK22.18 showed 23% HB9$^+$ MN but only 11% ISL1$^+$ MNs pinpointing the need of examining several MN markers in parallel as carried out in this study.

Taken together, early *in-vitro* MN cultures exhibited rather comparable amounts of HB9$^+$ (20-30%) or ISL1$^+$ (~20%) cells with reasonable efficiency on day 8 when summed up according to their phenotype. By trend, MN cultures of asymptomatic discordant women contained the fewest HB9$^+$ (~16%) or ISL1$^+$ MNs (~12%).

Nonetheless, the detrimental effect of SMN loss in MN maintenance became obvious after three weeks of further maturation (Fig. 42 **B**). On day 27, MN cultures were stained for MN markers HB9, ISL1, SMI-32 and additionally mature MN marker ChAT. MN cultures of SMA I patient line HGK1 barely contained any ISL1$^+$ or HB9$^+$/ChAT$^+$ MNs anymore whereas in discordant individuals HGK27.13 (SMA III) and HGK16 (asymptomatic) as well as healthy control line r12 MNs expression of the aforementioned markers was demonstratively detectable. Yet, in comparison to day 8 HGK27.13 exhibited already an apparent decline in MN number on day 27. Notably, expression of SMI-32 did not seem to be negatively affected in cell lines with disease-related background apparently.

Counting HB9$^+$ and ISL1$^+$ cells in such MN cultures evidently pointed out these trends (Fig. 43). From three independent MN differentiation runs (n=3), cells with these markers were manually counted (HB9: 800-1,700 cells; ISL1: 300-900 neurons in total) and their ratios calculated relative to total number of cells (HB9) and total number of β III-tubulin$^+$ neurons (ISL1), respectively. Note that owing to technical reasons three trials could not be evaluated for every cell line (see tables in Fig. 43 **C**, **D**).

Healthy control line r12 exhibited the highest percentage of HB9$^+$ MNs (~21%) on day 27 whereas SMA I patient HGK1 suffered from a drastic drop in MN number losing almost entirely its HB9$^+$ cells (~0.7%) (Fig. 43 **C**). With varying range, SMA III cell lines and their corresponding asymptomatic siblings' cell lines generally revealed 3-5% HB9$^+$ MNs after three weeks. Only

HGK21.1, HGK27.10, HGK27.13 and HGK28.9 presented a higher HB9 number (8-13.5%). However, for HGK21.1 there was only a single sample available depriving its validity. The other three cell lines strongly expressed HB9 on day 8 so that their loss of HB9$^+$ cells began from a high level. Nevertheless, in comparison to control line r12 the decline of HB9$^+$ MNs was only significant with respect to SMA I HGK1. This statistically valid difference also held true in the phenotypic overview (Fig. 43 **G**): While there was no significant difference detected among healthy control, SMA III samples or asymptomatic samples on day 27, differences between healthy control and SMA I was very significant.

Yet, in respect of number of ISL1$^+$ MNs there were no such clear differences detectable within single cell lines (Fig. 43 **D**). Indeed, healthy control line r12 revealed the most ISL1$^+$ MNs (23%) on day 27. Similarly, severely affected SMA I line HGK1 heavily lost ISL1$^+$ MNs leaving only 2.3% from original ~20% on day 8. In cell lines from discordant family members, the amount of remaining ISL1$^+$ MNs ranged either between ~5-7.5% (HGK13, HGK16, HGK21.8 and HGK22.18) or ~9-17% (HGK22.17, HGK27.10, HGK28.9). Surprisingly, SMA III patient line HGK27.13 nearly reached the level of control line r12 (~21%). However, in comparison to day 8 HGK27.13 had to bear a loss of ~7% whereas r12 presented even a slight increase in ISL1$^+$ cell number (from ~21% to ~23%). Slow growing asymptomatic cell line HGK28.11 showed again the least number of all discordant cell lines (2.8%) ranging hardly above the results of SMA I HGK1. So, the only statistically significant difference was observed between control r12 and SMA I HGK1 (Fig. 43 **D**). Understandably, those individual results were exactly reflected in the phenotype summary (Fig. 43 **H**). Between classified samples of SMA I, SMA III or asymptomatic individuals, the only significant difference in ISL1 number was present between SMA III and SMA I MN cultures on day 27. Neither was there a significant change measured when SMA III or asymptomatic samples were likened to healthy control. Just SMA I samples showed a very significant difference in comparison to healthy control.

In summary, matured *in-vitro* MN cultures on day 27 revealed only in SMA I phenotype a significant decrease in MN survival and drastic drop of ISL1$^+$ and HB9$^+$ cell numbers. Even though healthy control lost ~8% HB9$^+$ MNs, it maintained number of ISL1$^+$ MNs on nearly equal level. MN death in SMA III or asymptomatic phenotype was insignificant concerning ISL1 and HB9. Still, by trend the number of ISL1$^+$ MNs was reduced almost halving when matched to values on day 8.

In Fig. 44 the individual changes of ISL1$^+$ and HB9$^+$ cell numbers between day 8 and day 27 were displayed with regard to the phenotype. Basically, in all four phenotype classes the number of HB9$^+$ MNs diminished within the three weeks of maturation (healthy control: 29.8% ↘20.8%; SMA I: 26.8% ↘0.7%; SMA III: 20.9% ↘8.9%; asymptomatic: 16.5% ↘6.3%) (Fig. 44 **A**). Yet, only SMA I had to cope with such a massive loss of HB9$^+$ MNs when day 8 was compared to day 27. A similar steep decline in ISL1$^+$ cell number was detected in SMA I phenotype (19.5% ↘2.3%) (Fig. 44 **B**). SMA III and asymptomatic phenotype illustrated a moderate decrease in ISL1$^+$ cell number (SMA III: 21.5 ↘14.7%; asymptomatic: 11.8% ↘7.2%) whereas healthy control even slightly increased its ISL1$^+$ amount (19.3% ↗23%).
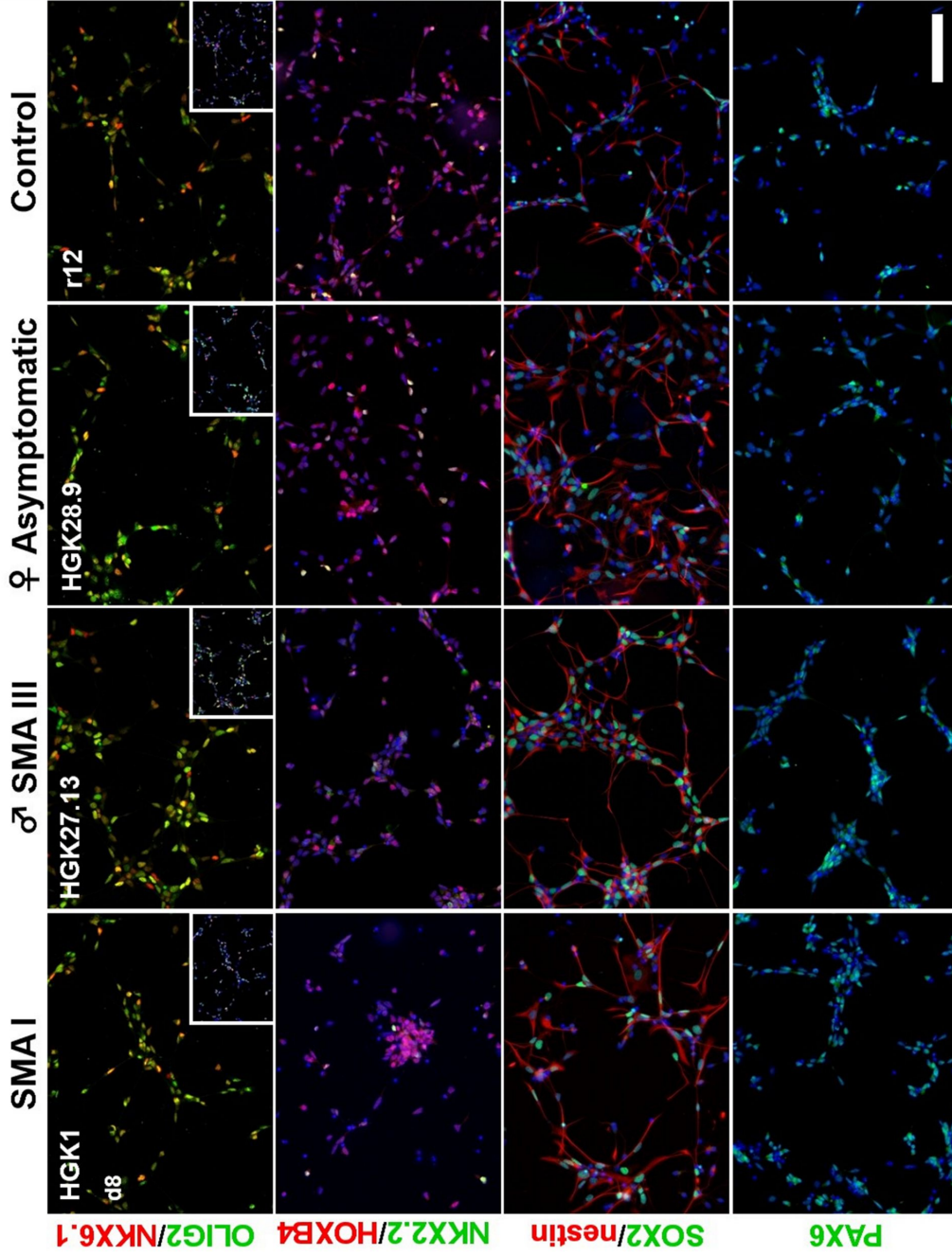
Fig. 41: Immunocytochemistry of four motoneuronally differentiated smNPC lines representing the respective phenotype classes (control r12, SMA I patient HGK1, SMA III patient HGK27.13 and asymptomatic sister HGK28.9) proved correct pMN-regionalisation on day 8. Pan-NSC markers SOX2 (green) and nestin (red) were clearly visible. Early CNS marker PAX6 (green) was moderately expressed. Cells broadly exhibited pMN-marker OLIG2 (green) and NKX6.1 (red). Strong co-localisation (yellow) of these markers underlined presence of true MN-progenitor cells. Moreover HOXB4 (red) expression verified sufficient spinal caudalisation. Only few NKX2.2⁺ cells (green) marked abidance of correct domain boundaries. Insets showed corresponding pictures with stained nuclei. Nuclei were counterstained with DAPI (blue) (scale bar 100 µm, valid for all images).
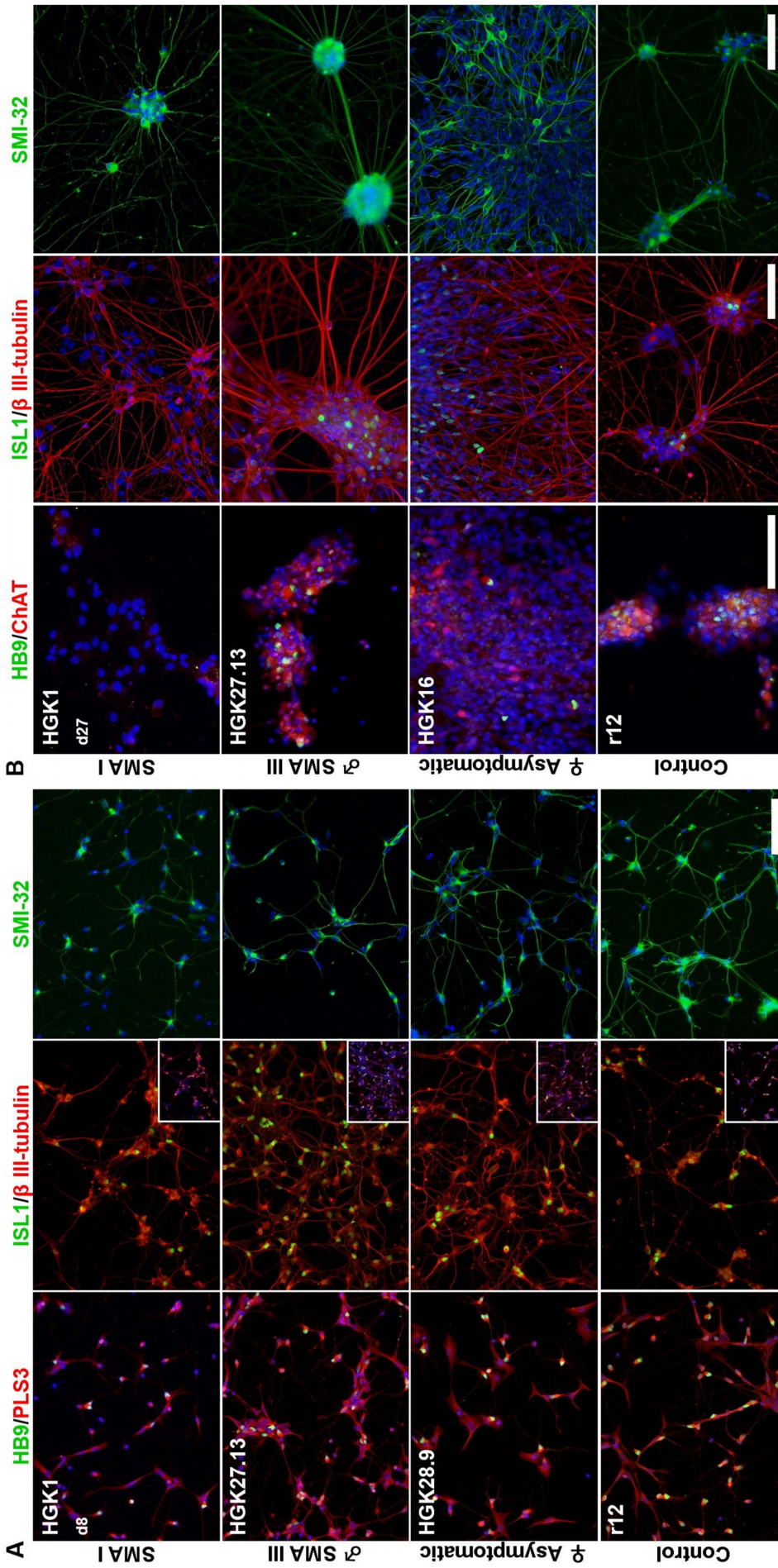
Fig. 42: **(A)** Immunocytochemical staining of four representative motoneuronally differentiated smNPC lines (control r12, SMA I patient HGK1, SMA III patient HGK27.13 and asymptomatic sister HGK28.9) demonstrated strong expression of classical MN marker HB9, ISL1 and SMI-32 (all green) on day 8 irrespective of their genetic background. HB9+ MNs expressed PLS3 (red) as well. **(B)** After three weeks further maturation, obvious changes in MN survival were visible. Severely affected SMA I patient HGK1 did not exhibit any ISL1+ (green) or HB9+(green)/ChAT+ (red) MNs anymore. On the other hand, MN cultures of control line r12, SMA III patient HGK27.13 and asymptomatic individual HGK16 still contained ISL1+ or HB9+/ChAT+ MNs. Contrarily, broad SMI-32 expression was detectable in all four cell lines on d27. Insets showed corresponding pictures with stained nuclei. Nuclei were counterstained with DAPI (blue) (scale bar 100 µm, valid for all images).
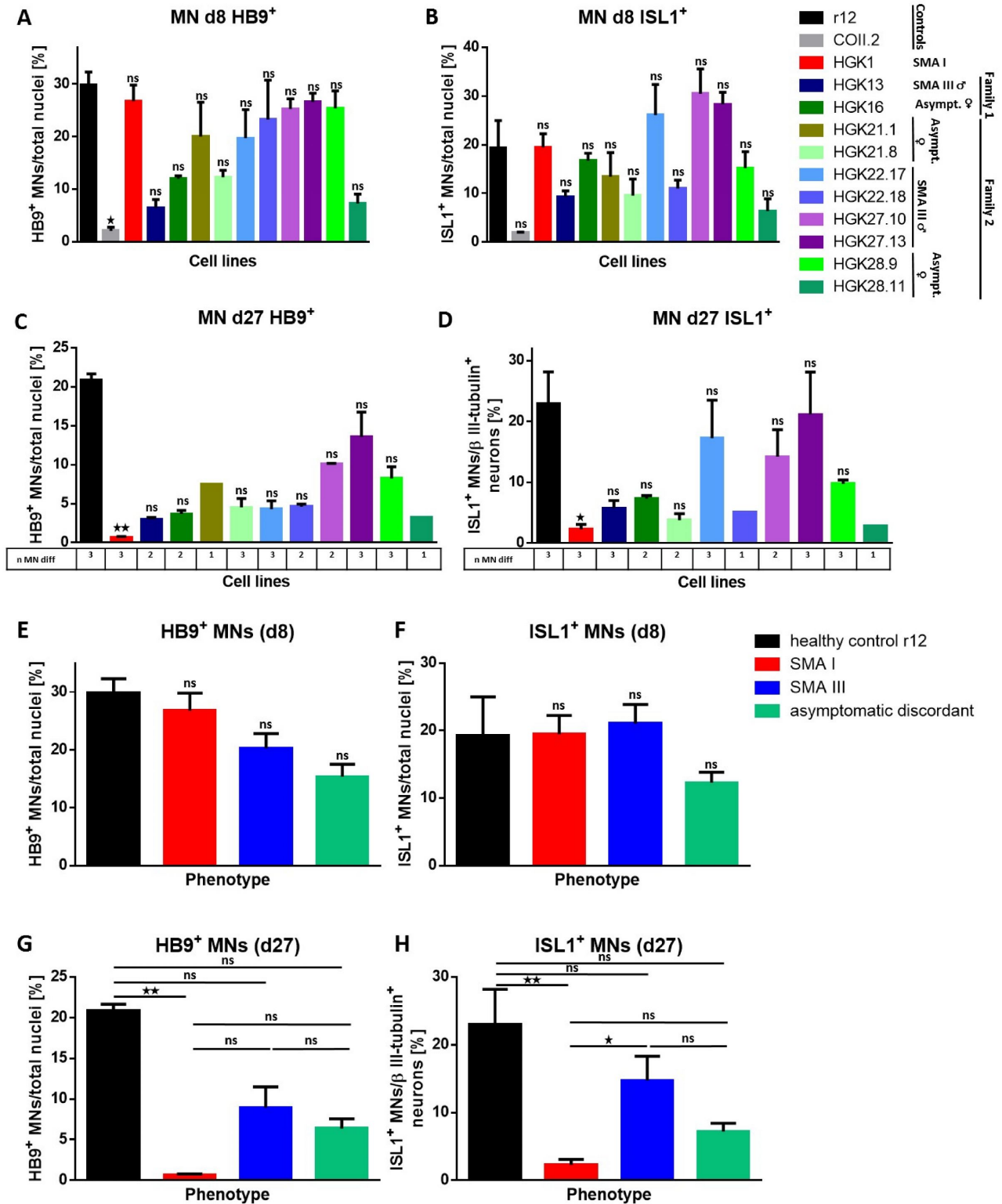
Fig. 43: Quantification of MN marker expression in smNPC-derived MN cultures of different healthy and SMA affected or asymptomatic individuals on day 8 and after three weeks maturation on day 27. Mean number of HB9+ MNs on day 8 (**A**), ISL1+ MNs on day 8 (**B**), HB9+ MNs on day 27 (**C**) and ISL1+ MNs on day 27 (**D**) were depicted for each individual cell line (day 8: HB9: 1,200-2,000 cells; ISL1: 1,400-2,400 cells counted in total; day 27: HB9: 800-1,700 cells; ISL1: 300-900 neurons counted in total). Additionally, mean values were summed up according to the phenotypic background for day 8 (**E**, **F**) and day 27 (**G**, **H**), respectively. (**A**) A reasonable amount of HB9+ MNs was visible within the individual cell lines ranging between 20-30% of all cells. Fewer HB9+ MNs (6-12%) were found in cell lines HGK13, HGK16, HGK21.8 and HGK28.11, even undercut by control line COII.2 (2%). Overt significant differences between controls r12 and COII.2 rather pointed out intrinsic features of individual cell lines. (**B**) Similarly, ISL1 expression on day 8 did not significantly differ amongst the cell lines. Thus,

no correlation between genetic background and MN number could be drawn on day 8. Nor were ISL1 and HB9 numbers congruent within a single cell line. (**E, F**) Grouping the data according to the four phenotypic classes did not reveal any statistically significant difference. (**C**) On day 27, control line r12 showed the highest amount of HB9$^+$ MNs (~21%) whereas all other cell lines faced a marked drop in HB9$^+$ number. SMA I line HGK1 almost completely lost its HB9$^+$ MNs (0.7%) rendering a significant difference compared to control r12. SMA III and asymptomatic cell lines ranged from 3-13%. (**G**) Therefore, when those results were grouped and phenotypes were likened to controls there was significant difference detectable. Between SMA-related phenotypes differences were not significant. (**D**) Evaluation of ISL1$^+$ cell survival did not present such a clear trend. Variances in ISL1$^+$ cell number were higher resulting in mostly insignificant differences. Only SMA I line HGK1 contained significantly lower ISL1$^+$ cell numbers. (**H**) Of course, these facts were reflected in the phenotype summary with the only significant difference between controls and SMA I. Note that control COII.2 was excluded in phenotypic MN culture overviews. Results showed the counting of three independent differentiation runs (n=3) for day 8 whose ratios were calculated in relation to total number of cells (HB9: 1,200-2,000 cells; ISL1: 1,400-2,400 cells counted in total). For day 27, one to three independent differentiation runs (see tables in **C, D**) were considered with at least half of the cell lines thrice (n=3). Mean ratios were computed relative to total number of cells (HB9) and total number of β III-tubulin$^+$ neurons (ISL1), respectively (HB9: 800-1,700 cells; ISL1: 300-900 neurons counted in total; Kruskal-Wallis test, $p < 0.05$ = *, $p < 0.01$ = **). Note that owing to technical reasons three trials could not be evaluated for every cell line. Error bars represented ± SEM of biological triplicates (**A, B, E, F, G**; control r12, SMA I & SMA III in **H**) and duplicates (asymptomatic in **H**), respectively. Error bars in **C, D** (day 27) represented ± SEM of n=MN differentiation runs as outlined in subordinated tables.
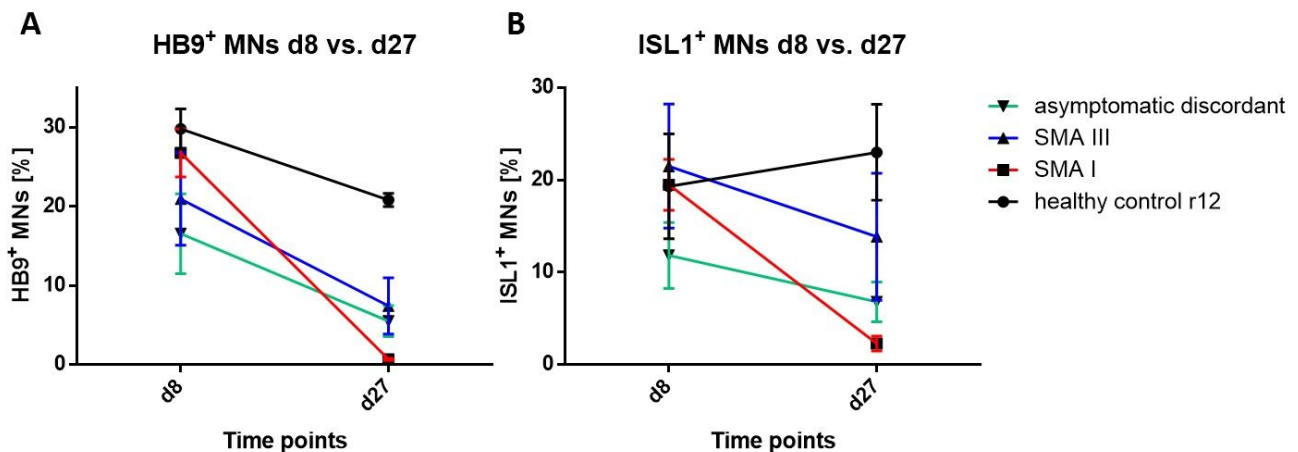
Fig. 44: Motoneuronal survival between day 8 and day 27 in smNPC-derived MN cultures of different healthy and SMA affected or asymptomatic individuals classified in regard of their phenotypic background. (**A**) In all four groups there was a loss of HB9$^+$ MNs observable (healthy control: 29.8% ↘20.8%; SMA I: 26.8% ↘0.7%; SMA III: 20.9% ↘8.9%; asymptomatic: 16.5% ↘6.3%). (**B**) Similarly, massive death of ISL1$^+$ MNs was only detected in SMA I phenotype (19.5% ↘2.3%) whereas the discordant family members just exhibited a mild decline in ISL1$^+$ cell numbers (SMA III: 21.5 ↘14.7%; asymptomatic: 11.8% ↘7.2%). Healthy controls even gained a minor percentage of ISL1$^+$ MNs (19.3% ↗23%). Error bars represented ± SEM of biological triplicates of three independent differentiation runs (n=3) (**A**; control r12, SMA I & SMA III in **B**) and duplicates (n=2) (asymptomatic on day 27 in **B**), respectively.

7.5 Analyses of SMN and PLS3 expression in various cell populations of different SMA phenotypes during MN development

Although PLS3 was supposed to be solely expressed in solid tissue but not in blood (Lin *et al.* 1999), asymptomatic siblings from discordant families evidently over-expressed PLS3 in blood-derived LB cell lines on RNA and protein levels (Oprea *et al.* 2008). However, the true situation in patients' MNs stayed unclear. Since data about SMN expression in MNs of patients investigated in this study were lacking as well, respective SMN levels ought to be checked.

To be able to follow possible changes of the expression rates during the developmental process of MN generation in SMA affected patients, PLS3 discordant siblings and healthy controls, the expression of PLS3 as well as SMN was examined on RNA and protein level in different cell populations, i.e. original fibroblasts, derived iPSCs, corresponding smNPCs and differentiated MN cultures on day 27.

7.5.1 *SMN* expression on RNA level in different SMA phenotypes during MN development

As the disease cause, *SMN* expression was investigated first. Samples of every cell line in each respective cell population were investigated by qRT-PCR. Data were normalised as well as graphically plotted relative to total RNA expression.

In fibroblasts, *SMN* expression in control lines r12 and COII.2 was almost equal (Fig. 45 **A**). SMA I patient line ML17 exhibited the least amount of *SMN* mRNA. Astonishingly, discordant family members showed an inconsistent *SMN* expression rate: Whereas asymptomatic ML11 and ML13 as well as SMA III ML12 displayed a moderate SMN expression (~40-60% relative to r12), the other lines asymptomatic ML101 and SMA III ML14 and ML102 nearly reached the expression level of healthy controls (75-100% relative to r12). Grouping this data according to the phenotypic background gave a more consistent view in which SMA I patients expressed only ~28% *SMN* mRNA and SMA III and asymptomatic discordant family members ~68-74% *SMN* mRNA relative to controls (Fig. 45 **B**). Thus, only SMA I demonstrated a very significant difference in *SMN* mRNA expression.

SMN expression in iPSCs conveyed a more homogeneous impression concerning single cell line expression (Fig. 45 **C**). Control lines r12 and COII.2 demonstrated the overall highest *SMN* expression. Moreover, SMA I line HGK1 showed the lowest amount of *SMN* expression which differed significantly from the control r12 amount. Discordant family 1 members HGK13 and HGK16 exhibited almost half the control amount (~50% relative to r12) reflecting the genetic background with three *SMN2* copies. Since siblings of discordant family 2 possessed four *SMN2* copies, expectedly the SMN expression rate was higher (60-80% relative to r12) than in other SMA phenotypes, however for most of the iPSC lines still distinctly lower than in control lines. Summarising these results in respect of the phenotype represented the same picture as in fibroblasts (Fig. 45 **D**). Controls expressed the highest amount of *SMN* whereas SMA III and asymptomatic siblings almost equally expressed ~65% relative to controls still rendering a significant decrease. SMA I depicted the lowest amount (27% relative to control) indicating very significant difference.

In smNPCs, both control lines r12 and COII.2 displayed the overall strongest *SMN* expression (Fig. 45 **E**). Again, SMA I line HGK1 showed a significantly lower amount when compared to control r12. The discordant family members basically revealed a stronger *SMN* expression rate (70-90% relative to r12) except for HGK21.8 with 46%. When the four phenotype classes were compared, they exhibited a picture congruent with the previous phenotype summaries (Fig. 45 **F**): A high *SMN* expression in controls, a significantly lower expression in SMA I (26% relative to controls) and a moderate significant *SMN* expression diminution in SMA III and asymptomatic groups (~65% relative to controls).

Analyses of MN culture samples revealed the highest *SMN* expression in control line r12 (Fig. 45 **G**). The least *SMN* expression was found in SMA I HGK1 and exceptionally in SMA III HGK13 being significantly different relative to r12. On the other hand, the remaining SMA III and asymptomatic individuals expressed a medium up to higher *SMN* amount (~43%-85% relative to r12) which was not significant. However, the graph represented only data from a

single MN differentiation run. Once samples of the two other runs were processed, the pooled data might give a more conclusive picture of *SMN* expression in MN cultures.

Nevertheless, grouped data in the phenotypic overview (Fig. 45 **H**) showed a firm *SMN* expression in healthy control r12 proving significantly higher than SMA I affected which delivered just approx. 25% expression rate. In contrast, in SMA III and asymptomatic samples *SMN* expression rate reached a medium level of ~56% and ~68%, respectively (relative to r12) marking only expression in SMA III as significantly diminished.

Taken together, *SMN* mRNA expression differed between healthy controls, SMA I, SMA III and asymptomatic discordant siblings according to their *SMN2* copy number. Cell line-specific variances were balanced to a conclusive phenotypic summary in which SMA I principally expressed roughly a quarter of the control amount (~26%) resulting in a significant difference. There was evidently a diminished *SMN* expression in SMA III or asymptomatic groups detectable in comparison to healthy controls so that variance in *SMN* expression was often significant, On average, in the four phenotypic classes SMA III and asymptomatic discordant expressed ~65% and ~68%, respectively.

Fig. 45: Quantitative analyses of *SMN* mRNA expression levels in different cell populations via qRT-PCR from healthy controls, SMA I and SMA III affected and asymptomatic discordant siblings. (**A**) In fibroblasts, control lines r12 and COII.2 expressed most *SMN* mRNA whereas SMA I ML17 the significantly least amount. Discordant family members showed a variant expression partially lower than controls, partially almost equal. (**B**) Fibroblast *SMN* expression in four phenotype classes exhibited no significant differences between SMA III and asymptomatic siblings in comparison to control lines. However, SMA I expression ranged very significantly lower. (**C**) In iPSCs, control line r12 displayed a significantly higher *SMN* expression towards SMA I line HGK1. Discordant family members individually revealed a significantly reduced *SMN* expression on medium level. (**D**) In phenotypic classes, the highest *SMN* expression was found in healthy controls whereas SMA I patient demonstrated a significantly decreased *SMN* amount. *SMN* reduction in discordant family members was significant, yet reaching a moderate expression level (~65%). (**E**) In smNPCs, *SMN* expression level was significantly lowered in SMA I line HGK1 relative to control line r12 whereas in individual discordant family members *SMN* amount was not significantly diminished nonetheless appeared still lower than control levels. (**F**) Phenotypic summary disclosed a similar picture as in previous cell populations leaving SMA I as group with the significantly lowest *SMN* amount. Still, *SMN* expression was significantly scaled down in SMA III and asymptomatic siblings. (**G**) In MN cultures (day 27), the significantly lowest *SMN* amount was exceptionally detected in SMA III HGK13 although SMA I HGK1 showed diminished *SMN* expression as well. The *SMN* expression rates of other discordant family members

ranged at an insignificant medium level mostly. (**H**) Consistently, phenotypic overview depicted in SMA I and SMA III a significant reduction relative to control r12. Contrarily, the *SMN* expression of asymptomatic siblings comprised a not significant medium range. Expression was normalised to total RNA levels and significance calculated relative to r12 and healthy controls, respectively (Kruskal-Wallis test, $p < 0.05$ = *, $p < 0.01$ = **). Error bars represented ± SEM of technical duplicates (n=2). MN culture displayed data of one MN differentiation run (n=1). Note that control COII.2 was excluded in MN culture analyses.

7.5.2 *PLS3* expression on RNA level in different SMA phenotypes during MN development

Since PLS3 was evidently proven to be the causative reason of protection in asymptomatic SMA III discordant individuals (Oprea *et al.* 2008), *PLS3* mRNA expression was also monitored within the different cell populations of all 13 cell lines by qRT-PCR. Data were normalised relative to total RNA expression.

In fibroblasts, cell lines showed various *PLS3* expression levels irrespective of their phenotypic background. Markedly lessened *PLS3* levels were measured in SMA I line ML17, asymptomatic ML11 and ML13 and in SMA III ML12 and ML102 with ML12 as least expressing line compared to controls (Fig. 46 **A**). Subsequently, solely significant differences were detected in pooled samples between controls and SMA III even though SMA I and asymptomatic by trend exhibited a light decrease in *PLS3* expression relative to controls (Fig. 46 **B**).

In iPSCs, inconsistent *PLS3* expression pattern still prevailed because cell lines disclosed diverse expression levels independent of their genetic background. In comparison to control line r12, SMA III HGK13 expressed lower *PLS3* amounts whilst most other discordant family lines showed expression levels similar to r12. Strong increase in *PLS3* expression was determined in control COII.2, SMA I line HGK1 and asymptomatic lines HGK21.1, HGK28.9 and HGK28.11 (Fig. 46 **C**). Therefore, phenotypic summary kept depicting an insignificant expression pattern in which SMA I group was almost equal to controls, SMA III was visibly diminished and expression in asymptomatic was slightly augmented (Fig. 46 **D**).

In smNPCs, individual expression rates scattered without any significant difference relative to control r12. However, strong expressing cell lines conspicuously comprised primarily asymptomatic cell lines beside control COII.2 and SMA I HGK1 (Fig. 46 **E**). Thus, phenotypic grouping revealed no significant difference in *PLS3* expression. Nonetheless, overall expression levels were noticeably elevated in SMA I and asymptomatic (Fig. 46 **F**).

In MN culture, *PLS3* expression in control line r12 was strikingly down-regulated giving the lowest expression rate. So, the other cell lines presented strongly higher expression rates relative to control with significant differences in asymptomatic HGK28.9 and HGK28.11. Remarkably, previously high *PLS3* levels in SMA I line HGK1 were attenuated. Principally, firm *PLS3* expression was observed among asymptomatic siblings with individual cell lines exceeding expression of control r12 up to 15fold (e.g. HGK28.11) (Fig. 46 **G**). After phenotypic grouping, *PLS3* expression of asymptomatic was very significantly increased relative to controls. Thereby, the previous trend was distinctly stabilised because *PLS3* expression more than doubled in asymptomatic samples compared to SMA I and SMA III (Fig. 46 **H**).

Taken together, *PLS3* mRNA expression in fibroblasts reached comparable levels among non-control phenotypic groups. Albeit expression rates were visibly decreased significant difference was only revealed between controls and SMA III. Ever since, in following cell populations expression levels in asymptomatic evidently rose in comparison to other classes resulting in a very significant difference in MN cultures. SMA I and SMA III samples fluctuated

in the same range. While control line r12 principally exhibited a stable expression rate in the first three cell populations, r12 was markedly down-regulated in MN cultures.
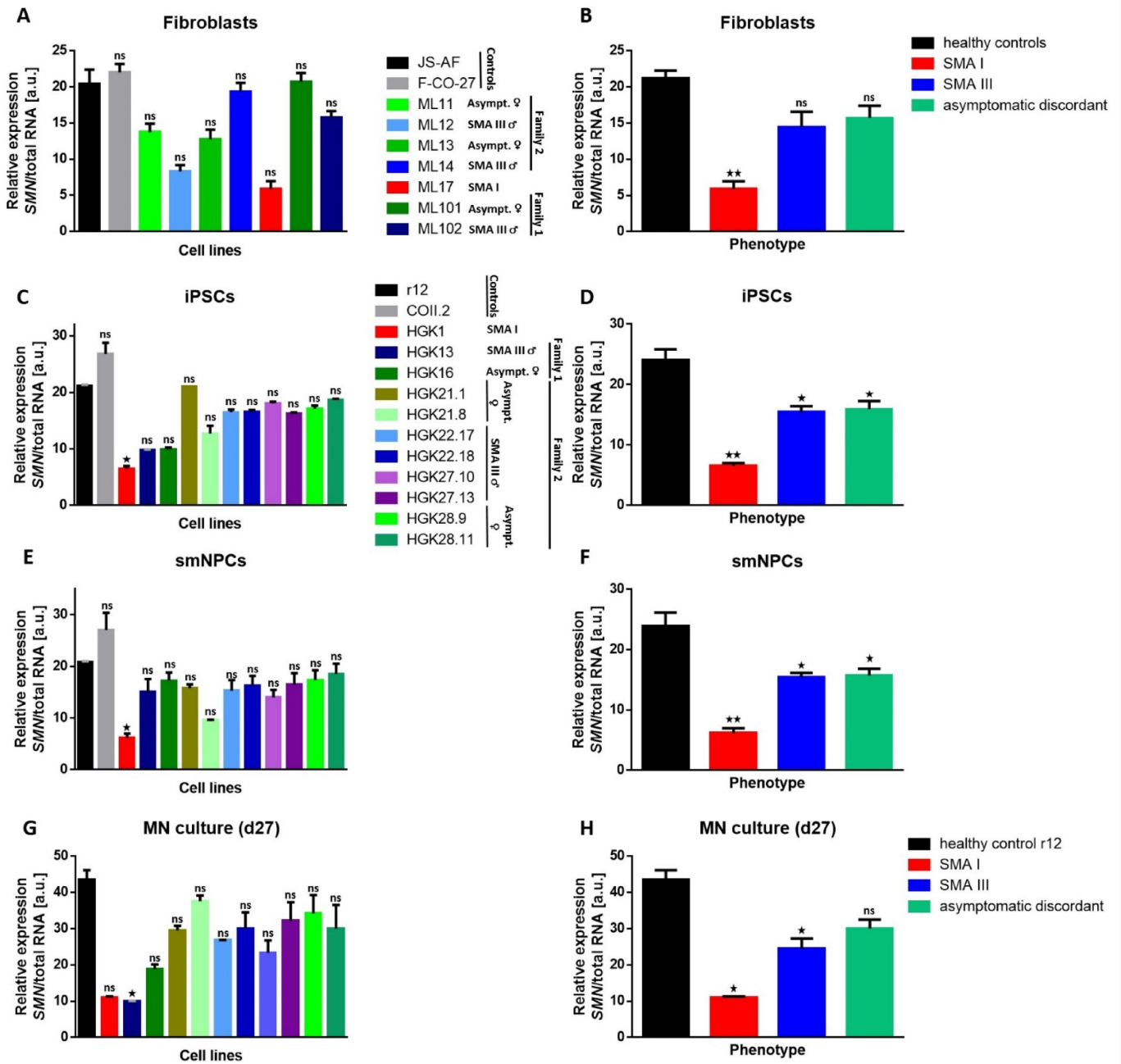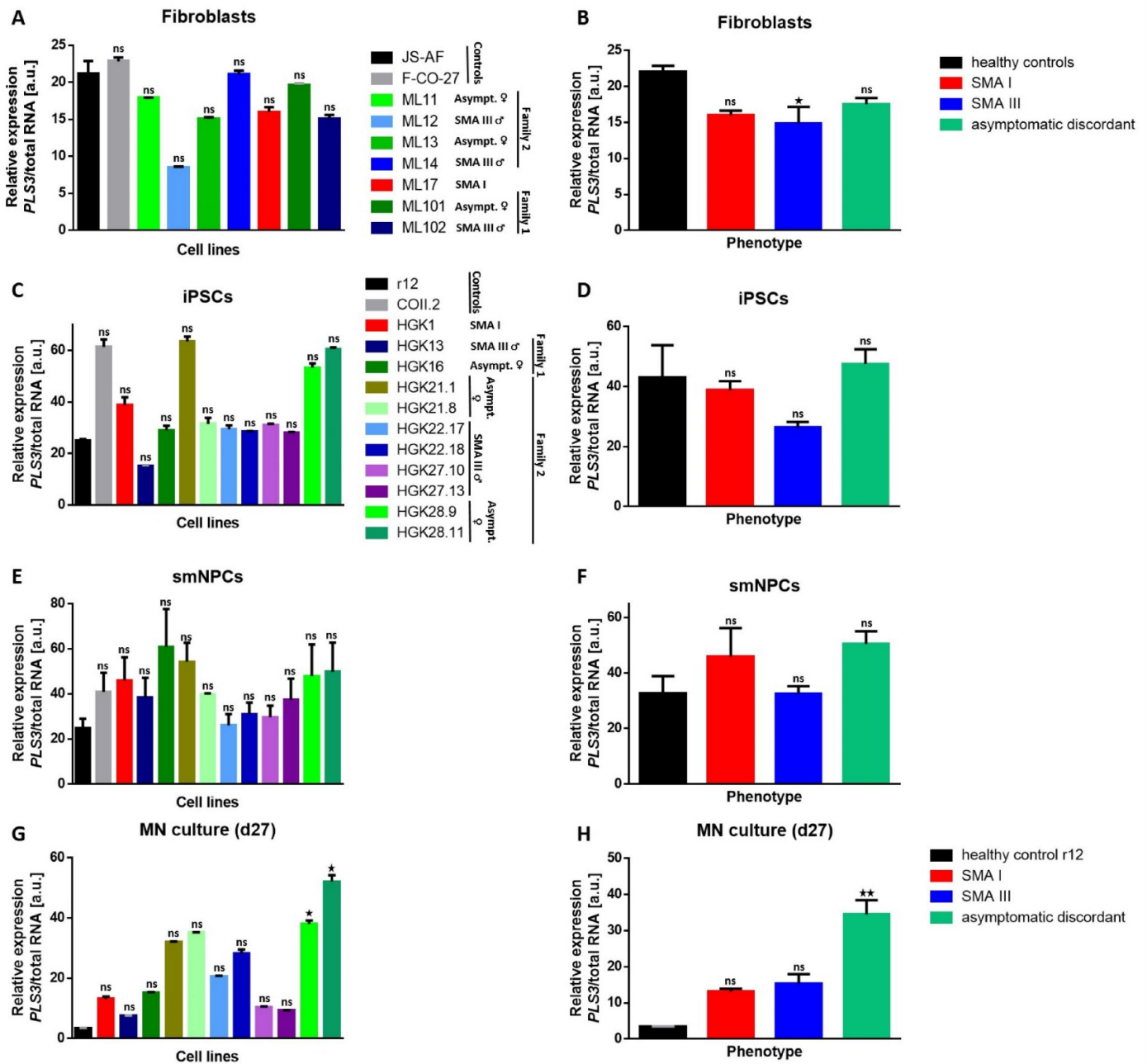

Fig. 46: Quantitative analyses of *PLS3* mRNA expression levels in different cell populations via qRT-PCR from healthy controls, SMA I and SMA III affected as well as asymptomatic discordant siblings. (**A**) In fibroblasts, *PLS3* expression levels fluctuated independently of the individual phenotypic background. Yet, distinctly lower expression was determined in SMA I line ML17, asymptomatic ML11 and ML13 and in SMA III ML12 and ML102 relative to control r12. (**B**) Phenotypic grouping ended up with slightly reduced expression rate in non-control classes which were nearly equal among themselves. (**C**) In iPSCs, control line r12 remained at *PLS3* levels previously seen in fibroblasts leaving only SMA III line HGK13 with a markedly lower *PLS3* expression. Whilst the majority of other cell lines reached control levels, other cell lines e.g. control COII.2, SMA I line HGK1 and asymptomatic lines HGK21.1, HGK28.9 and HGK28.11 topped expression in r12. (**D**) Phenotypic classification largely erased individual fluctuations so that no difference was significant relative to controls. Nevertheless, expression in SMA I and SMA III was visibly decreased and gently raised in asymptomatic. (**E**) In smNPCs, a light trend developed in noticeably higher *PLS3* levels in asymptomatic cell lines. Moreover, control COII.2 and SMA I line HGK1 expressed more *PLS3* mRNA relative to control r12 whereas SMA III cell lines reached comparable levels still with no significance at all. (**F**) Differences amongst phenotypic classes were not significant. Still, a considerably higher expression rate was pointed out in SMA I and asymptomatic compared to controls whereas

SMA III exhibited a similar expression level. (**G**) In MN cultures (day 27), individual cell lines presented various expression rates. Since control line r12 strikingly disclosed lowest *PLS3* expression, remaining cell lines exhibited high elevation of *PLS3* expression yet significant differences only with HGK28.9 and HGK28.11. While asymptomatic cell lines mostly oscillated at high levels, SMA I line HGK1 and SMA III lines reached medium or lower expression levels. (**H**) Phenotypic grouping revealed comparable expression levels between SMA I and SMA III without significant differences. However, expression level in asymptomatic was very significantly increased relative to control r12 manifesting the previous trend of strong *PLS3* expression in asymptomatic siblings. Expression was normalised to total RNA levels and significance computed relative to r12 and healthy controls, respectively (Kruskal-Wallis test, *p* <0.05 = *, *p* <0.01 = **). Error bars represented ± SEM of technical duplicates (n=2). MN culture displayed data of one MN differentiation run (n=1). Note that control COII.2 was excluded in phenotypic MN culture analyses.

7.5.3 SMN and PLS3 expression on protein level in different SMA phenotypes during MN development

To confirm SMN expression rates on protein level, whole cell extracts of all 13 cell lines in the respective cell populations were analysed by Western blotting and subsequent immunoblotting. Membranes were probed with antibodies against PLS3, SMN and β-actin. Data were normalised as well as graphically plotted relative to β-actin expression.

Principally, the bands on the blots evidently represented the correct weight of the respective proteins (PLS3: 72 kDa; β-actin: 50 kDa; SMN: 36 kDa) with equalised β-actin bands granting proper normalisation (Fig. 47). In fibroblasts, PLS3 protein was detected as a single distinct band, however, an overt difference in signal intensity was not visible (Fig. 47 **A**). If several bands were detectable, upper band was identified as correct PLS3 band (10.5, Fig. 65). Contrarily, SMN bands clearly exhibited diverse signal intensity with SMA I line ML17 and SMA III line ML12 as the least expressing cell lines.

In iPSCs, PLS3 protein was visualised as two bands ranging at the assumed size of 70 kDa. (Fig. 47 **B**). PLS3 *in vitro* knock-down in cell lines by Mohsen Hosseini identified the upper band as correct specific PLS3 signal (10.5, Fig. 65). So, in iPSCs thick bands revealed obvious differences in signal intensity among the present cell lines (Fig. 47 **B**). Control lines r12 and COII.2 as well as SMA III lines HGK22.17, HGK22.18, HGK27.10 and HGK27.13 displayed a rather moderate band intensity. On the contrary, asymptomatic lines HGK16, HGK21.8, HGK28.9 and HGK28.11 and SMA I line HGK1 demonstrated a visibly elevated signal intensity. Astonishingly, SMA III line HGK13 and asymptomatic line HGK21.1 apparently expressed the lowest PLS3 amount. Yet, SMN protein showed a different expression pattern with SMA I line HGK1 delivering the faintest signal. Expression in control lines r12 and COII.2 as well as asymptomatic lines HGK16 and HGK21.8 seemed the strongest whereas the other cell lines displayed a signal intensity in-between.

In smNPCs, PLS3 protein was detected as two distinct bands (Fig. 47 **C**) like in iPSCs. Signal strength was remarkably higher in SMA I line HGK1, asymptomatic lines HGK16, HGK21.1, HGK21.8 and HGK28.9 and control line r12. Weaker signal intensity was discernible in the other cell lines with SMA III lines HGK13 and HGK22.17 as lowest expressing cell lines. The SMN expression pattern expectedly reflected the differences in *SMN1*/*SMN2* gene copies since the band of SMA I line HGK1 was hardly observable. In control lines r12 and COII.2, the strongest bands were detected whereas the discordant family members depicted a medium luminance.

In MN culture samples, prominent PLS3 expression was observed in asymptomatic lines HGK21.1, HGK21.8, HGK28.9 and HGK28.11 (Fig. 47 **D**). Other cell lines generated a moderate signal intensity including SMA I line HGK1. Notably, the band of control line r12 vanished almost completely. On the contrary, control line r12 displayed a considerable amount of SMN

protein. The band of SMA I line HGK1 had nearly disappeared while discordant family members disclosed rather medium intense band signals.
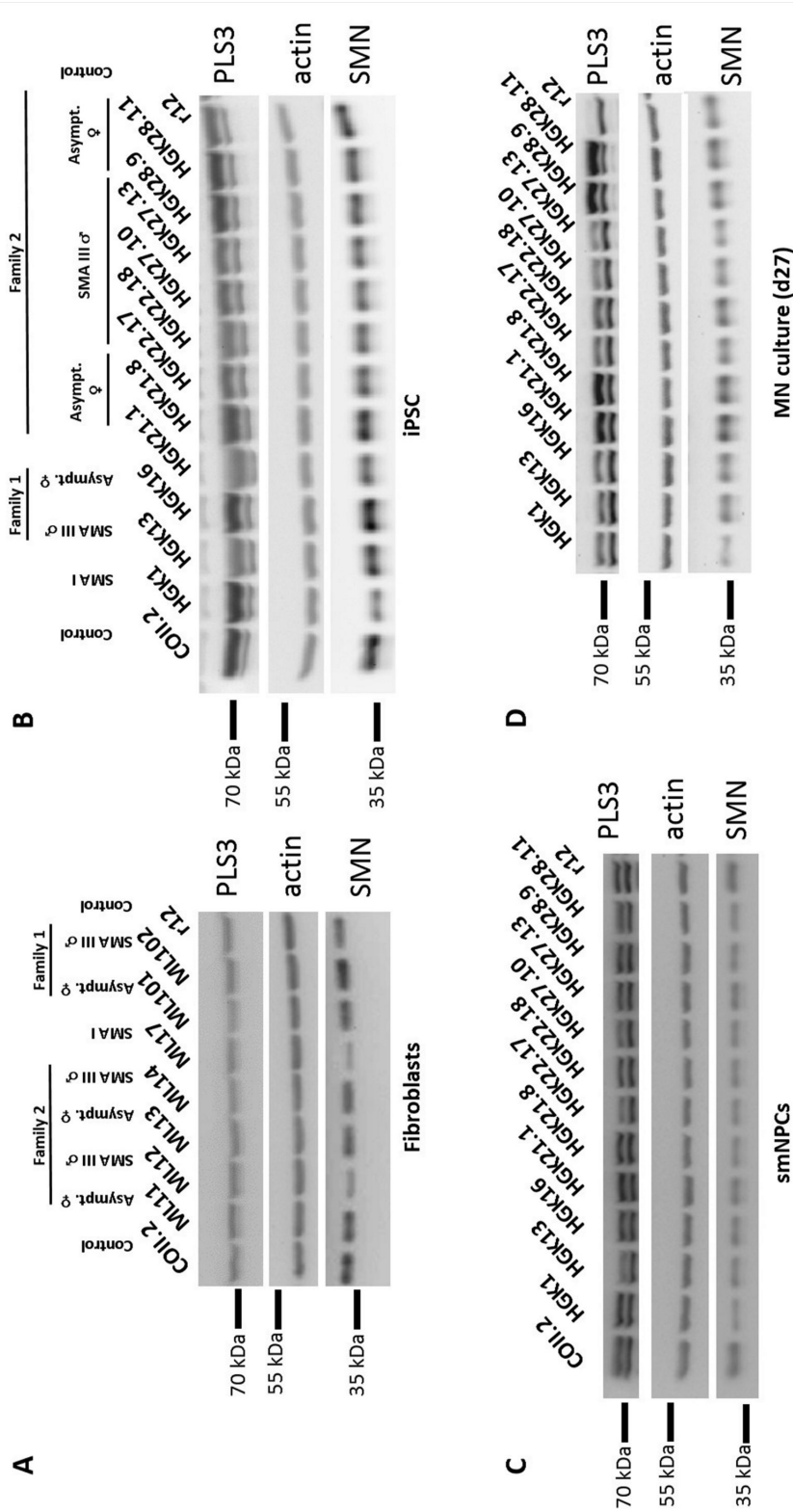
Fig. 47: Qualitative assessment of PLS3 and SMN protein expression via Western blotting and subsequent immunoblotting. Distinct bands clearly evinced correct weight of the respective proteins (PLS3: 72 kDa; actin: 50 kDa; SMN: 36 kDa) with equalised actin bands allowing reliable normalisation. (**A**) In fibroblasts, there were no obvious differences in PLS3 signal intensity identifiable among the cell lines. SMN was contrarily expressed in visibly different signal strength with SMA I line ML17 and SMA III line ML12 expressing the least. (**B**) In iPSCs, PLS3 was recognisably differently expressed with strongest signal intensity in asymptomatic lines HGK16, HGK21.8, HGK28.9 and HGK28.11 and SMA I line HGK1. Note that SMA III line HGK13 and asymptomatic line HGK21.1 expressed the least PLS3 amount. However, SMN expression level was almost evened apart from SMA I line HGK1 disclosing a discernible SMN reduction. Control lines r12 and COII.2 as well as asymptomatic lines HGK16 and HGK21.8 apparently expressed more SMN. (**C**) In smNPCs, differences in PLS3 expression intensity were noticeably elevated in SMA I line HGK1, asymptomatic lines HGK16, HGK21.1, HGK21.8 and HGK28.9 and control line r12. Weakest signal strength was found in SMA III lines HGK13 and HGK22.17. SMN expression mirrored individual genetic background with control lines r12 and COII.2 possessing the strongest bands whereas discordant family members depicted a medium signal intensity. Low expressing SMA I line HGK1 exhibited only a slim faint band. (**D**) In MN cultures, gross increase in PLS3 expression was distinguishable in asymptomatic lines HGK21.1, HGK21.8, HGK28.9 and HGK28.11. Take heed of control line r12 whose band nearly disappeared. On the contrary, control line r12 displayed an intense signal of SMN protein. While SMA I line HGK1 presented a thin SMN band with weak luminance, discordant family members exhibited a considerable SMN amount. Note that control COII.2 was excluded in MN culture analyses.

Quantification of SMN protein expression

Fig. 48: Quantitative analyses of SMN protein expression levels in different cell populations via immunoblotting from healthy controls, SMA I and SMA III affected and asymptomatic discordant siblings. (**A**) In fibroblasts, control line r12 disclosed a deviant low SMN expression level. SMA I line ML17 and SMA III line ML12 showed the least amount of SMN. Unexpectedly, other discordant family members revealed quite strong SMN expression, however no significant difference became overt in general. (**B**) Subsequently, phenotype groups did not significantly differ although SMN expression in SMA I just amounted to ~18% in comparison to healthy control. SMA III and asymptomatic siblings even reached control expression level despite different *SMN1*/*SMN2* copy number. (**C**) In iPSCs, SMN expression levels displayed in expected manner with control r12 as high expressing line and SMA I line HGK1 as the least. Discordant family members exhibited a slightly diminished SMN expression. (**D**) Thus, phenotype groups revealed considerably less SMN expression in SMA I (~46% relative to controls) and a marginally lessened SMN amount in SMA III and asymptomatic siblings (~89% and ~83%, respectively). (**E**) In smNPCs, individual SMN expression pattern resembled the previous one, yet discordant family members revealed an overall lesser expression rate at medium level compared to control. SMA I line HGK1 expressed the least SMN amount. (**F**) Grouped phenotypes mirrored these results so that SMA I demonstrated only ~30% SMN

expression when likened to control values. SMA III and asymptomatic siblings disclosed ~53-60% at least. (**G**) In MN culture, standard control line r12 suffered an abnormal drop in SMN expression, its expression level outnumbered by those of several discordant cell lines. Nonetheless, SMA I line HGK1 delivered the poorest SMN amount. (**H**) Therefore, in phenotype classes SMA I only showed ~31% SMN expression (relative to control) whereas SMA III and asymptomatic siblings evinced ~88% and ~126%, respectively. Expression was normalised to β-actin protein levels and significance calculated relative to r12 and healthy controls, respectively (Kruskal-Wallis test). In fibroblasts, error bars represented ± SEM of technical duplicates (n=2). iPSCs and smNPCs showed data of a single immunoblotting (n=1) with error bars representing pooled samples (**D**, **F**). MN culture (day 27) displayed data of three independent MN differentiation runs (n=3) with error bars representing ± SEM of biological triplicates (n=3). Note that control COII.2 was excluded in phenotypic MN culture analyses.

Quantification of individual expression ratios clarified previous impressions from the immunoblots. In fibroblasts, SMA I line ML17 showed the least expression. Despite the presence of three *SMN2* copies, SMA III line ML12 surprisingly displayed a similarly low SMN amount. Also control line r12 exhibited an unusually low SMN expression whereas control line COII.2 as well as further discordant family members disclosed strong SMN expression rates. Thus, no significant difference was detected in comparison to standard control r12 (Fig. 48 **A**). Phenotypic grouping of these results revealed a comparably high SMN protein expression between controls, SMA III and asymptomatic siblings in spite of differences in *SMN1*/*SMN2* copy number. Furthermore, SMN expression in SMA I was the least (~18% relative to controls), yet the difference was not significant in any way (Fig. 48 **B**).

In iPSCs, quantified SMN expression values pictured a more consistent pattern on the other hand: Control lines r12 and COII.2 presented high expression rates while SMA I line HGK1 expectedly expressed the least amount. On average, discordant family members displayed a quite strong SMN expression (Fig. 48 **C**). In phenotypic summary, controls possessed the strongest SMN expression. However, in discordant family members the respective SMN expression levels almost amounted to the controls' level (~89% and ~84%, respectively). Still, SMA I generated the lowest amount of SMN (~46% relative to controls) in iPSCs (Fig. 48 **D**).

In smNPCs, quantification accorded the immunoblot signal intensity rendering control lines COII.2 and r12 the strongest expressing lines and SMA I line HGK1 the weakest expressing line. Expression levels of discordant family members were located at a medium range with varying minor differences (Fig. 48 **E**). Such variances were flattened in the phenotypic overview so that SMA III and asymptomatic siblings both expressed approx. 53-60% when compared to healthy controls. The difference between controls and SMA I was even larger (~30% relative to controls) (Fig. 48 **F**).

In MN cultures, control line r12 acted as outlier because it exhibited an aberrantly low SMN expression ratio. Still, it was asymptomatic line HGK21.8 which disclosed the highest SMN expression rate. In general, the other discordant family members presented expression levels ranging around the control value (Fig. 48 **G**). Pooling these individual results according to the phenotype classes revealed markedly decreased SMN expression in SMA I samples (~31% relative to controls). Unexpectedly, SMA III and asymptomatic discordant samples showed an overall SMN expression level of ~88% and ~126%, respectively, exceeding the expectable SMN amount (Fig. 48 **H**).

In summary, SMN protein expression did not give such a clear distribution pattern reflecting the *SMN2* copy number as it was seen on RNA level between healthy controls, SMA I, SMA III and asymptomatic discordant siblings. Indeed, apparent variances of individual cell lines were flattened by phenotypic grouping. Nevertheless, in particular control line r12 often expressed an unexpectedly low SMN amount. Still, severely affected SMA I samples constantly gave the poorest expression SMN rate counting only approx. a third (relative to controls) on average of all four cell populations. Yet, on average of all four cell populations SMA III and asymptomatic

discordant reached remarkably high SMN expression levels which topped the expected SMN protein delivery of 3-4 *SMN2* copies in these cell lines.
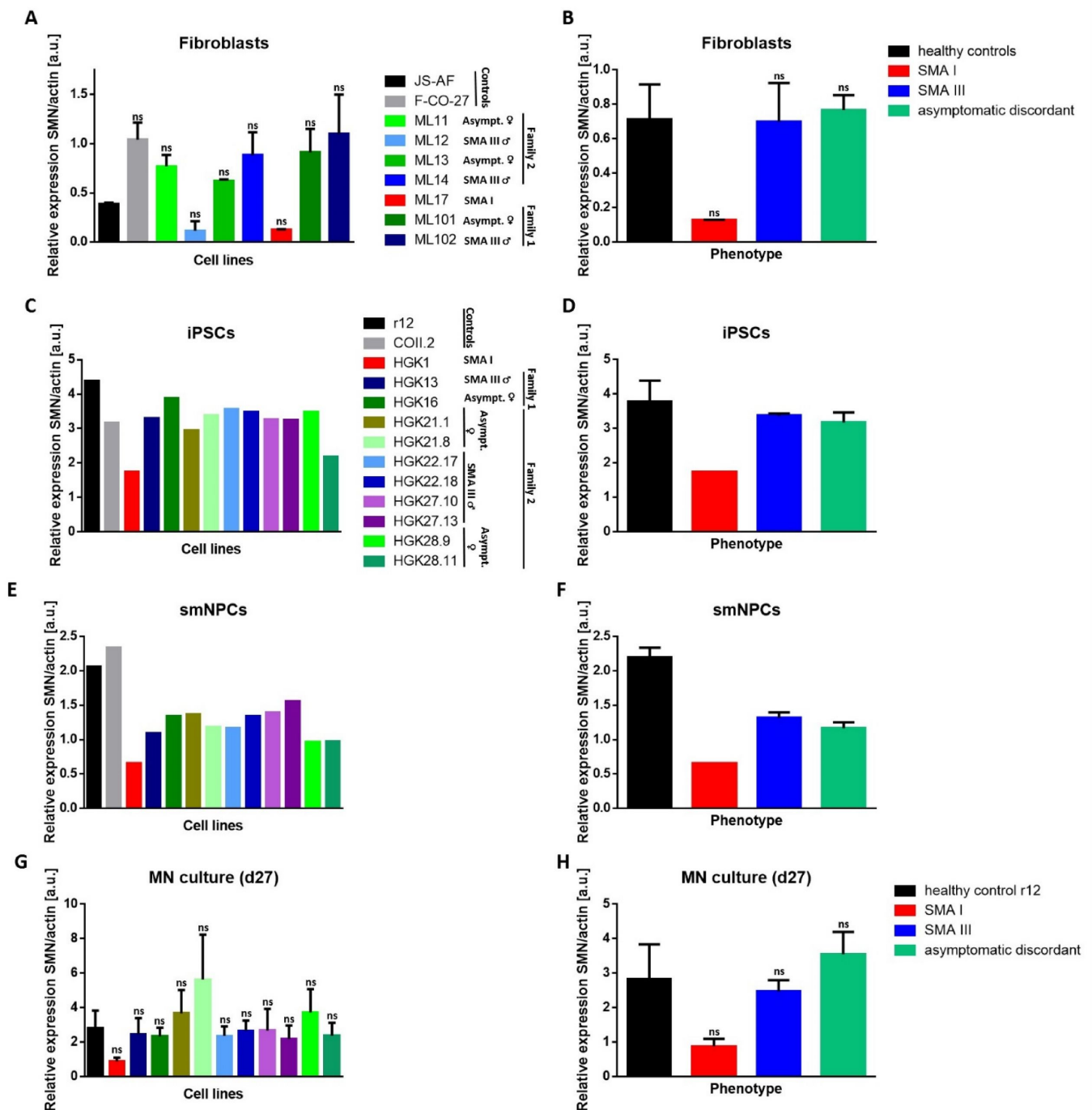
Quantification of PLS3 protein expression
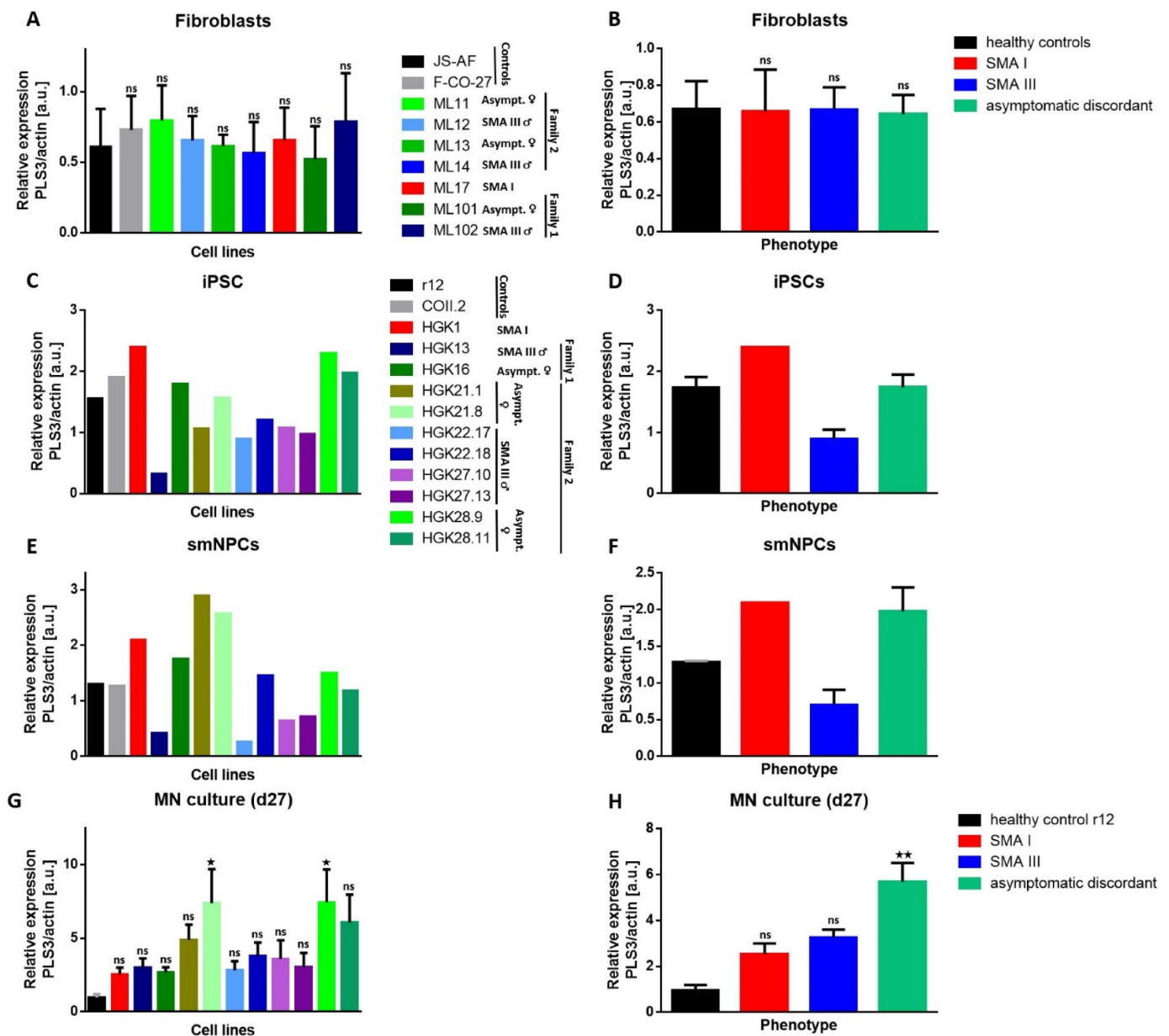
Fig. 49: Quantitative analyses of PLS3 protein expression levels in different cell populations via immunoblotting from healthy controls, SMA I and SMA III affected and asymptomatic discordant siblings. (**A**) In fibroblasts, expression equally ranged at comparable level irrespective of phenotypic background. (**B**) Thus, no significant difference was observed after summarising data to phenotype groups. (**C**) In iPSCs, both control lines exhibited similar expression rates. Astonishingly, SMA I line HGK1 outperformed other cell lines in expression. Still, asymptomatic lines e.g. HGK16, HGK21.8 or HGK28.9 strongly expressed PLS3. Consistently minor expression rates were found in SMA III lines. (**D**) Phenotypic grouping demonstrated nearly equal expression levels between controls and asymptomatic. SMA III reached only half the expression rate relative to control while SMA I distinctly showed more PLS3 expression. (**E**) In smNPCs, control lines and SMA I line HGK1 basically kept the previous iPSC expression levels with minor reduction in HGK1. Additionally, asymptomatic lines demonstrated a stably high PLS3 expression. SMA III lines HGK13 and HGK22.17 struck a visible decline in PLS3 expression and further SMA III lines did not improve either. (**F**) Phenotype classes revealed SMA I and asymptomatic as top expressing groups while SMA III occupied the last rank just delivering approx. 50% relative to controls. (**G**) In MN culture, control line r12 did not up-regulate PLS3 expression rendering it the least expressing line. SMA I HGK1 also kept previous expression rates. Contrarily, asymptomatic cell lines except for HGK16 strikingly boosted PLS3 expression. SMA III

lines also disclosed elevated expression yet reaching medium expression levels. (**H**) This development was reflected in phenotypic overview with control as least expression line. SMA I quantitatively expressed a similar PLS3 amount as in earlier populations. Yet, SMA III and particularly asymptomatic towered above with ~335% and ~588% PLS3 amount relative to control r12, respectively. Nonetheless, differences were solely very significant in asymptomatic siblings relative to control. Expression was normalised to β-actin protein levels and significance calculated relative to r12 and healthy controls, respectively (Kruskal-Wallis test, p <0.05 = *, p <0.01 = **). In fibroblasts, error bars represented ± SEM of technical duplicates (n=2). iPSCs and smNPCs showed data of a single immunoblotting (n=1) with error bars representing pooled samples. MN culture (day 27) displayed data of three independent MN differentiation runs (n=3) with error bars representing ± SEM of biological triplicates (n=3). Note that COII.2 was excluded from phenotypic overview in MN culture analyses.

Quantification of individual PLS3 expression ratios substantiated previous optic assessment of the immunoblots. In fibroblasts, homogenous signal intensity was correctly mirrored in individual expression rates. Cell-line specific variances did not point out any significant differences amongst cell lines (Fig. 49 **A**). Hence, phenotypic grouping revealed an expression rate on equal level (Fig. 49 **B**). In iPSCs, individual expression levels diversified: SMA I line HGK1 amazingly topped other cell lines in PLS3 expression. Control lines exhibited a solidly high expression rate comparable to most asymptomatic cell lines whilst SMA III cell lines presented a diminished PLS3 expression rate relative to control making HGK13 the least expressing line (Fig. 49 **C**). Phenotypic classes reflected these facts because asymptomatic siblings expressed equally to controls whereas SMA I demonstrated an elevated expression rate and SMA III a minimised expression rate (Fig. 49 **D**). In smNPCs, visibly attenuated signal intensity in the immunoblot with SMA III lines HGK13 and HGK22.17 perfectly transferred into the quantification making both lines hit the bottom-line of expression. Except for HGK22.18, the other SMA III lines expressed little PLS3 as well. While control lines disclosed a firm expression level, SMA I line HGK1 and particularly asymptomatic lines HGK16, HGK21.1, HGK21.8 and HGK28.9 strongly expressed PLS3 (Fig. 49 **E**). In phenotypic overview, SMA I demonstrated a strongly increased PLS3 expression compared to controls. While averaged expression rate in SMA III was almost halved compared to controls, expression level approx. equally rose in asymptomatic (~154%) relative to controls (Fig. 49 **F**). In MN cultures, the overall PLS3 expression rate was noticeably increased. Comparably, control r12 expressed low PLS3 amounts as in previous cell populations. SMA I line HGK1 appeared low expressing yet it was the globally higher expression level in the remaining cell lines which conveyed this impression. In particular, asymptomatic sisters of family 2 exhibited a massive up-regulation in PLS3 expression as indicated by prominent immunoblot signal intensity beforehand (Fig. 47 **D**). Compared to previous cell populations, SMA III lines also increased expression rates still outplayed by asymptomatic lines (Fig. 49 **G**). Phenotypic classification revealed a large significant up-regulation of PLS3 expression in asymptomatic almost sextupling the averaged control amount (Fig. 49 **H**). Moreover, SMA I and SMA III disclosed higher expression levels relative to control as well. Although differences between the latter two groups were not significant compared to control distinct trends in expression patterns were set (Fig. 49 **H**).

7.5.4 Comparative overview in SMN and PLS3 expression on RNA and protein level in different SMA phenotypes during *in vitro* MN development

Plotting the data obtained from summaries of the phenotypic classes according to the four cell populations revealed a conclusive insight into phenotype-specific changes in SMN and PLS3 expression on RNA and protein level during *in vitro* development (Fig. 50).

SMN mRNA expression followed a stringent line depicting an almost parallel course in fibroblasts, iPSCs and smNPCs. Expectedly, SMA I disclosed the least expression level and healthy control the highest with SMA III and asymptomatic in-between. Admittedly, the overall intervals did not appear very broad. Just in MN cultures, all cell lines befell a visible increase in SMN expression with the smallest increment in SMA I and the strongest rise in healthy controls (Fig. 50 **A**).

SMN protein expression illustrated a more oscillating course since the overall SMN protein amount in fibroblasts was astonishingly low in controls, SMA III and asymptomatic. Although the overall SMN amount rose in subsequent cell populations, the interval between controls and SMA III/asymptomatic did not match the given *SMN1*/*SMN2* copy number ratio in which discordant family members were supposed to deliver only 40-70% of healthy controls. Here, SMA III and discordant expressed comparable SMN amounts in fibroblasts and iPSCs. Only in smNPCs, the expression rates fit the expected ratios. In MN cultures, SMA III reached approx. ⅔ of control expression whereas asymptomatic expressed ~87%. At least, SMA I depicted a considerably low expression throughout development (Fig. 50 **B**). Remarkably, SMA III and asymptomatic presented nearly identical SMN expression rates on both RNA and protein level. Solely in MN cultures, there was a drastic increase detectable in asymptomatic group unusually overtopping control amount.

PLS3 mRNA expression pictured a unique expression course. While in fibroblasts *PLS3* expression barely differed among phenotype classes, asymptomatic revealed the highest expression rate in following cell populations. Surprisingly, SMA I exhibited a continuously high expression rate as well. From iPSCs onwards, *PLS3* expression in healthy controls was increasingly attenuated. SMA III was constantly the least expressing group apart from MN cultures in which control r12 expressed barely any *PLS3* mRNA. In principle, *PLS3* expression peaked in iPSCs and smNPSCs before expression decremented in MN cultures (Fig. 50 **C**).

PLS3 protein expression was equally low in fibroblasts and spread then with SMA I as highest expressing group in iPSCs. SMA III stayed the lowest expressing class in iPSCs and smNPCs. In smNPCs, expression levels diversified rendering SMA I and asymptomatic the high expressing classes while healthy controls disclosed a medium expression rate. The overall PLS3 expression levels demonstrated relatively low in iPSCs and smNPCs. Finally, PLS3 levels remarkably rose in asymptomatic MN cultures exhibiting here an almost 2fold increase compared to SMA I and SMA III and even a 6fold increase in comparison to control. While expression levels remained fairly unchanged in control and SMA I MN cultures compared to those in iPSCs and smNPCs, SMA III presented a surprising augmentation overtaking the previously mentioned two phenotype classes in PLS3 expression in MN cultures (Fig. 50 **D**).

Tab. 17 listed the relative expression percentage in comparison to healthy control(s) (100%) within individual phenotypic groups in specific cell populations. Except for MN cultures (only control r12), controls meant r12 and COII.2 (in fibroblasts, iPSCs and smNPCs).

Table 17: SMN and PLS3 expression percentage in phenotypic classes was itemised relative to healthy control(s) (100%) in cell populations during *in vitro* MN development

	SMN mRNA expression			SMN protein expression		
Population	SMA I	SMA III	Asymptomatic	SMA I	SMA III	Asymptomatic
Fibroblast	27%	68%	74%	18%	98%	108%
iPSC	27%	64%	65%	46%	89%	84%
smNPC	26%	64%	65%	30%	60%	53%
MN culture	25%	56%	68%	31%	88%	126%
	PLS3 mRNA expression			PLS3 protein expression		
Population	SMA I	SMA III	Asymptomatic	SMA I	SMA III	Asymptomatic
Fibroblast	73%	68%	80%	99%	100%	96%
iPSC	90%	61%	110%	138%	51%	100%
smNPC	140%	99%	154%	163%	54%	154%
MN culture	382%	445%	1003%	262%	335%	588%
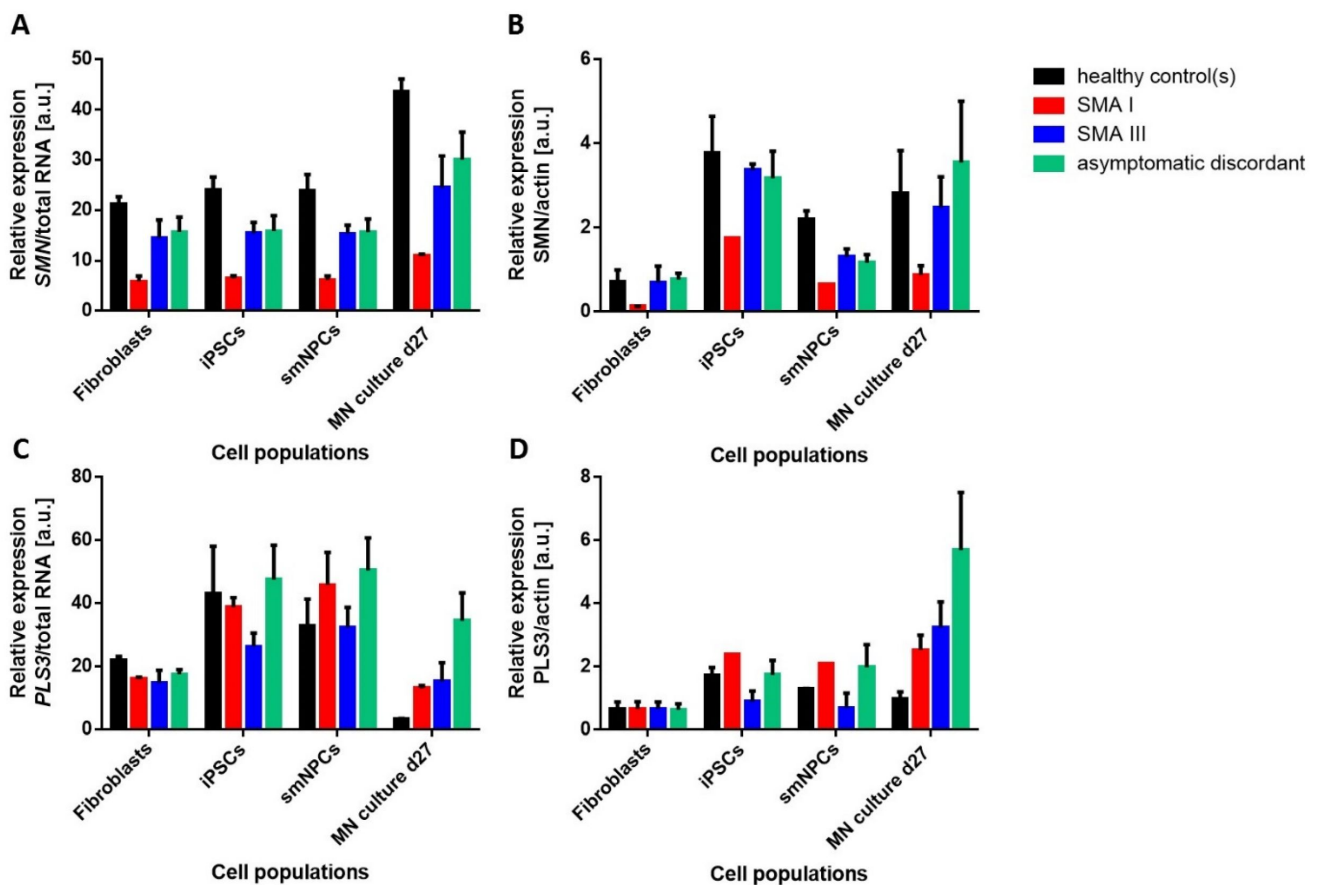
Fig. 50: Comparative overview in SMN and PLS3 expression during *in vitro* MN development. (**A**) On generally lower levels, *SMN* mRNA expression proceeded in comparable pattern in fibroblasts, iPSCs and smNPCs with controls at the top, SMA III and asymptomatic similarly in the middle and SMA I at the bottom-line matching the *SMN1*/*SMN2* copy number. In MN culture, an overall increment was detected yet leaving the previous expression pattern unchanged except for broader intervals. (**B**) SMN protein expression did not exactly display mRNA expression levels because the SMN amount in controls, SMA III and asymptomatic was basically equal denying the absence of *SMN1* copies in discordant family members. Indeed, SMA I expressed always the poorest while controls overran SMA III/asymptomatic classes in following cell populations. Still, discordant family members unusually expressed much SMN particularly asymptomatic in MN cultures (see Tab. 17). (**C**) *PLS3* mRNA expression depicted a less stringent distribution. While in fibroblasts, expression levels barely differed among the classes, iPSCs showed a wider spreading with asymptomatic at the top, SMA I and controls following close and SMA III at lowest expression rates. While asymptomatic prevailed as strongest expressing group which underlined putative over-expression, controls suffered from a continuous decline in *PLS3* expression leaving

hardly any detectable in MN cultures. Also expression in SMA I dropped to equal levels as in SMA III in MN cultures. (**D**) In fibroblasts, equal mRNA amounts were exactly mirrored on protein level. Subsequently, an expression increase was observable in iPSCs with SMA I at the top, controls and asymptomatic in the middle and SMA III at the bottom. This picture recurred in smNPCs, however, asymptomatic gradually incremented resulting in strong expression in MN cultures after all. Also expression in SMA III augmented in MN cultures overrunning SMA I and controls. *SMN* and *PLS3* mRNA levels were normalised relative to total RNA levels. SMN and PLS3 protein levels were normalised relative to β-actin levels. Apart from MN cultures (control only r12), controls meant r12 and COII.2 (in fibroblasts, iPSCs and smNPCs). Graphs were summarised from data of Fig. 45, Fig. 46, Fig. 48 and Fig. 49.

7.5.5 Determination of gems in different SMA phenotypes during MN development

Concomitantly to SMN loss, diminution of SMN containing foci ("gems") in the cell nucleus is a crucial hallmark of SMA. So, the number of gems was determined in all cell populations of every donor fibroblast line, iPSC line and their derived smNPC lines and differentiated MN cultures. Fig. 51 pictured immunocytochemical staining of SMN in different cell lines representative for the four phenotypic classes (i.e. healthy control, SMA I, SMA III and asymptomatic discordant) in varying developmental stages (i.e. original fibroblasts, derived iPSCs, corresponding smNPCs and differentiated MN cultures on day 8 and day 27). On the one hand, SMN was diffusely dispersed in the cytoplasm, on the other hand, there were gems present as distinct nuclear agglomerations with obviously variable size depending on the nucleus size.

In fibroblasts, control line JS-AF abundantly exhibited gems, every now and then even several gems per nucleus. Already in discordant sibling pair ML13 and ML14 gems were more sparsely distributed whereas in SMA I line ML17 there were barely found any gems (Fig. 51).

In iPSCs, gems were wide-spread in control line r12 whereas discordant sibling pair HGK21.1 and HGK22.17 contained visibly fewer gems in densely grown iPSCs. SMA I line possessed no noticeable gems (Fig. 51).

In smNPC control line r12, gems were distributed in fewer numbers in comparison to iPSCs in spite of a similarly growth density. Discordant family members HGK13 and HGK16 disclosed a visible gem number comparable to previous cell populations. The same held true for SMA I line HGK1 in which only sporadic gems could be visualised (Fig. 51).

In MN culture on day 8, a considerable number of gems was counted in control line r12. In discordant family 2 members HGK21.1 and HGK22.18, gems were more scattered within the mixed neuronal culture whereas SMA I line HGK1 barely displayed any gem (Fig. 51).

After three week maturation, gems were frequently recorded in mixed MN culture of control line r12 on day 27. In discordant sibling pair HGK28.9 and HGK27.13, gems amounted to a lower number while SMA I line HGK1 failed to present recognisable gems at all (Fig. 51).

For quantification (Fig. 52), gems were manually counted and their ratios calculated relative to total number of nuclei. Fibroblasts: 150-300 cells in total from duplicates (n=2); iPSCs: 950-1,300 cells in total from triplicates (n=3); smNPCs: 1,200-1,700 cells in total from triplicates (n=3); MN cultures: 300-450 cells (day 8) and 200-550 cells (day 27) in total from three independent MN differentiation runs (n=3).
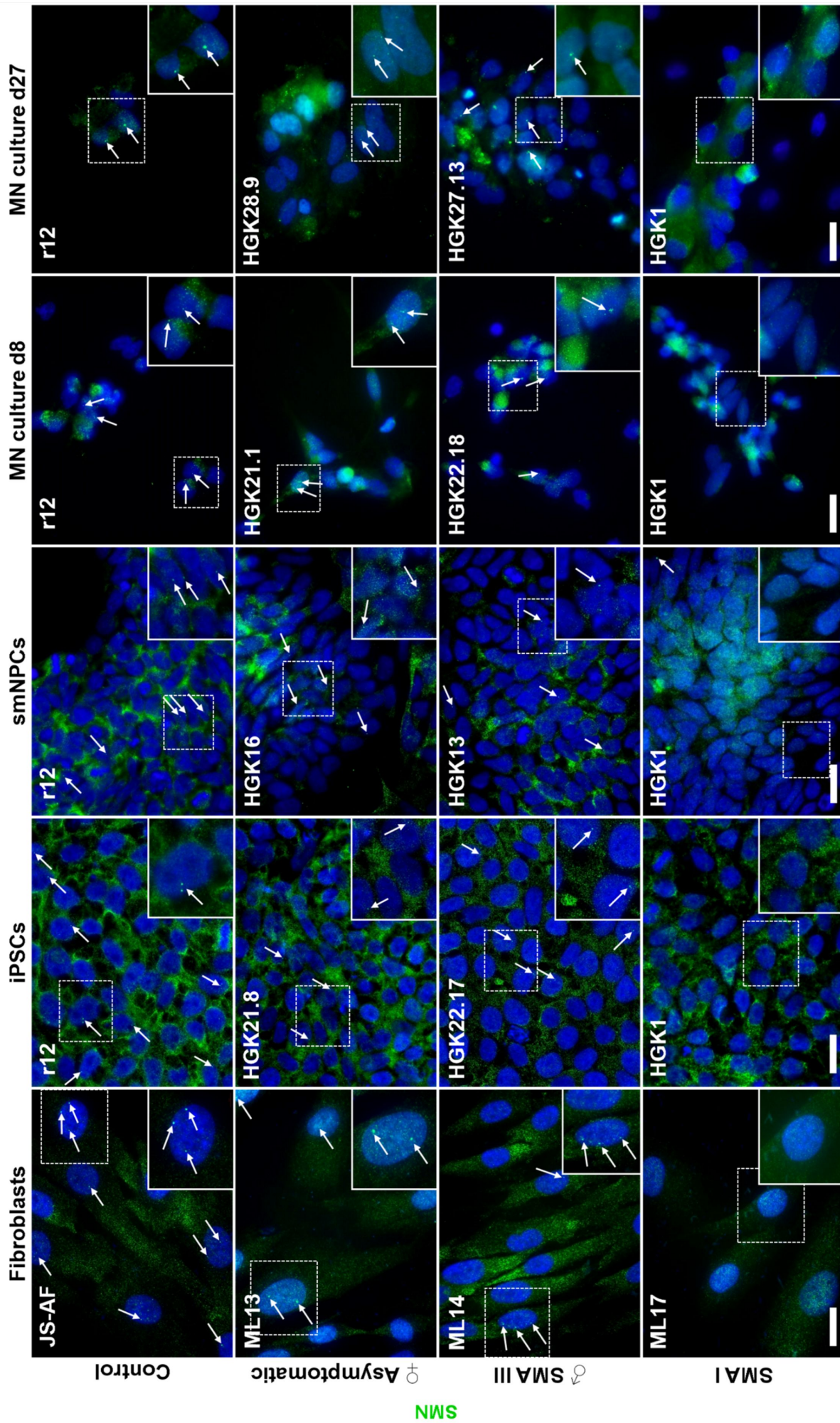
Fig 51: Immunocytochemical staining of cell lines representing the four phenotype classes in different cell populations during *in vitro* MN development. Principally, SMN (green) was either cytoplasmatically spread as diffuse fog or visible in distinct dot-like nuclear accumulations, i.e. gems (arrows). Control fibroblast JS-AF and corresponding progeny lines r12 displayed a variable gem number according to the cell population yet always observably topping the other cells in gem number. Opposite impressions were conveyed by SMA I line ML17 and respective offspring line HGK1 in which gems were hardly visualised. Members of discordant families continuously disclosed a moderate gem number irrespective of cell line or developmental stage. Nuclei were counterstained with DAPI (blue). Dashed line inclosed area magnified in insets (scale bar 20 μm, valid for all images).
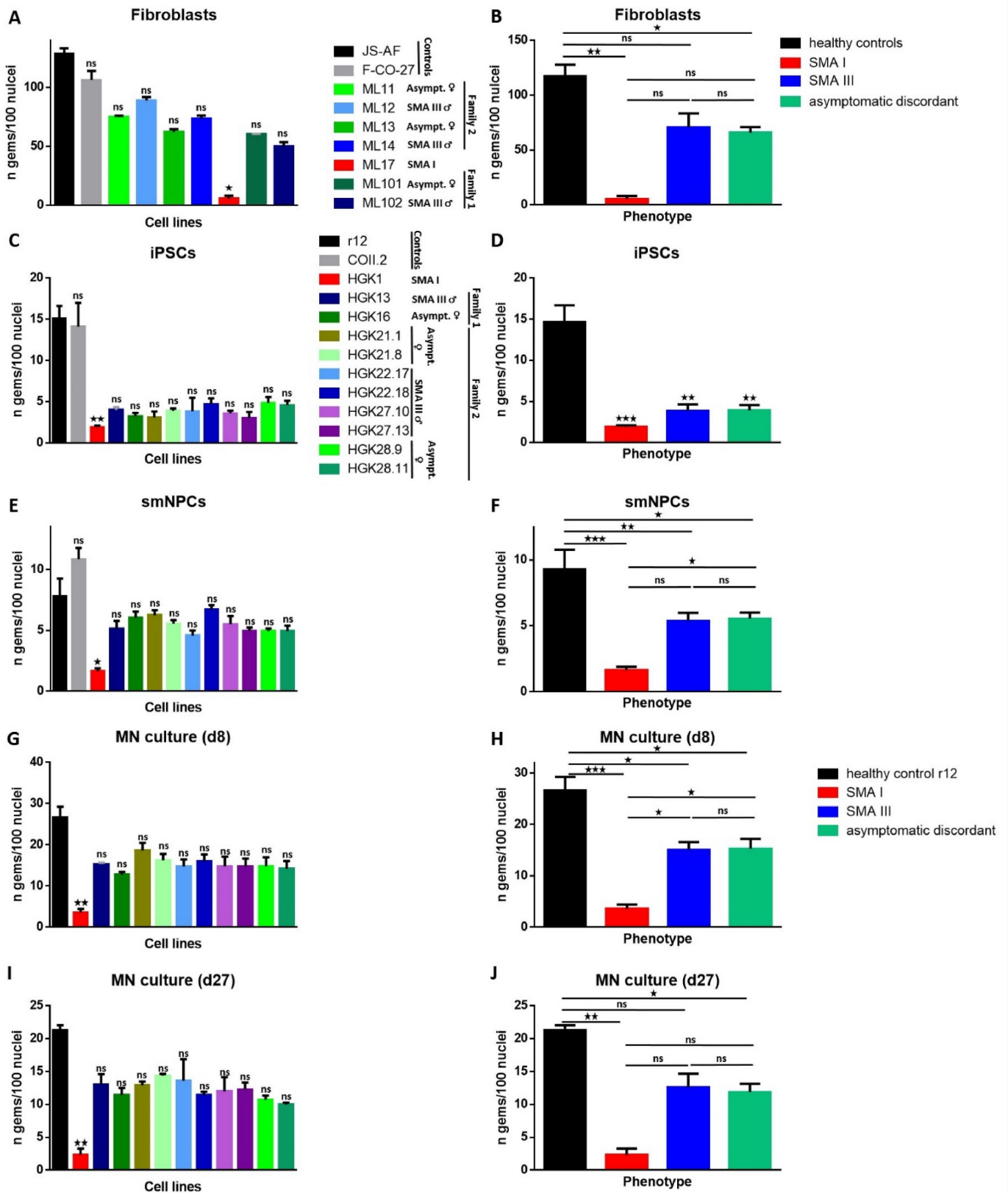
Fig. 52: Quantitative determination of gem number in different cell populations. (**A**) In fibroblasts, massive gem reduction was overt in SMA I line ML17 while discordant family members displayed a minor decrease. Still, diminished gem numbers were significant relative to controls. (**B**) Phenotypic groups indicated significant gem decrease in SMA I and asymptomatic while gem reduction in SMA III remained insignificant as among non-control groups. (**C**) In iPSCs, non-control lines exhibited very reduced gem numbers. Nonetheless, SMA I line HGK1 presented the fewest number. (**D**) Summarising single results to phenotypic classes pictured a very significant diminution in SMA I, SMA III and asymptomatic relative to controls. (**E**) In smNPCs, SMA I line HGK1 disclosed a

significantly low gem number whereas discordant family lines possessed overall more gems, yet compared to control line r12 visible reduced. (**F**) Phenotypic grouping evidently visualised significant decline in gem number in SMA I, SMA III and asymptomatic relative to controls. Clearly, discordant family members equally showed a medium gem number which was significantly higher than SMA I gem number (relative to asymptomatic). (**G**) In early MN culture (day 8), only SMA I line HGK1 disclosed a significant gem reduction in comparison to r12. Indeed, discordant family lines exhibited a decreased gem number, still without significance due to an unexpectedly lower total gem number in control r12. (**H**) In phenotype classes, gem number decrease was proved with strong significance in non-control phenotypes on the other hand. SMA I kept showing the fewest gems while SMA III and asymptomatic presented a moderate reduction. (**I**) In late MN culture (day 27), strongest significant decline was observable in SMA I HGK1. Gem numbers of individual discordant family lines remained at medium high level. (**J**) Phenotype classification illustrated a strong significant reduction in SMA I and asymptomatic with fewest gem number in SMA I again. Medium expression clearly represented more *SMN2* copy numbers in SMA III and asymptomatic. Error bars represented ± SEM of duplicates in fibroblasts (n=2) and triplicates in all other cell populations (n=3). MN cultures displayed data of three independent MN differentiation runs (n=3) (Kruskal-Wallis test, $p < 0.05$ = *, $p < 0.01$ = **, $p < 0.001$ = ***). Note that control COII.2 was excluded from analyses in MN culture day 8 and day 27.

In fibroblasts, both controls exhibited an extraordinarily high gem number virtually furnishing every nucleus counted with more than one gem on average. Contrarily, gem number in SMA I line ML17 was diminished in strong significance. Gems in discordant family members amounted to a considerable number so that corresponding reduction was insignificant relative to control line JS-AF (Fig. 52 **A**). Summing up these results according to phenotypic classes strikingly pointed out a significant decrease in gem numbers between controls and SMA I and asymptomatic, respectively. However, the difference between SMA III and healthy controls was insignificant as amongst non-control groups (Fig. 52 **B**).

In iPSCs, control lines r12 and COII.2 contained almost equal gem numbers whereas other cell lines exhibited a remarkable decrease in gem number with SMA I HGK1 showing the fewest gems and significant reduction. Gem number in discordant family members was found ~2-2.5fold higher than HGK1 but still lower than in controls (Fig. 52 **C**). Phenotypic classification mirrored this consistent gem number distribution with a very significant decline in gem number relative to controls: SMA I delivered only ~13% while SMA III and asymptomatic discordant equally exhibited ~26-27% gems (Fig. 52 **D**).

smNPCs control lines r12 and COII.2 comprised a reasonable gem number. Gem number in SMA I HGK1 was very significantly lowered whereas gem numbers in discordant family members resided at higher levels (Fig. 52 **E**). Grouped according to phenotypes gem number was very significantly lessened in SMA I smNPCs (~18%) and still significantly reduced in discordant family members compared to controls. SMA III and asymptomatic discordant reached ~57-59% of gem number in controls rendering also a significant difference when asymptomatic are compared to SMA I (Fig. 52 **F**).

In MN cultures on day 8, control line r12 revealed a relatively high gem number. Thus, minimised gem numbers in discordant cell lines was not significant when likened to control r12. In general, within discordant family members gem number consistently ranged between ~47-70% relative to control. SMA I HGK1 kept displaying a significant diminution in gem number relative to r12 (Fig. 52 **G**). Phenotypic classification again disclosed a significant reduction in SMA I, SMA III and asymptomatic discordant relative to control r12. SMA I possessed only ~13% of gems in controls whereas SMA III and asymptomatic contained ~56% and ~57%, respectively ranging significantly higher in comparison to SMA I (Fig. 52 **H**).

MN cultures on day 27 illustrated a similar picture as on day 8 with decreased gem number in non-control cell lines. However, after three weeks maturation, control line r12 demonstrated the most gems. An overall higher gem number on average in discordant family members was observed remaining insignificant in comparison to control r12. In addition, SMA I line HGK1

presented a highly significant drastic decrease in gem number (Fig. 52 **I**). The phenotypic overview depicted an identical gem number distribution as before the maturation phase. Relative to controls, gem number in SMA I was very significantly lowered (~11%) and markedly decreased in SMA III and asymptomatic (~59% and ~56%, respectively). Yet, significant difference was solely determined between asymptomatic and control. (Fig. 52 **J**).

Scrutinising gem number in so many cell lines of different populations enabled a thorough insight in developmental changes (Fig. 53). Generally, in fibroblasts the highest gem number was found in all four phenotype classes. Nevertheless, gem number in SMA I stayed on very low level throughout further cell populations. Conversion into iPSCs led to a massive drop in gem number in controls, SMA III and asymptomatic siblings quenching the latter ones almost to the level of SMA I. Additionally, in smNPCs the least differences among the four classes were visible. Motoneuronal differentiation again broadened the intervals in gem number between the four phenotypes setting controls at top, SMA III and asymptomatic in the middle and SMA I at the bottom line. Remarkably, discordant family groups (SMA III and asymptomatic) presented nearly equal gem number in all cell populations.

Taken together, albeit there were overall differences in total gem numbers within single phenotypic classes dependant on the cell population, SMN deficiency was solidly mirrored in various cell types by gem number determination. SMA I contained just 12% of control gems on average while in SMA III and asymptomatic averaged 52% and 51% of control gems were observable. Percentage of gem numbers in comparison to healthy control (100%) was itemised in Tab. 18.
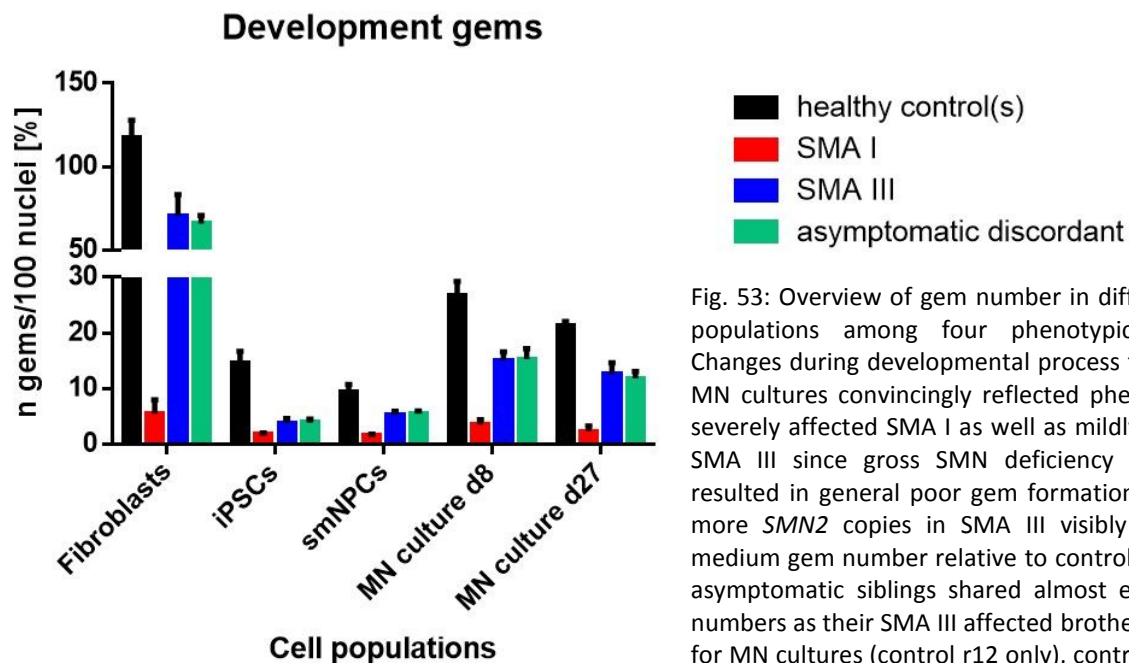
Fig. 53: Overview of gem number in different cell populations among four phenotypic classes. Changes during developmental process to mature MN cultures convincingly reflected phenotype in severely affected SMA I as well as mildly affected SMA III since gross SMN deficiency in SMA I resulted in general poor gem formation whereas more *SMN2* copies in SMA III visibly led to a medium gem number relative to control. Notably, asymptomatic siblings shared almost equal gem numbers as their SMA III affected brothers. Except for MN cultures (control r12 only), controls meant r12 and COII.2 (in fibroblasts, iPSCs and smNPCs). Graph was summarised from data of Fig. 52.

Table 18: Percentage of gem number in phenotypic classes was itemised relative to healthy controls (100%) in cell populations during *in vitro* MN development

Population	no. gems		
	SMA I	SMA III	Asymptomatic
Fibroblast	5%	60%	56%
iSPC	13%	26%	27%
smNPC	18%	58%	60%
MN culture d8	14%	57%	58%
MN culture d27	11%	59%	56%

7.5.6 Measurement of neurite length in MN cultures of different SMA phenotypes

To examine whether PLS3 over-expression also impacted on the neuronal outgrowth of differentiated smNPCs, on day 8 MN cultures of all 13 cell lines were immunocytochemically stained for neuron-specific filament marker β III-tubulin and motoneuronal filament marker SMI-32, respectively. The individual neurite outgrowth of HB9^{+}, ISL1^{+} or SMI-32^{+} MNs was then measured based on an assay developed by Kristina Dobrindt (personal communication) (Fig. 54).

The overall neurite length did not significantly differ between the individual cell lines neither with β III-tubulin as general neuronal marker (Fig. 55 **A**) nor with SMI-32 as motoneuronal marker (Fig. 55 **C**). Grouping the results into the four disease-related phenotypic classes did not demonstrate a significant difference between the phenotypes either (Fig. 55 **B**, **D**). Principally, the variance in neurite length was very broad.

The average length of β III-tubulin[+] neurites generally ranged between 70-80 µm independent of the genetic background. Only HGK28.9 exhibited a mean neurite length of 90 µm, yet also showing the highest variance in neurite length (Fig. 55 **A**). On average, the neurites in SMI-32^{+} MNs appeared basically longer, however, the length was also more variant (100-160 µm) between the individual cell lines (Fig. 55 **C**). Indeed, summing up the latter results according to the phenotype levelled these differences because within the four phenotypic classes the neurite length of SMI-32^{+} MNs was nearly equal ranging between 117-130 µm (Fig. 55 **D**).
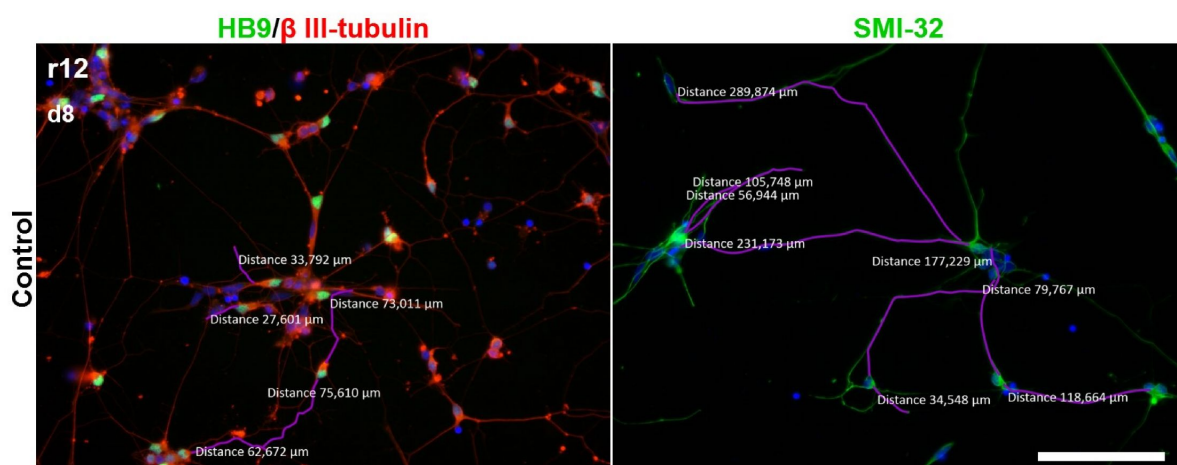
Fig. 54: Exemplary immunocytochemical staining of β III-tubulin[+] (red) and SMI-32^{+} (green) neurites, respectively, in MN cultures of representative control line r12 on day 8. Individual neurite outgrowth of HB9^{+} or SMI-32^{+} MNs (both green) was assayed (purple lines) and corresponding distances (white) registered. Nuclei were counterstained with DAPI (blue) (scale bar 100 µm, valid for all images).
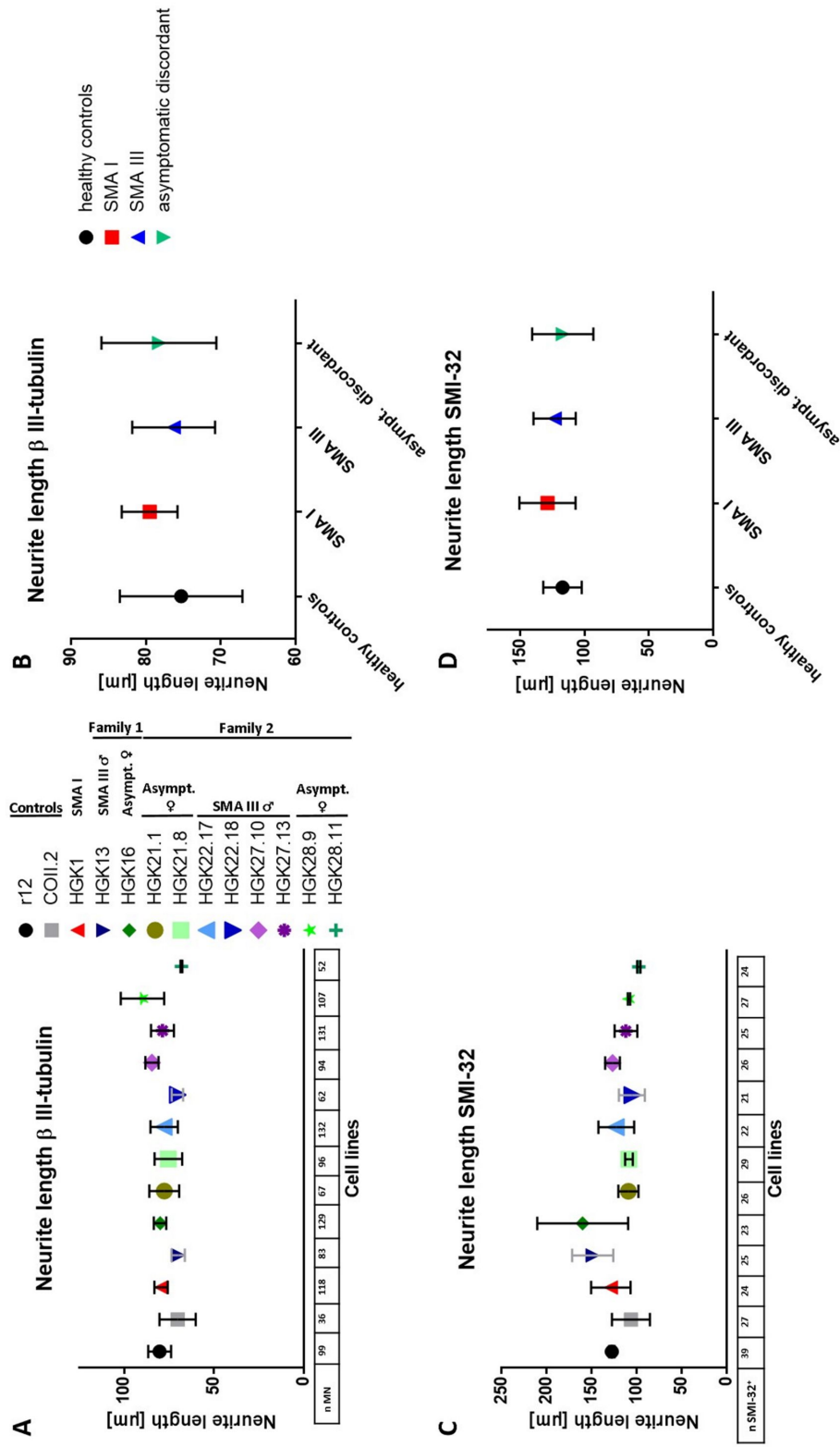
Fig. 55: Quantification of neurite length survey in smNPC-derived MN cultures of different healthy and SMA affected or asymptomatic individuals on day 8. Mean neurite length of β III-tubulin⁺ MNs (HB9⁺ or ISL1⁺) (**A**) or SMI-32⁺ MNs (**C**) were depicted for each individual cell line. Tables below denoted individual MN number per cell line. Additionally, mean values were summarised according to the phenotypic background (**B**, **D**). Basically, a rather broad variance within the individual cell lines was visible. So, when the phenotypes were compared there was no significant difference detectable either. Subordinated tables listed total number of HB9⁺/ISL1⁺ (**A**) or SMI-32⁺ MNs (**B**) per cell line. Results showed the measurements of three independent MN differentiation runs (n=3) for β III-tubulin (90-160 neurites in total) and two independent MN differentiation runs (n=2) for SMI-32 (30-60 neurites in total). Error bars represented ± SEM (Kruskal-Wallis test).

7.6 Visualisation of axonal growth cones in MN cultures

The presence of PLS3 at motoneuronal axon tips is regarded as one key feature of PLS3-mediated protection. Differentiation of patient-derived iPSCs via smNPCs into MN culture renders possible to examine whether PLS3 in asymptomatic siblings co-localises with actin at putative MN growth cones. Originally, endogenous Pls3 accumulated in F-actin rich growth cones of primary mouse MNs (Oprea *et al.* 2008). In PLS3 over-expressing mouse fibroblasts, an overt strong co-localisation was visible at filopodia (Ackermann *et al.* 2013). Axonal outgrowth was visualised by punctiform seeding of pMN-primed smNPCs and further cultivation for three weeks (6.8.1). Presence of growth cones was verified by triple immunocytochemical staining and possible co-localisation of actin and PLS3 assessed by confocal laser scanning microscopy in nine samples. Evidently, MAPT[+] axonal protrusions ended in cones with very delicate thin branches which did contain PLS3 and actin (Fig. 56 **A**).
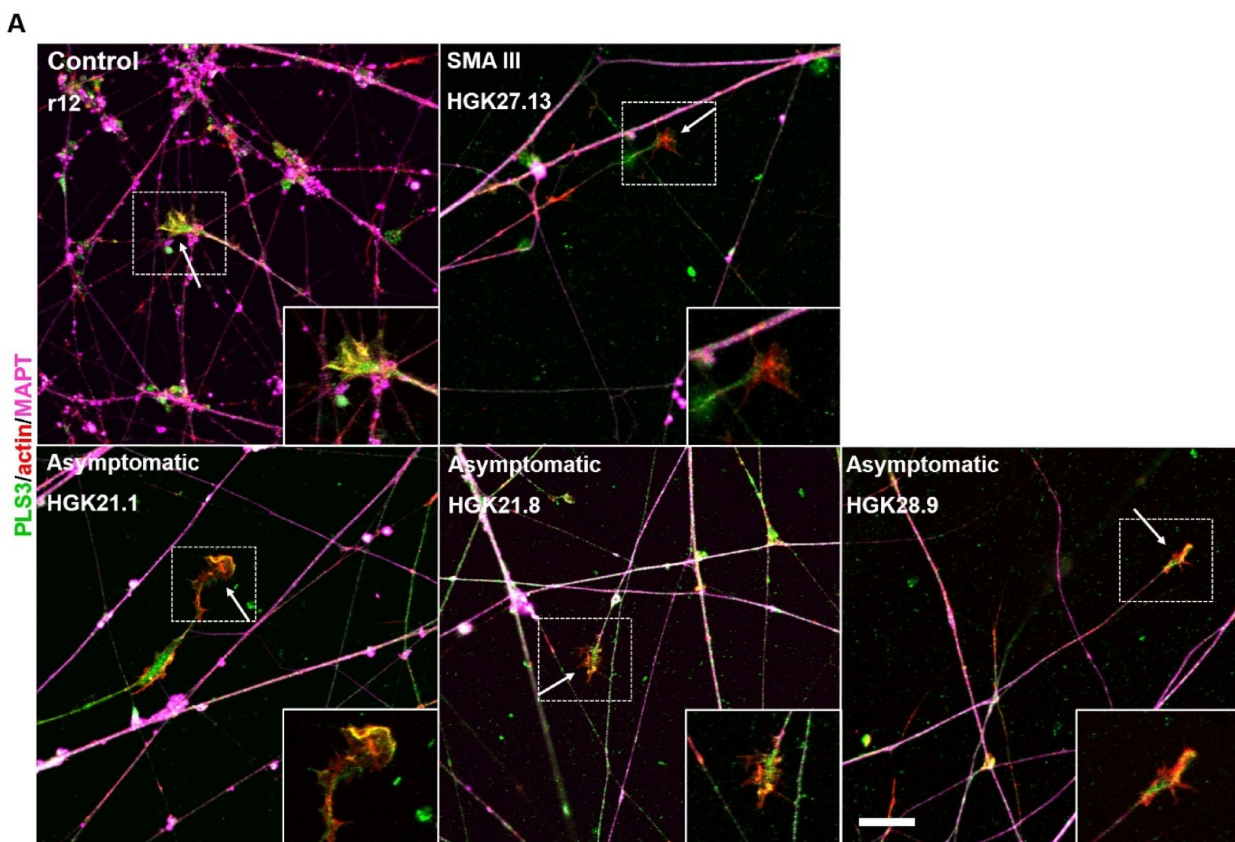
Fig. 56: (**A**) Visualisation of growth cones in maturing MN cultures from healthy control (r12) and PLS3 discordant siblings (SMA III patient HGK27.13 and his asymptomatic sisters HGK21.1, HGK21.8 and HGK28.9) on day 27. MAPT[+] (magenta) axons ended in delicately arborized growth cones (arrows) detectably comprising phalloidin-actin (red) and PLS3 (green). Co-localisation appeared already in control r12 and asymptomatic HGK21.1, HGK21.8 and HGK28.9 while such was not directly visible in SMA III HGK27.13. Following figures presented growth cones of control r12 (**B**), SMA III HGK27.10 (**C**) and asymptomatic HGK28.9 (**D**) with single staining in left panels and an overlay in the centre. Growth cones were magnified in PLS3/actin merge and collected Z-stacks analysed (right panels). Subordinated graph pictured fluorescence intensity of given YZ plane for both PLS3 (green) and actin (red) when cut distance [nm] was plotted against intensity. (**B**) Sagittal plane of control growth cone visualised PLS3 and actin nearly equally distributed, however, frequently co-localised at the rim. Overlaid signal intensities supported this impression. (**C**) In SMA III HGK27.10, presence of PLS3 and actin was visibly proved. Yet, distinct co-localisation and congruent signal intensity patterns as in control r12 were not detected. (**D**) In asymptomatic HGK28.9, intense PLS3 expression was imaged particularly in the rod end and growth cone central domain whereas actin allocated especially at the edges. Remarkably, PLS3 observably concentrated in such actin-rich areas. Z-stack analysis of such foci pictured clear PLS3/actin co-localisation. Additionally plotted signal intensities delineated in areas of strong actin accumulation an equally intense PLS3 concentration (scale bar 20 µm, **A**; 10 µm **B**-**D**).

D actin PLS3 MAPT

Asymptomatic
HGK28.9

XZ YZ
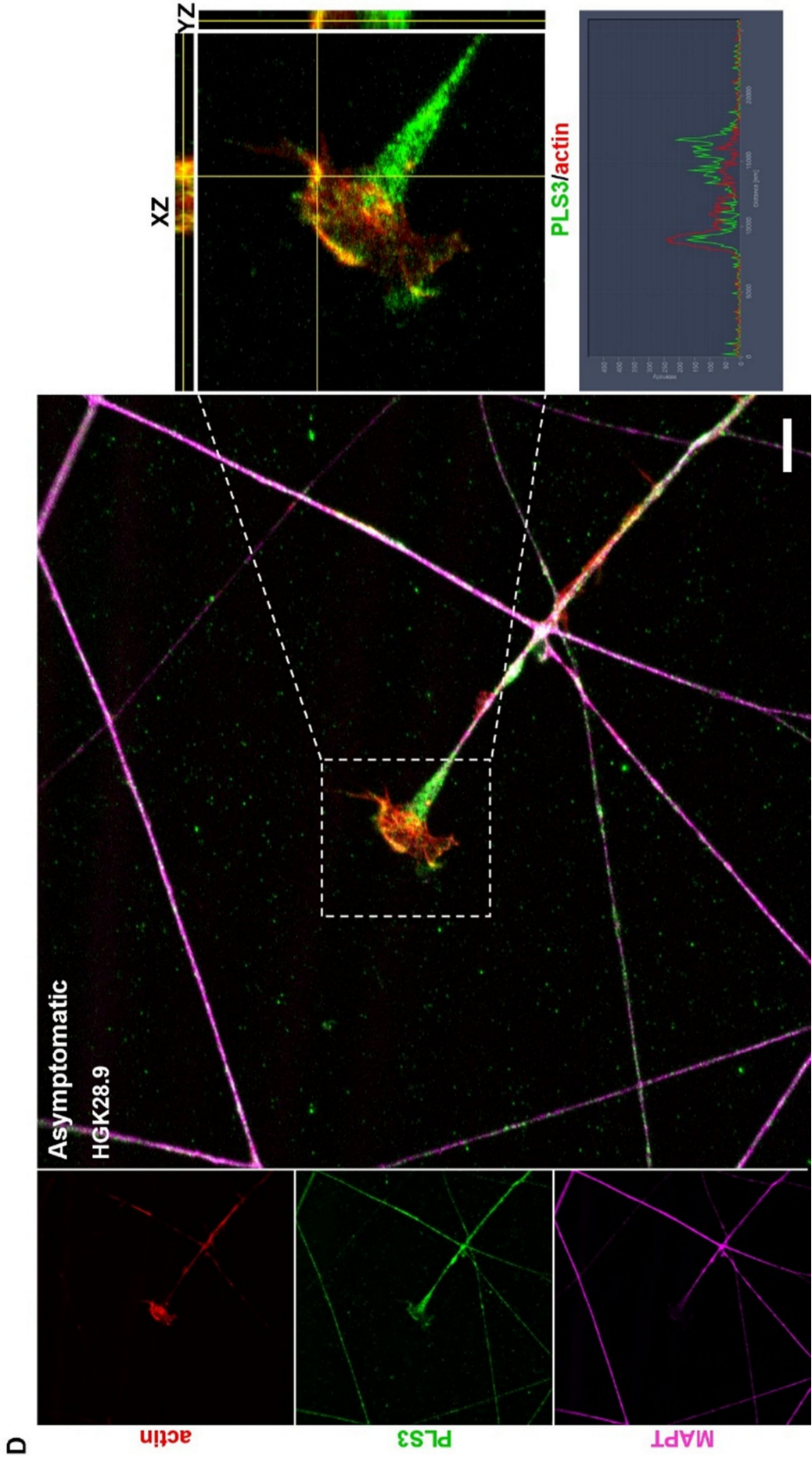
PLS3/actin

In control line r12, confocal laser scanning microscopy revealed an almost even distribution of actin and PLS3 in the growth cone resulting in frequent co-localisation. Z-stack analysis confirmed visible co-localisation of PLS3 and actin. Intensity measurements backed view of equal PLS3 and actin allocation (Fig. 56 **B**).

On the other hand, SMA III patient HGK27.10 did not display such an equal distribution (Fig. 56 **C**). Indeed, PLS3 and actin were also present in this growth cone, however, Z-stack analysis failed to denote consistent co-localisation. Moreover, signal intensity graphs rather shifted between each other.

In asymptomatic HGK28.9, intense PLS3 expression was observed in axon rod and growth cone centre while actin accumulated especially at the rims (Fig. 56 **D**). Intriguingly, PLS3 allocated in such actin-rich areas. Such co-localisation was visibly corroborated by Z-stack analyses and signal intensity. Corresponding graphs delineating strong actin expression went along with concomitantly high PLS3 expression yet not *vice versa* since areas of strong PLS3 expression (e.g. axonal rod) were almost devoid of detectable actin. SMA I line HGK1 failed to exhibit usable growth cones (data not shown).

7.7 Mixed motoneuronal cultures exhibited early signs of NMJ formation when co-cultured with human myotubes

Signal transduction to target muscles is the essential feature of proper functionality in motoneurons. Generation and maintenance of NMJs has ever since been in the focus of elucidating the pathomechanism of SMA (Kariya *et al.* 2008; Kong *et al.* 2009; Bowerman *et al.* 2012).

Even though there are miscellaneous co-culture methods published in which putative NMJ formation is displayed, no robust standard protocol exists so far (Marchetto *et al.* 2008; Hu *et al.* 2009; Guo *et al.* 2011; Son *et al.* 2011; Stockmann *et al.* 2011). Moreover, co-culturing myotubes and motoneurons is an extremely time-consuming process for it requires a long cultivation period until a fully stable connection between pre- and post-synaptic sites is accomplished. Stockmann and colleagues showed in 2011 that even after 12–14 weeks *in vitro*, cultivated MNs were obviously still proceeding in NMJ-development (Stockmann *et al.* 2011).

In order to examine the most appropriate protocol, several different methods were tried out varying in cell types, medium composition or addition of growth factors and small compounds (data not shown). Initially used murine myocyte line C2C12 was replaced by healthy human myocyte control line hMC to obtain a single-species xeno-free *in vitro* system. Human myocyte line hMC was a kind gift of Prof. Hanns Lochmüller (University of Newcastle, UK). When motoneuronal neurospheres were seeded on top of a human myotube layer, intense neuronal outgrowth was visible contacting neighbouring myotubes (Fig. 57).

However, prolonged co-cultivation in motoneuronal maturation medium MN1 resulted only sporadically in very early developmental signs of NMJ formation indicated by punctual bungarotoxin positive (BTX[+]) AChR clustering nearby myotube nuclei accumulation. Nonetheless, obvious AChR clustering was mostly visible in close proximity to axons (Fig. 58). Moreover, the addition of laminin and agrin – an extracellular matrix (ECM) proteoglycan – is regarded as beneficial for NMJ formation. Agrin is synthesised by the elongating MN axon and secreted into the synaptic cleft. There, it essentially fosters AChR clustering on skeletal muscle surfaces during maturation (Weston *et al.* 2007). Both ECM components were also part of the enriched co-culture medium utilised by Guo and colleagues. Yet, a remarkable increase in BTX[+]

AChR clusters was not observable when our MN1 medium was supplemented with laminin and agrin (data not shown).
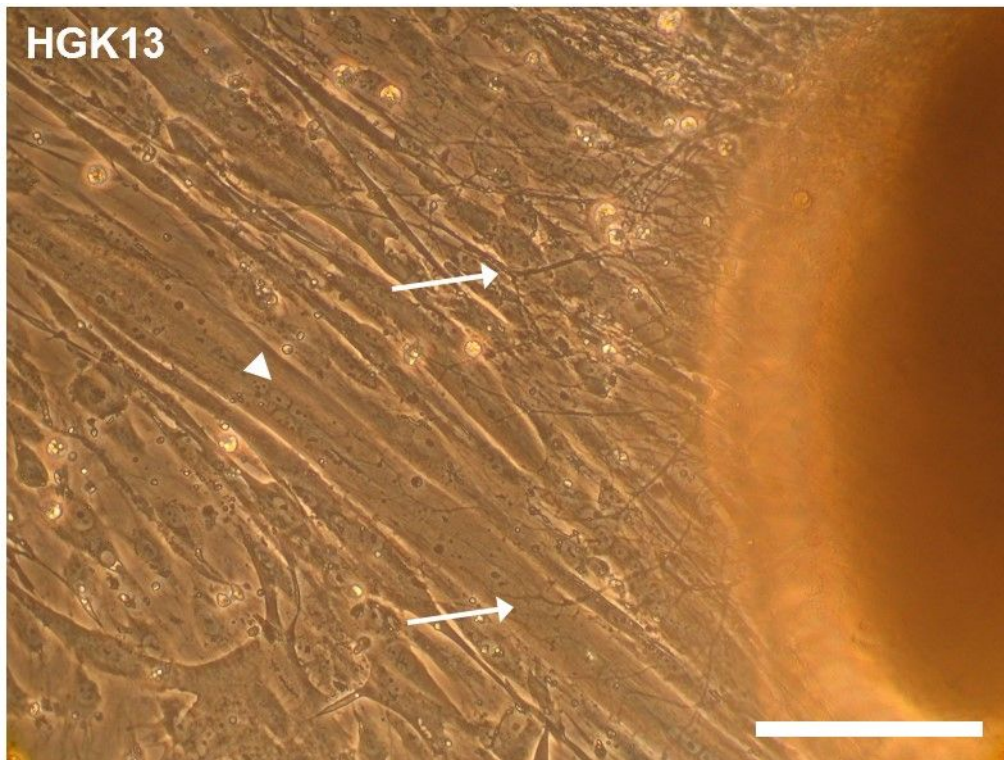
Fig. 57: Phase image of co-culture of human myotubes hMC with motoneuronally primed neurosphere derived from SMA III iPSC line HGK13. Immediately after plating, strong neuronal outgrowth (arrows) took place on day 4 starting from the seeded neurosphere (right). The axonal protrusions evidently contacted vicinal thick multi-nucleated myotubes (arrowhead) (scale bar 200 µm).

Another possibly benefiting option was presented by Peng and colleagues: In *Xenopus laevis*, they demonstrated that upon neurotrophic withdrawal MNs had the propensity to induce synaptogenesis on contact with the target muscle cell (Peng *et al.* 2003). During synaptogenesis, the MN axon outgrowth had eventually to halt in order to allow the establishment of a stable connection between the pre-synaptic and post-synaptic partners (Sanes *et al.* 1999). Neurotrophic factors such as BDNF or GDNF down-regulated the expression of agrin in MNs thereby inhibiting synaptogenesis (Peng *et al.* 2003). On the other hand, Schwann cell-conditioned medium (SC-CM) was able to override the retarding effects of neurotrophic factors concerning synapse formation *in vitro* (Peng *et al.* 2003).

Thus, mixed motoneuronal cultures were sown onto a human myotube layer and ever since co-cultured with SC-CM for seven weeks. Murine Schwann cell line iMS32 was a kind gift of Rebecca Conrad/Dr. Michael Karus (University of Bochum, Germany). Obviously, SC-CM strongly enhanced clustering of BTX[+] AChRs on the myotube surface (Fig. 59). Grooved plaque-like patches were spread over large areas of the myotube surface. Many axonal protrusions of SV2^{+} mature neurons extended towards the myotubes and contacted AChR plaques. Nevertheless, a clear direct co-localisation of a presumable MN growth cone and an AChR patch was not detectable so far.

NF/BTX

Fig. 58: Immunocytochemical staining visualized punctual bungarotoxin (BTX) positive AChR agglomeration (red) on hMC myotube surface in close proximity to neurofilament (NF) positive axons (green) of motoneuronally differentiated control iPSC line r1 after 15 days of co-culture. Note several myonuclei were strung together in the early myotube. Nuclei were counterstained with DAPI (blue) (scale bar 20 µm).

SV2/BTX

Fig. 59: (**A**) Immunocytochemical staining revealed that BTX[+] AChRs (red) strongly clustered on myotube surface when co-cultured with motoneuronally differentiated iPSC line HGK16 in Schwann-cell conditioned medium (SC-CM) for seven weeks. Note the plaque-like wide-spread AChR agglomeration on the myotube surface as in comparison to single sparsely scattered BTX[+] punctae after 15 days co-culture in Fig. 58. (**B**) Mature SV2^{+} neurons (green) did extend axonal protrusions towards these AChR clusters (arrows). (**C**) However, a clear NMJ-like co-localisation was not identifiable yet. Nuclei were counterstained with DAPI (blue) (scale bar 100 µm, **A**, **B**; 20 µm, **C**).

7.8 Application of iPSC-derived lt-NES®SCs for examination of cell-specific responsiveness to VPA treatment

Among potential therapeutic agents for curing SMA, histone deacetylase (HDAC) inhibitor valproic acid (VPA) played a promising role (Brichta *et al.* 2006; Swoboda *et al.* 2011). VPA exerted its beneficial effect by loosening chromatin structure via histone hyperacetylation, thus amongst others stimulating transcription of remaining *SMN2* copies in SMA patients (Garbes *et al.* 2013). However, deeper investigations demonstrated different responses towards VPA administration in patients' cohorts, resulting in an ameliorative, indifferent or damaging effect in patients. Obviously, patients reacted as positive (pos-) responders, non-responders or negative (neg-) responders thwarting VPA application as prospective drug (Brichta *et al.* 2006; Kissel *et al.* 2011; Piepers *et al.* 2011).

To elucidate the molecular reasons of this divergent responsiveness, in 2013 Garbes and colleagues published an in-depth study in which different tissues of VPA pos-, non- and neg-responders were treated with VPA revealing altered fatty acid uptake as underlying rationale. In patients' blood and fibroblasts, response to VPA treatment was measured by changes in expression of *FL-SMN2* mRNA and SMN protein (Garbes *et al.* 2013).

Furthermore, VPA was known to interfere with neuronal GABA synthesis leading to elevated GABA levels in GABAergic CNS neurons (Johannessen 2000). This hypothesis would mean a stop of GABA degradation in VPA pos-responder thereby causing an increase in GABA release. So, respective lt-NES®SC lines were derived from control ESC line HB9-GFP (Placantonakis *et al.* 2009), pos-responder iPSC line HGK1 and non-responder iPSC line HGK4 according to Koch *et al.*, 2009, and differentiated into GABAergic neurons whose supernatant GABA release was determined by ELISA after manufacturer's instructions (see (Garbes *et al.* 2013)).

When lt-NES®SC lines were immunocytochemically stained, all three cell lines evidently displayed pan-neuronal markers SOX2 and nestin. In addition, typical rosette-markers ZO-1 and PLZF were recognisably picturing the petal-like arrangement of rosette-like NSCs. Thus, valid lt-NES®SC traits were proven in these cell lines (Fig. 60 **A**). Once lt-NES®SC lines were subjected to directed GABAergic differentiation, immunocytochemical staining revealed considerable presence of GABAergic neurons indicated by expression of GABAergic marker GAD65/67 and concomitantly neuronal marker β III-tubulin (Fig. 60 **B**).

Subsequently, 500 µM VPA were administered to GABAergic neurons for nine days. RNA was sampled and checked for *SMN* expression by qRT-PCR. Clearly, VPA exerted a boosting effect in pos-responder HGK1, resulting in augmented *SMN* mRNA level. On the contrary, control ESC and non-responder HGK4 did not illustrate a shift in *SMN* levels (Fig. 60 **C**). Finally, supernatant of GABAergic cultures was collected and assayed for GABA content. Indeed, a significantly increased GABA release was measured in pos-responder HGK1 whereas control ESC remained asymptomatic by VPA application. Non-responder HGK4 even displayed a detectable decline in GABA release (Fig. 60 **D**).

Taken together, VPA responsiveness was maintained in GABAergic neurons not only pointing out the importance to verify cellular patient-specific features but also the feasibility and reliability of iPSC-derived neuronal *in vitro* systems.
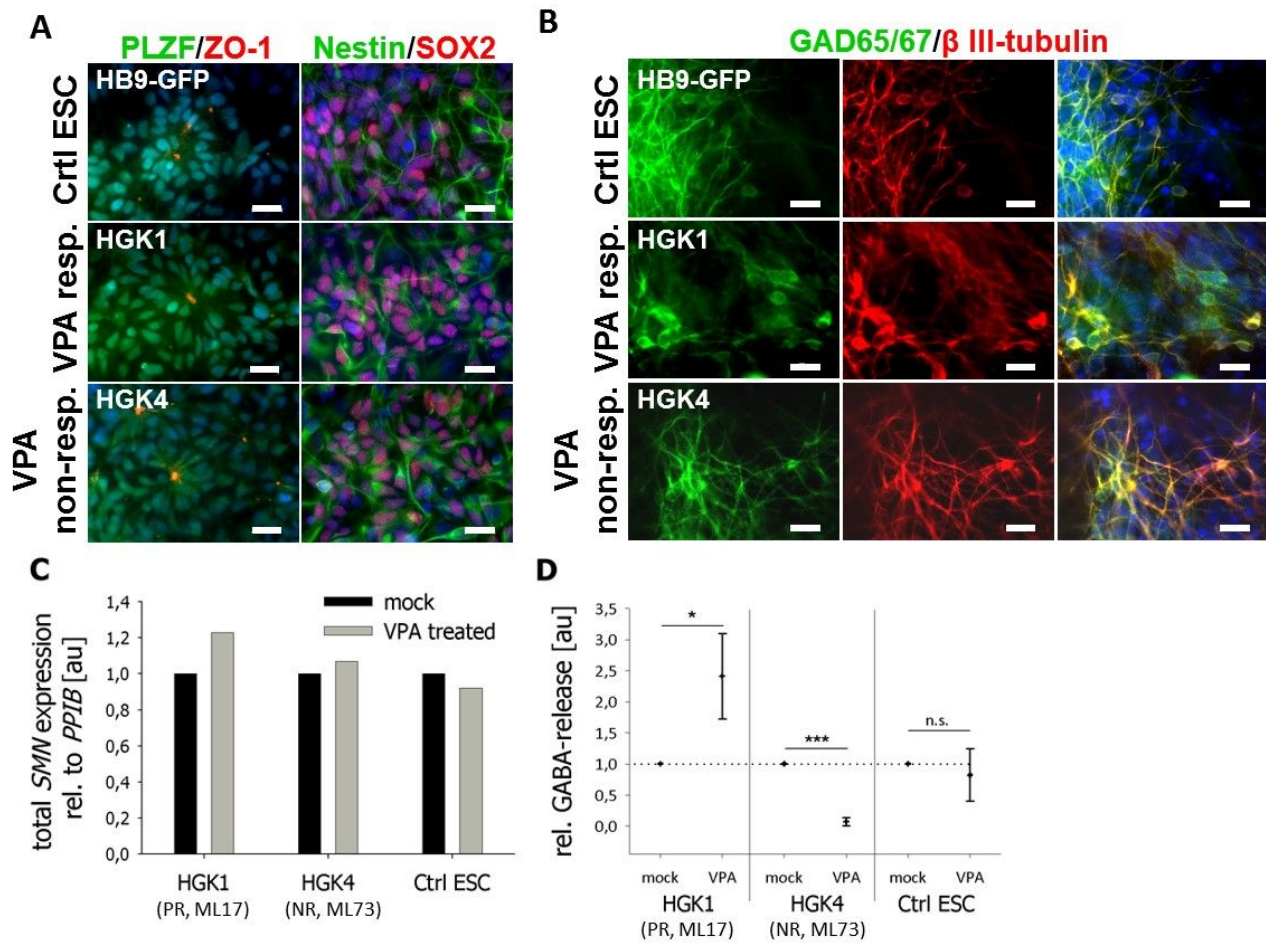
Fig. 60: Assessment of VPA-mediated GABA release in lt-NES®SC-derived GABAergic neurons of VPA pos-responder HGK1, VPA non-responder HGK4 and control ESC line HB9-GFP. (**A**) Immunocytochemical staining demonstrated characteristic petal-shape arrangement of rosette-like lt-NES®SCs with PLZF+ (green) cells fanned around the ZO-1+ (red) apical centre. Additional presence of wide-spread expression of general neuronal markers SOX2 (red) and nestin (green) verified lt-NES®SC character. (**B**) Following directed GABAergic differentiation, all three cell lines featured overt presence of true GABAergic neurons marked by GABAergic neuron marker GAD65/67 (green) and neuronal marker β III-tubulin (red) in immunocytochemical staining. Nuclei were counterstained with DAPI (blue) (scale bar 20 µm). GABAergic neurons were treated with 500 µM VPA for nine days. Subsequently, expression of *SMN* mRNA was determined by qRT-PCR in neuronal RNA extracts. (**C**) VPA treatment raised SMN levels in pos-responder HGK1 while control and non-responder HGK4 remained unaffected. Expression was normalised to *PPIB* (cyclophilin B) levels. Analysis represented data from one single GABAergic differentiation (n=1). (**D**) Quantifying relative GABA release in lt-NES®SC-derived GABAergic neurons recorded a significant approx. 2.5fold elevation in GABA release in pos-responder HGK1 while non-responder HGK4 even disclosed a significant diminution in GABA release. Mock comprised treatment with VPA solvent (i.e. H_2O dest.). Error bars represented ± SD of duplicates (n=2) (two-tailed Student's *t*-test, *p* <0.05 = *, *p* <0.001 = ***). Corresponding donor fibroblast cell lines and VPA status (PR=pos-responder, NR=non-responder) were bracketed below cell line names. Figure adapted from original publication (Garbes *et al.* 2013).

8. Discussion

8.1 iPSC-derived *in vitro* cell culture models grant more exact access to SMA-specific features in MNs than animal models

Several well established SMA mouse models reasonably phenocopy different stages of disease severity in humans (Hsieh-Li *et al.* 2000; Monani *et al.* 2000; Le *et al.* 2005; Bowerman *et al.* 2009). Thus, they and further animal models provide a valuable platform to investigate the molecular and cellular pathomechanisms inhering SMA.

Examination of the effects of SMA modifying genes or drug responsiveness is of particular interest in SMA research since they bespeak deeper evidence into SMA pathophysiology and may grant access to possible therapeutic measures. Plastin 3 (PLS3), an actin bundling cytoskeletal protein, was discovered as protective modifier in *SMN1*-deleted siblings of discordant SMA families (Oprea *et al.* 2008). This finding was affirmed by further studies (Stratigopoulos *et al.* 2010), yet PLS3 over-expression was not detected in blood of all asymptomatic individuals (Bernal *et al.* 2011). A PLS3 over-expressing SMA mouse model exhibited general improvements in MN-synapse architecture, function and neuromuscular connectivity (Ackermann *et al.* 2013). However, the overall survival rate was not extended whereas human PLS3 over-expressing individuals exhibit no SMA deficits and possess a regular life expectancy.

Hence, every animal disease model can only approximate the true human state incompletely. Since living human motoneurons cannot be sampled from SMA patients, the actual target tissue of SMA remains inaccessible. So, the exact events of SMA pathology stay elusive. This gap between SMA animal models and human SMA patients was bridged by the introduction of direct reprogramming technique in which patient-derived somatic cells are converted into induced pluripotent stem cells (iPSCs) (Takahashi *et al.* 2006; Takahashi *et al.* 2007). Those iPSCs are capable of differentiating into cells of various lineages so that also human motoneurons were cultivable *in vitro* (Dimos *et al.* 2008; Ebert *et al.* 2009). Indeed, iPSC-derived motoneurons were successfully obtained from SMA I patients displaying the characteristic features of SMA pathology, e.g. MN degeneration, diminished number of gems, reduced SMN levels and phenotypic rescue by SMN increase (Ebert *et al.* 2009; Chang *et al.* 2011).

In order to circumvent the aforementioned shortcomings of a PLS3 over-expressing SMA mouse model, the establishment of a personalised iPSC-derived *in vitro* cell culture model from PLS3 discordant family members and VPA (non-)responders was the main goal of this doctoral thesis.

8.1.1 State-of-the-art reprogramming via SeV technology reliably delivered integration-free iPSC lines from PLS3 discordant fibroblasts

The ectopic expression of four pluripotency-related reprogramming factors (4F = OCT4, SOX2, KLF4 and c-MYC) converts human fibroblasts into iPSCs (Takahashi *et al.* 2007). In total, eight fibroblast cell lines (5.8.3, Tab. 13, 7.1, Fig. 10) were reprogrammed in this thesis. Classical reprogramming strategy involved 4F introduction via retrovirus infection. Dr. John Dimos from iPierian Inc. (San Francisco, USA) succeeded in reprogramming ML17 (SMA I, VPA responder), ML73 (SMA II, VPA non-responder) and family 1 siblings ML101 (asymptomatic, PLS3 discordant) and ML102 (SMA III, PLS3 discordant) by 4F retroviruses.

Retroviral vectors represent a suitable tool to stably introduce exogenous DNA into mitotic mammalian host cells (Barquinero *et al.* 2004). The transfer of the four Yamanaka factors during the first reprogramming studies was carried out by such retroviral transduction rendering a reasonably moderate efficiency rate of 0.01-1% (Takahashi *et al.* 2006; Robinton *et al.* 2012). After the transduction, multiple random insertions (1-40) of the four factors in varying copy numbers took place into the host genome (Wernig *et al.* 2007; Okita *et al.* 2011). Therefore, standard technology applied for reprogramming *per se* raised serious concerns regarding the safe use of genetically modified cells bearing exogenous proviral transgenes randomly integrated in their genome (Sun *et al.* 2010; Sancho-Martinez *et al.* 2011). Furthermore, transplantation of heterogeneous iPSC populations containing cells with incomplete reprogramming or reactivation of transgenic oncogene c-Myc had been strongly associated with tumorigenicity in mouse models (Okita *et al.* 2007; Miura *et al.* 2009). Thus, insufficient silencing of proviral transgenes may represent a serious problem for subsequent applications (e.g. lineage-specific differentiation) (Sommer *et al.* 2012; Toivonen *et al.* 2013) although the specific pMXs-plasmid backbone ought to promote transgene silencing (Takahashi *et al.* 2006).

Indeed, retrovirus-mediated reprogramming failed in generating proper iPSC colonies from human fibroblast cell lines of SMA discordant family 2 (7.1, Fig. 10) asymptomatic members (ML11, ML13) and SMA III patients (ML12, ML14) when carried out at the Institute of Reconstructive Neurobiology (Bonn) during this study. An inverse correlation between reprogramming efficiency and donor age and passage number was reported (Sommer *et al.* 2010). Considering a relatively elevated donor age (see 5.8.3, Tab. 13) as well as a high passage number, fibroblast cell lines ML11, ML12, ML13 and ML14 might behave reluctantly towards retroviral reprogramming.

To overcome these pitfalls, diverse alternative reprogramming methods have been developed within the recent years: Subsequent removal of transgenes from iPSCs by transposon-based approaches with *piggyBac* (Woltjen *et al.* 2009) or excision of a *loxP* site flanked reprogramming cassette via *Cre* recombinase treatment (Kaji *et al.* 2009); transient 4F expression by adenoviruses (Stadtfeld *et al.* 2008; Zhou *et al.* 2009b) or episomal vectors (Yu *et al.* 2009); omission of any DNA vector like zinc finger nuclease (ZFN) technology (Ramalingam *et al.* 2012), application of synthetic 4F mRNAs (Warren *et al.* 2010), 4F proteins (Kim *et al.* 2009; Zhou *et al.* 2009a) or miRNAs (Anokye-Danso *et al.* 2011; Miyoshi *et al.* 2011). Despite this broad line-up of various alternative methods, unequivocal backlashes inhere in all of them: Labour-intensive screening for excised transgene-free iPSC lines or tedious sub-cloning, cumbersome repeated transfection cycles and an overall very poor efficiency lessening the original efficiency rate (Robinton *et al.* 2012).

To avoid these overt deficits, a novel reprogramming approach by non-integrative Sendai virus (SeV) was chosen for reprogramming human fibroblast cell lines ML11, ML12, ML13 and ML14 turning out as efficient and successful method in our hands. The non-integrative RNA SeV replicates only in the cytoplasm. Hence, neither a DNA-intermediate nor integration into the host genome will occur. SeV vectors simply decrease over time delivering transgene-free iPSC lines (Fusaki *et al.* 2009).

Patients' fibroblasts tolerated single spinfection with 4F SeV vectors well (7.1, Fig. 12). Time-lapse analyses pictured the process of morphological conversion from fibroblast to iPSC resulting in emergence of typical iPSC colonies (Araki *et al.* 2010). Every now and then, the reprogramming process is not completed yet and gets stuck in intermediate states instead (Mikkelsen *et al.* 2008). Therefore, accurate choice of putative iPSC colonies is essential for further propagation and cell line integrity. Intact new iPSC colonies are characterised by

roundish colony form, flat growth behaviour, small cell body with high nucleus/cytoplasma ratio and prominent nucleoli and a distinct well-defined edge to the surrounding MEF-feeder layer (Takahashi *et al.* 2007; Smith *et al.* 2009). Indeed, SeV-mediated reprogramming yielded a high number of putative iPSC colonies on primary plates. Only colonies fulfilling the aforementioned obvious morphological quality criteria were chosen from which scores of clonal iPSC lines were picked from every target cell line (see 10.1, Tab. 19).

Summarised, eight fibroblast cell lines of different SMA background were successfully reprogrammed into iPSCs.

8.1.2 Human iPSC lines are validated as fully pluripotent

Validation of iPSCs is mandatory to prove full pluripotency and to reject faulty and inappropriate iPSC clones. Cellular conversion during reprogramming is not always complete. Thus, cells may become trapped in intermediate states (Chan *et al.* 2009). These partially reprogrammed cell lines show reactivation of a distinctive subset of SC-related genes, yet an incomplete repression of lineage-specifying transcription factors (Mikkelsen *et al.* 2008). Repeatedly, possible iPSC colonies stopped growing on primary TC dishes, collapsed or began excessive proliferation with characteristic brown outgrowth (7.1, Fig. 13 **A**). Therefore, also SeV-mediated reprogramming gave rise to such improper intermediate states.

Hence, assessment of successful reprogramming commenced with identification of compact colonies on primary TC dishes. Such putative iPSC colonies had distinct borders with well-defined edges and they were comprised of cells with a large nucleus, bigger nucleoli and scant cytoplasm (Robinton *et al.* 2012). Exclusively, colonies fulfilling this primary morphologic quality criterion were picked (7.1, Fig. 13 **B**).

However, only a combination of several criteria reliably verifies *bona fide* pluripotency in human iPSCs: Pluripotent SCs are karyotypically normal (Brivanlou *et al.* 2003), possess a distinctive nuclear architecture concerning lamina, nuclear speckles and heterochromatin domains (Meshorer *et al.* 2006) and exhibit rapid proliferative behaviour with a shortened G1-phase (Ghule *et al.* 2008). In addition, pluripotent SCs express typical surface markers (SSEA-3, SSEA-4, TRA-1-60 and TRA-1-81), a unique set of miRNAs, telomerase, alkaline phosphatase and pluripotency sustaining TFs OCT4, SOX2 and NANOG whose promoters are hypophosphorylated reflecting their transcriptionally active state (Nichols *et al.* 1998; Mitsui *et al.* 2003; Suh *et al.* 2004; Wernig *et al.* 2007; Smith *et al.* 2009).

Upon further propagation, human iPSC lines HGK13, HGK16, HGK21, HGK22, HGK27 and HGK28 stably grew and maintained typical pluripotent morphology throughout passaging (7.2.1, Fig. 14). In addition, all iPSC lines were AP[+] and expressed typical pluripotency surface markers (7.2.1, Fig. 14). This held also true for iPSC SMA I line HGK1 and SMA II line HGK4 (Garbes *et al.* 2013).

Albeit standard karyotyping was frequently observed in publications to prove genomic integrity in iPSCs, it did not suffice our quality requirements because more subtle mutations were not covered. Moreover, established human iPSC lines initially declared as "genomically intact" after traditional karyotyping exhibited genomic aberrations which cannot be ruled out to interfere with subsequent applications (Hussein *et al.* 2011). Thorough SNP-array analyses of iPSC lines HGK13, HGK16, HGK21, HGK22, HGK27 and HGK28 verified genomic integrity in all respective clones (7.2.3, Fig. 16, Tab. 16). Lines HGK1 and HGK4 also passed this quality criterion (Garbes *et al.* 2013).

Possible drawbacks in using retroviral reprogramming were disclosed in examining transgene silencing in HGK1, HGK4, HGK13 and HGK16. The latter both iPSC lines still exhibited residual

transgene activity (7.2.4, Fig. 17) as HGK1 did (Garbes *et al.* 2013). Even though no broad silencing defect was detectable, leaky exogenous transgenes would perhaps yield unknown detrimental effects in future applications, yet some studies reported no inhibition of MN differentiation by persistent transgene expression (Boulting *et al.* 2011). In contrast, generated own iPSC lines HGK21, HGK22, HGK27 and HGK28 were demonstrably transgene-free. Neither did they express SeV surface marker protein HN (7.2.5, Fig. 18) nor did they contain viral *NP* mRNA after several passages in culture (7.2.5, Fig. 19). Moreover, this fact underlined the importance of analysing more than one clone per iPSC line to skip problematic clones in case. Unfortunately, just one single previously unvalidated clone from HGK1, HGK4, HGK13 and HGK16 was delivered by iPierian Inc.

To verify pluripotency in reprogrammed cells, it must be demonstrated that they are capable of differentiating into all cell types in the developing organism. By the formation of embryoid bodies (EBs), spontaneously formed spherical SC clusters resembling the gastrulating embryo, the development of all three germ layers *in vitro* was achieved (Itskovitz-Eldor *et al.* 2000). Certainly, every investigated iPSC line generated progeny of all three germ layers (7.2.6, Fig. 20) and (Garbes *et al.* 2013). Nonetheless, EB-formation pictured just random differentiation processes lacking the complex organisational interplay of embryonic organogenesis. Hence, a stronger quality criterion represented *in vivo* data. Unlike with mouse iPSCs, injection into a host blastocyst resulting in germ line competent chimeras at last (Okita *et al.* 2007) was not accomplishable with human iPSCs for ethical reasons albeit human/mouse chimeras were generated with human ESCs (James *et al.* 2006) which was legally not allowed in Germany. Instead, teratoma formation assay was performed when reprogrammed cells were injected into immuno-compromised SCID mice producing a teratoma-like neoplasia which contained offspring of all three germ layers (Smith *et al.* 2009). Verifiably, all iPSC lines developed into tissues of different embryonic lineages (7.2.7, Fig. 21) and (Garbes *et al.* 2013). In conclusion, novel state of the art SeV reprogramming technique was successfully applied to obtain integration-free fully characterised iPSC lines from PLS3 discordant SMA family members.

8.2 Human PLS3 discordant iPSCs differentiated into mixed motoneuronal cultures

Despite a generalised improvement concerning NMJ maintenance and function in a PLS3 over-expressing SMA mouse model, a rescue with regard to viability was not achieved in severely affected SMA mice (Ackermann *et al.* 2013). Hence, amelioration on molecular and cellular levels was not translated into enhanced long-term survival. Obviously, PLS3 exerted its protective effect only in mildly affected SMA patients. Therefore, the establishment of an iPSC-based MN-model of mildly affected SMA III patients and asymptomatic siblings from PLS3 discordant families was essential for future analyses of PLS3 mediated protection.

As outlined in 3.2.4, iPSC-based cell models may serve as valuable novel platform for *in vitro* pathogenesis research, drug discovery and evaluation of potential therapeutics promising "personalised" medicine. Additionally, differentiability of iPSCs into plenty of various cell lineages circumvents the inaccessibility of diseased neurons, for example.

Among the first to profoundly recapitulate the phenotype in disease-specific iPSCs, Ebert *et al.* derived iPSCs from a SMA I patient and his unaffected mother (Ebert *et al.* 2009). Subsequently, the authors differentiated these human iPSC into spinal motoneurons phenocopying the cellular deficits of SMA-affected MNs. In SMA I iPSC-derived MNs, the authors reported fewer gems, lesser MN size, diminished SMI-32$^+$ and ChAT$^+$ MN survival rate

and pre-synaptic maturation delay *in vitro*. Initially, SMA-iPSCs were able to produce a comparable amount of MNs which however degenerated during time-course. The overall amount of β III-tubulin⁺ neurons remained unchanged between WT and SMA I, though, highlighting the MN-specific damage due to SMN deficiency. This MN loss obviously reflected the prevailing view of SMA as defect in MN maintenance, not in MN generation. Furthermore, the authors managed to lift SMN protein levels by application of TSA and VPA (see 3.1.5), hence rescuing SMA-MNs (Ebert *et al.* 2009). Moreover, a *SMN1* knock-down in human ESCs modelled this disease phenotype. Neither did SMN depletion interfere with neural induction nor with subsequent MN specification (Wang *et al.* 2013).

These findings were supported by following studies: SMA I iPSC-derived MN cultures disclosed diminished MN formation ability and neurite growth impairment whereas such deficits were relieved by ectopic SMN1 expression (Chang *et al.* 2011). iPSCs of two SMA I patients and correspondent healthy controls gave rise to comparably equal amounts of SMI-32⁺ MNs at the start of final maturation (approx. 5%) (Sareen *et al.* 2012). However, during subsequent cultivation the number of SMI-32⁺ MNs declined in SMA cultures. A similar observation was made in human SMA I iPSC-derived MNs between five and eight weeks *in vitro* cultivation (Corti *et al.* 2012).

Nevertheless, every study about iPSC-based MN-differentiation in SMA patients issued so far dealt with congenital severe SMA I cases only. Thus, to decipher likely more subtle pathologic changes in milder SMA cases, a suitable *in vitro* cell model was necessary.

8.2.1 Modifications in EB-based run-through protocol facilitated stable differentiation of PLS3 discordant iPSCs to mixed MN cultures

Specification of different neuronal subtypes during *in vitro* differentiation of human pluripotent SCs remains an elaborate challenge. Eventually, every differentiation protocol mimics the natural principles of neurulation during human embryogenesis (see 3.3.2). In brief, clearance of BMP and other TGFβ ligands by specific inhibitors such as chordin, noggin or follistatin propels acquisition of neural fate in pluripotent ectodermal SCs (Weinstein *et al.* 1999; Muñoz-Sanjuán *et al.* 2002; Smukler *et al.* 2006). Developing neuroepithelial primitive NSCs are subsequently further specified into manifold neuronal or glial lineages since their cellular plasticity allows them to respond to morphogenic patterning (Seaberg *et al.* 2003; Smukler *et al.* 2006).

If human ESCs are grown as EB aggregates in chemically defined neural medium without any exogenous patterning morphogen, they tend to acquire an anterior identity (Pankratz *et al.* 2007). Therefore, neural precursor cells (NPCs) seem to adopt a rostral "forebrain-like" positional state by default during embryogenesis. Hence, cells of caudal character (such as midbrain, hindbrain and spinal cord) are generated by specification of rostral cells (Wilson *et al.* 2001). The use of morphogens which activate or inhibit key developmental pathways enables specifically directed neuronal differentiation (Hardingham *et al.* 2010).

In mammals, post-mitotic MNs derive from a narrow region in the ventral part of the neural tube denoted as pMN domain (see 3.3.2). The joint expression of TFs, above all OLIG2, PAX6 and NKX6.1, specifies the pMN domain and is caused by morphogens SHH and RA (3.3.2, Fig. 6). In respect of motoneuronal differentiation with human pluripotent SCs *in vitro*, initial studies imitated these developmental processes (Wichterle *et al.* 2002; Li *et al.* 2005; Li *et al.* 2008) resulting in several protocols for differentiation of functional motoneurons from human pluripotent stem cells (Wichterle *et al.* 2002; Ebert *et al.* 2009; Patani *et al.* 2011; Amoroso *et al.* 2013; Li *et al.* 2005; Li *et al.* 2008; Hu *et al.* 2009). Many of those protocols as well as

protocols provided by iPierian Inc. were used for MN differentiation of iPSCs. After all, an EB-based run-through protocol proved as most reliable (Hu *et al.* 2009).

In Hu *et al.*, the authors claimed to obtain 50% HB9$^+$ MNs from original human ESC progenies. The first study using this protocol for motoneuronal differentiation of human iPSCs did not evaluate the amount of HB9$^+$ MNs (Karumbayaram *et al.* 2009). Instead, the number of ISL1$^+$/β III-tubulin$^+$ neurons was given ranging between 28%-33% depending on iPSC line.

Nevertheless, the EB-based run-through protocol by Hu and Zhang was chosen as standard MN differentiation protocol in this thesis (7.3, Fig. 22). Yet, the differentiation process was modified at first step. In order to kick off the tendency to develop into neural tissue, iPSC-derived EBs were subjected to dual SMAD-signalling inhibition: TGFβ-inhibitor SB431542 and BMP-inhibitor dorsomorphin synergistically promoted neural conversion of human pluripotent SCs (Chambers *et al.* 2009; Kim *et al.* 2010a). Thus, generation of neuroepithelial NSCs was enhanced. Moreover, dual SMAD-signalling inhibition could rescue "under-performing" human iPSC clones in MN differentiation (Boulting *et al.* 2011). So, support of neural induction apparently overcame differentiation impediments.

However, this protocol failed to yield a reasonable number of correctly patterned pMN-progenitors or mature MNs (7.3.1, Fig. 23). Therefore, to elevate the overall amount of MNs, further protocol modifications were introduced: The concentration of RA was lifted to 0.75 µM to ensure full caudalisation. Adequate RA signalling is required for NKX6$^+$ cells to progress to an OLIG2$^+$ state as MN progenitors (Diez del Corral *et al.* 2003). Karumbayaram *et al.* also administered 1 µM RA with human iPSCs, albeit 0.1 µM RA was titrated as sufficient amount for motoneuronal patterning with human ESC-derived NSCs (Hu *et al.* 2009). Nonetheless, alternative MN differentiation protocols applied 1 µM RA as well (Wichterle *et al.* 2002; Amoroso *et al.* 2013).

In addition, RA administration occurred earlier (on day 7 instead of day 10). A previous study conceptualised a specific time window in which NSCs stay responsive towards morphogenic stimuli (Li *et al.* 2005). Hence, day 10 proved the optimal date for RA application in MN *in vitro* differentiation (Hu *et al.* 2009). However, this protocol lacked boosted neurulation owing to dual SMAD-signalling inhibition. If generation of neuroepithelial cells is sped up then, the optimal time point would be postponed as well. Therefore, an earlier date for RA employment seemed recommendable.

Synthetic small molecule agonists acting in the SHH signalling pathway were suitable surrogates for purified recombinant SHH protein of original studies. The purine derivative purmorphamine (Pur) and chlorobenzothiophene Smoothened agonist (SAG) both activated the SHH signalling pathway (Mas *et al.* 2010) and were successfully used in ventralisation during motoneuronal differentiation (Li *et al.* 2008; Wada *et al.* 2009).

8.2.2 Human iPSC lines showed a low MN efficiency when subjected to EB-based run-through protocol

Truly, correct regionalisation of PLS3 discordant iPSC-derived neuroepithelial cells was visible when staining for typical ventral neural tube markers OLIG2, NKX6.1 and NKX2.2 (Li *et al.* 2008) (7.3.2, Fig. 24). Expression of upper spinal cord marker HOXB4 signalled posteriorisation. In total, the amount of proper pMN-progenitor cells convincingly appeared higher than samples differentiated according to the original run-through protocol (7.3.1, Fig. 23). However, the MN yield did not meet expected efficacy. The number of MNs ranged between 3-10% for HB9$^+$ neurons and 6-12% ISL1$^+$ neurons, respectively (7.3.4, Fig. 29). Moreover, healthy control lines often depicted the poorest MN differentiation efficiency.

Besides, identification of the cellular composition of mixed MN cultures appeared meaningful to exclude wrong NSC specification as reason (7.3.4, Fig. 30). Apart from scarce dopaminergic neurons and occasional glial cells, predominantly gluatmatergic and GABAergic neurons overbalanced. Presumably, these populations represented interneurons since GABAergic interneurons derive from p2 domain and glutamatergic interneurons stem from p3 domain (Alaynick *et al.* 2011). Both progenitor domains border the pMN domain indicating a strong ventralisation of neuroepithelial cells. Yet, quantitative analysis of different non-motoneuronal populations would be necessary to determine the exact constitution of mixed cultures. As a matter of fact, a lack of MN differentiability in our iPSC lines had to be stated. This raised the question why the efficiency had developed improperly.

A number of technical obstacles accompany iPSC-based research in neurological disorders: Clonal variation of iPSCs influencing differentiation abilities, heterogeneity of target neurons and glial cells and the time-consuming nature of experiments have to be subdued in order to reproducibly detect new cellular phenotypes (Ito *et al.* 2012). Additionally, the lack of a standardised motoneuron differentiation protocol complicates comparability between results of different studies. Thus, reproducing published MN efficiencies was also hampered.

Comparable previous studies reported 10-17% SMI-32$^+$ MNs of healthy controls after ten weeks differentiation (Sareen *et al.* 2012) or 25% ChAT$^+$/β III-tubulin$^+$ neurons of healthy controls after six weeks differentiation (Ebert *et al.* 2009). Maximum 10% HB9$^+$ neurons of total cells were obtained when a human control ESC line had been differentiated and even less (1%) with a SMA I iPSC line (Chang *et al.* 2011). Stockmann *et al.* voiced electrophysiologically functional MNs positive for MN markers HB9, ISL1, SMI-32 and vesicular acetylcholine transporter VAChT from healthy individuals (Stockmann *et al.* 2011). Up to 40% of differentiated cells were sorted as SMI-32$^+$ MNs which formed mature synapses *in vitro*.

Notably, in many studies quantification was performed by determining the number of SMI-32$^+$ cells. SMI-32 antibody binds non-phosphorylated neurofilament-H in neurons associated with MN identity (Carriedo *et al.* 1996). On the other hand, SMI-32 antibody also detects neurons in the PNS and CNS such as human GABAergic cortical neurons (Campbell *et al.* 1989). Therefore, comparative quantification of unequivocal MN markers HB9 and ISL1 would have given more valid data impact in those studies. Moreover, just one or two SMA or control cell lines were employed and no different clones per cell line (Ebert *et al.* 2009; Sareen *et al.* 2012). Application of different iPSC lines and several respective clones balances the inter-line variances as outlined in 2011 by Boulting *et al.* (Boulting *et al.* 2011). Taken together, presentation of published MN differentiation efficiencies depends on selectable parameters. The iPSC-based run-through protocol yielded an overall low number of *bona fide* MNs in mixed cultures in spite of our positive modifications. This poor outcome was either caused by intrinsic cellular obstructions of the respective cell lines or general technical reasons.

Several different clones from different individuals and families tended to show a sub-optimal MN number. This trend points rather to a general differentiation impediment than to a deficit inhering in each iPSC line. Of course, it cannot be ruled out that a mutation was causative for this low efficiency. However, genomic integrity was thoroughly scrutinised (7.2.3). The original mutations detectable in donor fibroblasts (7.2.3, Tab. 16) were unlikely to exert any deleterious effect because the siblings did not show any physiologic deficits apart from the SMA III phenotype in affected individuals. On genomic level, established early human iPSC lines presented indeed a number of genomic aberrations particularly *de novo* copy number variations (CNVs) rendering mostly disadvantageous features (Hussein *et al.* 2011; Laurent *et al.* 2011). These studies regarded such CNVs as intrinsic feature of the reprogramming process. Expansion of human iPSCs in culture would rapidly selected against mutated cells (Hussein *et*

al. 2011). However, a following study indicated such CNVs as sign of somatic mosaicism in parental fibroblasts and their subsequent manifestation in human iPSCs owing to their clonal origin (Abyzov *et al.* 2012). Since MN differentiations were undertaken with stable iPSC lines (passage 10-25), such mutated cells should have vanished in the meantime. Furthermore, all iPSC lines robustly fulfilled validation criteria (7.2), particularly the capability to differentiate into all three germ layers *in vitro* and *in vivo* (7.2.6, Fig. 20; 7.2.7, Fig. 21). In summary, it thus seems unlikely that all cell lines are affected by mutations impacting MN differentiation.

Yet, the parental epigenetic traits are obviously not absolutely obliterated during reprogramming. Apparently, an "epigenetic memory" is retained since early passage iPSCs exhibit residual DNA methylation signatures of the original cell rendering iPSCs more efficient in re-differentiation to their lineage of origin (Kim *et al.* 2010b; Bar-Nur *et al.* 2011). This phenomenon was found in iPSC lines generated in different laboratories by varying strategies with diverse donor cells and could be partially explained by insufficient promoter methylation of somatic genes (Ohi *et al.* 2011). Yet, continuous propagation largely attenuated this feature in murine iPSCs, at least (Polo *et al.* 2010). Perhaps these findings contribute explanatory clues with regard to the discrepancies seen in the developmental behaviour since some murine and human iPSC lines differentiated less efficiently *in vitro* and *in vivo* than the ESC counterparts (Robinton *et al.* 2012). Therefore, remnants of the originating fibroblast (i.e. mesodermal) epigenetic traits might hamper neuroectodermal differentiation capability in this study. Some authors even prefer iPSCs derived from donor cells of ectodermal origin, like keratinocytes for instance, for they may serve better as starting population for neuronal differentiation (Stockmann *et al.* 2011).

Furthermore, differentiation propensity varied also within human ESCs (Osafune *et al.* 2008). In a broad panel of 16 human iPSCs and six ESCs, Boulting and colleagues evaluated their ability to differentiate into MNs (Boulting *et al.* 2011). The developmental capacity between ESCs and iPSCs was comparable, nonetheless, the differentiation efficiency between separate iPSC lines varied (HB9^{+} cells: 1-6%; ILS1^{+} cells: 5-20% of all cells on day 32). Notwithstanding all iPSCs in this study passed standard validation successfully, the individual propensity to terminal MN differentiation evidently fluctuated. In particular, donor identity and donor sex influenced the efficiency of MN differentiation (Boulting *et al.* 2011).

The lack of an unambiguous human spinal MN surface marker impedes MN enrichment out of such mixed MN cultures (Wada *et al.* 2009). Although distinct spinal MN markers exist as mentioned before, not all unambivalently discriminate MNs: ChAT and VAChT mark cholinergic neurons. However, cholinergic identity is not exclusively restricted to spinal MNs for there are cholinergic interneurons of the dorsal striatum (Witten *et al.* 2010). SMI-32 antibody does not only label neurons with MN morphology and location (Carriedo *et al.* 1996) but also other neurons of the PNS and CNS (Campbell *et al.* 1989). In addition, these markers are all intracellularly located like the motoneuronal TFs HB9, ISL1 and LIM3. Nonetheless, enrichment of murine spinal MNs was performed by panning assays of mixed spinal cord isolates via lectin or antibodies specifically binding neurotrophin receptor p75[NTR] (Wiese *et al.* 2010; Conrad *et al.* 2011). Utilising the p75[NTR] antibody is however an expensive approach considering the number of cell lines in our study. Besides, these two protocols have only been conducted with mouse spinal cord. To which extent these panning methods are feasible in human iPSC-derived mixed MN cultures remains elusive. On the contrary, gradient centrifugation successfully enriched human ESC- and iPSC-derived spinal MNs from *in vitro* cultures (Corti *et al.* 2012; Wada *et al.* 2009). Also substrate rigidity of cultivation dishes influenced MN differentiation yield (Sun *et al.* 2014).

Regardless of any possible explanations, the low level of overall MN differentiation efficiency hampered proper analyses in this PLS3 discordant iPSC-based MN *in vitro* model. Ergo, this difficulty was tackled by a new experimental approach.

8.3 smNPC-derived motoneuronal cultures serve as beneficial platform for disease-modelling in SMA discordant families

8.3.1 Stable NSC lines serve as standardised starting population for MN differentiation with high efficiency

To circumnavigate the recalcitrance of individual iPSC lines towards highly efficient MN differentiation via an EB-based run-through protocol, generation of a suitable neuroepithelial NSC population seemed sensible. As mentioned in 7.4.1, already neurally designated precursor populations shorten the duration of MN differentiation. Precisely, in this study the smNPC-based MN differentiation lasted four weeks compared to eight weeks in the EB-based run-through protocol. They are more homogenous and easily patternable. Several NPC populations have been generated within the recent years of which all were successfully differentiated into MNs: Directed differentiation of lt-NES®SCs yielded approx. 15% HB9^{+}/β III-tubulin^{+} neurons (Koch *et al.* 2009) whereas rosette neural cells delivered roughly 25% HB9^{+} MNs (Elkabetz *et al.* 2008). Flow cytometry analysis of MN-differentiated primitive NSCs showed 53.7% neurons positive for ISL1 and microtubule-associated protein (MAP) (Li *et al.* 2011). The most recent NSCs population, i.e. small molecule NPCs (smNPCs), was reported to generate 50% HB9^{+}/β III-tubulin^{+} neurons (Reinhardt *et al.* 2013).

Due to the cost-effective rapid generation, easy maintenance and feasibility even in functional electrophysiological studies with smNPC-derived MNs (Naujock *et al.* 2014), smNPC generation was chosen (7.4.1, Fig. 31) and successfully applied in healthy control, SMA I, SMA III and discordant asymptomatic iPSC lines in the present study (7.4.1, Fig. 32). Although all smNPC lines exhibited the same marker profile as given in the original publication, some lines (e.g. HGK21.8) revealed early signs of rosette formation when grown densely indicated by ZO-1^{+} ring-like centres within smNPC colonies. Therefore, present smNPC lines may constitute a more heterogenous and plastic NSC population perhaps owing to increased Pur concentration (1 µM) and different basal medium composition during standard cultivation compared to Reinhardt *et al.*, 2013.

In advance, proof-of-principle experiments with an OLIG2-GFP smNPC reporter cell line heralded promising results concerning MN differentiation. Since SHH pathway agonist SAG had already been successfully applied in motoneuronal differentiation of human ESCs (Wada *et al.* 2009), SAG was added to the original differentiation regimen to promote additional ventralisation. Upon motoneuronal specification via treatment with RA, SAG and Pur, effective regionalisation was visualised by OLIG2-GFP reporter gene expression (7.4.2, Fig. 33) and immunocytochemical staining of pMN markers (7.4.2, Fig. 34). Final MN maturation indicated expression of ISL1, HB9, ChAT and SMI-32 and delivery of a visible amount of HB9^{+} MNs at last (7.4.2, Fig. 35).

Moreover, smNPCs seemed to be convertible into rosette-type cells similar to lt-NES®SCs by simple changes in culture conditions (7.4.3, Fig. 36, Fig. 37). Already the original publication revealed comparable convertibility upon FGF2 application (Reinhardt *et al.* 2013). Addition of growth factors bFGF, EGF and B27 indeed transformed smNPCs into rosette-like lt-NES®SCs and enabled further propagation as individual NSC population. Upon such treatment, smNPC-

derived OLIG2-GFP reporter lt-NES®SCs expressed typical NSC markers like ESC-derived lt-NES®SCs (Koch *et al.* 2009) (7.4.3, Fig. 38) and were successfully differentiated into proper MNs (7.4.3, Fig. 39).

When OLIG2-GFP reporter lt-NES®SCs were patterned during regular cultivation with SAG (1 µM) and rather low RA concentration (150 nM), decent GFP fluorescence indicated expression of OLIG2 already after one week treatment (7.4.3, Fig. 37 **D**). Nonetheless, patterned lt-NES®SCs retained their typical appearance and growth behaviour (7.4.3, Fig. 37 **C**). When it may be possible to stably enrich the amount of OLIG2$^+$ pMN-primed progenitor cells in NSC lines during regular cultivation, the number of proper MNs should increase afterwards. Forced Olig2 expression in murine ESC-derived NSCs dramatically increased motoneuron generation *in vitro* from 10% to 90% HB9$^+$/ISL1$^+$ MNs of all β III-tubulin$^+$ neurons (Panman *et al.* 2011) undoubtedly corroborating the importance of the initial yield of OLIG2$^+$ NSCs. Successful pMN patterning with high OLIG2$^+$ numbers may launch correspondently efficient MN generation.

To verify whether this assumption held true, OLIG2-GFP reporter lt-NES®SCs were simultaneously treated with 150 nM RA and 1 µM SAG for eleven days or 21 days or maintained in standard medium without patterning morphogens. Effectiveness of pre-patterning was visualised by evident presence of *bona fide* MNs expressing ChAT, HB9, ISL1 and SMI-32 after 16 days final maturation in comparison to untreated samples (7.4.3, Fig. 39 **B**). A separate patterning step without growth factors bFGF and EGF and with more RA like in Koch *et al.*, 2009 as outlined in Fig. 36 might even enhance the MN differentiation efficiency.

Admittedly, for discovery of statistical significant differences concerning pre-patterning effects several experiments must be performed and substantiated with cell counting or GFP FACS analysis for quantification. Yet, conducting MN differentiation experiments with PLS3 discordant and SMA cell lines giving really meaningful data was prioritised.

In conclusion, smNPCs represented a homogenous stably cultivable NSC population which responded to desired morphogenic patterning. Thus, they proved to be very suitable for accelerated and efficient MN generation. Generation of correspondent smNPCs from healthy control, SMA I, SMA III and discordant asymptomatic iPSC lines decisively enlivened the continuance of our study.

8.3.2 iPSC-derived mixed motoneuronal cultures represent the first *in vitro* cell model of a mild SMA phenotype and asymptomatic PLS3 over-expressing siblings

According to their marker expression profile, smNPCs were *a priori* localised to the neural plate border with moderately dorsal hindbrain character (Reinhardt *et al.* 2013). On the other hand, MN differentiation implies relocating smNPCs towards a ventral-caudal fate.

Therefore, pre-patterning technique was adapted to smNPC cultivation for boosting high yield MN differentiation. Instead of 0.5 µM Pur standard smNPC culture medium NPC1 contained 1 µM Pur (7.4.4, Fig. 40). Together with 3 µM CHIR99021, such an increase of Pur was shown to simultaneously elevate the expression of MN progenitor markers NKX6.1 and OLIG2 on mRNA level and in immunocytochemistry (Reinhardt *et al.* 2013). Thus, it was assumed that smNPCs were even more easily shifted into the correct pMN-domain during pre-patterning.

Indeed, immunocytochemical staining of such pre-treated smNPCs distinctly depicted proper expression of essential markers defining spinal MN progenitors such as ventral markers OLIG2 and NKX6.1 or caudal marker HOXB4 (7.4.4, Fig. 41). Parallel use of ventralising agents Pur and

SAG during pre-patterning and regular patterning did not thrust smNPCs too ventral because p3 marker NKX2.2 was barely expressed proving an exact hit of the desired pMN domain in these smNPCs. However, recent data demonstrated that unlike in mice NKX2.2 encroached into the OLIG2-expressing domain in human neural tube even resulting in MN generation obviously (Marklund *et al.* 2014).

After having circumnavigated the obstacles of iPSC-based MN differentiation via application of smNPCs, immunocytochemical staining undoubtedly identified *bona fide* MNs by expression of characteristic MN markers HB9, ISL1, ChAT and SMI-32 on day 8 and day 27, respectively (7.4.4, Fig. 42). Quantification of ISL1$^+$ and HB9$^+$ cells was set relative to total cell number or β III-tubulin$^+$ neurons as also other studies preferred calculating the ratio of motoneurons:β III-tubulin$^+$ neurons (Karumbayaram *et al.* 2009). In addition, a possible bias of different neurogenic potential in various cell lines is lowered thereby.

Data presented valid MN numbers for most cell lines, the amount of HB9$^+$ or ISL1$^+$ cells ranged between 20%-30% relative to total cell number presenting an overall meaningful yield in comparison to MN differentiation efficiency in other NSC populations: lt-NES®SCs delivered approx. 15% HB9$^+$/β III-tubulin$^+$ neurons (Koch *et al.* 2009), rosette neural cells yielded roughly 25% HB9$^+$ MNs (Elkabetz *et al.* 2008) and MN-differentiated primitive NSCs showed 53.7% ISL1$^+$ neurons (Li *et al.* 2011).

Still, number of HB9$^+$ cells remained conspicuously below published data: ~23% in control line r12 on day 27 compared to ~50% in healthy iPSC1-derived MN culture on day 21 (Reinhardt *et al.* 2013). Unlike the original publication, DAPT was administered during final maturation in this study. Inhibition of notch-signalling by γ-secretase inhibitor DAPT propelled neuronal differentiation of NSCs (Borghese *et al.* 2010; Crawford *et al.* 2007). In MN cultures devoid of DAPT treatment, differentiation of existing pMN-primed progenitors into MNs would be deferred over time and thereby HB9$^+$ MN pool would be constantly replenished. Contrarily, DAPT treatment in this study irreversibly pushed neurogenesis of all pMN-primed progenitors present at day 8 at once. Thus, total number of MN progenitor cells maturing over time may differ between this study and the original study by Reinhardt *et al.*, 2013. Moreover, different propensity towards MN differentiability might explain lower total MN number since MN numbers obviously differed between cell lines and clones of one cell line (7.4.4, Fig. 43, **A**-**D**). Unlike in the original publication, MN maturation medium NPC3 was supplemented with low RA (50 nM) and Pur (0.5 μM) concentrations for seven days (d8-d14) (7.4.4, Fig. 40) because reduced concentrations of these two morphogens promoted division of OLIG2$^+$ progenitors in MN cultures (Hu *et al.* 2009; Li *et al.* 2008). Anyway, cross-comparison of MN differentiation protocols between different laboratories and experimenters remain challenging unless standardised differentiation and quantification methods are introduced.

With the majority of all single smNPC lines differentiated into MNs three times, the phenotypic grouping validly highlighted differences in MN survival over time (7.4.4, Fig. 43 **E**-**H**). Intriguingly, there was no significant difference in HB9$^+$ or ISL1$^+$ MN number detectable between healthy controls, SMA I, SMA III and discordant asymptomatic in early MN cultures on day 8. SMN knock-down in human ESCs did not impair subsequent MN differentiation proving that regular SMN amounts are not mandatory for MN differentiation (Wang *et al.* 2013). Neither were initially lower MN numbers detected in early iPSC-derived MN cultures of SMA I patients in previous studies corroborating present findings (Ebert *et al.* 2009; Sareen *et al.* 2012).

Still, asymptomatic siblings denoted always the lowest MN number on day 8. However, it has to be considered that asymptomatic comprised fewer counting data. For instance, data from HGK21.1 was wholly missing in ISL1$^+$ quantification thereby possibly biasing the data set (7.4.4,

Fig. 43 **D**). Furthermore, cell-specific features bore detrimental effects obviously. Asymptomatic cell line HGK28.11 disclosed the slowest growth and lowest cell number during differentiation regimen thereby spoiling pooled data of asymptomatic additionally. Similarly, healthy control line COII.2 absolutely underperformed during MN differentiation. Albeit COII.2 behaved normally until patterning started on day 0, neurogenesis subsequently failed delivering more epithelial-like or glial-like cells but hardly any β III-tubulin⁺ neurons, let alone MNs. This explained the poor MN yield on day 8 (7.4.4, Fig. 43 **A**, **B**) and further justified the exclusion of that cell line for quantification because COII.2 did not represent a proper MN culture. Cortical differentiation succeeded with this line (Kristina Dobrindt, Swetlana Ritzenhofen, personal communication), however adherent generation and cultivation into smNPCs failed too (Bea Weykopf, personal communication). Generally, individual cell lines behaved differently strongly advocating the use of several cell lines with several clones per line to even this putative bias in overview panels as performed in this study.

Human ESC-derived neurons resembled foetal brain more than adult brain in terms of molecular maturation (Patani *et al.* 2012). Likewise, human iPSC-derived MNs rather may represent a pre-natal/young post-natal state. Intriguingly, severely affected SMA I exhibited almost equally high MN numbers compared to controls on day 8. This finding underlines that SMA is not a disorder of MN formation but MN maintenance (Sleigh *et al.* 2011).

Strikingly, three weeks differentiation until day 27 pictured a totally different impression of MN survival in these *in vitro* MN cultures (7.4.4, Fig. 43 **G**, **H**). Relative to day 8, MN number massively declined in SMA I (HB9⁺: ↘97%; ISL1⁺: ↘88%) (7.4.4, Fig. 44) phenocopying the severe phenotype already seen in human SMA I foetuses where motoneuronal degeneration already occurs *in utero* (Markowitz *et al.* 2004) and in severe SMA mouse models which revealed normal MN number on post-natal day 1 but massive MN waste during following days (Hsieh-Li *et al.* 2000; Monani *et al.* 2000).

Additionally, SMA III and asymptomatic siblings suffered from considerable loss in HB9⁺ MN number compared to day 8 (SMA III: ↘57%; asymptomatic: ↘62%). Additionally, reduction in ISL1⁺ MNs stayed insignificant yet obvious at glance (SMA III: ↘31%; asymptomatic: ↘39%). Intermediate SMA mouse models reported significant MN loss in murine spinal cord and brain stem as well (Bowerman *et al.* 2012a). Usually, SMA III manifests after the first 18 months (Kugelberg *et al.* 1956). Still, clinical symptoms penetrate with delayed onset and only a mild phenotype during childhood and early adolescence. In SMA III patients HGK22 and HGK27 the disorder was diagnosed with 18 years and 13 years, respectively. So, the rather strong loss of MNs in the *in vitro* model at this early time point in development is explainable since MN dysfunction expresses just after many years. Thus, PLS3 over-expression in asymptomatic siblings apparently did not result in enhanced MN survival since asymptomatic lines HGK21.8 and HGK28.9 revealed high PLS3 expression rates (7.5.3, Fig. 49 **G**) while MN numbers ranged low (7.4.4, Fig. 43 **C**, **D**). This data suggested a PLS3-mediated protective effect rather in other parts of the motor circuit than in MN maintenance itself. Hence, formation or stabilisation of NMJs might prevent penetration of mild SMA III phenotype in asymptomatic.

Astonishingly, HB9 number also diminished (↘30%) in controls during three weeks maturation questioning whether cultivation conditions might interfere with MN survival. In contrast, number of ISL1⁺ MNs even slightly increased (↗19%) in controls during MN maturation rebutting the assumption that external and not cell-autonomous effects elicit MN death. Murine Hb9 expression persists in most adult post-mitotic MNs owing to its requirement for the maintenance of Isl1 expression in post-mitotic MNs (Arber *et al.* 1999). However, HB9 expression is down-regulated for assignation of specific motor column identities in the developing spinal cord (William *et al.* 2003). Moreover, in maturing ESC-derived MN cultures,

number of HB9 expressing cells decreased after three weeks concomitantly with proportionally increasing ChAT expression (Hu *et al.* 2009; Li *et al.* 2005). Likewise, this finding was observed in MN cultures of ESC line HB9-GFP (Placantonakis *et al.* 2009) and was additionally outlined in an overview of stem cell-based in vitro MN differentiation (Davis-Dusenbery *et al.* 2014). Such processes may be causal for general disappearance of HB9 signal. On the other hand, ISL1 function is obligatory for all spinal MNs (Pfaff *et al.* 1996) therefore serving as more meaningful tool for MN survival determination. ISL1$^+$ and HB9$^+$ MNs are not absolutely identical and respective expression does not always overlap *in vivo* or *in vitro*. Instead, separate staining only marks MN subsets (Amoroso *et al.* 2013). This fact points out the importance of employing several MN markers for quantification as it was conducted in this study whereas previous studies mostly relied on a single MN marker.

When the presented *in vitro* system resembled an early post-natal stage of human development, deleterious effect of SMN loss was already visible in SMA I at this early time-point. Instead, milder SMA III phenotype and discordant asymptomatic showed tendency to delayed MN loss being congruent with the patients' disease progress. In most studies with severe early-onset SMA I patients, total MN differentiation time amounted to 6-10 weeks (Corti *et al.* 2012; Sareen *et al.* 2012). Since human neurons developed ten times slower than in murine systems (Stockmann *et al.* 2011), a longer differentiation period might be recommendable to carve out more subtle changes in ISL1$^+$ MN survival among SMA III and asymptomatic MN cultures.

SMA III MNs may require additional exposition to biological, chemical or environmental stressors to accelerate disease progression and to reveal pathological phenotypes as it was carried out in a stem cell model of Parkinson's Disease (Nguyen *et al.* 2011). Undeniably, oxidative stress had been associated with SMA pathology in respect of MN degeneration (Hayashi *et al.* 2002; Wang *et al.* 2013) or disturbed SMN complex formation (Wan *et al.* 2008). So, employment of stressors like hydrogen peroxide (H_2O_2) in the SMA III *in vitro* model might sensitise MNs for expressing a more pronounced disease phenotype.

In summary, an *in vitro* SMA model of mild SMA III and PLS3 discordant asymptomatic individuals based on iPSC-differentiation was introduced in this doctoral thesis for the first time. The present *in vitro* cell model feasibly sufficed then as platform for further studies in PLS3 discordant families.

8.3.3 MN neurite length did not differ among healthy controls, SMA I, SMA III and asymptomatic in MN *in vitro* model

Since MN loss in SMA was associated with a dying-back axonopathy (Cifuentes-Diaz *et al.* 2002; Fallini *et al.* 2012), maintenance of neuronal protrusions such as axons was always focussed on in SMA research. Furthermore, PLS3 over-expression was capable of rescuing axonal growth defects in smn depleted zebrafish or mice (Oprea *et al.* 2008; Hao le *et al.* 2012, Ackermann *et al.* 2013). Therefore, measurement of neurite length in PLS3 discordant MN cultures seemed reasonable.

Neurites are regarded as transient protrusions of early *in vitro* neurons which develop further into axons or dendrites (Alberts *et al.* 2002). The former can be selectively discriminated by staining for Tau proteins (axons), the latter by microtubule-associated protein 2 (MAP2) (dendrites), for instance (Rossoll *et al.* 2003) as late structures of mature neurons.

On day 8, there was no significant length difference observed in healthy controls, SMA I, SMA III and asymptomatic MN cultures regarding β III-tubulin$^+$ or SMI-32$^+$ neurites (7.5.6,

Fig. 55). A previous study reported a significantly delayed neurite outgrowth in iPSC-derived MN cultures (Chang *et al.* 2011) which our data apparently contradict.

The authors referred to earlier publications: After five days cultivation, primary MNs from a severe SMA mouse model indeed revealed significantly shorter axons (Rossoll *et al.* 2003). In zebrafish, SMN deficiency caused reduced axonal length but exerted no negative effect on dendrites (McWhorter *et al.* 2003). Isolated primary murine MNs of control, heterozygous and SMA I mice showed short axons and disturbed neurite network in SMA I samples (Ting *et al.* 2007). Notably, these studies always explicitly measured axonal length and not neurite length. Although defects in neurite networks of SMA I primary mouse MNs were observed, neurite length measurement was not presented (Ting *et al.* 2007). Thus, careful discrimination has to occur between axons and neurites.

Moreover, different experimental approaches have to be considered: Between two time-points (day 2 and day 5), Chang and colleagues monitored β III-tubulin$^+$ neurite growth from seeded neurospheres in SMA I MN cultures and ESC healthy control. Contrarily, our measurement comprised only a single time-point yet distinctly in HB9$^+$, ISL1$^+$ or SMI-32$^+$ MNs. Otherwise, cellular clustering in maturing MN cultures would have prevented unequivocal identification of MNs and appending neurites.

In our very young MN cultures (day 8), the detrimental effect of SMN loss in neurite outgrowth might not have been displayed. Murine studies investigated primary spinal cord MNs, i.e. fully matured MNs (Rossoll *et al.* 2003; Ting *et al.* 2007). Therefore, singularisation of older MN cultures (day 27 *et seq.*) may enable to measure axons and neurites in our human *in vitro* system. However, poor recovery rate of singularised MN cultures thwarted such attempts hitherto (data not shown).

Averaged neurite length amounted to ~220 µm (ESC control) and ~100 µm (SMA I) on day 2 but were not proved significant (Chang *et al.* 2011). Significant differences became just observable after prolonged cultivation (5 days) and SMN rescue (Chang *et al.* 2011). Still, in their study β III-tubulin$^+$ neurites grew longer in comparison to our study (~75 µm, control and ~80 µm, SMA I) (7.5.6, Fig. 55 **B**). However, measurements were performed directly one day after seeding and not after two days as in Chang *et al.*, 2011. Of course, increasing the numbers of neurites counted particularly in SMI-32$^+$ MNs will solidify our data.

8.4 Examination of SMN and PLS3 expression in different cell populations mirrors SMA phenotypes

Genetic expression rates were monitored in parental fibroblasts, derived iPSCs, corresponding smNPCs and differentiated MN cultures on day 27 comprising the entire *in vitro* MN differentiation process of the four phenotype classes (healthy controls, SMA I, SMA III and asymptomatic). RNA and protein extractions from all these conditions suited well for downstream analyses of SMN and PLS3 expression rates, respectively.

8.4.1 SMN expression levels mimic effects of *SMN1*/*SMN2* copy number in phenotype classes during *in vitro* MN development

Deletion or conversion of *SMN1* gene in SMA patients inevitably leads to MN death and consequently SMA phenotype (Burghes 1997; Lefebvre *et al.* 1995). Yet, remaining *SMN2* genes still provide approx. 10% FL-SMN mRNA/protein per copy thereby easing disease severity with increasing number (Brahe 2000; Helmken *et al.* 2003; Wirth *et al.* 2006b). As

outlined in 5.8.3, Tab. 13, *SMN1*-deleted lines SMA I HGK1 possesses 2 *SMN2* copies, discordant family 1 members HGK13 and HGK16 comprise 3 *SMN2* copies and discordant family 2 members HGK21, HGK22, HGK27 and HGK28 present 4 *SMN2* copies. Accordingly, the amount of FL-SMN mRNA/protein ought to range between 20-40% in comparison to healthy controls with 2 *SMN1* copies delivering 100% FL-SMN mRNA/protein. Previous studies already proved diminished SMN expression rates in iPSC-derived SMA I models (Corti *et al.* 2012; Ebert *et al.* 2009).

Indeed, concerning mRNA levels significantly decreased *SMN* expression levels could be recapitulated in SMA I affected relative to controls (7.5.1, Fig. 45; 7.5.4 Fig. 50 **A**). SMA I reached approx. a quarter of control expression levels in all cell populations (7.5.4, Tab. 17) fitting the low *SMN2* copy number. However, in SMA III and asymptomatic significant differences were detected in iPSCs, smNPCs and SMA III MN cultures compared to controls albeit a visible decrement in *SMN* mRNA expression emerged also in other cell populations (7.5.1, Fig. 45). Still, the decline in *SMN* amount disclosed at a higher level (mostly 60-75% relative to control) than 3-4 SMN2 copies expectedly should deliver (7.5.4, Tab. 17). Anyway, this distribution pattern typically recurred throughout MN development in all cell populations very consistently (7.5.1, Fig. 45). Of course, inclusion of more controls and SMA I or SMA II might enhance the validity of this data.

Preliminary results from SMN protein analyses did not resemble the expected distribution pattern with respect to *SMN1*/*SMN2* copy number (7.5.3, Fig. 48, 7.5.4 Fig. 50 **B**). Grouped according to their phenotypes, controls, SMA III and asymptomatic fibroblasts presented similar SMN protein amounts while SMA I showed a considerable diminution in expression (7.5.3, Fig. 48 **B**). Previous determination of SMN expression in family 2 fibroblasts (ML11-ML14) revealed no significant difference between SMA III and asymptomatic either (Helmken *et al.* 2003). Similar results were obtained in iPSCs with an overall higher protein expression rate in all phenotypes resulting in nearly equal SMN amounts in controls, SMA III and asymptomatic (7.5.3, Fig. 48 **D**). Surprisingly, SMA I iPSCs delivered almost half the SMN amount relative to control topping the expectable quantity from 2 *SMN2* copies. Despite higher total SMN protein amounts in WT iPSCs any significant differences in SMN protein between WT control and SMA I iPSCs were not reported in previous studies (Ebert *et al.* 2009). Not until the start of *in vitro* MN differentiation via smNPCs into early MN cultures, the distribution pattern shaped the way better suiting *SMN1*/*SMN2* copy numbers in phenotype classes (7.5.3, Fig. 48 **F**, **H**): While SMA I delivered roughly ~30% SMN protein compared to controls, SMA III and asymptomatic positioned at a medium expression level (53-60% relative to controls) in smNPCs (7.5.4, Tab. 17). However, ~88% SMN protein expression in SMA IIII and ~126% SMN expression in asymptomatic MN cultures acted as outlier. Relying on a single control line (r12) in MN cultures might bias these results in case r12 samples exhibited unforeseen variance in SMN expression as indicated by large error bar (7.5.3, Fig. 48 **H**). Naturally, preliminary SMN protein results have to be confirmed by consecutive immunoblotting or inclusion of other controls to obtain scientifically valid numbers particularly in iPSCs and fibroblasts which might clarify unusual SMN expression levels.

Significant differences with regard to SMN RNA/protein expression rates were evidently demonstrated in humans between healthy controls and SMA patients of various severities and in mouse models (Coovert *et al.* 1997; Hsieh-Li *et al.* 2000; Lefebvre *et al.* 1995; Monani *et al.* 2000). SMN protein levels ranged higher in foetal tissue than in post-natal (Burlet *et al.* 1998). More precisely, SMN is low expressed in adult fibroblasts and blood (lymphocytes), medium expressed in muscle and highly in brain, kidney, liver and spinal cord but a 100fold reduction

was observed in SMA I spinal cord (Coovert *et al.* 1997) illustrating the obvious link between SMA pathology, MN death and locally insufficient SMN expression.

Evidently, our study provided comparable findings since somatic differentiated foetal-like MN cultures exhibited an overall higher *SMN* expression rate in all phenotype classes (7.5.1, Fig. 45 **H**) whereas total *SMN* expression rate was detectably lower in adult fibroblasts, iPSCs and smNPCs (7.5.1, Fig. 45 **B**, **D**, **F**). Additionally, global SMN protein levels in adult fibroblasts ranged conspicuously below those in iPSCs or foetal-like MN cultures matching results of former studies (7.5.3, Fig. 48 **B**, **D**, **H**).

Of course, fibroblasts depicted varying growth behaviour and proliferation speed due to passage-related senescence (data not shown). Thus, stem cell populations such as iPSCs and smNPCs may prove more homogeneous. Wang and colleagues determined *FL-SMN* expression at different steps of human ESC-based MN run-through differentiation protocol (Wang *et al.* 2013). Like in iPSCs and smNPCs of our study, healthy ESCs and early neuroepithelial progenitors expressed almost equal SMN amounts, yet upon differentiation into proper MNs SMN rate considerably rose comparable to the course in this study (7.5.4, Fig. 50 **A**). SMN levels were up-regulated in differentiating PC12-derived NSCs (Navascues *et al.* 2004; Oprea *et al.* 2008) and increased in human neuroblastoma cell line SH-SY5Y upon MN differentiation (Clelland *et al.* 2009). Comparably, SMN expression rose on RNA and protein levels after MN induction compared to smNPCs (7.5.4, Fig. 50 **A**, **B**).

Besides, *SMN2* copies were declared as not fully equal due to conversion or fusion events causing hybrid copies (Hahnen *et al.* 1996; Chen *et al.* 2011): Gem number and SMN expression levels differed among SMA I and SMA II patients despite nominally sharing the same *SMN2* copy number (Coovert *et al.* 1997; Wirth 2000). In addition, percentage of FL-SMN RNA and protein obtained from *SMN2* copies varied between 10-30% according to several studies (Coovert *et al.* 1997; Lefebvre *et al.* 1997; Helmken *et al.* 2003; Sendtner 2010). Thus, mildly affected SMA III and asymptomatic siblings might also express more than 10% *SMN* RNA per *SMN2* copy resulting in fluctuating expression rates.

Already in MN cultures derived by the EB-based run-through protocol overt differences in SMN expression were observable. SMA III HGK13 and asymptomatic HGK16 delivered comparably significantly lower SMN amounts (~30%, mRNA; ~50%, protein) relative to controls (7.3.3, Fig. 27, Fig. 28). Expectedly, scarce amount of MNs in such cultures did not influence the overall SMN expression in a neuronal system. Hence, previous results from smNPC-derived cultures were demonstratively backed.

In conclusion, from SMN expression rates of different phenotype classes throughout *in vitro* MN differentiation it can be deduced that the present iPSC-based cell system is definitely suitable to mimic SMN deficiency during development lending support to further SMA-related studies.

8.4.2 Gem number reliably depicts SMN deficiency in different phenotype classes throughout development

While cytoplasmatic SMN protein is diffusely spread, nuclear SMN agglomerates into distinct ~0.1–1 µm sized structures termed "gems" nearby Cajal bodies (Liu *et al.* 1996). Loss of gems correlates with low SMN expression in SMA patients as a sign of SMA pathology (Coovert *et al.* 1997).

Previously, presence of gems was quantitatively assessed in fibroblasts, iPSCs (control ~50 gems/100 nuclei, SMA I ~8 gems/100 nuclei) and iPSC-derived neurons and astrocytes (Ebert *et al.* 2009), again in iPSCs (control ~60 gems/100 nuclei, SMA I ~8 gems/100 nuclei)

(Corti *et al.* 2012) and in fibroblasts (control ~2 gems/nucleus, SMA I ~0 gems/nucleus) (Chang *et al.* 2011). Similarly, gems were quantified in this study, however, more cell lines comprising different SMA phenotypes were examined to improve data validity. Moreover, gem number assessment was performed at important stations of *in vitro* MN developmental course, i.e. in original fibroblasts, derived iPSCs, corresponding smNPCs and differentiated MN cultures on day 8 and on day 27 thereby deepening the insight in SMN-specific changes during development and exceeding the data base provided in previous studies.

Although absolute gem number per 100 nuclei differed among cell populations, a recurrent distribution pattern was detectable between the phenotype groups within a single cell population (7.5.5, Fig. 52). Healthy controls abundantly exhibited highest gem number per 100 nuclei (fibroblasts: ~117; iPSCs: ~15; smNPCs: ~9; MN culture d8: ~27; MN culture d27: ~21) mirroring sufficient *SMN1* expression. However, *SMN1*-deleted individuals held gem numbers equivalent to their *SMN2* copy number. SMA I line HGK1 (2 *SMN2* copies) betokened the significantly lowest gem number in all cell populations (fibroblasts: ~5; iPSCs: ~2; smNPCs: ~1.5; MN culture d8: ~2; MN culture d27: ~3.5) in comparison to controls. Partially, SMA I gem numbers even ranged significantly lower when compared to mildly affected SMA III and discordant asymptomatic. Furthermore, SMA III and asymptomatic revealed nearly always the same gem numbers which were significantly lessened compared to controls however reflecting the medium *SMN2* (3-4) copy number (fibroblasts: ~66-71; iPSCs: ~4; smNPCs: ~5-6; MN culture d8: ~15; MN culture d27: ~12-13). Consequently, the first time ever individual gem numbers were continuously strung together through several different cell populations even reflecting phenotypic differences during developmental processes in solid significance (7.5.5, Fig. 53).

Total gem numbers in fibroblasts matched previous results of controls and SMA patients with various severity in which also a direct correlation between *SMN1/SMN2* copies, gem numbers and disease severity was found (Coovert *et al.* 1997). Roughly simplified, SMA III and asymptomatic exhibited ~55-60% relative to control gem number mirroring the medium FL-SMN protein delivery from 3-4 *SMN2* copies. In iPSCs, exceptionally only a quarter of gems (~25%) were visualised.

SMN protein complexes appear as independent sub-nuclear structures during embryonic development and like other RNA-processing nuclear compartments e.g. Cajal bodies, gems are subjected to temporo-spatial regulation during developmental processes (Young *et al.* 2001). Diverse human foetal tissue samples all presented gems (Young *et al.* 2001), yet in rapidly proliferating undifferentiated cells, gems were only detected in a small proportion (Carvalho *et al.* 1999). Additionally, SMN-containing gems were barely detectable in undifferentiated PC12-derived neural precursor cells until neuronal differentiation was induced (Navascues *et al.* 2004). Taken together, these findings give explanatory clues to overall lower gem numbers in highly proliferative iPSCs and smNPCs.

The number of RNA-processing compartments like Cajal bodies linked to SMN via coilin correlates with neuronal soma size (Pena *et al.* 2001). While some authors reported fewer gem numbers in adult neuronal tissues or explanted adult neurons (Pena *et al.* 2001; Young *et al.* 2001), other studies claimed an abundance of gems in differentiated PC12-derived neurons (Navascues *et al.* 2004) whereas the former *in vitro* systems rather approach the true *in vivo* state. Thus, early smaller neurons are expected to contain fewer gems than mature neurons. Congruent with this common view of increasing gem number upon neuronal differentiation, smNPC-derived MN cultures in this study globally exhibited higher gem numbers with regard to control, SMA III and asymptomatic when compared to precedent cell

populations. Only in SMA I gem number stagnated throughout development at very low number (7.5.5, Fig. 53).

Although the gem distribution pattern pictured the different *SMN* copy numbers of phenotype classes more precisely and consistently than corresponding SMN protein data particularly concerning SMA III and asymptomatic (7.5.4, Fig. 50 **B**), admittedly, the present gem percentage of SMA III and asymptomatic (~55-60% relative to control gem number) beat the expected rate because 3-4 *SMN2* copies were supposed to generate just 10% FL-SMN/copy, hence totally 30-40% FL-SMN protein (Brahe 2000; Wirth *et al.* 2006b). As already outlined in the previous section (8.4.1), *SMN2* copies are not absolutely identical on account of preceding conversion events influencing regulatory sequences (Coovert *et al.* 1997; Feldkötter *et al.* 2002; Mailman *et al.* 2002). Thus, SMN protein with different capabilities of accumulation in gems was generated which may explain relatively high gem number in SMA III and asymptomatic.

Taking into account the absolute SMN expression levels of all phenotype groups (8.4.1), gem numbers were not directly reflected. Much SMN protein did not automatically correspond to high gem number since in iPSCs, gem numbers were low (7.5.5, Fig. 53) while SMN protein levels were high (7.5.4, Fig. 50 **B**). Indeed, absolute SMN amount does not necessarily transfer into respective gem number because additional nuclear assembly factors are required and gems also serve as nuclear SMN storage (Young *et al.* 2000).

Really, gems were prior detected in iPSC-derived MN cultures, yet no quantification was performed (Corti *et al.* 2012; Ebert *et al.* 2009). Minimum counted iPSC or fibroblast cell number amounted to 100 cells (Corti *et al.* 2012; Ebert *et al.* 2009) or sometimes even less (35-60 cells) (Chang *et al.* 2011).

In contrast, this study coherently reveals for the first time phenotype-specific changes in SMN expression and subsequent gem formation during *in vitro* MN differentiation. The large number of cell lines plus additional sub-clones as well as high number of cells assessed firmly fortifies present results and extends data of previous studies.

8.4.3 PLS3 expression notifies cell type-specific as well as phenotype-related differences amongst phenotypic classes during *in vitro* MN development

Inaccessibility of neural tissue samples from PLS3 discordant family members impeded elucidation of PLS3-mediated amelioration in mild SMA phenotype. Actin-bundling protein PLS3 is expressed in all solid tissues including spinal cord (Lin *et al.* 1999). PLS3 expression on RNA and protein level in LB cell lines of rare discordant family individuals distinctly differed among discordant siblings revealing a strong PLS3 over-expression in blood of asymptomatic individuals which eventually led to the discovery of PLS3 as protective modifier in SMA III (Oprea *et al.* 2008).

In fibroblasts, PLS3 protein is visualised as distinct single band, however, no difference between SMA III and asymptomatic siblings was detected on RNA or protein levels (Bernal *et al.* 2011; Oprea *et al.* 2008). Similarly, *PLS3*/PLS3 expression in fibroblasts of healthy controls, SMA I, SMA III and asymptomatic did not significantly differ (7.5.4, Fig. 50 **C**, **D**) strengthening results of previous studies. Considering absolute expression values, *PLS3*/PLS3 expression in fibroblasts was generally quite low compared to other cell populations (7.5.4, Fig. 50 **C**, **D**).

From iPSCs onwards, asymptomatic cell lines commenced to gradually augment *PLS3*/PLS3 expression levels individually and grouped, particularly once subjected to neural development into smNPCs and MN cultures (7.5.2, Fig. 46; 7.5.3, Fig. 49). In contrast, SMA III patients displayed the lowest PLS3 protein amount within the four phenotype groups despite rising

PLS3 mRNA rates (7.5.4, Fig. 50 **C**, **D**). Remarkably, SMA I line HGK1 presented throughout strong *PLS3*/PLS3 expression until MN cultures (7.5.4, Fig. 50 **C**, **D**). PLS3 expression rate was not determined in this patient's blood why an over-expression state cannot be defined. Any possible existing PLS3 over-expression did not rescue this severe SMA phenotype with only two *SMN2* copies anyway. Amazingly, healthy control line r12 maintained absolute *PLS3* expression level until MN differentiation when *PLS3* expression was massively down-regulated (7.5.2, Fig. 46 **G**). Comparably, PLS3 protein amount did not rise during development unlike in other cell lines (7.5.3, Fig. 49 **G**). Since control line COII.2 did not represent a proper MN culture, its data were only included when presenting as flawless population (i.e. fibroblast, iPSC, smNPC). Of course, results included very preliminary data from iPSCs and smNPCs which had to be confirmed by repetition, yet by trend results would fit the overall view.

Since iPSCs and smNPCs represent transient structures during human neural development, fibroblasts and MN cultures with mature post-mitotic cells reflect more the *in vivo* state. Of course, MN cultures as target tissue displayed the most interesting cell population.

Already in MN cultures derived by the EB-based run-through protocol obvious differences in PLS3 expression were detected. SMA III HGK13 denoted a conspicuous reduction in *PLS3*/PLS3 expression compared to controls whereas asymptomatic HGK16 delivered comparable PLS3 amounts relative to controls exhibiting no over-expression on RNA or protein level however (7.3.3, Fig. 27, Fig. 28). In smNPC-derived MN cultures of these two lines, similar results were obtained for *PLS3* mRNA levels (7.5.2, Fig. 46 **G**). However, on protein level HGK13 and HGK16 almost expressed the same PLS3 amount (7.5.3, Fig. 49 **G**). Concerning individual absolute expression strength, such inconsistency in PLS3 expression was sometimes seen between SMA III affected and asymptomatic siblings as well as among discordant asymptomatic individuals themselves (Bernal *et al.* 2011; Oprea *et al.* 2008) most probably reflecting individuals' intrinsic features and familial differences. Still, asymptomatic siblings verifiably expressed more PLS3 in blood than their SMA III siblings (Bernal *et al.* 2011; Oprea *et al.* 2008). More importantly, this fact points out the necessity to employ several cell lines to validly discover a specific phenotype as it was done in this study.

Similar to a recently introduced mouse model in which PLS3 rescued just mildly affected SMA mice (Ackermann *et al.* 2013), PLS3 over-expression only improved MN survival in *SMN1* depleted individuals comprising ≥3 *SMN2* copies (i.e. SMA III and asymptomatic) but not in SMA I affected (2 *SMN2* copies). Unlike in zebrafish where decreasing Pls3 protein amounts accompanied declining Smn protein amounts (Hao le *et al.* 2012), data from our *in vitro* MN system did not suggest a direct dependency between both proteins since SMA I line HGK1 frequently exhibited high PLS3 expression rates despite overt SMN deficiency (7.5.4, Fig. 50).

Relation to age and sex were examined in PLS3 expression. Pre-pubertal females and younger males (<11 years) exhibited an almost 2fold increase in *PLS3* expression in blood relative to older males and post-pubertal women (Stratigopoulos *et al.* 2010). Moreover, *PLS3* levels of post-pubertal female SMA III patients ranged higher than in more severely affected post-pubertal female patients alluding to a gender-specific feature since *PLS3* gene maps to Xq23 (Stratigopoulos *et al.* 2010). Intriguingly, healthy infant controls (≤3 years) principally denoted higher *PLS3* expression levels in blood in comparison to older healthy children insinuating an age-dependent down-regulation during development (Yanyan *et al.* 2014). Since healthy, SMA III and asymptomatic fibroblast cell lines were sampled from older individuals (18-61 years, see 5.8.3, Tab. 13) thereby reflecting the person's true age, the comparably low overall and within almost equal PLS3 expression would be explainable (7.5.3, Fig. 49 **B**).

The reprogramming process is assumed to erase any somatic trait and reset a juvenile state in iPSCs (Jaenisch *et al.* 2008). Thus, any previous age-related influence on *PLS3*/PLS3 expression should be eradicated in iPSCs and derived cell lines. Nonetheless, a basically higher *PLS3* expression rate in infant SMA patients (≤3 years) relative to controls was reported as compensatory effect in such patients (Yanyan *et al.* 2014). This may explain the up-regulated *PLS3*/PLS3 expression in SMA I, SMA III and asymptomatic siblings in MN cultures while healthy control r12 did not increase *PLS3*/PLS3 expression (7.5.4, Fig. 50 **C**, **D**). Admittedly, the present MN cultures are far away from the border age (3 years) after which differences were seen in Yanyan *et al.* Still, it cannot be ruled out that such transcriptional regulatory processes begin earlier in neural lineages than in blood.

Additionally, there was no significantly different *PLS3* expression rate in blood between healthy controls, SMA I, SMA II and SMA III patients below three years of age (Yanyan *et al.* 2014). Comparably, PLS3 expression in our developmentally young MN cultures is expected to present equal amounts of PLS3 among SMA I and SMA III patients which holds true indeed (7.5.3, Fig. 49 **H**). Yet, control lines ranged even lower. Besides, over-expression in asymptomatic siblings strikingly outlined a persisting PLS3 over-expression obviously counteracting deleterious effects of SMN deficiency which already struck their symptomatic SMA III siblings.

As known, PLS3 was vastly expressed in actively dividing cells (Rao *et al.* 2003) perfectly going in line with increasing PLS3 expression rates in iPSCs and smNPCs of all phenotype classes (7.5.4, Fig. 50 **C**, **D**). Since PLS3 is highly expressed in spinal cord (Oprea *et al.* 2008), evident presence of PLS3 in HB9+ MNs (7.4.4, Fig. 42 **A**) would reflect respective expression rates in mixed MN cultures addressing the decisive question if PLS3 over-expression in blood is mirrored in MN cultures thereby corroborating current hypothesis that PLS3 mediates protection specifically in spinal cord.

MN content in smNPC-derived MN cultures did not obviously correlate with PLS3 expression. While SMA III lines HGK22.17, HGK27.10 or HGK27.13 still exhibit relatively high numbers of HB9+ and ISL1+ MNs (7.4.4, Fig. 43 **C**, **D**), PLS3 expression was fairly low (7.5.3, Fig. 49 **G**). In contrast, asymptomatic lines HGK21.8 and HGK28.9 depicted globally lower MN numbers (7.4.4, Fig. 43 **C**, **D**) while PLS3 expression demonstrably exceeded all others (7.5.3, Fig. 49 **G**). Furthermore, SMA I line HGK1 still expressed PLS3 reasonably although SMA I MN cultures were virtually devoid of MNs.

Of course, in a mixed *in vitro* MN culture it was impossible to figure out whether remaining MNs or other CNS populations in asymptomatic siblings were responsible for this striking PLS3 over-expression. To address that question MNs have either to be enriched (Corti *et al.* 2012) or differentiated into specific CNS populations e.g. astrocytes and GABAergic or glutamatergic interneurons and subsequently checked for PLS3 expression. Since smNPCs already reveal a visible PLS3 over-expression in asymptomatic, it might be speculated that neural lineages and especially MN-specific differentiation indeed exposed or even triggered PLS3 over-expression in those asymptomatic. Future analyses of pMN-primed smNPCs or other NSC populations will provide quick proof. Of course, inclusion of more SMA I patients and healthy control will fortify this data since data of single SMA I line HGK1 puts common validity on narrow grounding.

Bernal *et al.* uttered doubts whether small positive variances in LB lines of asymptomatic individuals indicating a PLS3 over-expression reflect the real state in individuals' spinal cord (Bernal *et al.* 2011). Present results of this study contrarily advocated a transfer of elevated PLS3 levels in blood into the CNS and impressively emphasised the apparent importance of increased PLS3 expression in MN cultures exerting its protective effect specifically in spinal cord.

8.5 PLS3 and actin apparently co-localise in neuronal growth cones of MN cultures

The morphology of growth cones is described as the outer axon tip where a rod of stable microtubule in the axon shaft terminates in a cone-shaped structure with highly dynamic actin-containing finger-like protrusions (Lowery *et al.* 2009) as it was demonstrated in isolated murine MNs (Jablonka *et al.* 2013). Co-localisation of Pls3 was demonstrated in primary murine MNs (Oprea *et al.* 2008) as well as in filopodia of PLS3 over-expressing MEFs (Ackermann *et al.* 2013).

Evident motor growth cone identification necessitates skilful experimental setting: Additional specific axon staining by microtubule associated protein τ (MAPT) or acetylated tubulin is mandatory to unambiguously discriminate the axon tip between dendrites. Furthermore, motor axons have to be identified by MN markers like ISL1, ChAT or SMI-32. A quadruple staining of PLS3, actin plus a MN-marker (e.g. ChAT) and an axonal marker (e.g. MAPT) was not feasible. Thus, (motor)neuronal identification markers (i.e. ChAT, ISL1, neurofilament) were verified in parallel with cytoskeletal markers (i.e. PLS3, actin, MAPT) in immunocytochemical staining. Calculation of MN amount per sample will proportionally depict number of putative motor growth cones.

Indeed, present growth cones of controls, SMA III and asymptomatic siblings were shaped accordingly and did display presence of PLS3 and actin in such growth cones (7.6, Fig. 56 **A**). MAPT$^+$ axons evidently denoted axons ending in such growth cones. In line with common knowledge (Lowery *et al.* 2009), actin allocated primarily in the peripheral zone and filopodia-like protrusions (7.6, Fig. 56). In all three phenotype groups examined, PLS3 and actin often overlaid. In SMA I line HGK1, no usable growth cone were detected (data not shown). In control r12, equal PLS3/actin distribution pattern met expected regular PLS3 function to bundle F-actin despite globally lower PLS3 expression rates (7.5.3, Fig. 49 **G**) indicating that present PLS3 amount sufficed to fulfil its function.

Unlike in SMA III, asymptomatic strikingly revealed that strong actin accumulation was always accompanied by PLS3 co-localisation. Contrarily, SMA III HGK27.10 evidently displayed an incongruent trend in both intensity graphs since high peaks of actin signals were not covered by respective PLS3 signals. In short, actin-rich areas entailed visible PLS3 amounts but not *vice versa* implying that high actin amounts may attract PLS3. Of course, too few growth cones were analysed to state any valid explanation. Speculating, this process might lead to retention of already fewer actin filaments and extended stabilisation in asymptomatic nonetheless. SMN depletion was evidently linked to disturbed axonal mRNA-transport and local *β-actin* mRNA translation (Rossoll *et al.* 2003; Hubers *et al.* 2010; Akten *et al.* 2011; Fallini *et al.* 2013; Yoo *et al.* 2013) as well as impaired NMJ maintenance which derived from growth cones (Akten *et al.* 2011). Thus, SMA III growth cones may suffer from F-actin diminution whose detrimental effects could not be compensated by overall surplus PLS3 expression rates in asymptomatic MN cultures.

Nevertheless, any meaningful conclusion cannot be drawn until now since too few growth cones were analysed. Data yield ranged very low for only nine growth cones were examined so far. After prolonged MN cultivation and subsequent immunocytochemical staining procedure, sensitive growth cones might have shrunk or collapsed. Anyway, detecting usable growth cones turned out as challenging task. Besides, Ackermann *et al.* were able to utilise V5-tagged PLS3 for strong immunocytochemical staining whereas in this model only endogenous PLS3 was stainable which may give weaker signals.

Motor growth cone identity was not defined either due to a lack of suitable staining combination. Parallel ISL1/HB9 quantification (7.4.4, Fig. 43 **C**, **D**) delivered just an approximate benchmark. Furthermore, without a proper method to quantify the exact amount of F-actin and PLS3 it will remain elusive whether overt PLS3 over-expression really leads to more local growth cone PLS3 in asymptomatic. Therefore, examining pivotal PLS3/actin co-localisation in NMJs would give more insight into PLS3-mediated protection as in a plain MN culture. Additionally, the problem of MN identity in growth cones was removed since only MNs generate NMJs (Manuel *et al.* 2011).

Still, the present system may deliver useful data concerning growth cone stability. Growth cones could be categorised with respect to their shape, for example dystrophic or regular.

8.6 Establishment of a co-culture model of mixed motoneuronal cultures and human myotubes decisively broadened the possibility in studying SMA-conditioned NMJ pathology

Maintenance defects in neuromuscular junctions (NMJs) have always been suspected as one principal reason for pathogenic effects in SMA. Upon SMN-depletion, lower α-motoneurons suffer from foetal developmental maturation anomalies which consequently lead to a postnatal retrograde axonal dying-back mechanism ending in motor axon disruption and eventually entire MN degeneration (Fidzianska *et al.* 2002; Ito *et al.* 2011; Fallini *et al.* 2012). Therefore, a reliable cellular *in vitro* model phenocopying synaptogenesis between MN and muscle and formation of NMJs is crucial for elucidating SMA pathology. In particular, PLS3 did exert its protective effect in a mouse model putatively in motor axon growth cones by actin stabilisation. Thus, synaptic function and neuromuscular connectivity were maintained and NMJ decay was countervailed (Ackermann *et al.* 2013). Therefore, establishment of a human co-culture model comprising iPSC-derived patient-specific motoneurons and human myotubes will come in handy to examine the exact working mechanism of PLS3 in SMA discordant motoneurons.

Indeed, the basic experimental set-up for such an *in vitro* model has successfully been established in this doctoral thesis. On the pre-synaptic site, human motoneurons were differentiated from iPSCs. On the post-synaptic site, human myotube formation was induced *in vitro*. During myogenesis, several post-mitotic myoblasts align and fuse to primitive primary myotubes, large syncytial multinucleated cells (Slater 2009). These relatively few primary myotubes were clearly on hand in this co-culture model. Moreover, neurons did contact these myotubes (7.7, Fig. 57) and long-term co-culture (up to seven weeks) succeeded.

A manifest sign of NMJ formation is a clustering of AChRs on the muscular surface (Slater 2009). During murine embryogenesis, MN-mediated agrin secretion induces cytoskeletal re-distribution of membrane-linked AChRs on the sarcolemma surface. Originally evenly dispersed AChRs coalesce to plaque-like patches in the centre of myotubes in late embryogenesis. During postnatal development, these patches form riffled shapes and perforate later to the characteristic pretzel-structure owing to massive sarcolemma folding when the motor axon tip bulges into this developing motoric end-plate (Sanes *et al.* 2001; Wu *et al.* 2010). In humans, comparable developmental processes are assumed.

Truly, these early developmental changes concerning size, shape and topography on the post-synaptic muscle site were mimicked in the present co-culture model. The early AChR clustering was rather punctiform and occurred in close proximity to a queue of myonuclei in the syncytial myotube (7.7, Fig. 58). In mammals, there is often an early postnatal

accumulation of such sub-synaptic myoneuclei (Slater 2009). Later, AChRs clearly arranged in a plaque-like furrowed shape indicating an early sign of NMJ formation (7.7, Fig. 59 **A**). These morphological differences visible between MN1 fed co-cultures (7.7, Fig. 58) and SC-CM fed co-cultures (7.7, Fig. 59 **A**) also reflected varying culture periods (15 days vs. 49 days), ergo the natural developmental process.

Even though motoneurons require neurotrophic factors *in vitro* and *in vivo* (Hughes *et al.* 1993), it is obviously not necessary to supplement a MN-myotube co-culture with further neurotrophic factors (e.g. NT3, BDNF, GDNF) since they are secreted by skeletal muscle cells. Then, these factors convey rather a local effect in developing NMJs than a general MN survival stimulus (Peng *et al.* 2003). Administration of additional neurotrophic factors even impeded synaptogenesis and NMJ formation on account of inhibition of agrin synthesis in pre-synaptic MNs (Peng *et al.* 2003). This might also explain the poor yield of NMJ-like structures in MN1 fed co-cultures because MN1 is supplemented with BDNF, GDNF and IGF-1.

Evidently, SC-CM gave the best results in respect to visual morphological changes in MN-myotube co-culture. SC-CM exerted its stimulatory synaptogenic effect most probably via a combination of mostly unknown factors. Although Schwann cells secrete agrin, SC-CM by itself did not increase AChR clustering on muscle (Yang *et al.* 2001). More likely, SC-CM factors directly act on MN gene expression thereby promoting proper synapse formation. In rat SC-CM, TGF-β1 signalling boosted motoneuronal agrin expression in a co-culture system (Feng *et al.* 2008).

Yet, no *bona fide* NMJs were found in the present co-cultures. Of course, the overall low number of MNs upon iPSC differentiation reduced the probability of MN-myotube contact. Moreover, the time of co-cultivation might have been too short. When data from different studies were compared, it became obvious that human neurons developed about ten times slower than cells from other well characterised murine model systems, for example (Stockmann *et al.* 2011). Even after 12–14 weeks MN-myotube co-culture, NMJ formation has not completed *in vitro* yet (Stockmann *et al.* 2011).

Still, this experimental set-up with SC-CM may serve as valuable platform for further studies in SMA pathogenesis and effects of modifiers when a higher MN number will be available with NSC-based MN differentiation. Nonetheless, in comparison to other publications (Hu *et al.* 2009; Guo *et al.* 2011; Stockmann *et al.* 2011) the SC-CM mediated co-culture system presented in this thesis showed a more distinct BTX[+] AChR clustering on the post-synaptic muscle site – the first hallmark of proper NMJ formation.

8.7 iPSC-derived GABAergic neuronal cultures evidently reflected molecular cause of diverging VPA responsiveness in SMA patients

Before the recent introduction of *SMN2* splicing compounds as highly potent drug in treatment of severe Δ7 mice (Naryshkin *et al.* 2014), histone deacetylase (HDAC) inhibitors such as valproic acid (VPA) were regarded as potentially promising therapeutic (Brichta *et al.* 2006; Swoboda *et al.* 2011). Notwithstanding, deeper analyses delineated a differing responsiveness towards VPA administration amongst SMA patients counteracting VPA application as cure (Brichta *et al.* 2006; Piepers *et al.* 2011). A recent study depicted altered fatty acid metabolism, precisely the fatty acid uptake by membrane translocase CD36 as causative (Garbes *et al.* 2013).

In addition, VPA is known to inhibit an enzymatic compound of GABA synthesis resulting in elevated GABA levels (Johannessen 2000). Thus, GABAergic neurons of VPA responders are supposed to respond particularly intensely upon VPA application. Indeed, lt-NES®SC-derived

GABAergic neuron cultures of VPA responder/non-responder iPSC lines notably reflected the according VPA response previously observed in fibroblasts and blood cell lines (Garbes *et al.* 2013). Supernatant of VPA responder culture contained measurably more GABA than control ESC line or VPA non-responder who even exhibited a significant lower GABA release (7.8, Fig. 60 **D**). Thus, an *in vitro* system representing the CNS strongly aided the discovery of CD36 as cause for different VPA responsiveness in SMA patients.

Of course, examining more than one VPA responder/non-responder each would have backed these findings with more validity. Additionally, differentiation into MN cultures will deliver the final proof of VPA response in patients' target tissue.

8.8 Summarised findings pinpoint advantages of an iPSC-based MN culture system and reliable validity in modelling SMA phenotype *in vitro*

Taken together, this study successfully applied iPSC technology in setting up patient-derived neuronal *in vitro* cell models for the first time with VPA (non-)responders and PLS3 discordant mildly SMA III affected or asymptomatic individuals in comparison to healthy controls and severe SMA I cases.

Firstly, a broad range of SMA patients' samples of different disease severity and PLS3 discordant siblings were converted into *bona fide* iPSC lines via retroviral or state-of-the-art SeV reprogramming. Secondly, generation of stably expandable and pMN-patternable NSC population (smNPCs) enabled robust MN differentiation with sufficient yield. Thirdly, accessibility of different cell populations, i.e. original fibroblasts, derived iPSCs, corresponding smNPCs and differentiated MN cultures facilitated monitoring of SMA-specific changes during the developmental process of human MN generation. Fourthly, not only was a significant decline in MN number observed in SMA I cultures but also gradually decremented MN numbers in SMA III and asymptomatic cultures. Fifthly, SMN expression on RNA and protein level revealed lowest expression rate in SMA I cultures and moderate reduction in SMA III and asymptomatic cultures recapitulating *SMN2* copy number effects and generally known SMN expression changes in adult versus foetal tissue and cell types. Sixthly, PLS3 expression on RNA and protein level indicated strong trend in over-expression of asymptomatic samples in iPSCs and neural lineages possibly pinpointing the protective effect of PLS3. Finally, differences in gem number perfectly matched respective diminished SMN expression rates in SMA I, SMA III and asymptomatic samples.

Moreover, successful set-up of a human MN-myotube co-culture model paved the way for future studies of NMJ formation in PLS3 discordant individuals. Furthermore, VPA-dependent changes of GABA release in GABAergic neuron cultures clearly corroborated molecular causes of altered fatty acid metabolism which underlay VPA responsiveness in SMA patients. In addition, this finding provided evidence that VPA responsiveness found in blood and fibroblasts similarly mirrored in a neuronal cell system.

In summary, data of this study profoundly displayed the advantageous applicability of iPSC-derived patient-specific SMA *in vitro* cell models – an indispensable benefit for further research mapping crucial mechanisms underlying modifier-mediated protection in SMA.

8.9 Outlook

After having established the fundamental experimental settings for a PLS3 discordant iPSC-based *in vitro* model mimicking evidently mild SMA progression in SMA III patients and PLS3 over-expression in asymptomatic siblings, following steps ought to be envisaged: Previous studies dealing with iPSC-based SMA models as well as PLS3 discordant mouse models demonstrated changes in axonal outgrowth, growth cone architecture or G-/F-actin ratio (Oprea *et al.* 2008; Ebert *et al.* 2009; Ackermann *et al.* 2013). Thus, such findings should be confirmed. Including SMA II line HGK4 would comprise all degrees of severity in this study. Additional examination of unrelated SMA III patients from non-discordant families may back present data. Shorter intervals of analysis and more samples throughout the *in vitro* differentiation would give more coherent insight in cell-specific PLS3 and SMN expression changes.

Moreover, insight is gained how the mode of action of PLS3 exerts its protective effect on molecular level in the context of the SMA pathomechanism. For instance, calcium binding was discovered as essential for PLS3 function in Smn-deficient MNs in zebrafish (Lyon *et al.* 2013) so that investigation of Ca^{2+} homeostasis in human MNs would be worth checking. Interestingly, PLS3 lacking its actin-binding domains was still able to rescue motor axons in smn morphants leading to the speculative assumption that PLS3 might exert its ameliorative function independent of the cytoskeleton (Lyon *et al.* 2013). Earlier studies uttered perturbations in neurotransmitter release and synaptic vesicle cycle (Torres-Benito *et al.* 2011) predestining endocytosis as future research topic in discordant MN cultures. Additionally, our group identified further modifying genes in SMA discordant families prefiguring involvement of these SMA modifiers in endocytotic processes (Dr. Markus Rießland, publication in preparation).

Correct mRNA localisation and on-site protein synthesis are essential processes required for synaptic development, function and activity (Wiersma-Meems *et al.* 2005; Liu-Yesucevitz *et al.* 2011). This aspect is emphasised by the connection between mRBPs such as FMRP and SMN and neurological diseases like fragile-X syndrome and SMA (Bassell *et al.* 2008; Piazzon *et al.* 2008). Particularly in SMA, this link provides a plausible insight into neuromuscular pathology since the entire process of endocytosis, neurotransmitter release and the SV cycle in the motor axon depends on proper actin dynamics, alluding to the pivotal role of SMN in NMJ maintenance. Hence, analysing the variability of endocytotic properties in iPSC-derived PLS3 discordant MN tips may unclose access to PLS3-mediated protection.

Even comparison between healthy control and diseased cell lines is just able to roughly approximate the true *in vivo* state because individual cell line-specific features of every cell line are benevolently left aside when drawing conclusions. Generation of age/gender-matched isogenic gene-corrected control cell lines carrying the same genetic variants apart from the disease-causing gene would find a remedy (Hargus *et al.* 2013; Sandoe *et al.* 2013).

As key feature of SMA pathogenesis, NMJ maintenance capability represents an important aspect in SMA research and was already assessed in SMA mouse models (Ackermann *et al.* 2013; Bowerman *et al.* 2012a). Highly efficient generation of iPSC-derived myocytes (Darabi *et al.* 2012; Salani *et al.* 2012) would enable the generation of a doubly patient-derived *in vitro* co-culture model dodging any putative biasing allogenic effect between MNs and myotubes. Transplanted iPSC-derived human MNs successfully formed functional connections with rat muscles (Su *et al.* 2013). In addition, rapid progress in biomaterial research even resulted in a murine 3D neuron-muscle construct displaying NMJ formation (Morimoto *et al.* 2013).

Rescue experiments always grant great significance to scientific studies. Therefore, monitoring effects of exogenous PLS3 over-expression in smNPCs/MNs of SMA III discordant patients and reciprocal of PLS3 knock-down in smNPCs/MNs of healthy control individuals or asymptomatic siblings might deliver valuable data about SMA pathology. Genome editing strategies like transcription activator-like effector nuclease (TALEN) or clustered regularly interspaced short palindromic repeats/Cas9 RNA-guided nucleases (CRISPR/Cas9) system also evolve very fast in context of SC research (Ding *et al.* 2013; Horii *et al.* 2013) thereby simplifying the feasibility. Additionally, generation of isogenic cell lines is manageable by such techniques. Variability of human pluripotent SCs in modelling disease phenotypes originates from genetic background and derivation method (Sandoe *et al.* 2013). To attenuate such experimental "noise" large patients' cohorts and many cell lines are necessary. However, isogenic cell lines better fulfil this purpose since fewer SC lines are needed to grant generalisibilty of results. Possibly more subtle differences between patients and controls could be carved out as well (Sandoe *et al.* 2013). Evidently, isogenic ESC lines demonstrated a more similar whole-genome expression profile compared to unrelated ESC lines (Soldner *et al.* 2011).

Since VPA-responsiveness was examined in a GABAergic neuronal system, generation of corresponding smNPC lines and subsequent MN differentiation may finalise research in this area by checking SMN expression levels in smNPCs/MNs upon VPA treatment in (non-)responders.

Direct transdifferentiation between somatic lineages elegantly circumvents reprogramming difficulties, time-consuming iPSC validation and subsequent differentiation. Inarguably, scientific groups succeeded in directly converting fibroblast into induced neurons (iNs) and even motoneurons (iMNs) (Vierbuchen *et al.* 2010; Son *et al.* 2011). Besides, iN technology successfully displayed familial Alzheimer's Disease phenotype on cellular level (Qiang *et al.* 2011). Notwithstanding, the efficiency remained very low and ectopic over-expression of several lineage-specific TFs required good technical practice. Still, improved techniques may facilitate iN application (Daniela Eckert, personal communication).

Stem cell research unavoidably fuels hopes to generate personalised cells or tissues and to employ these in cellular engraftment strategies as potential custom-made therapy. However, replacement of fully functional MNs seems an insurmountable obstacle because motor axon guidance through limbs and subsequent synapse formation via NMJs remains virtually impossible in post-natal humans. Hence, diseased MNs in SMA patients cannot be replaced. Still, the idea was seized in impressive publications in which primary mouse NSCs, later murine ESC-derived NSCs or human iPSC-derived genetically corrected SMA MNs were injected in cerebrospinal fluid of post-natal SMA mice (Corti *et al.* 2008; Corti *et al.* 2010; Corti *et al.* 2012). Implanted cells differentiated primarily into neuronal cells or partially into glial cells, yet also retained NSC or MN states, respectively. Ameliorative effects were exerted via secretion of neuroprotective growth factors thus stabilising endogenous SMA MNs or establishment of new NMJs by donor MNs. Therefore, a promising trail to follow in humans might focus on supportive cell types in the motor circuit. SMN depletion evidently affected also murine Schwann cells (Hunter *et al.* 2014) and human iPSC-derived astrocytes (McGivern *et al.* 2013) intrinsically. Hence, such cell populations may prove more feasible for transplantation in older humans. Nevertheless, potential benefits must be carefully pondered with respect to risks of tumorigenicity or unknown long-term effects after engraftment of exogenous cells.

Indeed, Nobel prize-awarded iPSC technology opened an avenue to spectacular new insights into manifold disease pathomechanisms.

9. Publications, oral & poster presentations

Original Publications

"VPA response in SMA is suppressed by the fatty acid translocase CD36"
Lutz Garbes, **Ludwig Heesen**, Irmgard Hölker, Tim Bauer, Julia Schreml, Katharina Zimmermann, Michaela Thoenes, Michael Walter, John Dimos, Michael Peitz, Oliver Brüstle, Raoul Heller and Brunhilde Wirth, **Hum Mol Genet. 2013** Jan; Vol. 22, No. 2, p.398-407

"Evaluation of SNPs in miR-146a, miR196a2 and miR-499 as low-penetrance alleles in German and Italian familial breast cancer cases"
Catucci I, Yang R, Verderio P, Pizzamiglio S, **Heesen L**, Hemminki K, Sutter C, Wappenschmidt B, Dick M, Arnold N, Bugert P, Niederacher D, Meindl A, Schmutzler RK, Bartram CC, Ficarazzi F, Tizzoni L, Zaffaroni D, Manoukian S, Barile M, Pierotti MA, Radice P, Burwinkel B, Peterlongo P, **Hum Mutat. 2010** Jan;31(1):E1052-7

Conferences

23rd May 2014	Annual Human Genetics meeting, Universität zu Köln, Cologne, Germany (poster presentation) Title: *Differentiating patient-derived iPS cells into motoneurons for tissue-specific analysis of SMN-specific changes in SMA patients* **Ludwig Heesen**, Michael Peitz, Lutz Garbes, Irmgard Hölker, Kristina Hupperich, John Dimos, Oliver Brüstle, Brunhilde Wirth
13th-14th February 2014	5th International Symposium "Crossroads in Biology" (CIB), Universität zu Köln, Cologne, Germany (member of organisational board) Website: http://crossroads.uni-koeln.de/
23rd-24th April 2013	7th International Stem Cell Network Meeting, Cologne, Germany
25th-27th January 2013	Neuromics Kick-off Meeting, Sitges, Spain (poster presentation) Title: *Differentiating patient-derived iPS cells into motoneurons for tissue-specific analysis of SMN-specific changes in SMA patients* **Ludwig Heesen**, Michael Peitz, John Dimos, Oliver Brüstle, Brunhilde Wirth
29th November 2012	Annual Human Genetics meeting, Universität zu Köln, Cologne, Germany (oral presentation) Title: *Generation of human iPSCs of PLS3 discordant families & re-differentiation to SMA motoneurons (MNs)* **Ludwig Heesen**, Michael Peitz, John Dimos, Oliver Brüstle, Brunhilde Wirth

21st-24th June 2012	16th International Families of SMA Meeting, Bloomington, USA (conference report for the Initiative SMA e.V.) Website: http://www.initiative-sma.de Header: 16. Kongress der Families of SMA
13th May 2011	Annual Human Genetics meeting, Universität zu Köln, Cologne, Germany (poster presentation) Title: *Differentiating patient-derived iPS cells into motoneurons for tissue-specific analysis of SMN-specific changes in SMA patients* **Ludwig Heesen**, Michael Peitz, John Dimos, Oliver Brüstle, Brunhilde Wirth
5th-6th April 2011	6th Internationales Stammzellnetzwerk Meeting, Essen, Deutschland
22nd-24th March 2010	9th Transgenic Technology Meeting, Berlin, Germany (poster presentation) Title: *Generating patient-derived iPS cells & motoneurons for tissue-specific analysis of SMN-specific changes in SMA patients* **Ludwig Heesen**, Michael Peitz, John Dimos, Oliver Brüstle, Brunhilde Wirth
9th October 2009	Annual Human Genetics meeting, Universität zu Köln, Cologne, Germany (poster presentation) Title: *Generation and application of iPS cells & motoneurons for tissue-specific analysis of SMN-specific changes in SMA patients* **Ludwig Heesen**, Brunhilde Wirth, Michael Peitz, Oliver Brüstle

10. References

Aasen, T., A. Raya, *et al.* (2008). "Efficient and rapid generation of induced pluripotent stem cells from human keratinocytes." Nat Biotechnol **26**(11): 1276-84.

Abmayr, S. and J. Chamberlain (2006). The structure and function of dystrophin. Molecular mechanisms of muscular dystrophies. S. Winder, Landes Bioscience: p. 14-34.

Abyzov A., J. Mariani, *et al.* (2012). "Somatic copy number mosaicism in human skin revealed by induced pluripotent stem cells." Nature **492**(7429):438-42

Ackermann, B., S. Kröber, *et al.* (2013). "Plastin 3 ameliorates spinal muscular atrophy via delayed axon pruning and improves neuromuscular junction functionality." Hum Mol Genet **22**(7): 1328-47.

Ahmad, S., Y. Wang, *et al.* (2012). "The zinc finger protein ZPR1 is a potential modifier of spinal muscular atrophy." Hum Mol Genet **21**(12): 2745-58.

Akten, B., M. J. Kye, *et al.* (2011). "Interaction of survival of motor neuron (SMN) and HuD proteins with mRNA cpg15 rescues motor neuron axonal deficits." Proc Natl Acad Sci U S A **108**(25): 10337-42.

Alaynick, W. A., T. M. Jessell, *et al.* (2011). "SnapShot: spinal cord development." Cell **146**(1): 178-178 e1.

Alberts, B., A. Johnson, *et al.* (2002). Molecular Biology of the Cell. New York, Garland Science.

Alias, L., S. Bernal, *et al.* (2009). "Mutation update of spinal muscular atrophy in Spain: molecular characterization of 745 unrelated patients and identification of four novel mutations in the SMN1 gene." Hum Genet **125**(1): 29-39.

Allendoerfer, K. L., J. L. Magnani, *et al.* (1995). "FORSE-1, an antibody that labels regionally restricted subpopulations of progenitor cells in the embryonic central nervous system, recognizes the Le(x) carbohydrate on a proteoglycan and two glycolipid antigens." Mol Cell Neurosci **6**(4): 381-95.

Amabile, G. and A. Meissner (2009). "Induced pluripotent stem cells: current progress and potential for regenerative medicine." Trends Mol Med **15**(2): 59-68.

Amit, M. and J. Itskovitz-Eldor (2002). "Derivation and spontaneous differentiation of human embryonic stem cells." J Anat **200**(Pt 3): 225-32.

Amoroso, M. W., G. F. Croft, *et al.* (2013). "Accelerated high-yield generation of limb-innervating motor neurons from human stem cells." J Neurosci **33**(2): 574-86.

Andreassi, C., J. Jarecki, *et al.* (2001). "Aclarubicin treatment restores SMN levels to cells derived from type I spinal muscular atrophy patients." Hum Mol Genet **10**(24): 2841-9.

Anokye-Danso, F., C. M. Trivedi, *et al.* (2011). "Highly efficient miRNA-mediated reprogramming of mouse and human somatic cells to pluripotency." Cell Stem Cell **8**(4): 376-88.

Aoi, T., K. Yae, *et al.* (2008). "Generation of pluripotent stem cells from adult mouse liver and stomach cells." Science **321**(5889): 699-702.

Araki, R., Y. Jincho, *et al.* (2010). "Conversion of ancestral fibroblasts to induced pluripotent stem cells." Stem Cells **28**(2): 213-20.

Arber, S., B. Han, *et al.* (1999). "Requirement for the homeobox gene Hb9 in the consolidation of motor neuron identity." Neuron **23**(4): 659-74.

Arnold, A. S., M. Gueye, *et al.* (2004). "Reduced expression of nicotinic AChRs in myotubes from spinal muscular atrophy I patients." Lab Invest **84**(10): 1271-8.

Arpin, M., E. Friederich, *et al.* (1994). "Functional differences between L- and T-plastin isoforms." J Cell Biol **127**(6 Pt 2): 1995-2008.

Avila, A. M., B. G. Burnett, *et al.* (2007). "Trichostatin A increases SMN expression and survival in a mouse model of spinal muscular atrophy." J Clin Invest **117**(3): 659-71.

Bao, L., L. He, *et al.* (2011). "Reprogramming of ovine adult fibroblasts to pluripotency via drug-inducible expression of defined factors." Cell Res **21**(4): 600-8.

Bar-Nur, O., H. A. Russ, *et al.* (2011). "Epigenetic memory and preferential lineage-specific differentiation in induced pluripotent stem cells derived from human pancreatic islet beta cells." Cell Stem Cell **9**(1): 17-23.

Barquinero, J., H. Eixarch*, et al.* (2004). "Retroviral vectors: new applications for an old tool." Gene Ther **11 Suppl 1**: S3-9.

Bassell, G. J. and S. T. Warren (2008). "Fragile X syndrome: loss of local mRNA regulation alters synaptic development and function." Neuron **60**(2): 201-14.

Battaglia, G., A. Princivalle*, et al.* (1997). "Expression of the SMN gene, the spinal muscular atrophy determining gene, in the mammalian central nervous system." Hum Mol Genet **6**(11): 1961-71.

Bäumer, D., S. Lee*, et al.* (2009). "Alternative splicing events are a late feature of pathology in a mouse model of spinal muscular atrophy." PLoS Genet **5**(12): e1000773.

Bernal, S., E. Also-Rallo*, et al.* (2011). "Plastin 3 expression in discordant spinal muscular atrophy (SMA) siblings." Neuromuscul Disord **21**(6): 413-9.

Bertrandy, S., P. Burlet*, et al.* (1999). "The RNA-binding properties of SMN: deletion analysis of the zebrafish orthologue defines domains conserved in evolution." Hum Mol Genet **8**(5): 775-82.

Bock, C., E. Kiskinis*, et al.* (2011). "Reference Maps of human ES and iPS cell variation enable high-throughput characterization of pluripotent cell lines." Cell **144**(3): 439-52.

Borghese, L., D. Dolezalova*, et al.* (2010). "Inhibition of notch signaling in human embryonic stem cell-derived neural stem cells delays G1/S phase transition and accelerates neuronal differentiation in vitro and in vivo." Stem Cells **28**(5): 955-64.

Boulting, G. L., E. Kiskinis*, et al.* (2011). "A functionally characterized test set of human induced pluripotent stem cells." Nat Biotechnol **29**(3): 279-86.

Bowerman, M., C. L. Anderson*, et al.* (2009). "SMN, profilin IIa and plastin 3: a link between the deregulation of actin dynamics and SMA pathogenesis." Mol Cell Neurosci **42**(1): 66-74.

Bowerman, M., L. M. Murray*, et al.* (2012a). "A critical smn threshold in mice dictates onset of an intermediate spinal muscular atrophy phenotype associated with a distinct neuromuscular junction pathology." Neuromuscul Disord **22**(3): 263-76.

Bowerman, M., D. Shafey*, et al.* (2007). "Smn depletion alters profilin II expression and leads to upregulation of the RhoA/ROCK pathway and defects in neuronal integrity." J Mol Neurosci **32**(2): 120-31.

Bowerman, M., K.J. Swoboda *et al.* (2012b). "Glucose metabolism and pancreatic defects in spinal muscular atrophy." Ann Neurol **72**(2): 256-68.

Bradford, M. M. (1976). "A rapid and sensitive method for the quantitation of microgram quantities of protein utilizing the principle of protein-dye binding." Anal Biochem **72**: 248-54.

Brahe, C. (2000). "Copies of the survival motor neuron gene in spinal muscular atrophy: the more, the better." Neuromuscul Disord **10**(4-5): 274-5.

Brichta L., Y. Hofmann, *et al.* (2003) Valproic acid increases the SMN2 protein level: a well-known drug as a potential therapy for spinal muscular atrophy. Hum Mol Genet **12**: 2481-9

Brichta, L., I. Hölker, *et al.* (2006). "*In vivo* activation of SMN in spinal muscular atrophy carriers and patients treated with valproate." Ann Neurol **59**(6): 970-5.

Briese, M., B. Esmaeili*, et al.* (2009). "Deletion of smn-1, the Caenorhabditis elegans ortholog of the spinal muscular atrophy gene, results in locomotor dysfunction and reduced lifespan." Hum Mol Genet **18**(1): 97-104.

Briese, M., B. Esmaeili*, et al.* (2005). "Is spinal muscular atrophy the result of defects in motor neuron processes?" Bioessays **27**(9): 946-57.

Briscoe, J. and J. Ericson (2001). "Specification of neuronal fates in the ventral neural tube." Curr Opin Neurobiol **11**(1): 43-9.

Brivanlou, A. H., F. H. Gage*, et al.* (2003). "Stem cells. Setting standards for human embryonic stem cells." Science **300**(5621): 913-6.

Brzustowicz, L. M., T. Lehner*, et al.* (1990). "Genetic mapping of chronic childhood-onset spinal muscular atrophy to chromosome 5q11.2-13.3." Nature **344**(6266): 540-1.

Burghes, A. H. (1997). "When is a deletion not a deletion? When it is converted." Am J Hum Genet **61**(1): 9-15.

Burghes, H. M. (2008). "Other forms of survival motor neuron protein and spinal muscular atrophy: an opinion." Neuromuscul Disord **18**(1): 82-3.

Bürglen, L., S. Lefebvre*, et al.* (1996). "Structure and organization of the human survival motor neurone (SMN) gene." Genomics **32**(3): 479-82.

Burkhardt, M. F., F. J. Martinez*, et al.* (2013). "A cellular model for sporadic ALS using patient-derived induced pluripotent stem cells." Mol Cell Neurosci **56C**: 355-364.

Burlet, P., C. Huber*, et al.* (1998). "The distribution of SMN protein complex in human fetal tissues and its alteration in spinal muscular atrophy." Hum Mol Genet **7**(12): 1927-33.

Burnett, B. G., E. Munoz*, et al.* (2009). "Regulation of SMN protein stability." Mol Cell Biol **29**(5): 1107-15.

Butchbach, M. E., J. D. Edwards*, et al.* (2007). "Abnormal motor phenotype in the SMNDelta7 mouse model of spinal muscular atrophy." Neurobiol Dis **27**(2): 207-19.

Campbell, K. and M. Götz (2002). "Radial glia: multi-purpose cells for vertebrate brain development." Trends Neurosci **25**(5): 235-8.

Campbell, M. J. and J. H. Morrison (1989). "Monoclonal antibody to neurofilament protein (SMI-32) labels a subpopulation of pyramidal neurons in the human and monkey neocortex." J Comp Neurol **282**(2): 191-205.

Carissimi, C., L. Saieva*, et al.* (2006). "Gemin8 is a novel component of the survival motor neuron complex and functions in snRNP assembly." J Biol Chem.

Carlson, B. M. (1999). Human Embryology & Developmental Biology 2nd ed., Elsevier Mosby.

Carpenter, M. B. (1991). Core Text of Neuroanatomy, 4th ed. Baltimore, MD, USA, Williams & Wilkins.

Carriedo, S. G., H. Z. Yin*, et al.* (1996). "Motor neurons are selectively vulnerable to AMPA/kainate receptor-mediated injury in vitro." J Neurosci **16**(13): 4069-79.

Cartegni, L. and A. R. Krainer (2002). "Disruption of an SF2/ASF-dependent exonic splicing enhancer in SMN2 causes spinal muscular atrophy in the absence of SMN1." Nat Genet **30**(4): 377-84.

Carvalho, T., F. Almeida*, et al.* (1999). "The spinal muscular atrophy disease gene product, SMN: A link between snRNP biogenesis and the Cajal (coiled) body." J Cell Biol **147**(4): 715-28.

Cauchi, R. J. (2010). "SMN and Gemins: 'we are family' ... or are we?: insights into the partnership between Gemins and the spinal muscular atrophy disease protein SMN." Bioessays **32**(12): 1077-89.

Chambers, S. M., C. A. Fasano*, et al.* (2009). "Highly efficient neural conversion of human ES and iPS cells by dual inhibition of SMAD signaling." Nat Biotechnol **27**(3): 275-80.

Chan, E. M., S. Ratanasirintrawoot*, et al.* (2009). "Live cell imaging distinguishes *bona fide* human iPS cells from partially reprogrammed cells." Nat Biotechnol **27**(11): 1033-7.

Chan, Y. B., I. Miguel-Aliaga*, et al.* (2003). "Neuromuscular defects in a Drosophila survival motor neuron gene mutant." Hum Mol Genet **12**(12): 1367-76.

Chang, H. C., D. N. Dimlich*, et al.* (2008). "Modeling spinal muscular atrophy in Drosophila." PLoS One **3**(9): e3209.

Chang, H. C., W. C. Hung*, et al.* (2004). "Degradation of survival motor neuron (SMN) protein is mediated via the ubiquitin/proteasome pathway." Neurochem Int **45**(7): 1107-12.

Chang, T., W. Zheng*, et al.* (2011). "Brief report: phenotypic rescue of induced pluripotent stem cell-derived motoneurons of a spinal muscular atrophy patient." Stem Cells **29**(12): 2090-3.

Chen, T. H., C. C. Tzeng*, et al.* (2011). "Identification of bidirectional gene conversion between SMN1 and SMN2 by simultaneous analysis of SMN dosage and hybrid genes in a Chinese population." J Neurol Sci **308**(1-2): 83-7.

Cifuentes-Diaz, C., S. Nicole*, et al.* (2002). "Neurofilament accumulation at the motor endplate and lack of axonal sprouting in a spinal muscular atrophy mouse model." Hum Mol Genet **11**(12): 1439-47.

Clelland, A. K., N. P. Kinnear*, et al.* (2009). "The SMN protein is a key regulator of nuclear architecture in differentiating neuroblastoma cells." Traffic **10**(11): 1585-98.

Cobb, M. S., F. F. Rose*, et al.* (2013). "Development and characterization of an SMN2-based intermediate mouse model of Spinal Muscular Atrophy." Hum Mol Genet **22**(9): 1843-55.

Cobben, J. M., H. H. Lemmink*, et al.* (2008). "Survival in SMA type I: a prospective analysis of 34 consecutive cases." Neuromuscul Disord **18**(7): 541-4.

Conrad, R., S. Jablonka, *et al.* (2011). "Lectin-based isolation and culture of mouse embryonic motoneurons." <u>J Vis Exp</u>(55).

Coovert, D. D., T. T. Le, *et al.* (1997). "The survival motor neuron protein in spinal muscular atrophy." <u>Hum Mol Genet</u> **6**(8): 1205-14.

Copp, A. J., N. D. Greene, *et al.* (2003). "The genetic basis of mammalian neurulation." <u>Nat Rev Genet</u> **4**(10): 784-93.

Corti, S., M. Nizzardo, *et al.* (2008). "Neural stem cell transplantation can ameliorate the phenotype of a mouse model of spinal muscular atrophy." <u>J Clin Invest</u> **118**(10): 3316-30.

Corti, S., M. Nizzardo, *et al.* (2010). "Embryonic stem cell-derived neural stem cells improve spinal muscular atrophy phenotype in mice." <u>Brain</u> **133**(Pt 2): 465-81.

Corti, S., M. Nizzardo, *et al.* (2012). "Genetic correction of human induced pluripotent stem cells from patients with spinal muscular atrophy." <u>Sci Transl Med</u> **4**(165): 165ra162.

Court, F. A., T. H. Gillingwater, *et al.* (2008). "Identity, developmental restriction and reactivity of extralaminar cells capping mammalian neuromuscular junctions." <u>J Cell Sci</u> **121**(Pt 23): 3901-11.

Cowan, C. A., J. Atienza, *et al.* (2005). "Nuclear reprogramming of somatic cells after fusion with human embryonic stem cells." <u>Science</u> **309**(5739): 1369-73.

Crawford, T. O. (2002). Spinal muscular atrophy. <u>Neuromuscular disorders of infancy and childhood, a clinician's approach</u>. Jones R, Darras BT and DeVivo DC. Woburn, MA, USA, Butterworth Heinemann.

Crawford, T. Q. and H. Roelink (2007). "The notch response inhibitor DAPT enhances neuronal differentiation in embryonic stem cell-derived embryoid bodies independently of sonic hedgehog signaling." <u>Dev Dyn</u> **236**(3): 886-92.

Curtis, M. A., M. Kam, *et al.* (2007). "Human neuroblasts migrate to the olfactory bulb via a lateral ventricular extension." <u>Science</u> **315**(5816): 1243-9.

Custer, S. K. and E. J. Androphy (2014). "Autophagy dysregulation in cell culture and animals models of spinal muscular atrophy." <u>Mol Cell Neurosci</u> **61**: 133-40.

Cutting, G. R. (2010). "Modifier genes in Mendelian disorders: the example of cystic fibrosis." <u>Ann N Y Acad Sci</u> **1214**: 57-69.

Czeizel, A. and J. Hamula (1989). "A Hungarian study on Werdnig-Hoffmann disease." <u>J Med Genet</u> **26**(12): 761-3.

D'Angelo, M. G. and N. Bresolin (2006). "Cognitive impairment in neuromuscular disorders." <u>Muscle Nerve</u> **34**(1): 16-33.

Damjanov (2000). <u>Pathology</u>, Saunders.

Darabi, R., R. W. Arpke, *et al.* (2012). "Human ES- and iPS-derived myogenic progenitors restore DYSTROPHIN and improve contractility upon transplantation in dystrophic mice." <u>Cell Stem Cell</u> **10**(5): 610-9.

Davis, H. E., J.R. Morgan, *et al.* (2002). "Polybrene increases retrovirus gene transfer efficiency by enhancing receptor-independent virus adsorption on target cell membranes." <u>Biophys Chem</u> **97**(2-3): 159-72.

Davis-Dusenbery, B. N., L. A. Williams, *et al.* (2014). "How to make spinal motor neurons." <u>Development</u> **141**(3): 491-501.

Delanote, V., J. Vandekerckhove, *et al.* (2005). "Plastins: versatile modulators of actin organization in (patho)physiological cellular processes." <u>Acta Pharmacol Sin</u> **26**(7): 769-79.

Dent, E. W. and F. B. Gertler (2003). "Cytoskeletal dynamics and transport in growth cone motility and axon guidance." <u>Neuron</u> **40**(2): 209-27.

DiDonato, C. J., X. N. Chen, *et al.* (1997). "Cloning, characterization, and copy number of the murine survival motor neuron gene: homolog of the spinal muscular atrophy-determining gene." <u>Genome Res</u> **7**(4): 339-52.

Diez del Corral, R., I. Olivera-Martinez, *et al.* (2003). "Opposing FGF and retinoid pathways control ventral neural pattern, neuronal differentiation, and segmentation during body axis extension." <u>Neuron</u> **40**(1): 65-79.

Dimitriadi, M., J. N. Sleigh, *et al.* (2010). "Conserved genes act as modifiers of invertebrate SMN loss of function defects." <u>PLoS Genet</u> **6**(10): e1001172.

Dimos, J. T., K. T. Rodolfa, *et al.* (2008). "Induced pluripotent stem cells generated from patients with ALS can be differentiated into motor neurons." <u>Science</u> **321**(5893): 1218-21.

Ding, Q., Y. K. Lee, *et al.* (2013). "A TALEN genome-editing system for generating human stem cell-based disease models." <u>Cell Stem Cell</u> **12**(2): 238-51.

Dominguez, E., T. Marais, *et al.* (2011). "Intravenous scAAV9 delivery of a codon-optimized SMN1 sequence rescues SMA mice." <u>Hum Mol Genet</u> **20**(4): 681-93.

Donnelly, C. J., M. Park, *et al.* (2013). "Axonally synthesized beta-actin and GAP-43 proteins support distinct modes of axonal growth." <u>J Neurosci</u> **33**(8): 3311-22.

Duester, G. (2008). "Retinoic acid synthesis and signaling during early organogenesis." <u>Cell</u> **134**(6): 921-31.

Ebert, A. D., J. Yu, *et al.* (2009). "Induced pluripotent stem cells from a spinal muscular atrophy patient." <u>Nature</u> **457**(7227): 277-80.

Eggert, C., A. Chari, *et al.* (2006). "Spinal muscular atrophy: the RNP connection." <u>Trends Mol Med</u>.

Elkabetz, Y., G. Panagiotakos, *et al.* (2008). "Human ES cell-derived neural rosettes reveal a functionally distinct early neural stem cell stage." <u>Genes Dev</u> **22**(2): 152-65.

Emery, A. E. (1991). "Population frequencies of inherited neuromuscular diseases--a world survey." <u>Neuromuscul Disord</u> **1**(1): 19-29.

Ericson, J., S. Morton, *et al.* (1996). "Two critical periods of Sonic Hedgehog signaling required for the specification of motor neuron identity." <u>Cell</u> **87**(4): 661-73.

Eriksson, P. S., E. Perfilieva, *et al.* (1998). "Neurogenesis in the adult human hippocampus." <u>Nat Med</u> **4**(11): 1313-7.

Esteban, M. A., J. Xu, *et al.* (2009). "Generation of induced pluripotent stem cell lines from Tibetan miniature pig." <u>J Biol Chem</u> **284**(26): 17634-40.

Evans, M. J. and M. H. Kaufman (1981). "Establishment in culture of pluripotential cells from mouse embryos." <u>Nature</u> **292**(5819): 154-6.

Fallini, C., G. J. Bassell, *et al.* (2012). "Spinal muscular atrophy: the role of SMN in axonal mRNA regulation." <u>Brain Res</u> **1462**: 81-92.

Fallini, C., J. P. Rouanet, *et al.* (2013). "Dynamics of survival of motor neuron (SMN) protein interaction with the mRNA-binding protein IMP1 facilitates its trafficking into motor neuron axons." <u>Dev Neurobiol</u>.

Fallini, C., H. Zhang, *et al.* (2011). "The survival of motor neuron (SMN) protein interacts with the mRNA-binding protein HuD and regulates localization of poly(A) mRNA in primary motor neuron axons." <u>J Neurosci</u> **31**(10): 3914-25.

Fan, L. and L. R. Simard (2002). "Survival motor neuron (SMN) protein: role in neurite outgrowth and neuromuscular maturation during neuronal differentiation and development." <u>Hum Mol Genet</u> **11**(14): 1605-14.

Farrar, M. A., S. Vucic, *et al.* (2012). "Corticomotoneuronal integrity and adaptation in spinal muscular atrophy." <u>Arch Neurol</u> **69**(4): 467-73.

Felderhoff-Mueser, U., K. Grohmann, *et al.* (2002). "Severe spinal muscular atrophy variant associated with congenital bone fractures." <u>J Child Neurol</u> **17**(9): 718-21.

Feldkötter, M., V. Schwarzer, *et al.* (2002). "Quantitative analyses of SMN1 and SMN2 based on real-time lightCycler PCR: fast and highly reliable carrier testing and prediction of severity of spinal muscular atrophy." <u>Am J Hum Genet</u> **70**(2): 358-68.

Feng, Z. and C. P. Ko (2008). "Schwann cells promote synaptogenesis at the neuromuscular junction via transforming growth factor-beta1." <u>J Neurosci</u> **28**(39): 9599-609.

Fidzianska, A. and J. Rafalowska (2002). "Motoneuron death in normal and spinal muscular atrophy-affected human fetuses." <u>Acta Neuropathol (Berl)</u> **104**(4): 363-8.

Finsterer, J. and C. Stöllberger (1999). "Cardiac involvement in Werdnig-Hoffmann's spinal muscular atrophy." <u>Cardiology</u> **92**(3): 178-82.

Foust, K. D., X. Wang, *et al.* (2010). "Rescue of the spinal muscular atrophy phenotype in a mouse model by early postnatal delivery of SMN." <u>Nat Biotechnol</u> **28**(3): 271-4.

Fredericksen, B. L., B.L. Wei, *et al.* (2002). "Inhibition of endosomal/lysosomal degradation increases the infectivity of human immunodeficiency virus." <u>J Virol</u> **76**(22): 11440-6.

Fusaki, N., H. Ban*, et al.* (2009). "Efficient induction of transgene-free human pluripotent stem cells using a vector based on Sendai virus, an RNA virus that does not integrate into the host genome." <u>Proc Jpn Acad Ser B Phys Biol Sci</u> **85**(8): 348-62.

Gabanella, F., M. E. Butchbach*, et al.* (2007). "Ribonucleoprotein assembly defects correlate with spinal muscular atrophy severity and preferentially affect a subset of spliceosomal snRNPs." <u>PLoS One</u> **2**(9): e921.

Gage, F. H. (2002). "Neurogenesis in the adult brain." <u>J Neurosci</u> **22**(3): 612-3.

Garbes, L., L. Heesen*, et al.* (2013). "VPA response in SMA is suppressed by the fatty acid translocase CD36." <u>Hum Mol Genet</u> **22**(2): 398-407.

Garcera, A., N. Bahi, *et al.* (2013). "Survival motor neuron protein reduction deregulates autophagy in spinal cord motoneurons *in vitro*." <u>Cell Death Dis</u> **4**: e686

Gavrilina, T. O., V. L. McGovern*, et al.* (2008). "Neuronal SMN expression corrects spinal muscular atrophy in severe SMA mice while muscle-specific SMN expression has no phenotypic effect." <u>Hum Mol Genet</u> **17**(8): 1063-75.

Ghule, P. N., Z. Dominski*, et al.* (2008). "Staged assembly of histone gene expression machinery at subnuclear foci in the abbreviated cell cycle of human embryonic stem cells." <u>Proc Natl Acad Sci U S A</u> **105**(44): 16964-9.

Giavazzi, A., V. Setola*, et al.* (2006). "Neuronal-specific roles of the survival motor neuron protein: evidence from survival motor neuron expression patterns in the developing human central nervous system." <u>J Neuropathol Exp Neurol</u> **65**(3): 267-77.

Glascock, J. J., M. Shababi*, et al.* (2012). "Direct central nervous system delivery provides enhanced protection following vector mediated gene replacement in a severe model of spinal muscular atrophy." <u>Biochem Biophys Res Commun</u> **417**(1): 376-81.

Glinka, M., T. Herrmann*, et al.* (2010). "The heterogeneous nuclear ribonucleoprotein-R is necessary for axonal beta-actin mRNA translocation in spinal motor neurons." <u>Hum Mol Genet</u> **19**(10): 1951-66.

Gogliotti, R. G., K. A. Quinlan*, et al.* (2012). "Motor neuron rescue in spinal muscular atrophy mice demonstrates that sensory-motor defects are a consequence, not a cause, of motor neuron dysfunction." <u>J Neurosci</u> **32**(11): 3818-29.

Golestaneh, N., M. Kokkinaki*, et al.* (2009). "Pluripotent stem cells derived from adult human testes." <u>Stem Cells Dev</u> **18**(8): 1115-26.

Gowing, G. and C. N. Svendsen (2011). "Stem cell transplantation for motor neuron disease: current approaches and future perspectives." <u>Neurotherapeutics</u> **8**(4): 591-606.

Grzeschik, S. M., M. Ganta*, et al.* (2005). "Hydroxyurea enhances SMN2 gene expression in spinal muscular atrophy cells." <u>Ann Neurol</u> **58**(2): 194-202.

Gubitz, A. K., W. Feng*, et al.* (2004). "The SMN complex." <u>Exp Cell Res</u> **296**(1): 51-6.

Guo, X., M. Das*, et al.* (2011). "Neuromuscular junction formation between human stem-cell-derived motoneurons and rat skeletal muscle in a defined system." <u>Tissue Eng Part C Methods</u> **16**(6): 1347-55.

Gurdon, J. B. (1962). "The transplantation of nuclei between two species of Xenopus." <u>Dev Biol</u> **5**: 68-83.

Hahnen, E., J. Schönling, *et al.* (1996). "Hybrid survival motor neuron genes in patients with autosomal recessive spinal muscular atrophy: new insights into molecular mechanisms responsible for the disease." <u>Am J Hum Genet</u> **59**(5): 1057-65.

Hamilton, G. and T. H. Gillingwater (2013). "Spinal muscular atrophy: going beyond the motor neuron." <u>Trends Mol Med</u> **19**(1): 40-50.

Hammond, S. M., R. G. Gogliotti*, et al.* (2010). "Mouse survival motor neuron alleles that mimic SMN2 splicing and are inducible rescue embryonic lethality early in development but not late." <u>PLoS One</u> **5**(12): e15887.

Han, X., J. Han*, et al.* (2011). "Generation of induced pluripotent stem cells from bovine embryonic fibroblast cells." <u>Cell Res</u> **21**(10): 1509-12.

Hanahan, D. (1983). "Studies on transformation of Escherichia coli with plasmids." J Mol Biol **166**(4): 557-80.

Hanna, J., S. Markoulaki*, et al.* (2008). "Direct reprogramming of terminally differentiated mature B lymphocytes to pluripotency." Cell **133**(2): 250-64.

Hanna, J., M. Wernig*, et al.* (2007). "Treatment of sickle cell anemia mouse model with iPS cells generated from autologous skin." Science **318**(5858): 1920-3.

Hao le, T., M. Wolman*, et al.* (2012). "Survival motor neuron affects plastin 3 protein levels leading to motor defects." J Neurosci **32**(15): 5074-84.

Hardingham, G. E., R. Patani*, et al.* (2010). "Human embryonic stem cell-derived neurons as a tool for studying neuroprotection and neurodegeneration." Mol Neurobiol **42**(1): 97-102.

Hargus, G., M. Ehrlich, *et al.* (2013). "Human stem cell models of neurodegeneration: a novel approach to study mechanisms of disease development." Acta Neuropathol **127**(2): 151-73.

Harland, R. and J. Gerhart (1997). "Formation and function of Spemann's organizer." Annu Rev Cell Dev Biol **13**: 611-67.

Hayashi, M., S. Araki*, et al.* (2002). "Oxidative stress and disturbed glutamate transport in spinal muscular atrophy." Brain Dev **24**(8): 770-5.

Hayashi, Y., T. Chan*, et al.* (2010). "Reduction of N-glycolylneuraminic acid in human induced pluripotent stem cells generated or cultured under feeder- and serum-free defined conditions." PLoS One **5**(11): e14099.

HD iPSC Consortium (2012). "Induced pluripotent stem cells from patients with Huntington's disease show CAG-repeat-expansion-associated phenotypes." Cell Stem Cell **11**(2): 264-78.

He, Q., C. Lowrie*, et al.* (2005). "Inherited motor neuron disease in domestic cats: a model of spinal muscular atrophy." Pediatr Res **57**(3): 324-30.

Helmken, C., Y. Hofmann, *et al.* (2003). "Evidence for a modifying pathway in SMA discordant families: reduced SMN level decreases the amount of its interacting partners and Htra2-beta1." Hum Genet **114**(1)

Helmken, C. and B. Wirth (2000). "Exclusion of Htra2-beta1, an up-regulator of full-length SMN2 transcript, as a modifying gene for spinal muscular atrophy." Hum Genet **107**(6): 554-8.

Helms, A. W. and J. E. Johnson (2003). "Specification of dorsal spinal cord interneurons." Curr Opin Neurobiol **13**(1): 42-9.

Hendrickson, B. C., C. Donohoe*, et al.* (2009). "Differences in SMN1 allele frequencies among ethnic groups within North America." J Med Genet **46**(9): 641-4.

Hirata, T., A. Iida, *et al.* (2002). "An improved method for recovery of F-defective Sendai virus expressing foreign genes from cloned cDNA." J Virol Methods **104**(2): 125-33.

Hochedlinger, K. and R. Jaenisch (2003). "Nuclear transplantation, embryonic stem cells, and the potential for cell therapy." N Engl J Med **349**(3): 275-86.

Holt, C. E. and S. L. Bullock (2009). "Subcellular mRNA localization in animal cells and why it matters." Science **326**(5957): 1212-6.

Horii, T., D. Tamura*, et al.* (2013). "Generation of an ICF syndrome model by efficient genome editing of human induced pluripotent stem cells using the CRISPR system." Int J Mol Sci **14**(10): 19774-81.

Hsieh-Li, H. M., J. G. Chang*, et al.* (2000). "A mouse model for spinal muscular atrophy." Nat Genet **24**(1): 66-70.

Hsu, Y. C., D. C. Lee*, et al.* (2007). "Neural stem cells, neural progenitors, and neurotrophic factors." Cell Transplant **16**(2): 133-50.

Hu, B. Y. and S. C. Zhang (2009). "Differentiation of spinal motor neurons from pluripotent human stem cells." Nat Protoc **4**(9): 1295-304.

Hua, Y., K. Sahashi *et al.* (2011). "Peripheral SMN restoration is essential for long-term rescue of a severe spinal muscular atrophy mouse model." Nature **478**(7367): 123-6.

Huangfu, D., K. Osafune*, et al.* (2008). "Induction of pluripotent stem cells from primary human fibroblasts with only Oct4 and Sox2." Nat Biotechnol **26**(11): 1269-75.

Hubers, L., H. Valderrama-Carvajal*, et al.* (2010). "HuD interacts with survival motor neuron protein and can rescue spinal muscular atrophy-like neuronal defects." Hum Mol Genet **20**(3): 553-79.

Hunter, G., A. Aghamaleky Sarvestany, *et al.* (2014). "SMN-dependent intrinsic defects in Schwann cells in mouse models of spinal muscular atrophy." Hum Mol Genet **23**(9): 2235-50.

Hussein, S. M., N. N. Batada*, et al.* (2011). "Copy number variation and selection during reprogramming to pluripotency." Nature **471**(7336): 58-62.

Inoue, M., Y. Tokusumi*, et al.* (2003). "Nontransmissible virus-like particle formation by F-deficient sendai virus is temperature sensitive and reduced by mutations in M and HN proteins." J Virol **77**(5): 3238-46.

Israel, M. A., S. H. Yuan*, et al.* (2012). "Probing sporadic and familial Alzheimer's disease using induced pluripotent stem cells." Nature **482**(7384): 216-20.

Ito, D., H. Okano*, et al.* (2012). "Accelerating progress in induced pluripotent stem cell research for neurological diseases." Ann Neurol **72**(2): 167-74.

Ito, Y., S. Kumada*, et al.* (2004). "Thalamic lesions in a long-surviving child with spinal muscular atrophy type I: MRI and EEG findings." Brain Dev **26**(1): 53-6.

Ito, Y., N. Shibata*, et al.* (2011). "New insights into the pathogenesis of spinal muscular atrophy." Brain Dev **33**(4): 321-31.

Itskovitz-Eldor, J., M. Schuldiner*, et al.* (2000). "Differentiation of human embryonic stem cells into embryoid bodies compromising the three embryonic germ layers." Mol Med **6**(2): 88-95.

Jablonka, S., M. Beck*, et al.* (2007). "Defective Ca2+ channel clustering in axon terminals disturbs excitability in motoneurons in spinal muscular atrophy." J Cell Biol **179**(1): 139-49.

Jablonka, S., B. Dombert*, et al.* (2013). "Mechanisms for axon maintenance and plasticity in motoneurons: alterations in motoneuron disease." J Anat.

Jády, B. E., X. Darzacq*, et al.* (2003). "Modification of Sm small nuclear RNAs occurs in the nucleoplasmic Cajal body following import from the cytoplasm." Embo J **22**(8): 1878-88.

Jaeger, J. and J. Reinitz (2006). "On the dynamic nature of positional information." Bioessays **28**(11): 1102-11.

Jaenisch, R. and R. Young (2008). "Stem cells, the molecular circuitry of pluripotency and nuclear reprogramming." Cell **132**(4): 567-82.

James, D., S. A. Noggle*, et al.* (2006). "Contribution of human embryonic stem cells to mouse blastocysts." Dev Biol **295**(1): 90-102.

Jarecki, J., X. Chen*, et al.* (2005). "Diverse small-molecule modulators of SMN expression found by high-throughput compound screening: early leads towards a therapeutic for spinal muscular atrophy." Hum Mol Genet **14**(14): 2003-18.

Jessell, T. M. (2000). "Neuronal specification in the spinal cord: inductive signals and transcriptional codes." Nat Rev Genet **1**(1): 20-9.

Johannessen, C. U. (2000). "Mechanisms of action of valproate: a commentary." Neurochem Int **37**(2-3): 103-10.

Kaji, K., K. Norrby*, et al.* (2009). "Virus-free induction of pluripotency and subsequent excision of reprogramming factors." Nature **458**(7239): 771-5.

Kallos, M. (2011). Embryonic Stem Cells - Basic Biology to Bioengineering, InTech.

Kanagawa, M. and T. Toda (2006). "The genetic and molecular basis of muscular dystrophy: roles of cell-matrix linkage in the pathogenesis." J Hum Genet **51**(11): 915-26.

Kanatsu-Shinohara, M., K. Inoue*, et al.* (2004). "Generation of pluripotent stem cells from neonatal mouse testis." Cell **119**(7): 1001-12.

Kariya, S., T. Obis*, et al.* (2014). "Requirement of enhanced Survival Motoneuron protein imposed during neuromuscular junction maturation." J Clin Invest **124**(2): 785-800.

Kariya, S., G. H. Park*, et al.* (2008). "Reduced SMN protein impairs maturation of the neuromuscular junctions in mouse models of spinal muscular atrophy." Hum Mol Genet **17**(16): 2552-69.

Karumbayaram, S., B. G. Novitch*, et al.* (2009). "Directed differentiation of human-induced pluripotent stem cells generates active motor neurons." Stem Cells **27**(4): 806-11.

Kashima, T. and J. L. Manley (2003). "A negative element in SMN2 exon 7 inhibits splicing in spinal muscular atrophy." Nat Genet **34**(4): 460-3.

Kim, D., C. H. Kim*, et al.* (2009a). "Generation of human induced pluripotent stem cells by direct delivery of reprogramming proteins." Cell Stem Cell **4**(6): 472-6.

Kim, D. S., J. S. Lee*, et al.* (2010a). "Robust enhancement of neural differentiation from human ES and iPS cells regardless of their innate difference in differentiation propensity." <u>Stem Cell Rev</u> **6**(2): 270-81.

Kim, J. B., B. Greber, *et al.* (2009b). "Direct reprogramming of human neural stem cells by OCT4." <u>Nature</u> **461**(7264): 649-3.

Kim, J. B., H. Zaehres*, et al.* (2008). "Pluripotent stem cells induced from adult neural stem cells by reprogramming with two factors." <u>Nature</u> **454**(7204): 646-50.

Kim, K., A. Doi*, et al.* (2010b). "Epigenetic memory in induced pluripotent stem cells." <u>Nature</u> **467**(7313): 285-90.

Kissel, J. T., C.B. Scott *et al.* (2011). "SMA CARNIVAL TRIAL PART II: a prospective, single-armed trial of L-carnitine and valproic acid in ambulatory children with spinal muscular atrophy." <u>PLoS One</u> **6**(7): e21296.

Ko, K., N. Tapia*, et al.* (2009). "Induction of pluripotency in adult unipotent germline stem cells." <u>Cell Stem Cell</u> **5**(1): 87-96.

Koch, P., P. Breuer*, et al.* (2011). "Excitation-induced ataxin-3 aggregation in neurons from patients with Machado-Joseph disease." <u>Nature</u> **480**(7378): 543-6.

Koch, P., T. Opitz*, et al.* (2009). "A rosette-type, self-renewing human ES cell-derived neural stem cell with potential for in vitro instruction and synaptic integration." <u>Proc Natl Acad Sci U S A</u> **106**(9): 3225-30.

Kong, L., X. Wang*, et al.* (2009). "Impaired synaptic vesicle release and immaturity of neuromuscular junctions in spinal muscular atrophy mice." <u>J Neurosci</u> **29**(3): 842-51.

Krencik, R. and S. C. Zhang (2011). "Directed differentiation of functional astroglial subtypes from human pluripotent stem cells." <u>Nat Protoc</u> **6**(11): 1710-7.

Ku, S., E. Soragni*, et al.* (2010). "Friedreich's ataxia induced pluripotent stem cells model intergenerational GAATTC triplet repeat instability." <u>Cell Stem Cell</u> **7**(5): 631-7.

Kugelberg, E. and L. Welander (1956). "Heredofamilial juvenile muscular atrophy simulating muscular dystrophy." <u>AMA Arch Neurol Psychiatry</u> **75**(5): 500-9.

Kwiatkowski, J. L., J. L. Rutkowski*, et al.* (1998). "Schwann cell-conditioned medium promotes neuroblastoma survival and differentiation." <u>Cancer Res</u> **58**(20): 4602-6.

Kwon, D. Y., W.W. Motley *et al.* (2011). "Increasing expression and decreasing degradation of SMN ameliorate the spinal muscular atrophy phenotype in mice." <u>Hum Mol Genet</u> **20**(18): 3667-77.

Kye, M. J., E. D. Niederst, *et al.* (2014). "SMN regulates axonal local translation via miR-183/mTOR pathway." <u>Hum Mol Genet</u>.

Laemmli, U. K. (1970). "Cleavage of structural proteins during the assembly of the head of bacteriophage T4." <u>Nature</u> **227**(5259): 680-5.

Landmesser, L. (1978). "The distribution of motoneurones supplying chick hind limb muscles." <u>J Physiol</u> **284**: 371-89.

Laurent, L. C., I. Ulitsky, *et al.* (2011). "Dynamic changes in the copy number of pluripotency and cell proliferation genes in human ESCs and iPSCs during reprogramming and time in culture." <u>Cell Stem Cell</u> **8**(1): 106-18.

Le, T. T., V. L. McGovern*, et al.* (2012). "Temporal requirement for high SMN expression in SMA mice." <u>Hum Mol Genet</u> **20**(18): 3578-91.

Le, T. T., L. T. Pham*, et al.* (2005). "SMNDelta7, the major product of the centromeric survival motor neuron (SMN2) gene, extends survival in mice with spinal muscular atrophy and associates with full-length SMN." <u>Hum Mol Genet</u> **14**(6): 845-57.

Lee, S. K. and S. L. Pfaff (2001). "Transcriptional networks regulating neuronal identity in the developing spinal cord." <u>Nat Neurosci</u> **4 Suppl**: 1183-91.

Lefebvre, S., L. Burglen*, et al.* (1995). "Identification and characterization of a spinal muscular atrophy-determining gene." <u>Cell</u> **80**(1): 155-65.

Lefebvre, S., P. Burlet, *et al.* (1997). "Correlation between severity and SMN protein level in spinal muscular atrophy." <u>Nat Genet</u> **16**(3): 265-9.

Leung, C. T., P. A. Coulombe*, et al.* (2007). "Contribution of olfactory neural stem cells to tissue maintenance and regeneration." <u>Nat Neurosci</u> **10**(6): 720-6.

Levine, A. J. and A. H. Brivanlou (2007). "Proposal of a model of mammalian neural induction." Dev Biol **308**(2): 247-56.

Li, W., W. Sun*, et al.* (2011). "Rapid induction and long-term self-renewal of primitive neural precursors from human embryonic stem cells by small molecule inhibitors." Proc Natl Acad Sci U S A **108**(20): 8299-304.

Li, X. J., Z. W. Du*, et al.* (2005). "Specification of motoneurons from human embryonic stem cells." Nat Biotechnol **23**(2): 215-21.

Li, X. J., B. Y. Hu*, et al.* (2008). "Directed differentiation of ventral spinal progenitors and motor neurons from human embryonic stem cells by small molecules." Stem Cells **26**(4): 886-93.

Liao, J., C. Cui*, et al.* (2009). "Generation of induced pluripotent stem cell lines from adult rat cells." Cell Stem Cell **4**(1): 11-5.

Lichtman, J. W. and H. Colman (2000). "Synapse elimination and indelible memory." Neuron **25**(2): 269-78.

Lin, C. S., R. H. Aebersold*, et al.* (1988). "Molecular cloning and characterization of plastin, a human leukocyte protein expressed in transformed human fibroblasts." Mol Cell Biol **8**(11): 4659-68.

Lin, C. S., Z. P. Chen*, et al.* (1993). "Characterization of the human L-plastin gene promoter in normal and neoplastic cells." J Biol Chem **268**(4): 2793-801.

Lin, C. S., A. Lau, *et al.* (1999). "Differential regulation of human T-plastin gene in leukocytes and non-leukocytes: identification of the promoter, enhancer, and CpG island." DNA Cell Biol **18**(1): 27-37.

Lin, C. S., W. Shen*, et al.* (1994). "Identification of I-plastin, a human fimbrin isoform expressed in intestine and kidney." Mol Cell Biol **14**(4): 2457-67.

Lin, W., H. B. Sanchez*, et al.* (2000). "Aberrant development of motor axons and neuromuscular synapses in erbB2-deficient mice." Proc Natl Acad Sci U S A **97**(3): 1299-304.

Lindl, T. (2002). Zell- & Gewebekultur, Spektrum Gustav Fischer.

Ling, K. K., M. Y. Lin*, et al.* (2010). "Synaptic defects in the spinal and neuromuscular circuitry in a mouse model of spinal muscular atrophy." PLoS One **5**(11): e15457.

Liu-Yesucevitz, L., G. J. Bassell*, et al.* (2011). "Local RNA translation at the synapse and in disease." J Neurosci **31**(45): 16086-93.

Liu, Q. and G. Dreyfuss (1996). "A novel nuclear structure containing the survival of motor neurons protein." Embo J **15**(14): 3555-65.

Liu, Q., U. Fischer*, et al.* (1997). "The spinal muscular atrophy disease gene product, SMN, and its associated protein SIP1 are in a complex with spliceosomal snRNP proteins." Cell **90**(6): 1013-21.

Liu, Y., P. Jiang*, et al.* (2011). "OLIG gene targeting in human pluripotent stem cells for motor neuron and oligodendrocyte differentiation." Nat Protoc **6**(5): 640-55.

Lorson, C. L., E. Hahnen*, et al.* (1999). "A single nucleotide in the SMN gene regulates splicing and is responsible for spinal muscular atrophy." Proc Natl Acad Sci U S A **96**(11): 6307-11.

Lorson, C. L., J. Strasswimmer*, et al.* (1998). "SMN oligomerization defect correlates with spinal muscular atrophy severity." Nat Genet **19**(1): 63-6.

Lorson, M. A. and C. L. Lorson (2012). "SMN-inducing compounds for the treatment of spinal muscular atrophy." Future Med Chem **4**(16): 2067-84.

Lorson, M. A., L. D. Spate*, et al.* (2011). "Disruption of the Survival Motor Neuron (SMN) gene in pigs using ssDNA." Transgenic Res.

Lotti, F., W. L. Imlach*, et al.* (2012). "An SMN-dependent U12 splicing event essential for motor circuit function." Cell **151**(2): 440-54.

Low, L. K. and H. J. Cheng (2006). "Axon pruning: an essential step underlying the developmental plasticity of neuronal connections." Philos Trans R Soc Lond B Biol Sci **361**(1473): 1531-44.

Lowery, L. A. and D. Van Vactor (2009). "The trip of the tip: understanding the growth cone machinery." Nat Rev Mol Cell Biol **10**(5): 332-43.

Ludwig, T. E., V. Bergendahl*, et al.* (2006). "Feeder-independent culture of human embryonic stem cells." Nat Methods **3**(8): 637-46.

Lunn, M. R., D. E. Root, *et al.* (2004). "Indoprofen upregulates the survival motor neuron protein through a cyclooxygenase-independent mechanism." <u>Chem Biol</u> **11**(11): 1489-93.

Luo, J., S. T. Suhr, *et al.* (2011). "Generation of leukemia inhibitory factor and basic fibroblast growth factor-dependent induced pluripotent stem cells from canine adult somatic cells." <u>Stem Cells Dev</u> **20**(10): 1669-78.

Luo, L. and D. D. O'Leary (2005). "Axon retraction and degeneration in development and disease." <u>Annu Rev Neurosci</u> **28**: 127-56.

Lutz, C. M., S. Kariya, *et al.* (2011). "Postsymptomatic restoration of SMN rescues the disease phenotype in a mouse model of severe spinal muscular atrophy." <u>J Clin Invest</u> **121**(8): 3029-41.

Lyon, A.N., R.H. Pineda, *et al.* (2013). "Calcium binding is essential for plastin 3 function in Smn-deficient motoneurons." <u>Hum Mol Genet</u> **23**(8): 1990-2004.

MacKenzie, A. (2012). "Sense in antisense therapy for spinal muscular atrophy." <u>N Engl J Med</u> **366**(8): 761-3.

MacLeod, M. J., J. E. Taylor, *et al.* (1999). "Prenatal onset spinal muscular atrophy." <u>Eur J Paediatr Neurol</u> **3**(2): 65-72.

Mahmoudi, S., S. Henriksson, *et al.* (2010). "WRAP53 is essential for Cajal body formation and for targeting the survival of motor neuron complex to Cajal bodies." <u>PLoS Biol</u> **8**(11): e1000521.

Mailman, M. D., J. W. Heinz, *et al.* (2002). "Molecular analysis of spinal muscular atrophy and modification of the phenotype by SMN2." <u>Genet Med</u> **4**(1): 20-6.

Manuel, M. and D. Zytnicki (2011). "Alpha, beta and gamma motoneurons: functional diversity in the motor system's final pathway." <u>J Integr Neurosci</u> **10**(3): 243-76.

Marchetto, M. C., A. R. Muotri, *et al.* (2008). "Non-cell-autonomous effect of human SOD1 G37R astrocytes on motor neurons derived from human embryonic stem cells." <u>Cell Stem Cell</u> **3**(6): 649-57.

Marklund, U., Z. Alekseenko, *et al.* (2014). "Detailed expression analysis of regulatory genes in the early developing human neural tube." <u>Stem Cells Dev</u> **23**(1): 5-15.

Markowitz, J. A., P. Singh, *et al.* (2012). "Spinal muscular atrophy: a clinical and research update." <u>Pediatr Neurol</u> **46**(1): 1-12.

Markowitz, J. A., M. B. Tinkle, *et al.* (2004). "Spinal muscular atrophy in the neonate." <u>J Obstet Gynecol Neonatal Nurs</u> **33**(1): 12-20.

Marti, E., D. A. Bumcrot, *et al.* (1995). "Requirement of 19K form of Sonic hedgehog for induction of distinct ventral cell types in CNS explants." <u>Nature</u> **375**(6529): 322-5.

Martínez-Hernández, R., S. Bernal, *et al.* (2013). "Synaptic defects in type I spinal muscular atrophy in human development." <u>J Pathol</u> **229**(1): 49-61.

Mas, C. and A. Ruiz i Altaba (2010). "Small molecule modulation of HH-GLI signaling: current leads, trials and tribulations." <u>Biochem Pharmacol</u> **80**(5): 712-23.

Mattis, V. B., A.D. Ebert *et al.* (2009). "Delivery of a read-through inducing compound, TC007, lessens the severity of a spinal muscular atrophy animal model." <u>Hum Mol Genet</u> **18**(20): 3906-13.

Mattis, V. B., C.W. Tom Chang *et al.* (2012). "Analysis of a read-through promoting compound in a severe mouse model of spinal muscular atrophy." <u>Neurosci Lett</u> **525**(1): 72-5.

McGivern, J. V., T.N. Patitucci, *et al.* (2013). "Spinal muscular atrophy astrocytes exhibit abnormal calcium regulation and reduced growth factor production." <u>Glia</u> **61**(9): 1418-28.

McGovern, V. L., T. O. Gavrilina, *et al.* (2008). "Embryonic motor axon development in the severe SMA mouse." <u>Hum Mol Genet</u> **17**(18): 2900-9.

McWhorter, M. L., K. L. Boon, *et al.* (2008). "The SMN binding protein Gemin2 is not involved in motor axon outgrowth." <u>Dev Neurobiol</u> **68**(2): 182-94.

McWhorter, M. L., U. R. Monani, *et al.* (2003). "Knockdown of the survival motor neuron (Smn) protein in zebrafish causes defects in motor axon outgrowth and pathfinding." <u>J Cell Biol</u> **162**(5): 919-31.

Meister, G., D. Buhler, *et al.* (2000). "Characterization of a nuclear 20S complex containing the survival of motor neurons (SMN) protein and a specific subset of spliceosomal Sm proteins." <u>Hum Mol Genet</u> **9**(13): 1977-86.

Meister, G., D. Buhler*, et al.* (2001). "A multiprotein complex mediates the ATP-dependent assembly of spliceosomal U snRNPs." Nat Cell Biol **3**(11): 945-9.

Melki, J., P. Sheth*, et al.* (1990). "Mapping of acute (type I) spinal muscular atrophy to chromosome 5q12-q14. The French Spinal Muscular Atrophy Investigators." Lancet **336**(8710): 271-3.

Mentis, G. Z., D. Blivis*, et al.* (2011). "Early functional impairment of sensory-motor connectivity in a mouse model of spinal muscular atrophy." Neuron **69**(3): 453-67.

Meshorer, E. and T. Misteli (2006). "Chromatin in pluripotent embryonic stem cells and differentiation." Nat Rev Mol Cell Biol **7**(7): 540-6.

Michalczyk, K. and M. Ziman (2005). "Nestin structure and predicted function in cellular cytoskeletal organisation." Histol Histopathol **20**(2): 665-71.

Miguel-Aliaga, I., E. Culetto*, et al.* (1999). "The Caenorhabditis elegans orthologue of the human gene responsible for spinal muscular atrophy is a maternal product critical for germline maturation and embryonic viability." Hum Mol Genet **8**(12): 2133-43.

Mikkelsen, T. S., J. Hanna*, et al.* (2008). "Dissecting direct reprogramming through integrative genomic analysis." Nature **454**(7200): 49-55.

Mitsui, K., Y. Tokuzawa*, et al.* (2003). "The homeoprotein Nanog is required for maintenance of pluripotency in mouse epiblast and ES cells." Cell **113**(5): 631-42.

Miura, K., Y. Okada*, et al.* (2009). "Variation in the safety of induced pluripotent stem cell lines." Nat Biotechnol **27**(8): 743-5.

Miyoshi, N., H. Ishii*, et al.* (2011). "Reprogramming of mouse and human cells to pluripotency using mature microRNAs." Cell Stem Cell **8**(6): 633-8.

Monani, U. R., M. Sendtner*, et al.* (2000). "The human centromeric survival motor neuron gene (SMN2) rescues embryonic lethality in Smn(-/-) mice and results in a mouse with spinal muscular atrophy." Hum Mol Genet **9**(3): 333-9.

Montes, J., A. M. Gordon*, et al.* (2009). "Clinical outcome measures in spinal muscular atrophy." J Child Neurol **24**(8): 968-78.

Morimoto, Y., M. Kato-Negishi, *et al.* (2013). "Three-dimensional neuron-muscle constructs with neuromuscular junctions." Biomaterials **34**(37): 9413-9.

Mullis, K. B., F. Faloona*, et al.* (1986). "Specific enzymatic amplification of DNA in vitro: the polymerase chain reaction." Cold Spring Harbor Symposium, Quant Biol(51): 263-273.

Muñoz-Sanjuán, I. and H. B. A (2001). "Early posterior/ventral fate specification in the vertebrate embryo." Dev Biol **237**(1): 1-17.

Munsat, T. L. and K. E. Davies (1992). "International SMA consortium meeting. (26-28 June 1992, Bonn, Germany)." Neuromuscul Disord **2**(5-6): 423-8.

Murray, L. M., L. H. Comley*, et al.* (2008). "Selective vulnerability of motor neurons and dissociation of pre- and post-synaptic pathology at the neuromuscular junction in mouse models of spinal muscular atrophy." Hum Mol Genet **17**(7): 949-62.

Mutsaers, C. A., T. M. Wishart*, et al.* (2011). "Reversible molecular pathology of skeletal muscle in spinal muscular atrophy." Hum Mol Genet **20**(22): 4334-44.

Nagy, K., H. K. Sung*, et al.* (2011). "Induced pluripotent stem cell lines derived from equine fibroblasts." Stem Cell Rev **7**(3): 693-702.

Nakagawa, M., M. Koyanagi*, et al.* (2008). "Generation of induced pluripotent stem cells without Myc from mouse and human fibroblasts." Nat Biotechnol **26**(1): 101-6.

Narver, H. L., L. Kong*, et al.* (2008). "Sustained improvement of spinal muscular atrophy mice treated with trichostatin A plus nutrition." Ann Neurol **64**(4): 465-70.

Naryshkin, N. A., M. Weetall, *et al.* (2014). "Motor neuron disease. SMN2 splicing modifiers improve motor function and longevity in mice with spinal muscular atrophy." Science **345**(6197): 688-93.

Naujock, M., N. Stanslowsky, *et al.* (2014). "Molecular and functional analyses of motor neurons generated from human cord blood derived induced pluripotent stem cells." Stem Cells Dev.

Navascues, J., M. T. Berciano, *et al.* (2004). "Targeting SMN to Cajal bodies and nuclear gems during neuritogenesis." Chromosoma **112**(8): 398-409.

Nguyen, H. N., B. Byers*, et al.* (2011). "LRRK2 mutant iPSC-derived DA neurons demonstrate increased susceptibility to oxidative stress." Cell Stem Cell **8**(3): 267-80.

Nichols, J., B. Zevnik*, et al.* (1998). "Formation of pluripotent stem cells in the mammalian embryo depends on the POU transcription factor Oct4." Cell **95**(3): 379-91.

Nieuwkoop, P. D. (1952). "Activation and organization of the central nervous system in amphibians." J. Exp. Zool. **120**(1): 1–108

Nishimura, K., M. Sano*, et al.* (2011). "Development of defective and persistent Sendai virus vector: a unique gene delivery/expression system ideal for cell reprogramming." J Biol Chem **286**(6): 4760-71.

Ohi, Y., H. Qin*, et al.* (2011). "Incomplete DNA methylation underlies a transcriptional memory of somatic cells in human iPS cells." Nat Cell Biol **13**(5): 541-9.

Okita, K., T. Ichisaka*, et al.* (2007). "Generation of germline-competent induced pluripotent stem cells." Nature **448**(7151): 313-7.

Okita, K., M. Nakagawa*, et al.* (2008). "Generation of mouse induced pluripotent stem cells without viral vectors." Science **322**(5903): 949-53.

Okita, K. and S. Yamanaka (2011). "Induced pluripotent stem cells: opportunities and challenges." Philos Trans R Soc Lond B Biol Sci **366**(1575): 2198-207.

Oprea, G. E., S. Kröber*, et al.* (2008). "Plastin 3 is a protective modifier of autosomal recessive spinal muscular atrophy." Science **320**(5875): 524-7.

Ory, D. S., B. A. Neugeboren*, et al.* (1996). "A stable human-derived packaging cell line for production of high titer retrovirus/vesicular stomatitis virus G pseudotypes." Proc Natl Acad Sci U S A **93**(21): 11400-6.

Osafune, K., L. Caron*, et al.* (2008). "Marked differences in differentiation propensity among human embryonic stem cell lines." Nat Biotechnol **26**(3): 313-5.

Osman, E. Y., P. F. Yen*, et al.* (2012). "Bifunctional RNAs targeting the intronic splicing silencer N1 increase SMN levels and reduce disease severity in an animal model of spinal muscular atrophy." Mol Ther **20**(1): 119-26.

Pachot, A., J. L. Blond*, et al.* (2004). "Peptidylpropyl isomerase B (PPIB): a suitable reference gene for mRNA quantification in peripheral whole blood." J Biotechnol **114**(1-2): 121-4.

Pankratz, M. T., X. J. Li*, et al.* (2007). "Directed neural differentiation of human embryonic stem cells via an obligated primitive anterior stage." Stem Cells **25**(6): 1511-20.

Panman, L., E. Andersson*, et al.* (2011). "Transcription factor-induced lineage selection of stem-cell-derived neural progenitor cells." Cell Stem Cell **8**(6): 663-75.

Park, G. H., Y. Maeno-Hikichi*, et al.* (2010). "Reduced survival of motor neuron (SMN) protein in motor neuronal progenitors functions cell autonomously to cause spinal muscular atrophy in model mice expressing the human centromeric (SMN2) gene." J Neurosci **30**(36): 12005-19.

Park, I. H., N. Arora*, et al.* (2008a). "Disease-specific induced pluripotent stem cells." Cell **134**(5): 877-86.

Park, I. H., R. Zhao*, et al.* (2008b). "Reprogramming of human somatic cells to pluripotency with defined factors." Nature **451**(7175): 141-6.

Patani, R., A. J. Hollins*, et al.* (2011). "Retinoid-independent motor neurogenesis from human embryonic stem cells reveals a medial columnar ground state." Nat Commun **2**: 214.

Patani, R., P. A. Lewis*, et al.* (2012). "Investigating the utility of human embryonic stem cell-derived neurons to model ageing and neurodegenerative disease using whole-genome gene expression and splicing analysis." J Neurochem **122**(4): 738-51.

Patel, A. A. and J. A. Steitz (2003). "Splicing double: insights from the second spliceosome." Nat Rev Mol Cell Biol **4**(12): 960-70.

Paushkin, S., B. Charroux*, et al.* (2000). "The survival motor neuron protein of Schizosacharomyces pombe. Conservation of survival motor neuron interaction domains in divergent organisms." J Biol Chem **275**(31): 23841-6.

Pearn, J. (1978). "Incidence, prevalence, and gene frequency studies of chronic childhood spinal muscular atrophy." J Med Genet **15**(6): 409-13.

Pellizzoni, L. (2007). "Chaperoning ribonucleoprotein biogenesis in health and disease." EMBO Rep **8**(4): 340-5.

Pellizzoni, L., J. Baccon, *et al.* (2001). "The survival of motor neurons (SMN) protein interacts with the snoRNP proteins fibrillarin and GAR1." Curr Biol **11**(14): 1079-88.

Pellizzoni, L., B. Charroux, *et al.* (1999). "SMN mutants of spinal muscular atrophy patients are defective in binding to snRNP proteins." Proc Natl Acad Sci U S A **96**(20): 11167-72.

Pena, E., M. T. Berciano, *et al.* (2001). "Neuronal body size correlates with the number of nucleoli and Cajal bodies, and with the organization of the splicing machinery in rat trigeminal ganglion neurons." J Comp Neurol **430**(2): 250-63.

Peng, H. B., J. F. Yang, *et al.* (2003). "Differential effects of neurotrophins and schwann cell-derived signals on neuronal survival/growth and synaptogenesis." J Neurosci **23**(12): 5050-60.

Pfaff, S. L., M. Mendelsohn, *et al.* (1996). "Requirement for LIM homeobox gene Isl1 in motor neuron generation reveals a motor neuron-dependent step in interneuron differentiation." Cell **84**(2): 309-20

Piazzon, N., F. Rage, *et al.* (2008). "In vitro and in cellulo evidences for association of the survival of motor neuron complex with the fragile X mental retardation protein." J Biol Chem **283**(9): 5598-610.

Piepers, S., J. M. Cobben, *et al.* (2011). "Quantification of SMN protein in leucocytes from spinal muscular atrophy patients: effects of treatment with valproic acid." J Neurol Neurosurg Psychiatry **82**(8): 850-2.

Placantonakis, D. G., M. J. Tomishima, *et al.* (2009). "BAC transgenesis in human embryonic stem cells as a novel tool to define the human neural lineage." Stem Cells **27**(3): 521-32.

Polo, J. M., S. Liu, *et al.* (2010). "Cell type of origin influences the molecular and functional properties of mouse induced pluripotent stem cells." Nat Biotechnol **28**(8): 848-55.

Porensky, P. N., C. Mitrpant, *et al.* (2012). "A single administration of morpholino antisense oligomer rescues spinal muscular atrophy in mouse." Hum Mol Genet **21**(7): 1625-38.

Prior, T. W., A. R. Krainer, *et al.* (2009). "A positive modifier of spinal muscular atrophy in the SMN2 gene." Am J Hum Genet **85**(3): 408-13.

Qiang, L., R. Fujita, *et al.* (2011). "Directed conversion of Alzheimer's disease patient skin fibroblasts into functional neurons." Cell **146**(3): 359-71.

Quarto, N., B. Leonard, *et al.* (2010). "Skeletogenic phenotype of human Marfan embryonic stem cells faithfully phenocopied by patient-specific induced-pluripotent stem cells." Proc Natl Acad Sci U S A **109**(1): 215-20.

Raker, V. A., K. Hartmuth, *et al.* (1999). "Spliceosomal U snRNP core assembly: Sm proteins assemble onto an Sm site RNA nonanucleotide in a specific and thermodynamically stable manner." Mol Cell Biol **19**(10): 6554-65.

Ramalingam, S., V. London, *et al.* (2012). "Generation and genetic engineering of human induced pluripotent stem cells using designed zinc finger nucleases." Stem Cells Dev **22**(4): 595-610.

Rao, R. M., S. Rama, *et al.* (2003). "Changes in T-plastin expression with human trophoblast differentiation." Reprod Biomed Online **7**(2): 235-42.

Raya, A., I. Rodriguez-Piza, *et al.* (2009). "Disease-corrected haematopoietic progenitors from Fanconi anaemia induced pluripotent stem cells." Nature **460**(7251): 53-9.

Redfern, P. A. (1970). "Neuromuscular transmission in new-born rats." J Physiol **209**(3): 701-9.

Reinhardt, P., M. Glatza, *et al.* (2013). "Derivation and expansion using only small molecules of human neural progenitors for neurodegenerative disease modeling." PLoS One **8**(3): e59252.

Ricard, M. J. and L. J. Gudas (2013). "Cytochrome P450 Cyp26a1 alters spinal motor neuron subtype identity in differentiating embryonic stem cells." J Biol Chem.

Riessland, M., B. Ackermann, *et al.* (2010). "SAHA ameliorates the SMA phenotype in two mouse models for spinal muscular atrophy." Hum Mol Genet **19**(8): 1492-506.

Riessland, M., L. Brichta, *et al.* (2006). "The benzamide M344, a novel histone deacetylase inhibitor, significantly increases SMN2 RNA/protein levels in spinal muscular atrophy cells." Hum Genet **120**(1): 101-10.

Robinton, D. A. and G. Q. Daley (2012). "The promise of induced pluripotent stem cells in research and therapy." Nature **481**(7381): 295-305.

Rossoll, W. and G. J. Bassell (2009). "Spinal muscular atrophy and a model for survival of motor neuron protein function in axonal ribonucleoprotein complexes." Results Probl Cell Differ **48**: 289-326.

Rossoll, W., S. Jablonka, et al. (2003). "Smn, the spinal muscular atrophy-determining gene product, modulates axon growth and localization of beta-actin mRNA in growth cones of motoneurons." J Cell Biol **163**(4): 801-12.

Rossoll, W., A. K. Kroning, et al. (2002). "Specific interaction of Smn, the spinal muscular atrophy determining gene product, with hnRNP-R and gry-rbp/hnRNP-Q: a role for Smn in RNA processing in motor axons?" Hum Mol Genet **11**(1): 93-105.

Rudnik-Schöneborn, S., C. Berg, et al. (2009). "Genotype-phenotype studies in infantile spinal muscular atrophy (SMA) type I in Germany: implications for clinical trials and genetic counselling." Clin Genet **76**(2): 168-78.

Rudnik-Schöneborn, S., R. Heller, et al. (2008). "Congenital heart disease is a feature of severe infantile spinal muscular atrophy." J Med Genet **45**(10): 635-8.

Ruegg, M. A. (2001). "Molecules involved in the formation of synaptic connections in muscle and brain." Matrix Biol **20**(1): 3-12.

Ruggiu, M., V. L. McGovern, et al. (2012). "A Role for SMN Exon 7 Splicing in the Selective Vulnerability of Motor Neurons in Spinal Muscular Atrophy." Mol Cell Biol **32**(1): 126-38.

Ruiz, R., J. J. Casañas, et al. (2010). "Altered intracellular Ca2+ homeostasis in nerve terminals of severe spinal muscular atrophy mice." J Neurosci **30**(3): 849-57.

Sakmann, B. and H. R. Brenner (1978). "Change in synaptic channel gating during neuromuscular development." Nature **276**(5686): 401-2.

Salani, S., C. Donadoni, et al. (2012). "Generation of skeletal muscle cells from embryonic and induced pluripotent stem cells as an in vitro model and for therapy of muscular dystrophies." J Cell Mol Med **16**(7): 1353-64.

Sanchez, G., A. Y. Dury, et al. (2012). "A novel function for the survival motoneuron protein as a translational regulator." Hum Mol Genet **22**(4): 668-84.

Sancho-Martinez, I., E. Nivet, et al. (2011). "The labyrinth of nuclear reprogramming." J Mol Cell Biol **3**(6): 327-9.

Sandoe J. and K. Eggan (2013). "Opportunities and challenges of pluripotent stem cell neurodegenerative disease models." Nat Neurosci **16**(7):780-9

Sanes, J. R. and J. W. Lichtman (1999). "Development of the vertebrate neuromuscular junction." Annu Rev Neurosci **22**: 389-442.

Sanes, J. R. and J. W. Lichtman (2001). "Induction, assembly, maturation and maintenance of a postsynaptic apparatus." Nat Rev Neurosci **2**(11): 791-805.

Sango, K., T. Suzuki, et al. (2006). "High glucose-induced activation of the polyol pathway and changes of gene expression profiles in immortalized adult mouse Schwann cells IMS32." J Neurochem **98**(2): 446-58.

Sareen, D., A. D. Ebert, et al. (2012). "Inhibition of apoptosis blocks human motor neuron cell death in a stem cell model of spinal muscular atrophy." PLoS One **7**(6): e39113.

Scarciolla, O., L. Stuppia, et al. (2006). "Spinal muscular atrophy genotyping by gene dosage using multiple ligation-dependent probe amplification." Neurogenetics **7**(4): 269-76.

Scheffer, H., J. M. Cobben, et al. (2001). "Best practice guidelines for molecular analysis in spinal muscular atrophy." Eur J Hum Genet **9**(7): 484-91.

Schrank, B., R. Götz, et al. (1997). "Inactivation of the survival motor neuron gene, a candidate gene for human spinal muscular atrophy, leads to massive cell death in early mouse embryos." Proc Natl Acad Sci U S A **94**(18): 9920-5.

Schreml, J., M. Riessland, et al. (2013). "Severe SMA mice show organ impairment that cannot be rescued by therapy with the HDACi JNJ-26481585." Eur J Hum Genet **21**(6): 643-52.

Seaberg, R. M. and D. van der Kooy (2003). "Stem and progenitor cells: the premature desertion of rigorous definitions." Trends Neurosci **26**(3): 125-31.

See, K., P. Yadav, *et al.* (2013). "SMN deficiency alters Nrxn2 expression and splicing in zebrafish and mouse models of spinal muscular atrophy." Hum Mol Genet **23**(7): 1754-70.

Selenko, P., R. Sprangers, *et al.* (2001). "SMN tudor domain structure and its interaction with the Sm proteins." Nat Struct Biol **8**(1): 27-31.

Sendtner, M. (2010). "Therapy development in spinal muscular atrophy." Nat Neurosci **13**(7): 795-9.

Serio, A. W., R. L. Jeng, *et al.* (2010). "Defining a core set of actin cytoskeletal proteins critical for actin-based motility of Rickettsia." Cell Host Microbe **7**(5): 388-98.

Setola, V., M. Terao, *et al.* (2007). "Axonal-SMN (a-SMN), a protein isoform of the survival motor neuron gene, is specifically involved in axonogenesis." Proc Natl Acad Sci U S A **104**(6): 1959-64.

Shababi, M., C. L. Lorson, *et al.* (2013). "Spinal muscular atrophy: a motor neuron disorder or a multi-organ disease?" J Anat.

Sharma, A., A. Lambrechts, *et al.* (2005). "A role for complexes of survival of motor neurons (SMN) protein with gemins and profilin in neurite-like cytoplasmic extensions of cultured nerve cells." Exp Cell Res **309**(1): 185-97.

Sine, S. M. (2012). "End-plate acetylcholine receptor: structure, mechanism, pharmacology, and disease." Physiol Rev **92**(3): 1189-234.

Singh, N. N., M. Shishimorova, *et al.* (2009). "A short antisense oligonucleotide masking a unique intronic motif prevents skipping of a critical exon in spinal muscular atrophy." RNA Biol **6**(3): 341-50.

Slater, C. R. (2009). Neuromuscular Junction (NMJ): Mammalian Development. Developmental Neurobiology. G. Lemke, Academic Press.

Sleeman, J. (2013). "Small nuclear RNAs and mRNAs: linking RNA processing and transport to spinal muscular atrophy." Biochem Soc Trans **41**(4): 871-5.

Sleigh, J. N., T. H. Gillingwater, *et al.* (2011). "The contribution of mouse models to understanding the pathogenesis of spinal muscular atrophy." Dis Model Mech **4**(4): 457-67.

Smith, J. L. and G. C. Schoenwolf (1997). "Neurulation: coming to closure." Trends Neurosci **20**(11): 510-7.

Smith, K. P., M. X. Luong, *et al.* (2009). "Pluripotency: toward a gold standard for human ES and iPS cells." J Cell Physiol **220**(1): 21-9.

Smukler, S. R., S. B. Runciman, *et al.* (2006). "Embryonic stem cells assume a primitive neural stem cell fate in the absence of extrinsic influences." J Cell Biol **172**(1): 79-90.

Sockanathan, S. and T. M. Jessell (1998). "Motor neuron-derived retinoid signaling specifies the subtype identity of spinal motor neurons." Cell **94**(4): 503-14.

Soldner, F., D. Hockemeyer, *et al.* (2009). "Parkinson's disease patient-derived induced pluripotent stem cells free of viral reprogramming factors." Cell **136**(5): 964-77.

Soldner, F., J. Laganière, *et al.* (2011). "Generation of isogenic pluripotent stem cells differing exclusively at two early onset Parkinson point mutations." Cell **146**(2):318-31

Sommer, C. A., C. Christodoulou, *et al.* (2012). "Residual expression of reprogramming factors affects the transcriptional program and epigenetic signatures of induced pluripotent stem cells." PLoS One **7**(12): e51711.

Sommer, C. A. and G. Mostoslavsky (2010). "Experimental approaches for the generation of induced pluripotent stem cells." Stem Cell Res Ther **1**(3): 26.

Son, E. Y., J. K. Ichida, *et al.* (2011). "Conversion of mouse and human fibroblasts into functional spinal motor neurons." Cell Stem Cell **9**(3): 205-18.

Soula, C., C. Danesin, *et al.* (2001). "Distinct sites of origin of oligodendrocytes and somatic motoneurons in the chick spinal cord: oligodendrocytes arise from Nkx2.2-expressing progenitors by a Shh-dependent mechanism." Development **128**(8): 1369-79.

Spemann, H. and H. Mangold (1924). "Über Induktion von Embryonalanlagen durch Implantation artfremder Organisatoren. 1924." Arch. Mikr. Anat. Entwicklngsmech(100): 599-638.

Stadtfeld, M., K. Brennand, *et al.* (2008a). "Reprogramming of pancreatic beta cells into induced pluripotent stem cells." Curr Biol **18**(12): 890-4.

Stadtfeld, M., M. Nagaya, *et al.* (2008b). "Induced pluripotent stem cells generated without viral integration." Science **322**(5903): 945-9.

StemcellTechnologies (Version 3.0.0). Maintenance of Human Pluripotent Stem Cells in mTeSR™1 and TeSR™2.

Stockmann, M., L. Linta, *et al.* (2011). "Developmental and Functional Nature of Human iPSC Derived Motoneurons." Stem Cell Rev **9**(4): 475-92.

Stratigopoulos, G., P. Lanzano, *et al.* (2010). "Association of plastin 3 expression with disease severity in spinal muscular atrophy only in postpubertal females." Arch Neurol **67**(10): 1252-6.

Su, H., L. Wang, *et al.* (2013). "Transplanted motoneurons derived from human induced pluripotent stem cells form functional connections with target muscle." Stem Cell Res **11**(1): 529-39.

Sugarman, E. A., N. Nagan, *et al.* (2012). "Pan-ethnic carrier screening and prenatal diagnosis for spinal muscular atrophy: clinical laboratory analysis of >72,400 specimens." Eur J Hum Genet **20**(1): 27-32.

Suh, M. R., Y. Lee, *et al.* (2004). "Human embryonic stem cells express a unique set of microRNAs." Dev Biol **270**(2): 488-98.

Sumner, C. J. (2006). "Therapeutics development for spinal muscular atrophy." NeuroRx **3**(2): 235-45.

Sumner, C. J. (2007). "Molecular mechanisms of spinal muscular atrophy." J Child Neurol **22**(8): 979-89.

Sun, N., M. T. Longaker, *et al.* (2010). "Human iPS cell-based therapy: considerations before clinical applications." Cell Cycle **9**(5): 880-5.

Sun, N., N. J. Panetta, *et al.* (2009). "Feeder-free derivation of induced pluripotent stem cells from adult human adipose stem cells." Proc Natl Acad Sci U S A **106**(37): 15720-5.

Sun, Y., K. M. Yong, *et al.* (2014). "Hippo/YAP-mediated rigidity-dependent motor neuron differentiation of human pluripotent stem cells." Nat Mater **13**(6): 599-604.

Swoboda, K. J., C. B. Scott, *et al.* (2011). "SMA CARNI-VAL trial part I: double-blind, randomized, placebo-controlled trial of L-carnitine and valproic acid in spinal muscular atrophy." PLoS One **5**(8): e12140.

Tachibana, M., P. Amato, *et al.* (2013). "Human embryonic stem cells derived by somatic cell nuclear transfer." Cell **153**(6): 1228-38.

Tada, M., Y. Takahama, *et al.* (2001). "Nuclear reprogramming of somatic cells by in vitro hybridization with ES cells." Curr Biol **11**(19): 1553-8.

Takahashi, K., K. Tanabe, *et al.* (2007). "Induction of pluripotent stem cells from adult human fibroblasts by defined factors." Cell **131**(5): 861-72.

Takahashi, K. and S. Yamanaka (2006). "Induction of pluripotent stem cells from mouse embryonic and adult fibroblast cultures by defined factors." Cell **126**(4): 663-76.

Talbot, K. (1999). "Spinal muscular atrophy." J Inherit Metab Dis **22**(4): 545-54.

Tanabe, Y., C. William, *et al.* (1998). "Specification of motor neuron identity by the MNR2 homeodomain protein." Cell **95**(1): 67-80.

Thomson, J. A., J. Itskovitz-Eldor, *et al.* (1998). "Embryonic stem cell lines derived from human blastocysts." Science **282**(5391): 1145-7.

Ting, C. H., C. W. Lin, *et al.* (2007). "Stat5 constitutive activation rescues defects in spinal muscular atrophy." Hum Mol Genet **16**(5): 499-514.

Todd, A. G., R. Morse, *et al.* (2010). "Analysis of SMN-neurite granules: Core Cajal body components are absent from SMN-cytoplasmic complexes." Biochem Biophys Res Commun **397**(3): 479-85.

Toivonen, S., M. Ojala, *et al.* (2013). "Comparative analysis of targeted differentiation of human induced pluripotent stem cells (hiPSCs) and human embryonic stem cells reveals variability associated with incomplete transgene silencing in retrovirally derived hiPSC lines." Stem Cells Transl Med **2**(2): 83-93.

Tomishima, M. (2012). "Midbrain dopamine neurons from hESCs." StemBook [Internet](Harvard Stem Cell Institute).

Torres-Benito, L., M. F. Neher, *et al.* (2011). "SMN requirement for synaptic vesicle, active zone and microtubule postnatal organization in motor nerve terminals." PLoS One **6**(10): e26164.

Twiss, J. L. and M. Fainzilber (2009). "Ribosomes in axons--scrounging from the neighbors?" Trends Cell Biol **19**(5): 236-43.

Urbach, A., O. Bar-Nur, *et al.* (2010). "Differential modeling of fragile X syndrome by human embryonic stem cells and induced pluripotent stem cells." Cell Stem Cell **6**(5): 407-11.

Utikal, J., N. Maherali, *et al.* (2009). "Sox2 is dispensable for the reprogramming of melanocytes and melanoma cells into induced pluripotent stem cells." J Cell Sci **122**(Pt 19): 3502-10.

van Bergeijk, J., K. Rydel-Konecke, *et al.* (2007). "The spinal muscular atrophy gene product regulates neurite outgrowth: importance of the C terminus." Faseb J **21**(7): 1492-502.

Van de Velde, H., G. Cauffman, *et al.* (2008). "The four blastomeres of a 4-cell stage human embryo are able to develop individually into blastocysts with inner cell mass and trophectoderm." Hum Reprod **23**(8): 1742-7.

Vezain, M., B. Gerard, *et al.* (2011). "A leaky splicing mutation affecting SMN1 exon 7 inclusion explains an unexpected mild case of spinal muscular atrophy." Hum Mutat.

Vierbuchen, T., A. Ostermeier, *et al.* (2010). "Direct conversion of fibroblasts to functional neurons by defined factors." Nature **463**(7284): 1035-41.

Wada, T., M. Honda, *et al.* (2009). "Highly efficient differentiation and enrichment of spinal motor neurons derived from human and monkey embryonic stem cells." PLoS One **4**(8): e6722.

Wan, L., D. J. Battle, *et al.* (2005). "The survival of motor neurons protein determines the capacity for snRNP assembly: biochemical deficiency in spinal muscular atrophy." Mol Cell Biol **25**(13): 5543-51.

Wan, L., E. Ottinger, *et al.* (2008). "Inactivation of the SMN complex by oxidative stress." Mol Cell **31**(2): 244-54.

Wang, Y., C. G. Zheng, *et al.* (2012). "Genetic correction of beta-thalassemia patient-specific iPS cells and its use in improving hemoglobin production in irradiated SCID mice." Cell Res **22**(4): 637-48.

Wang, Z. B., X. Zhang, *et al.* (2013). "Recapitulation of spinal motor neuron-specific disease phenotypes in a human cell model of spinal muscular atrophy." Cell Res **23**(3): 378-93.

Watanabe, K., M. Ueno, et al. (2007). "A ROCK inhibitor permits survival of dissociated human embryonic stem cells." Nat. Biotechnol. **25**(6):681-6.

Weinstein, D. C. and A. Hemmati-Brivanlou (1999). "Neural induction." Annu Rev Cell Dev Biol **15**: 411-33.

Wen, H. L., Y. T. Lin, *et al.* (2010). "Stathmin, a microtubule-destabilizing protein, is dysregulated in spinal muscular atrophy." Hum Mol Genet **19**(9): 1766-78.

Wen, H. L., C. H. Ting, *et al.* (2012). "Decreased stathmin expression ameliorates neuromuscular defects but fails to prolong survival in a mouse model of spinal muscular atrophy." Neurobiol Dis **52**: 94-103.

Werdnig, G. (1891). "Zwei frühinfantile hereditäre Fälle von progressiver Muskelatrophie unter dem Bilde der Dystrophie, aber auf neurotischer Grundlage." Archiv für Psychiatrie und Nervenkrankheiten **22**: 437-480.

Wernig, M., A. Meissner, *et al.* (2007). "In vitro reprogramming of fibroblasts into a pluripotent ES-cell-like state." Nature **448**(7151): 318-24.

Weston, C. A., G. Teressa, *et al.* (2007). "Agrin and laminin induce acetylcholine receptor clustering by convergent, Rho GTPase-dependent signaling pathways." J Cell Sci **120**(Pt 5): 868-75.

Wichterle, H., I. Lieberam, *et al.* (2002). "Directed differentiation of embryonic stem cells into motor neurons." Cell **110**(3): 385-97.

Wiersma-Meems, R., J. Van Minnen, *et al.* (2005). "Synapse formation and plasticity: the roles of local protein synthesis." Neuroscientist **11**(3): 228-37.

Wiese, S., T. Herrmann, *et al.* (2010). "Isolation and enrichment of embryonic mouse motoneurons from the lumbar spinal cord of individual mouse embryos." Nat Protoc **5**(1): 31-8.

William, C. M., Y. Tanabe, *et al.* (2003). "Regulation of motor neuron subtype identity by repressor activity of Mnx class homeodomain proteins." Development **130**(8): 1523-36.

Williams, B. Y., S. L. Hamilton, *et al.* (2000). "The survival motor neuron protein interacts with the transactivator FUSE binding protein from human fetal brain." FEBS Lett **470**(2): 207-10.

Wilmut, I., A. E. Schnieke*, et al.* (1997). "Viable offspring derived from fetal and adult mammalian cells." <u>Nature</u> **385**(6619): 810-3.

Wilson, K. D., S. Venkatasubrahmanyam*, et al.* (2009). "MicroRNA profiling of human-induced pluripotent stem cells." <u>Stem Cells Dev</u> **18**(5): 749-58.

Wilson, L. and M. Maden (2005). "The mechanisms of dorsoventral patterning in the vertebrate neural tube." <u>Dev Biol</u> **282**(1): 1-13.

Wilson, S. I. and T. Edlund (2001). "Neural induction: toward a unifying mechanism." <u>Nat Neurosci</u> **4 Suppl**: 1161-8.

Winkler, C., C. Eggert*, et al.* (2005). "Reduced U snRNP assembly causes motor axon degeneration in an animal model for spinal muscular atrophy." <u>Genes Dev</u> **19**(19): 2320-30.

Wirth, B. (2000). "An update of the mutation spectrum of the survival motor neuron gene (SMN1) in autosomal recessive spinal muscular atrophy (SMA)." <u>Hum Mutat</u> **15**(3): 228-37.

Wirth, B., L. Brichta*, et al.* (2006a). "Spinal muscular atrophy: from gene to therapy." <u>Semin Pediatr Neurol</u> **13**(2): 121-31.

Wirth, B., L. Brichta*, et al.* (2006b). "Mildly affected patients with spinal muscular atrophy are partially protected by an increased SMN2 copy number." <u>Hum Genet</u> **119**(4): 422-8.

Wirth, B., L. Garbes*, et al.* (2013). "How genetic modifiers influence the phenotype of spinal muscular atrophy and suggest future therapeutic approaches." <u>Curr Opin Genet Dev</u> **23**(3): 330-8.

Wirth, B., M. Herz*, et al.* (1999). "Quantitative analysis of survival motor neuron copies: identification of subtle SMN1 mutations in patients with spinal muscular atrophy, genotype-phenotype correlation, and implications for genetic counseling." <u>Am J Hum Genet</u> **64**(5): 1340-56.

Wirth, B., M. Riessland*, et al.* (2007). "Drug discovery for spinal muscular atrophy." <u>Expert Opin Drug Discov</u> **2**(4): 437-51.

Wirth, B., T. Schmidt*, et al.* (1997). "*De novo* rearrangements found in 2% of index patients with spinal muscular atrophy: mutational mechanisms, parental origin, mutation rate, and implications for genetic counseling." <u>Am J Hum Genet</u> **61**(5): 1102-11.

Wishart, T. M., J. P. Huang*, et al.* (2010). "SMN deficiency disrupts brain development in a mouse model of severe spinal muscular atrophy." <u>Hum Mol Genet</u> **19**(21): 4216-28.

Wishart, T. M., C. A. Mutsaers, *et al.* (2014). "Dysregulation of ubiquitin homeostasis and beta-catenin signaling promote spinal muscular atrophy." <u>J Clin Invest</u> **124**(4): 1821-34.

Witten, I. B., S. C. Lin*, et al.* (2010). "Cholinergic interneurons control local circuit activity and cocaine conditioning." <u>Science</u> **330**(6011): 1677-81.

Wolpert, L. (1969). "Positional information and the spatial pattern of cellular differentiation." <u>J Theor Biol</u> **25**(1): 1-47.

Wolstencroft, E. C., V. Mattis*, et al.* (2005). "A non-sequence-specific requirement for SMN protein activity: the role of aminoglycosides in inducing elevated SMN protein levels." <u>Hum Mol Genet</u> **14**(9): 1199-210.

Woltjen, K., I. P. Michael*, et al.* (2009). "piggyBac transposition reprograms fibroblasts to induced pluripotent stem cells." <u>Nature</u> **458**(7239): 766-70.

Workman, E., L. Saieva*, et al.* (2009). "A SMN missense mutation complements SMN2 restoring snRNPs and rescuing SMA mice." <u>Hum Mol Genet</u> **18**(12): 2215-29.

Workman, E., A. Veith, *et al.* (2013). "U1A Regulates 3' Processing of the Survival Motor Neuron mRNA." <u>J Biol Chem</u>.

Wu, H., W. C. Xiong*, et al.* (2010). "To build a synapse: signaling pathways in neuromuscular junction assembly." <u>Development</u> **137**(7): 1017-33.

Yang, J. F., G. Cao*, et al.* (2001). "Schwann cells express active agrin and enhance aggregation of acetylcholine receptors on muscle fibers." <u>J Neurosci</u> **21**(24): 9572-84.

Yanyan, C., Q. Yujin*, et al.* (2014). "Correlation of PLS3 expression with disease severity in children with spinal muscular atrophy." <u>J Hum Genet</u> **59**(1): 24-7.

Yoo, S., H. H. Kim*, et al.* (2013). "A HuD-ZBP1 ribonucleoprotein complex localizes GAP-43 mRNA into axons through its 3' untranslated region AU-rich regulatory element." <u>J Neurochem</u> **126**(6): 792-804.

Young, P. J., T. T. Le, *et al.* (2001). "Nuclear gems and Cajal (coiled) bodies in fetal tissues: nucleolar distribution of the spinal muscular atrophy protein, SMN." <u>Exp Cell Res</u> **265**(2): 252-61.

Young, P. J., T. T. Le, *et al.* (2000). "The relationship between SMN, the spinal muscular atrophy protein, and nuclear coiled bodies in differentiated tissues and cultured cells." <u>Exp Cell Res</u> **256**(2): 365-74.

Yu, J., K. Hu, *et al.* (2009). "Human induced pluripotent stem cells free of vector and transgene sequences." <u>Science</u> **324**(5928): 797-801.

Yu, J., M. A. Vodyanik, *et al.* (2007). "Induced pluripotent stem cell lines derived from human somatic cells." <u>Science</u> **318**(5858): 1917-20.

Zapletalova, E., P. Hedvicakova, *et al.* (2007). "Analysis of point mutations in the SMN1 gene in SMA patients bearing a single SMN1 copy." <u>Neuromuscul Disord</u> **17**(6): 476-81.

Zerres, K., S. Rudnik-Schöneborn, *et al.* (1995). "Genetic basis of adult-onset spinal muscular atrophy." <u>Lancet</u> **346**(8983): 1162.

Zerres, K., S. Rudnik-Schöneborn, *et al.* (1997). "A collaborative study on the natural history of childhood and juvenile onset proximal spinal muscular atrophy (type II and III SMA): 569 patients." <u>J Neurol Sci</u> **146**(1): 67-72.

Zhang, H., L. Xing, *et al.* (2006). "Multiprotein complexes of the survival of motor neuron protein SMN with Gemins traffic to neuronal processes and growth cones of motor neurons." <u>J Neurosci</u> **26**(33): 8622-32.

Zhang, H. L., F. Pan, *et al.* (2003). "Active transport of the survival motor neuron protein and the role of exon-7 in cytoplasmic localization." <u>J Neurosci</u> **23**(16): 6627-37.

Zhang, J., Q. Lian, *et al.* (2011). "A human iPSC model of Hutchinson Gilford Progeria reveals vascular smooth muscle and mesenchymal stem cell defects." <u>Cell Stem Cell</u> **8**(1): 31-45.

Zhang, M. L., C. L. Lorson, *et al.* (2001). "An in vivo reporter system for measuring increased inclusion of exon 7 in SMN2 mRNA: potential therapy of SMA." <u>Gene Ther</u> **8**(20): 1532-8.

Zhang, Z., F. Lotti, *et al.* (2008). "SMN deficiency causes tissue-specific perturbations in the repertoire of snRNAs and widespread defects in splicing." <u>Cell</u> **133**(4): 585-600.

Zhou, H., S. Wu, *et al.* (2009a). "Generation of induced pluripotent stem cells using recombinant proteins." <u>Cell Stem Cell</u> **4**(5): 381-4.

Zhou, W. and C. R. Freed (2009b). "Adenoviral gene delivery can reprogram human fibroblasts to induced pluripotent stem cells." <u>Stem Cells</u> **27**(11): 2667-74.

11. Appendix

11.1 List of all iPSC clones picked

**Cell line
HGK21 (= ML11)**

Clone #	% confluence	% differentiated cells
1	90	0
2	95	5
3	90	5
4	60	30
5	90	15
6	70	15
7	80	20
8	80	15
9	65	10
10	80	10
11	80	5
12	75	5
13	75	15
14	85	5
15	90	10
16	90	5

**Cell line
HGK27 (= ML12)**

Clone #	% confluence	% differentiated cells
1		
2	80	20
3	90	15
4	70	15
5	85	20
6	90	50
7	100	50
8	80	10
9	80	30
10	90	5
11	90	50
12	95	30
13	95	15
14		
15	90	50
16	90	50
17	80	60
18	90	60

**Cell line
HGK22 (= ML14)**

Clone #	% confluence	% differentiated cells
1	90	15
2	100	40
3	100	40
4	75	5
5	70	20
6	70	20
7	70	20
8		
9	80	45
10	70	50
11	85	10
12	90	15
13	70	15
14	80	15
15		
16	75	20
17	45	0
18	50	0

**Cell line
HGK28 (= ML13)**

Clone #	% confluence	% differentiated cells
1	75	30
2	90	15
3	90	20
4	90	35
5	85	5
6	70	25
7	80	5
8	85	10
9	75	5
10	80	15
11	80	5
12	90	10
13	90	10
14	90	15
15	90	10
16	95	15

Tab. 19: Overview of all new iPSC clones with percentage of confluence and degree of contamination by differentiating cells before first split. Highlighted in red are clones not having grown properly after picking. Highlighted in yellow are clones which failed SNP-array analysis. Highlighted in turquoise are clones matching all validation criteria so far.

11.2 SNP-array data

Fig. 61: Schematic karyograms of new iPSC lines and corresponding parental fibroblasts. gDNA is extracted and amplified for whole-genome SNP-array. Each chromosome is depicted together with its corresponding B allele frequency (upper panel) and Log R ration (lower panel). Note that regular SNPs show a Log R ratio of 0 and a B allele frequency of 0, 0.5 or 1 when homozygous. A heterozygous deletion will result in a Log R ratio of <0 and a B allele frequency of only 0 or 1, whereas a duplication will cause a Log R ratio of >0 and a B allele frequency of 0, ⅓, ⅔, or 1. Any major aberration visible here is an original pre-existing mutation as already seen in the parental fibroblast cell lines (7.2.3, Tab. 16).
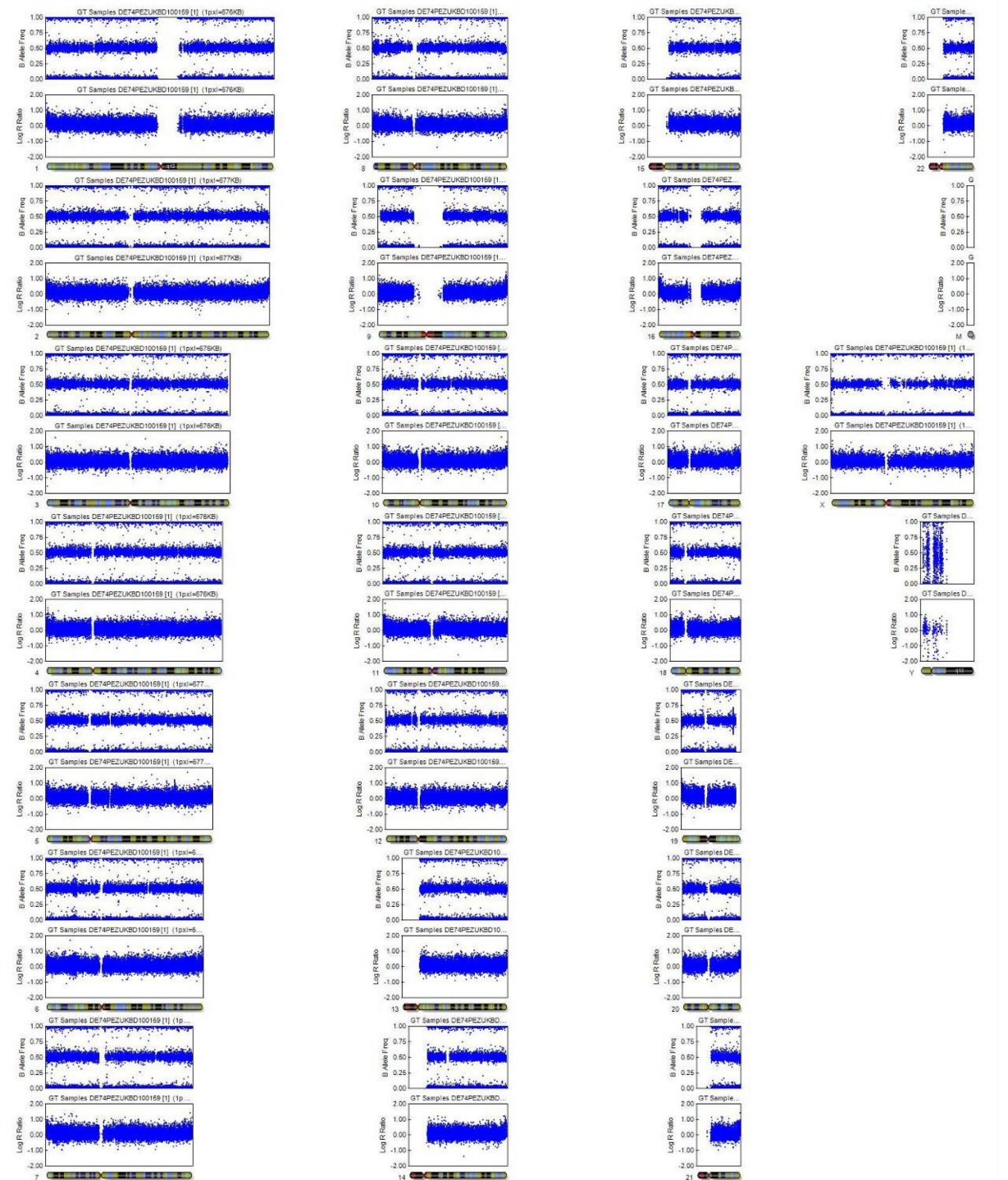
Fibroblast ML11
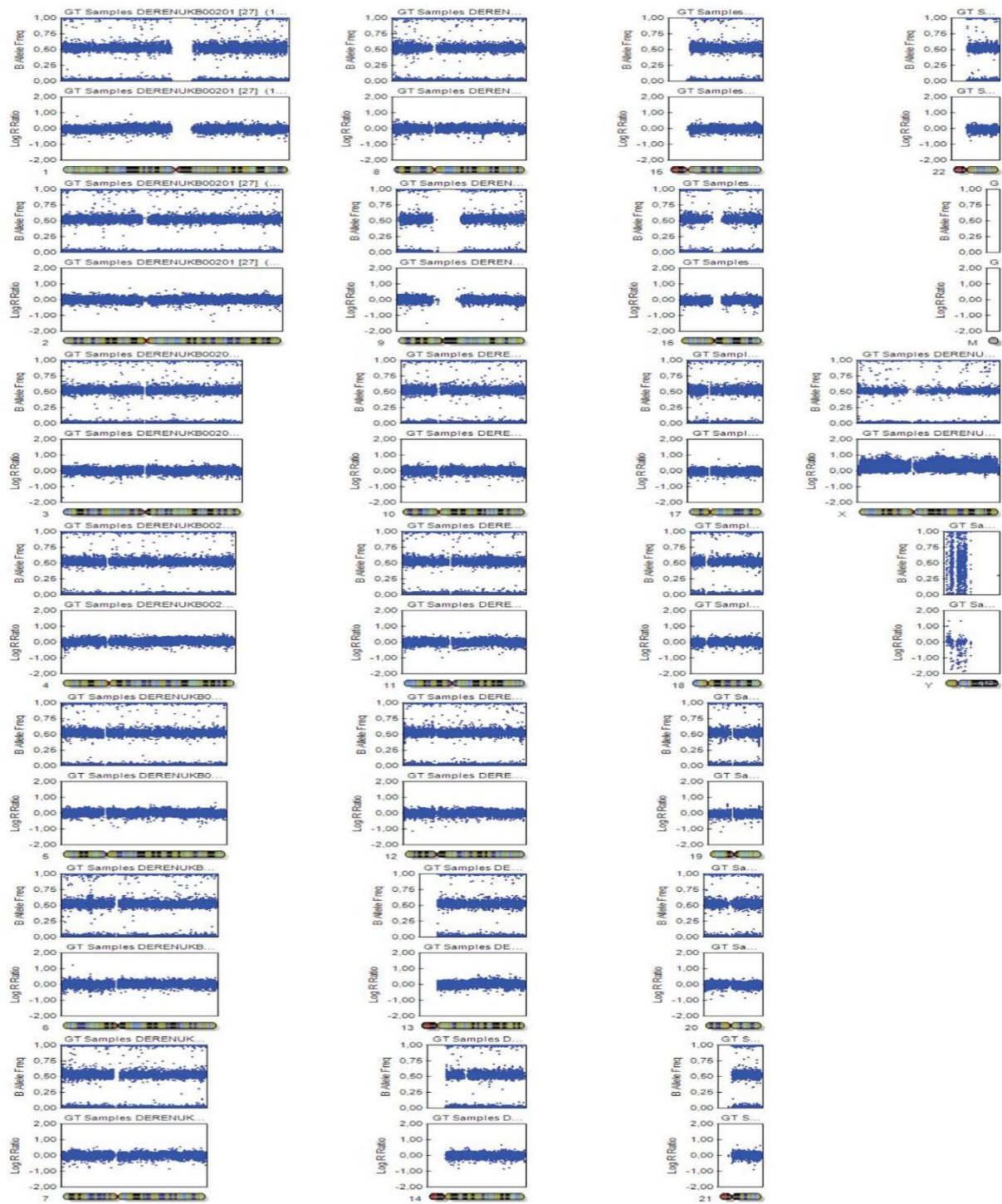
iPSC HGK21.8
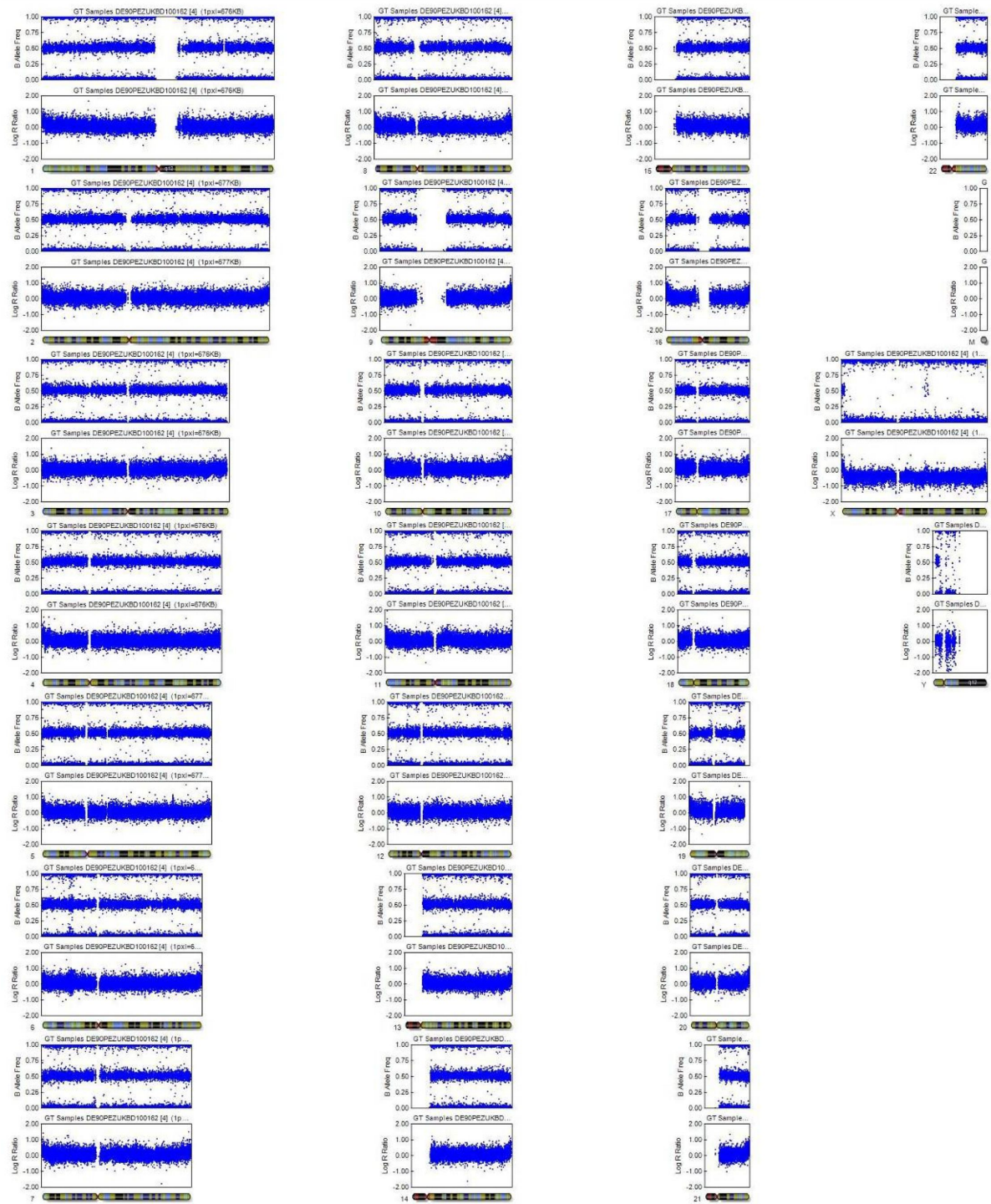
Fibroblast ML14
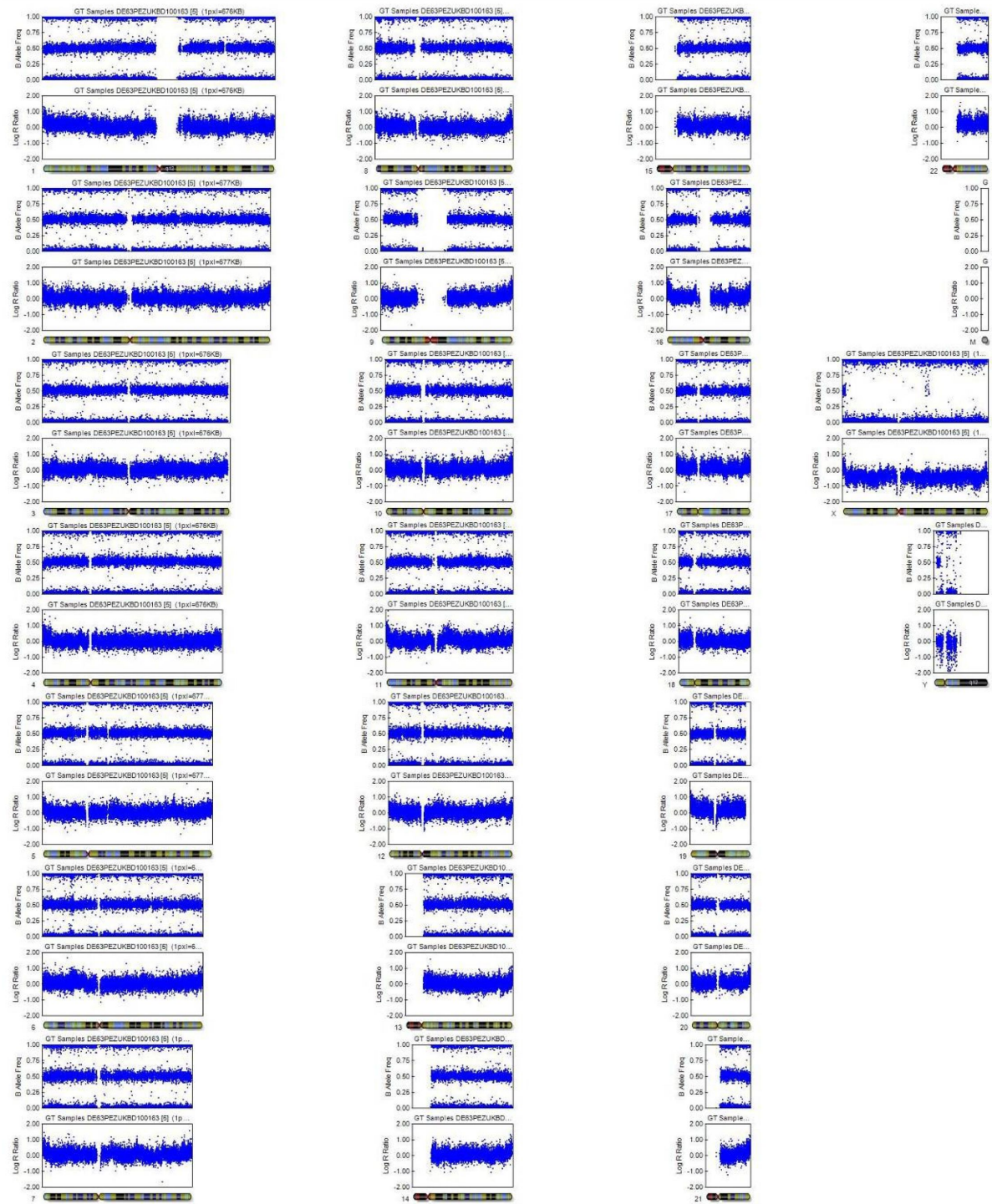
iPSC HGK22.17
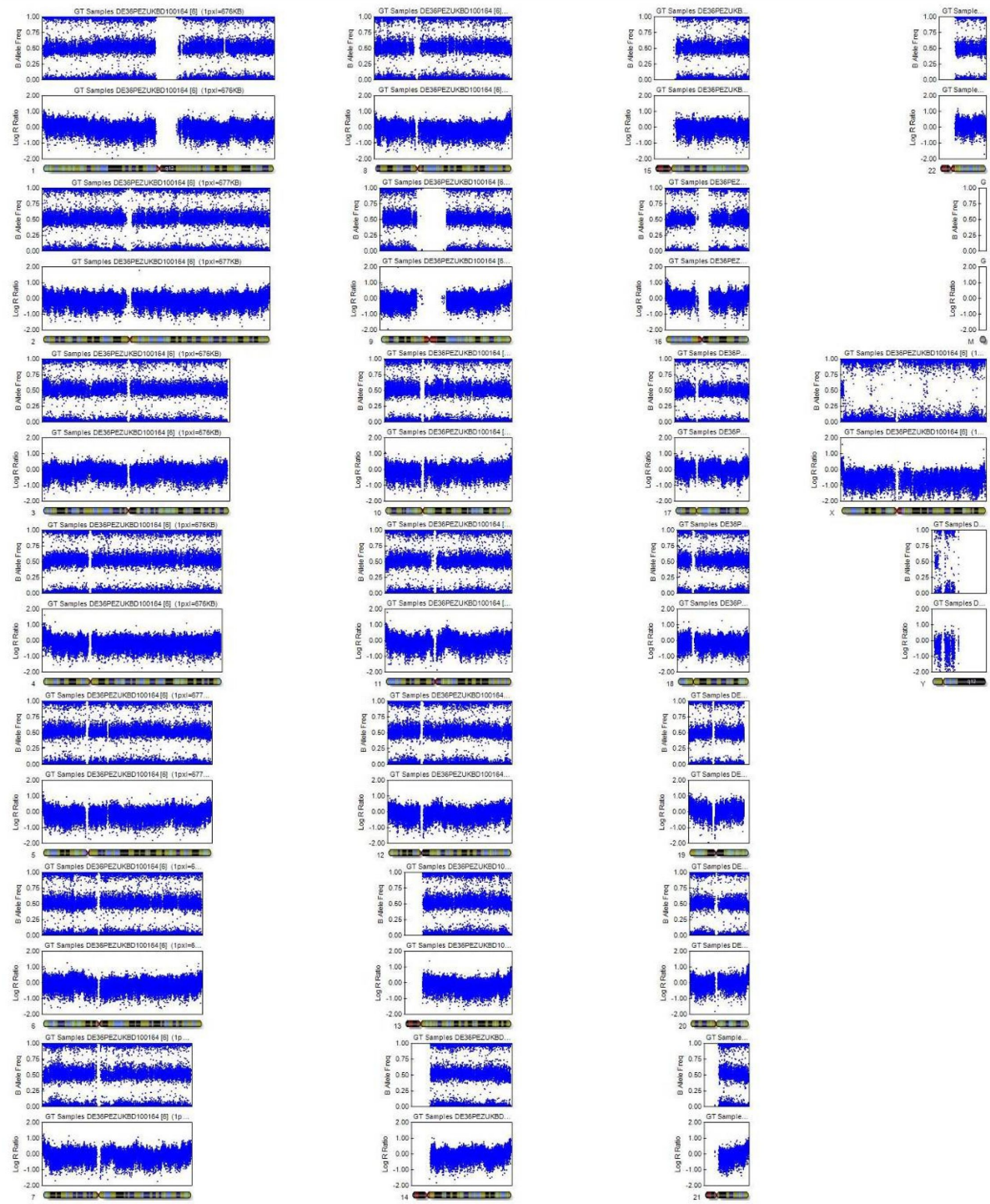
iPSC HGK22.18
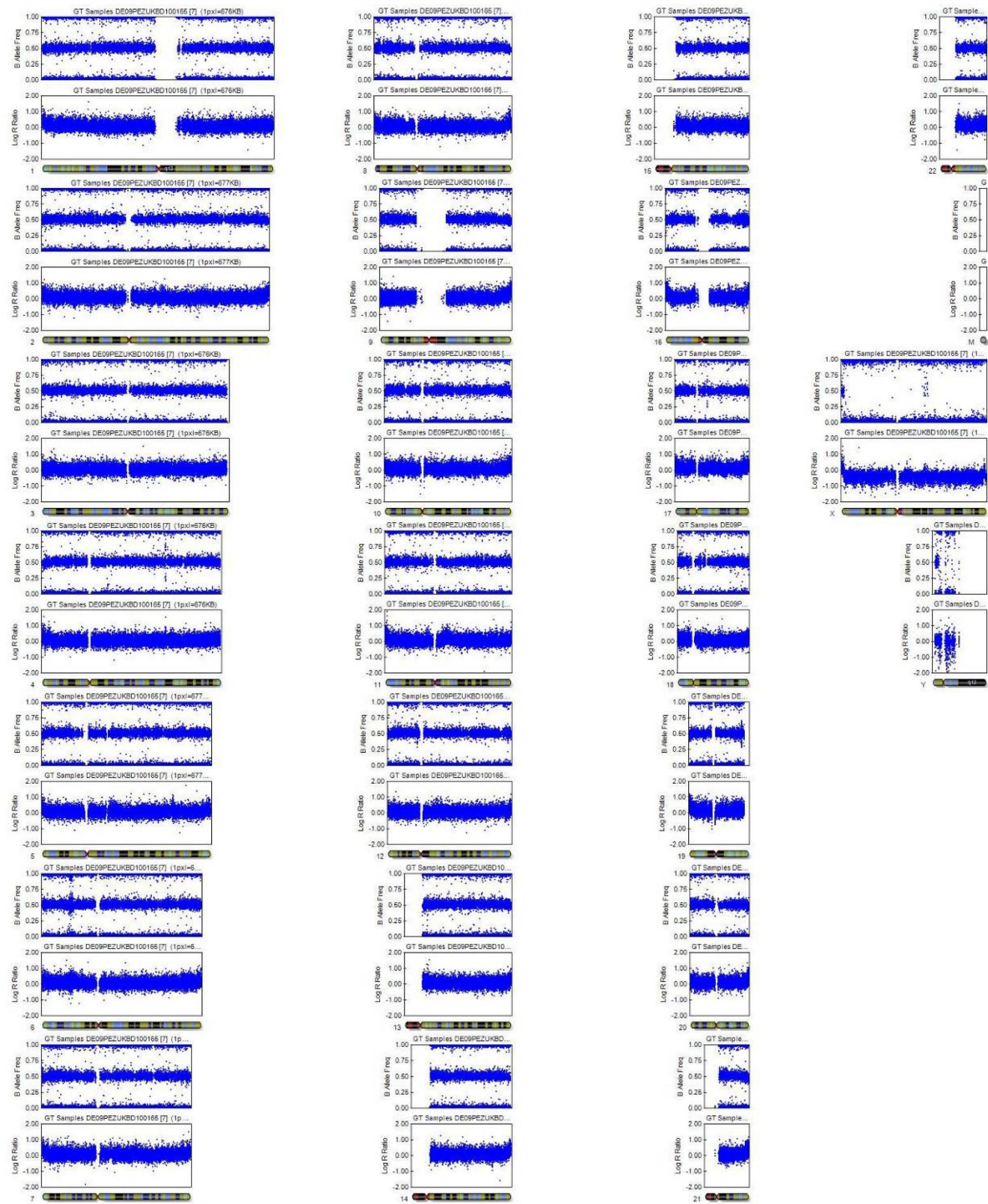
Fibroblast ML12
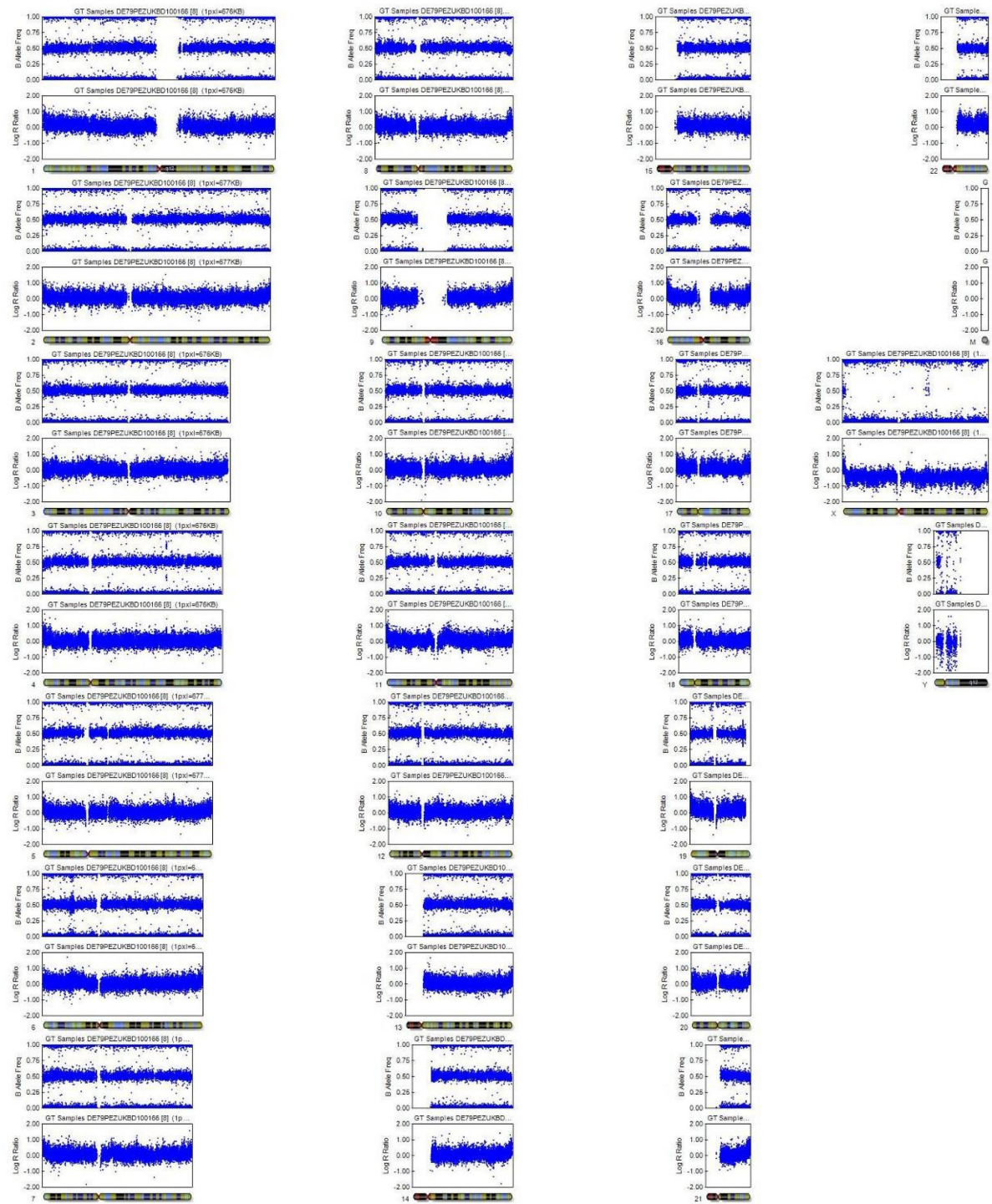
iPSC HGK27.10
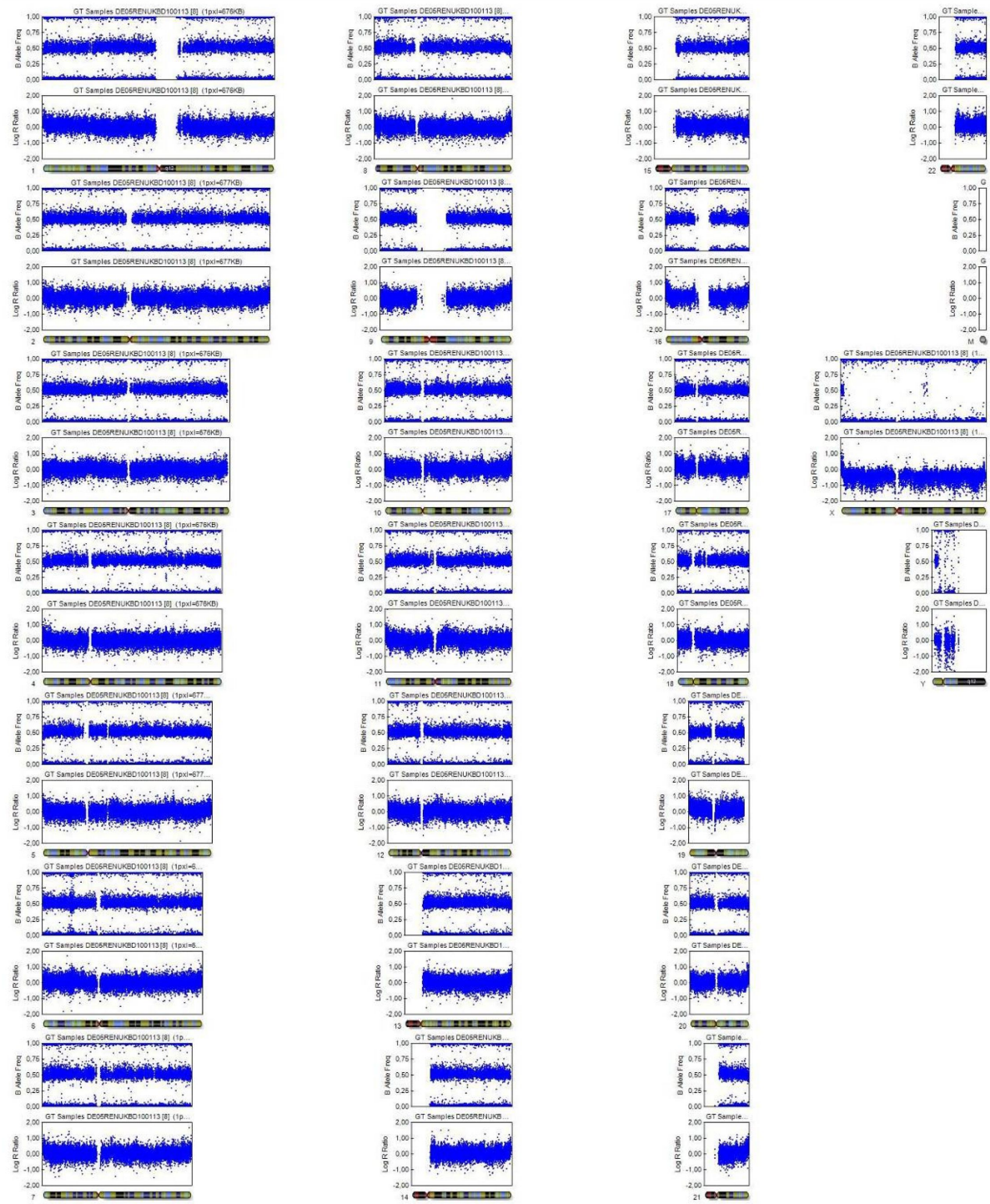
iPSC HGK27.13
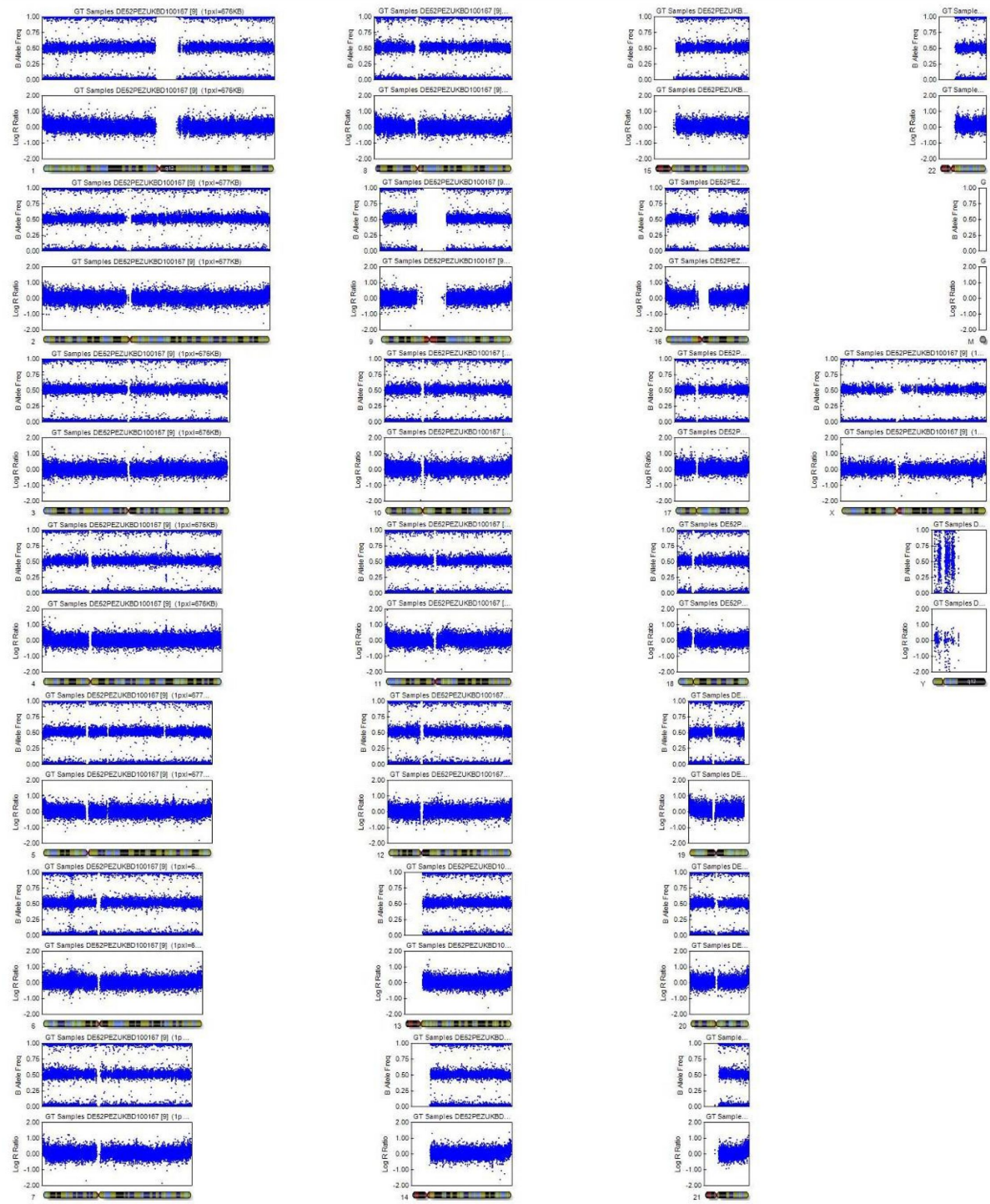
Fibroblast ML13
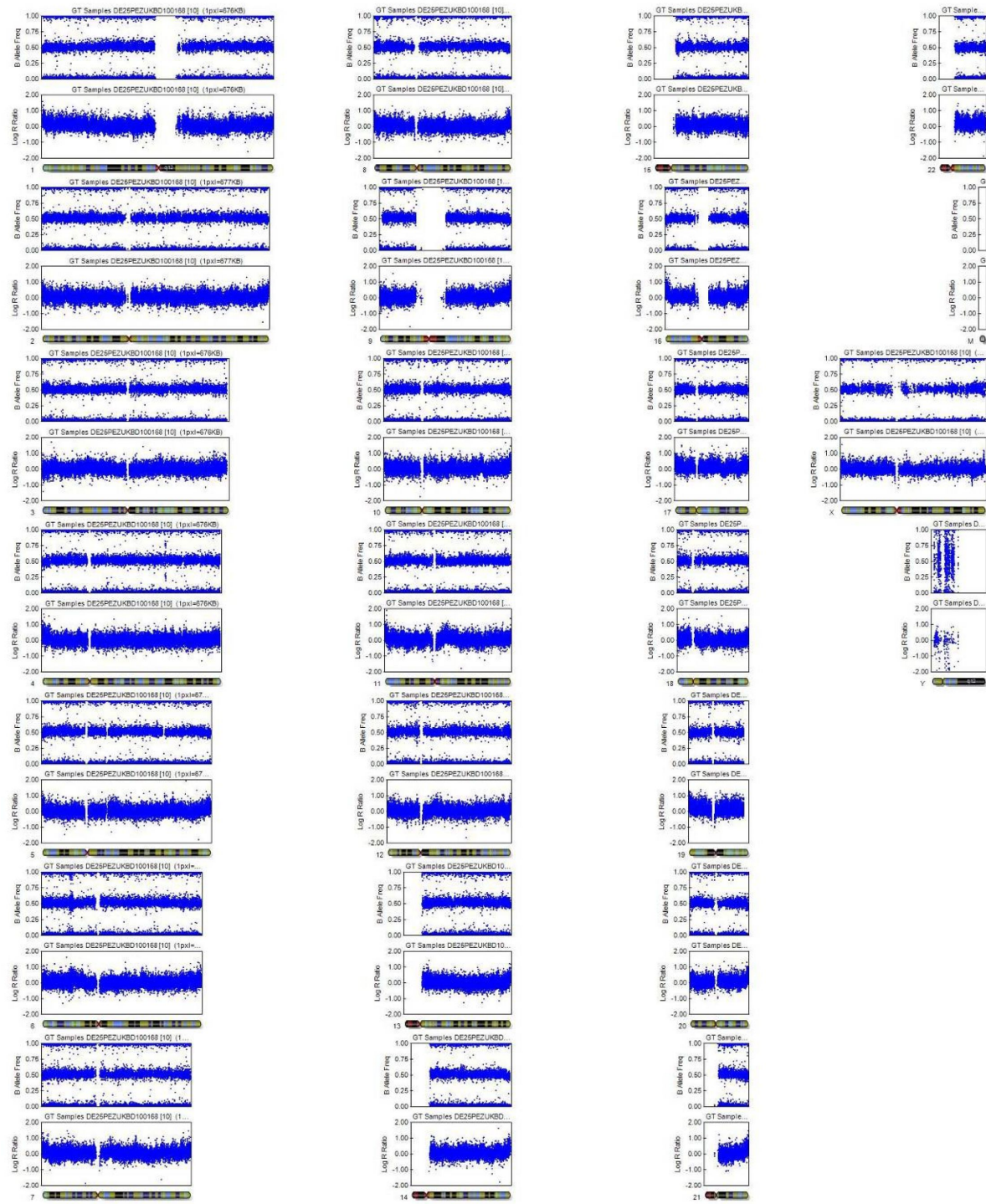
iPSC HGK28.9
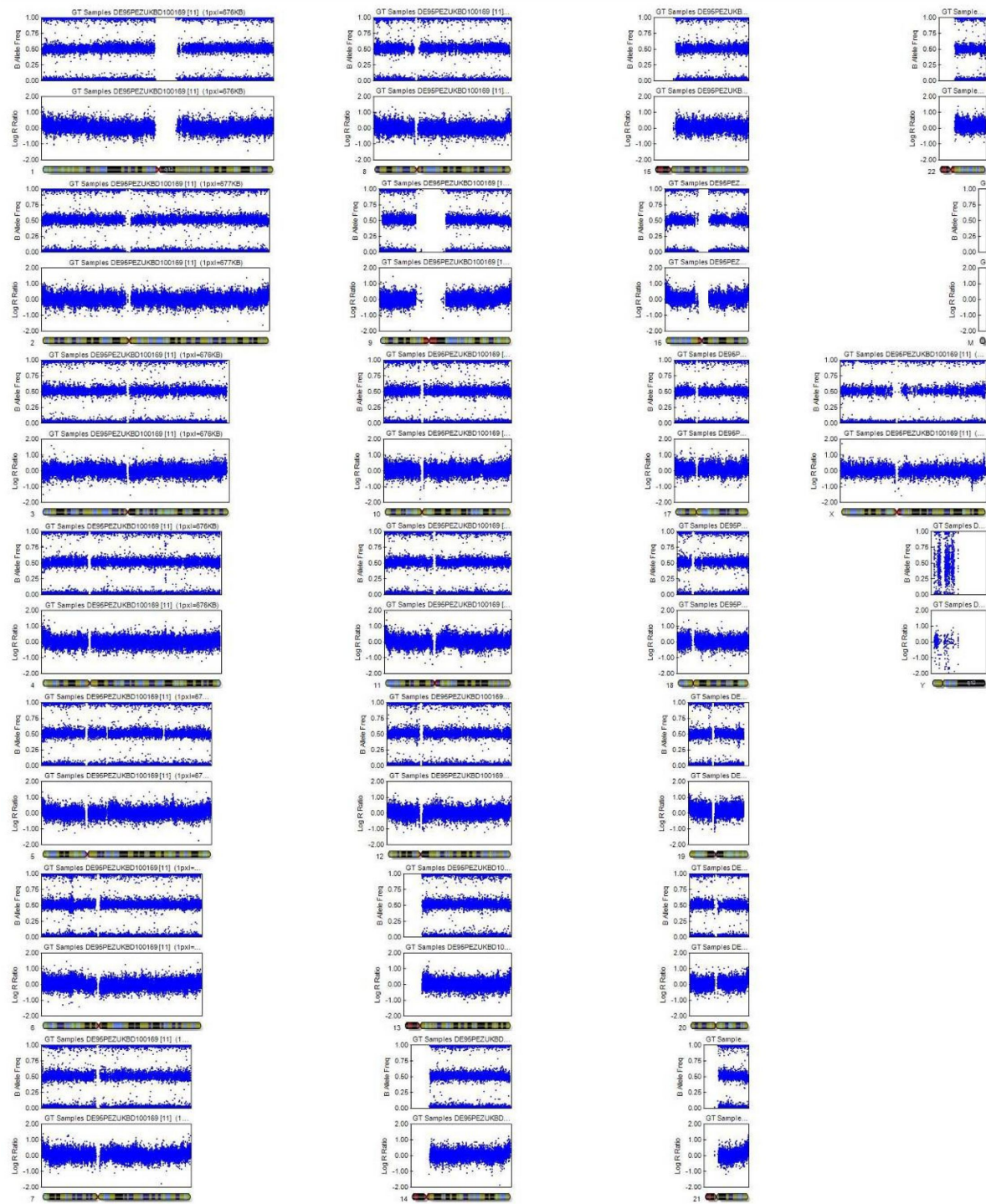
iPSC HGK28.11

Fig. 62: Cluster signals plotted in human iPSC lines HGK13 and HGK16 (red dots) with corresponding fibroblast donor cell lines ML102 and ML101 (blue dots). Physical intactness of the genome is demonstrated by SNP-array analysis in iPSC lines HGK13 versus parental fibroblast line ML102 and HGK16 versus parental fibroblast line ML101.

iPSC line HGK13 versus fibroblast line ML102
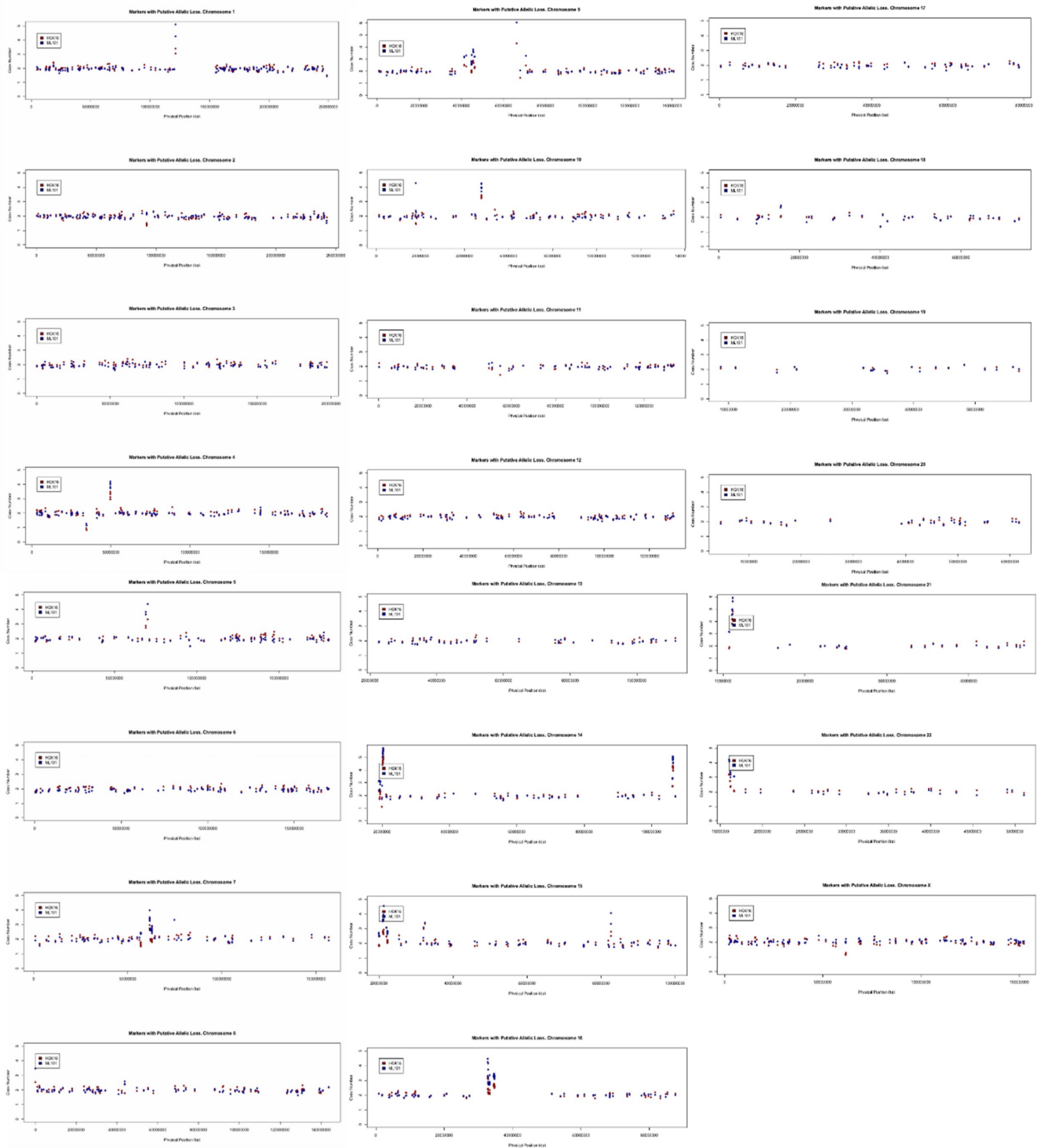
iPSC line HGK16 versus fibroblast line ML101

11.3 pMXs vector maps

Fig. 63: Vector maps of retro-DNA plasmids pMXs-hOCT4, pMXs-hSOX2, pMXs-hKLF4, pMXs-hc-Myc (© Addgene Inc., USA).
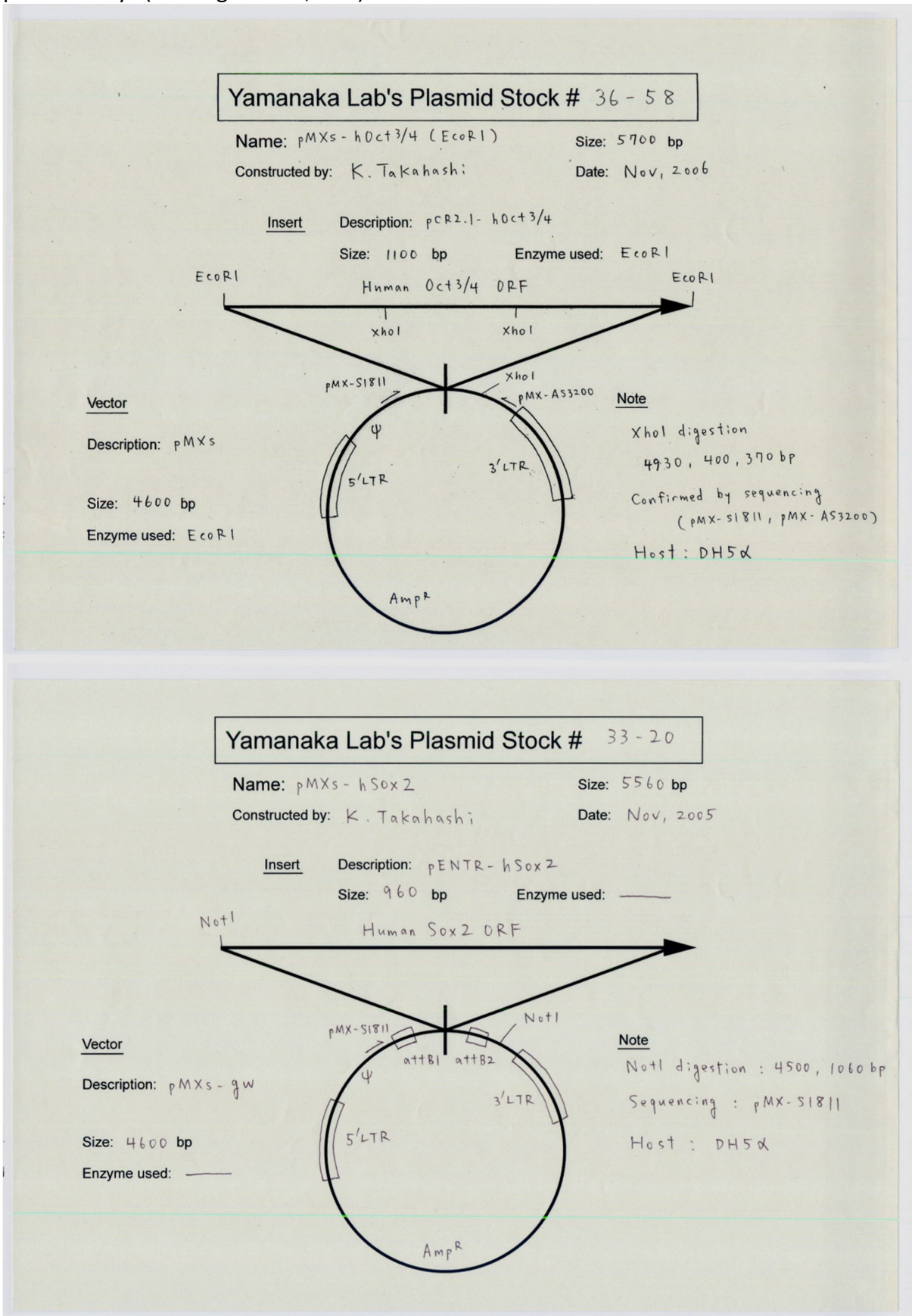
Yamanaka Lab's Plasmid Stock # 33 - 22

Name: pMXs-hKlf4   Size: 6020 bp

Constructed by: K. Takahashi   Date: Nov, 2005

Insert   Description: pENTR-hKlf4

Size: 1420 bp   Enzyme used: ———

NotI

Human Klf4 ORF

pMX-S1811   NotI

Vector   attB1   attB2

Description: pMXs-gw

ψ

Size: 4600 bp   3'LTR

Enzyme used: ———   5'LTR

AmpR
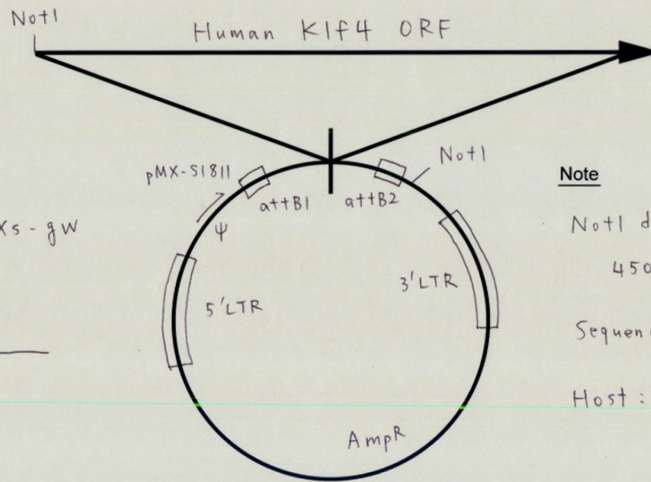
Note

NotI digestion
    4500, 1520 bp

Sequencing: pMX-S1811

Host: DH5α

Yamanaka Lab's Plasmid Stock # 33 - 24

Name: pMXs-hc-Myc   Size: 5920 bp

Constructed by: K. Takahashi   Date: Nov, 2005

Insert   Description: pENTR-hc-Myc

Size: 1320 bp   Enzyme used: ———

NotI

Human c-Myc ORF

pMX-S1811   NotI

Vector   attB1   attB2

Description: pMXs-gw

ψ

Size: 4600 bp   3'LTR

Enzyme used: ———   5'LTR

AmpR
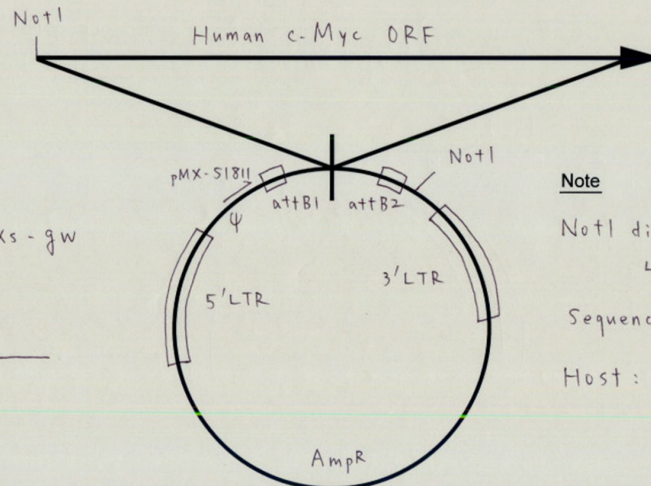
Note

NotI digestion
    4500, 1420 bp

Sequencing: pMX-S1811

Host: DH5α

11.4 SeV plasmid

A
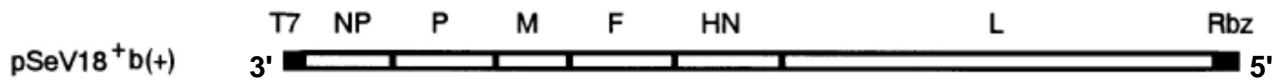
B
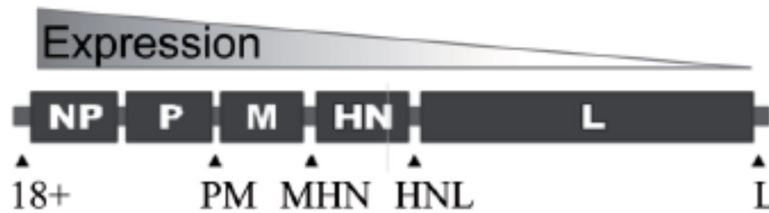
Fig. 64: Schematic illustration of SeV plasmids. (**A**) The plasmid pSeV18+b(+) (~15,000 nt) carries original full-length SeV cDNA. (**B**) In F-protein deficient SeV vector, genes of reprogramming factors are inserted at 18+, PM, MHN, HNL and L, respectively. The polar effect controls the expression rate of inserted genes according to their position (T7, T7 phage promoter; Rbz, hepatitis deltavirus ribozyme sequence) (modified from (Hirata *et al.* 2002; Fusaki *et al.* 2009)).

11.5 Identification of PLS3 bands on immunoblots
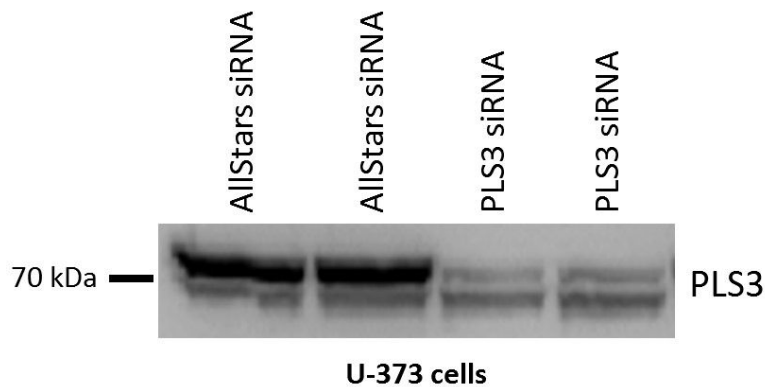
Fig. 65: Immunoblot revealed identity of correct PLS3 band in duplicate. Human glioblastoma cell line U-373 was treated with 50 ng/ml small interfering RNA (siRNA) directed against PLS3 and AllStars Negative Control siRNA. Proteins were isolated 48 h after knock-down. Evidently, strong expression intensity of upper PLS3 band was dimmed in comparison to AllStars Negative Control defining this band as correct PLS3 band. Thus, this specific upper band was subsequently analysed in all immunoblots (see Fig. 47). Results were successfully repeated in HEK cells too (Mohsen Hosseini, personal communication). All data and supportive information were kindly provided by Mohsen Hosseini.

11.6 Validation of smNPCs
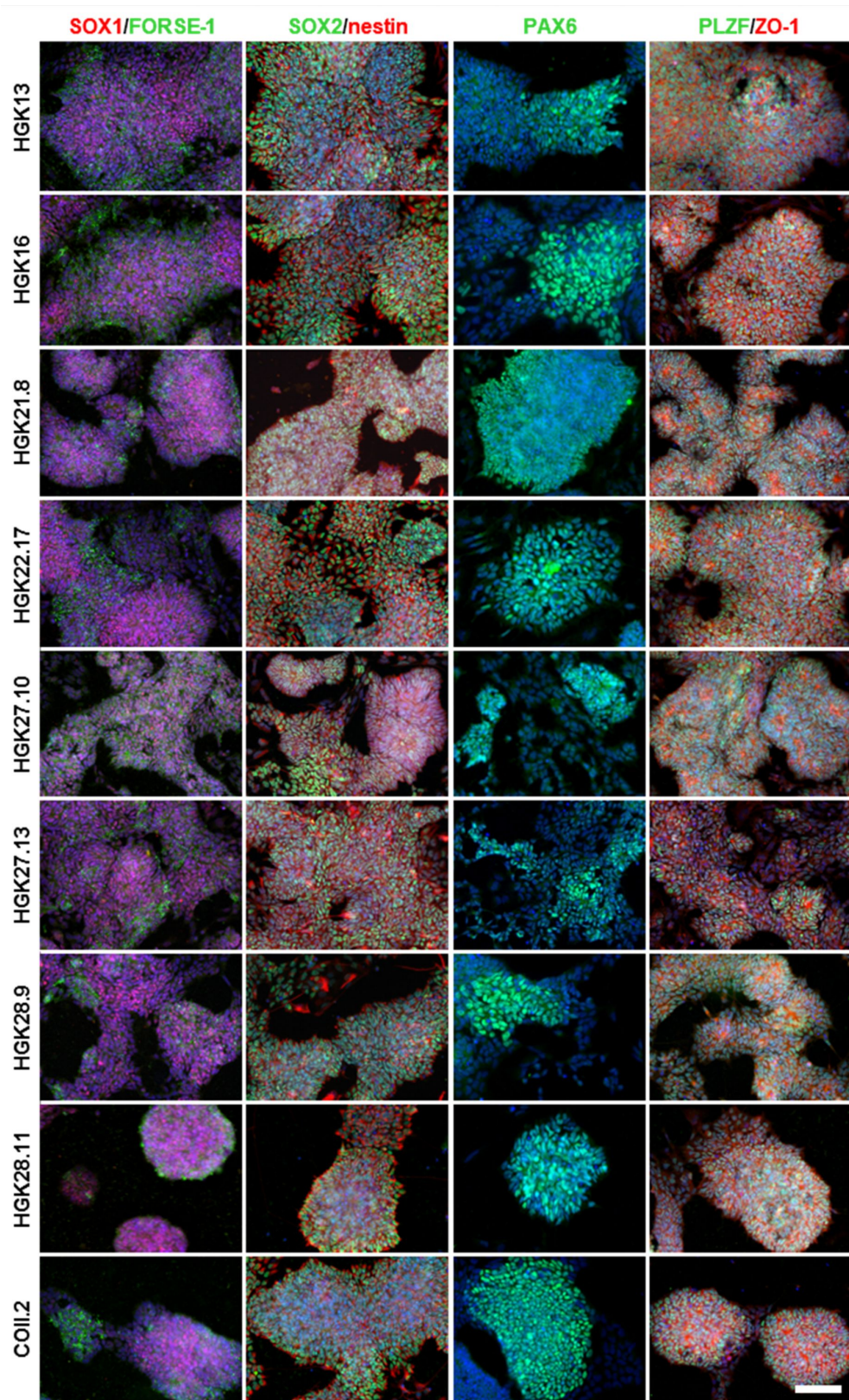
Fig. 66: Further iPSC-derived smNPC lines clearly presented typical NSC markers PAX6 (green), SOX1 (red), SOX2 (green), nestin (red) as well as anterior marker FORSE-1 (green). Since smNPCs possess an early pre-rosette NSC fate expression of characteristic rosette-markers PLZF (green) and ZO-1 (red) did not show the typical petal-like arrangement of lt-NES®SCs unless some lines (e.g. HGK21.8 and HGK27.10) grew densely. Then, ZO-1^{+} rings emerged. In summay, the marker profile of all smNPC lines was comparable to data in the original publication. Nuclei were counterstained with DAPI (blue) (scale bar 100 μm, valid for all images).

12. Danksagung

194

Unbowed, unbent, unbroken

13. Erklärung

Ich versichere hiermit, dass ich die von mir vorgelegte Dissertation selbständig angefertigt, die benutzten Quellen und Hilfsmittel vollständig angeben und die Stellen der Arbeit – einschließlich Tabellen, Karten und Abbildungen –, die anderen Werken im Wortlaut oder dem Sinn nach entnommen sind, in jedem Einzelfall als Entlehnung kenntlich gemacht habe; dass diese Dissertation noch keiner anderen Fakultät oder Universität zur Prüfung vorgelegen hat; dass sie – abgesehen von der unten angegebenen Teilpublikation – noch nicht veröffentlicht worden ist sowie, dass ich eine solche Veröffentlichung vor Abschluss des Promotionsverfahrens nicht vornehmen werde.

Die Bestimmungen der Promotionsordnung sind mir bekannt. Die von mir vorgelegte Dissertation ist von Prof. Dr. rer. nat. Brunhilde Wirth und Prof. Dr. rer. nat. Jürgen Dohmen betreut und in den Arbeitsgruppen von Prof. Dr. rer. nat. Brunhilde Wirth und Prof. Dr. med. Oliver Brüstle (Universität Bonn) durchgeführt worden.

Teilpublikationen sind in Kapitel 9 angegeben.

Köln, den

_____ (Ludwig Heesen, Dipl.-Biologe)

14. Curriculum vitae

Persönliche Daten

Name	Ludwig Heesen
Geburtstag	4. Januar 1982
Geburtsort	Essen
Familienstand	ledig
Staatsangehörigkeit	deutsch

Wissenschaftliche Tätigkeit

Feb 2009 – Okt 2014	Promotion bei Prof. Brunhilde Wirth am Institut für Humangenetik der Universität zu Köln in Kooperation mit dem Institut für Rekonstruktive Neurobiologie (Prof. Oliver Brüstle, Dr. Michael Peitz), Universität Bonn Titel: Analyses of spinal muscular atrophy (SMA) modifiers and drug-dependent responses using motoneurons (MNs) derived from induced pluripotent stem cells (iPSCs)
Jun – Nov 2008	wissenschaftlicher Mitarbeiter bei Prof. Barbara Burwinkel im Deutschen Krebsforschungszentrum (DKFZ), Heidelberg

Hochschulausbildung

Sep 2002 – Mär 2008	Diplomstudium Biologie an der Bayerischen Julius-Maximilians-Universität, Würzburg Hauptfach: Mikrobiologie Nebenfächer: Zell- & Entwicklungsbiologie und Humangenetik Diplomarbeit bei Prof. Clemens Müller-Reible am Institut für Humangenetik Titel: Expression und Mutagenese des Calpain 3-Gens *in vitro* Diplom ***(Gesamtnote: Sehr gut)***

Schulbildung

1988 – 2001	Grundschule und Gymnasium in Meerbusch Abitur als Bester des Jahrgangs **(1,0)** Leistungskurse: Biologie und Englisch
Sep 1998 – Jan 1999	Schüler-Austausch an der King Edward VI School in Bury St. Edmunds/Großbritannien

Köln, den

_____ (Ludwig Heesen, Dipl.-Biologe)